January 2020

Non-Canonical Targets, Reaction Kinetics, And Cellular Potency Of Amino Acid-Linked Platinum(ii) Compounds

Bett Kimutai
Wayne State University

NON-CANONICAL TARGETS, REACTION KINETICS, AND CELLULAR POTENCY OF AMINO ACID-LINKED PLATINUM(II) COMPOUNDS

by

BETT KIMUTAI

DISSERTATION

Submitted to Graduate School

of Wayne State University

Detroit, Michigan

in partial fulfillment of the requirements

for the degree of

DOCTOR OF PHILOSOPHY

2020

MAJOR: Chemistry (Biochemistry)

Approved By:

_____

Advisor Date

_____

_____

_____

DEDICATION

To my parents and wife, Mercy Chepngeno Langat, for their love, encouragement, and support.

ACKNOWLEDGEMENTS

Foremost, I would like to thank my doctoral advisor, Dr. Christine Chow, for taking me into her research lab. Since I joined, Dr. Chow has provided immense guidance and advice that enabled me to grow in research. Dr. Chow also created an enabling environment and opportunities to explore various career paths in preparation of life after graduate school for which I am grateful. I am thankful to all my dissertation committee members, including Dr. Young-Hoon Ahn, Dr. M. T. Rodgers, and Dr. Weilong Hao for their commitment and advice through my PhD dissertation. I also acknowledge Dr. Louis Romano who had earlier served in my committee until his retirement and grateful to Dr. Y. H. Ahn for having accepted to join the committee later on. I acknowledge Dr. M. T. Rodgers and her lab for the collaborative research projects that we had together for a number of years. I am grateful for the great expertise and contribution of Dr. M. T. Rodgers and her former student, Dr. C. C. He, toward the collaboration. The collaboration was very fruitful and enabled us to have publications. Working alongside Dr. C. C. He was also a great experience as I learnt a lot from her talent and knowledge. I would also like to thank Dr. Y. H. Ahn for allowing me to use a number of his research instruments and lab space. I am also grateful to his former student, Dr. Fidelis Ndombera, for training me to perform mammalian cell experiments.

During my time as a graduate student I was surrounded by supportive and friendly colleagues. I am grateful to my past labmates including Dr. Jun Jiang, Dr. Xun Bao, Dr. Gayani Dedduwa-Mudalige, Dr. Danielle Dremann, Dr. Hyosuk Seo, Dr. Nisansala Muthunayake, Dr. Supuni Thalalla Gamage, and Dr. Prabuddha Madubashitha for their advice, expertise, and training on various lab techniques. I am thankful to Dr. Supuni Thalalla Gamage for the fruitful discussions that we had in our collaborative projects and appreciate her talented input in some of the challenging experiments. I am also appreciative of the current Chow lab members including Evan Jones, Rabiul Islam, Alan Mlotkowski, and Deepak Shrestha for being collaborative in our research and providing valuable input from their areas of expertise. All the past and current labmates exemplified comradery in day to day activities that enabled us to grow in science and

also to be great friends outside of lab. I would like to thank all the former and current undergraduate students in our lab whom I worked with including Andrew Roberts, Marcel L. Jones, Ken Dada, Nicolas Nunez, and Mateusz Sileski. Each of them was very helpful and provided valuable contributions in various projects. I am also grateful to all the past and current members of Dr. Ahn and Dr. Bhagwat labs for the fruitful interactions that we had while assisting each other in various lab activities or discussions.

I would like to thank the staff at Lumigen instrument center (LIC) for providing me with the training and guidance on how to run various instruments. I particularly acknowledge Dr. Dennis Anderson, Evan Jones, Dr. Jun Jiang, and Dr. Phil Martin for their expertise and assistance in collecting some of the data. I am also grateful to Dr. Johnna Birbeck, Dr. Olena Danylyuk, and Dr. Nicholas Peraino for training me on the use of various mass spectrometry techniques. I am thankful for some of the materials provided generously by a number of labs including Dr. Y. H. Ahn, Dr. Kenneth V. Honn, and Dr. Zhihui Qin from where I acquired mammalian cell lines. I am also grateful for some chemical supplies provided generously by Dr. Klaus Friedrich from University of Detroit Mercy.

I acknowledge WSU-BEST and ReBUILDetroit programs for the career development opportunities that they provided. In winter 2018, I had a semester-long internship to explore a teaching career through these programs. I worked and interacted with exceptional people including Dr. Jazhara Mayes Otoo and Dr. Jeanne Andreoli from University of Detroit Mercy, and Dr. Andrea Matti from Wayne State University during this teaching internship. They provided such immerse guidance and environment for career development. I am also grateful to my advisor, Dr. Chow, and Dr. Heidi Kenaga who were an integral part of the BEST program and its opportunities. I would also like to acknowledge the WSU chapter of NOBCChE, its officials, and members for working together towards its mission and goals. Personally, being part of this incredible team gave me an opportunity to develop leadership skills and other soft career skills especially when I served as its vice-president.

I am grateful to Wayne State University and the Chemistry department for the opportunity to be part of this institution and the department. I am thankful for the environment and all the resources provided by WSU and the department for me to work on my PhD dissertation. I thank Melissa Rochon for her time and resourcefulness through the entire process.

I would like to thank my parents, Joseph Langat and Florence Langat, their love and support through all the years. I would also like to thank Hellen Jones and my friend Dr. Ezra Mutai at Cornell University who have always been encouraging in my professional and personal life. Lastly, I would like to thank my wife, Mercy Langat, for her love, support and patience. She has been very encouraging, full of life, and a continued source of inspiration since we met.

TABLE OF CONTENTS

LIST OF TABLES

LIST OF FIGURES

LIST OF SCHEMES

LIST OF ABBREVIATIONS

DNA	deoxyribonucleic acid
RNA	ribonucleic acid
cisPt,	*cis*-diamminedichloridoplatinum(II)
dGuo	2′-deoxyguanosine
dAdo	2′-deoxyadenosine
Guo	guanosine
Ado	adenosine
dThd	2′-deoxythymidine
dCyd	2′-deoxycytidine
Cyd	cytidine
Urd	uridine
AAPt	amino acid-linked platinum(II) compounds
AlaPt	alanine-linked platinum(II) compound
OrnPt	ornithine-linked platinum(II) compound
ArgPt	arginine-linked platinum(II) compound
HSAB	hard-soft acid-base
rRNA	ribosomal RNA
tRNA	transfer RNA
mRNA	messenger RNA
lncRNA	long noncoding RNA
GSH	glutathione
NER	nucleotide excision repair
AKI	acute kidney injury
hSOD	human superoxide dismutase
ROS	reactive oxygen species

HPLC	high performance liquid chromatography
NMR	nuclear magnetic resonance
HSQC	heteronuclear single quantum correlation
ESI-MS	electrospray ionization mass spectrometry
MALDI	matrix-assisted laser desorption ionization
LC-MS	liquid chromatography-mass spectrometry
ICP-MS	inductively coupled plasma mass spectrometry
ICP-OES	inductively coupled plasma optical emission spectroscopy
MTT	3-(4,5-dimethylthiazol-2-yl)-2,5- diphenyltetrazolium bromide
MTS	3-(4,5-dimethylthiazol-2-yl)-5-(3-carboxymethoxyphenyl)-2-(4sulfophenyl)-2H-tetrazolium
XTT	2,3-bis-(2-methoxy-4-nitro-5-sulfophenyl)-2H-tetrazolium-5carboxanilide
WST	2-(2-methoxy-4-nitrophenyl)-3-(4-nitrophenyl)-5-(2,4-disulfophenyl)-2H-tetrazolium
DMSO	dimethylsulfoxide
3-HPA	3-hydroxypicolinic acid
DACH	1,2-diamminocylohexane
DMSO	dimethylsulfoxide
ER-CID	energy-resolved collision-induced dissociation
PBS	phosphate-buffered saline
FBS	fetal bovine serum
IC_{50}	half maximal inhibitory concentration

CHAPTER 1

INTRODUCTION

1.1 Abstract

DNA serve as an ideal target where drugs such as cisplatin (cisPt) bind and exert their anticancer activities. CisPt is known to preferentially coordinate with DNA leading to formation of cisPt-deoxyguanosine (dGuo) adducts. The adducts distort the DNA structure and contribute to inhibition of DNA-mediated cellular functions and ultimately cancer cell death. Despite its utilization as an anticancer drug, cisPt has a number of drawbacks, which include toxic side effects and cellular resistance. Resistance occurs through processes such as repair of damaged DNA and inactivation of cisPt present in the cell. To overcome these challenges, the aim of this thesis work was to synthesize and investigate compounds that coordinate to different sites from those targeted by cisPt, including sites found in RNA. In this highly collaborative dissertation project, amino acid-linked platinum(II) compounds were synthesized and studied as alternatives to cisPt. The reactivity preferences of these compounds towards DNA/RNA nucleosides and oligonucleotides were determined through pseudo-first-order kinetics. The products formed by the reactions of amino acid-linked platinum(II) compounds with DNA and RNA were studied by electrospray ionization mass spectrometry (ESI-MS) to determine the type of adducts formed by the compounds. NMR spectroscopy was used to determine the non-canonical adducts formed by the compounds that include platination of the N1, N3, or N7 positions of RNA adenosine (Ado) residues. Features of amino acid-linked platinum(II) compounds that impact the glycosidic bond stability of Ado residues were explored by using tandem mass spectrometry in collaboration with the Rodgers laboratory. Furthermore, cytotoxicity assays and inductively coupled plasma mass spectrometry (ICP-MS) were used to determine the potency and accumulation of the compounds in cancer cells. Altogether, the unique characteristics of the amino acid-linked compounds such as altered reactivity preferences, formation of adducts at non-canonical residues, destabilization of glycosidic bonds, selective potency, and higher accumulation in cancer cells are important

features that could circumvent drug resistance faced by the currently available platinum-based drugs.

1.2 Introduction to discovery, mechanism of action, and kinetics of cisPt

1.2.1 Discovery of cisPt and its application in cancer therapy

CisPt, *cis*-diamminedichloridoplatinum(II), is a widely used platinum-based antitumor drug [1] that has come a long way since it was first synthesized in 1844 by an Italian chemist, Michele Peyrone (**Fig.1.1**) [2]. Peyrone was interested in the synthesis and reactivity of various platinum-based compounds. He documented some of the physical and chemical properties of cisPt, which at the time was called Peyrone's salt [3]. Although Peyrone described some of the properties of cisPt, the structure of the compound was not fully elucidated at that time [2]. In 1893, Alfred Werner, a scientist interested in the coordination chemistry of inorganic compounds proposed that the structure of cisPt consists of a square-planar geometry [4]. After Werner's findings, cisPt went into obscurity for many years until the 1960s when crystallographic studies of the compound were done [5] . A crystal structure confirmed the *cis* configuration of cisPt, while also revealing that transplatin (*trans*-diamminedichloridoplatinum(II), is an isomer of cisPt with the *trans* configuration (**Fig. 1.2**).

The biological applications of cisPt were not realized until the 1960s when Barnett Rosenberg serendipitously discovered its antitumor activity [6-7]. This discovery occurred while Rosenberg and coworkers were investigating the effects of electrical fields on the growth of *E. coli*. They observed inhibition of cell division, along with dramatic changes in the cell morphology, when the bacteria were exposed to an electrical current with platinum electrodes in an ammonium chloride buffer [6]. Further investigation revealed that these effects were not due to the electric current, but rather because cisPt was being formed from a reaction between the buffer and the platinum electrodes [6]. Using cisPt and related platinum-based compounds, Rosenberg, VanCamp, and co-workers carried out antitumor testing with animal models [7]. They treated tumor mice models using various concentrations of the compounds, and observed that the mice

had remarkable tumor regression after low doses of cisPt. This work contributed to discovery of the antitumor activity of cisPt in mammals, and led to the introduction of cisPt as a clinical platinum-based antitumor candidate in 1969 [7-8]. After more clinical investigation was done, cisPt was approved by the FDA in 1978 to be used for treatment of testicular and bladder cancer, becoming the first platinum-based anticancer drug [9].

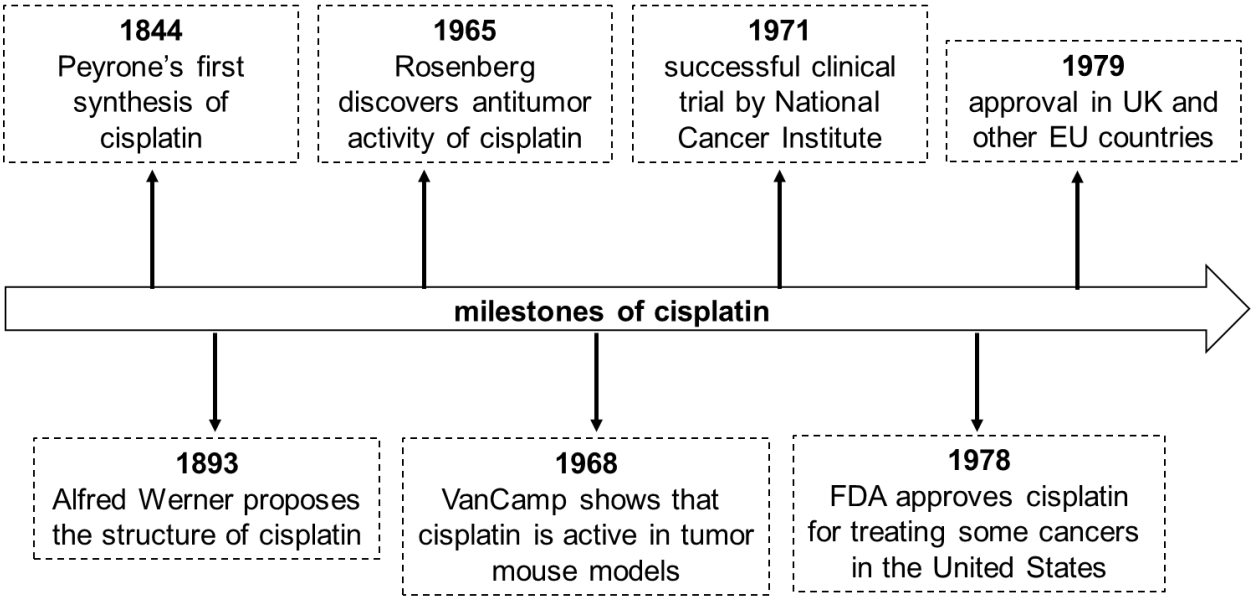

Figure 1.1. Timeline for discovery, development, and applications of cisPt. CisPt was first synthesized more than 150 years ago, but its application in human cancer therapy did not take place until the1970s [10].

cisplatin (cisPt) transplatin

Figure 1.2. The structures of cisplatin (cisPt) and transplatin with their respective configurations. Both of the isomeric compounds assume a square-planar geometry.

Since its approval by the FDA, cisPt has been used for treatment of several other forms of cancer, including testicular, ovarian, colorectal, prostate, lung, breast, and head and neck cancer [9, 11]. The response of the various forms of cancer to cisPt treatment varies from one

tissue to another. Testicular cancer is the most responsive, with a cure rate of 90-100%, especially when discovered and treated with cisPt early [11-12]. Other forms of cancer such as non-small lung cancer are not as responsive, and cancer regression can be hampered by development of cisPt resistance with each round of dosage given to the patient [13-14].

1.2.2 Structural components of cisPt

CisPt, $[PtCl_2(NH_3)_2]$, is a platinum-based complex with a square-planar *cis* geometry (**Fig. 1.3**). The platinum metal element has atomic number 78 and exists as various stable isotopes with the most abundant being ^{195}Pt. Platinum has two valence states, (II) and (IV), which have different numbers of coordinated ligands. CisPt has a Pt(II) center coordinated by two ammine and two chlorido ligands. According to the hard-soft acid-base (HSAB) principle, the platinum is a soft acid that prefers coordination to softer bases such as amines compared to chlorine [15]. Because coordination to the N-containing ligands is more thermodynamically stable, the two ammines are referred to as 'non-leaving groups', whereas the two chlorido ligands are referred to as the 'leaving groups' (**Fig. 1.3**). These two different ligand types determine the various chemical properties of cisPt, ranging from the kinetic reactivities of the compound to the preferred biological targets [16-17].

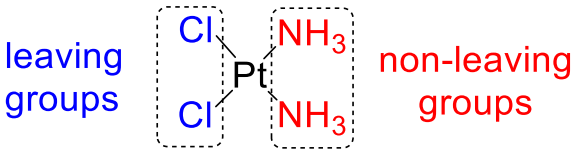

Figure 1.3. **The structural components of cisPt**. The two chlorido ligands are referred to as leaving groups, because they can be replaced during reactions with the target. The two ammines are thermodynamically stable and remain coordinated.

1.2.3 Mechanism of action, reaction kinetics, and adduct formation of cisPt

The mechanism of action of cisPt has been studied extensively over the past 50 years in an effort to understand its clinical efficacy [16, 18]. CisPt is administered intravenously into the bloodstream from where it can enter cells through various modes, including passive diffusion [19-20]. Passive diffusion is driven by the different cisPt concentrations inside and outside of the cell

(**Fig. 1.4**) [20-21]. Other modes of cisPt uptake are active and facilitated transport. For example, copper transporters in cancer cells facilitate the regulation and intake of cisPt [22-24]. Presence of such facilitated transport is crucial to the biological activity of cisPt, since upregulation of copper transporters increases the sensitivity of cancer cells to cisPt [22]. Downregulation of facilitated transporters and reliance on passive diffusion is one factor that may lead to cellular resistance to cisPt treatment [22].

Blood serum has a high chloride concentration of approximately 100 mM, which inhibits the loss of the chlorido ligands of cisPt and enables the compound to reach the cell membrane in its intact neutral form, $[PtCl_2(NH_3)_2]^0$ [25]. However, aquation (replacement with an aqua ligand) occurs once cisPt is inside the cell where the chloride concentration is much lower (2-30 mM) [25] (**Fig. 1.4**). The aquated cisPt can include the monoaquated form, $[PtCl(H_2O)(NH_3)_2]^+$, or the bis-aquated form, $[Pt(H_2O)_2(NH_3)_2]^{2+}$, in which either one or both of the chlorido ligands are replaced by aqua ligands, respectively [19]. The aquated forms of cisPt are positively charged and can interact with negatively charged nucleic acids through electrostatic interactions before coordination to the nucleobase occurs [19]. The aquated forms of cisPt preferentially coordinate to neighboring dGuo residues of DNA [26-27]. Formation of these adducts alters the DNA structure and inhibits biological processes such as replication and transcription [11]. The adducts trigger other cellular responses, including cell cycle arrest, DNA repair, and apoptosis [1]. Aside from DNA, cisPt can also coordinate with other cellular biomolecules including RNA, thiol containing metabolites, and S-containing proteins (**Fig. 1.4**) [28-30]. These interactions play different roles, from contributing to the potent activity of cisPt in the cell to cellular resistance towards the same compound [28-31].

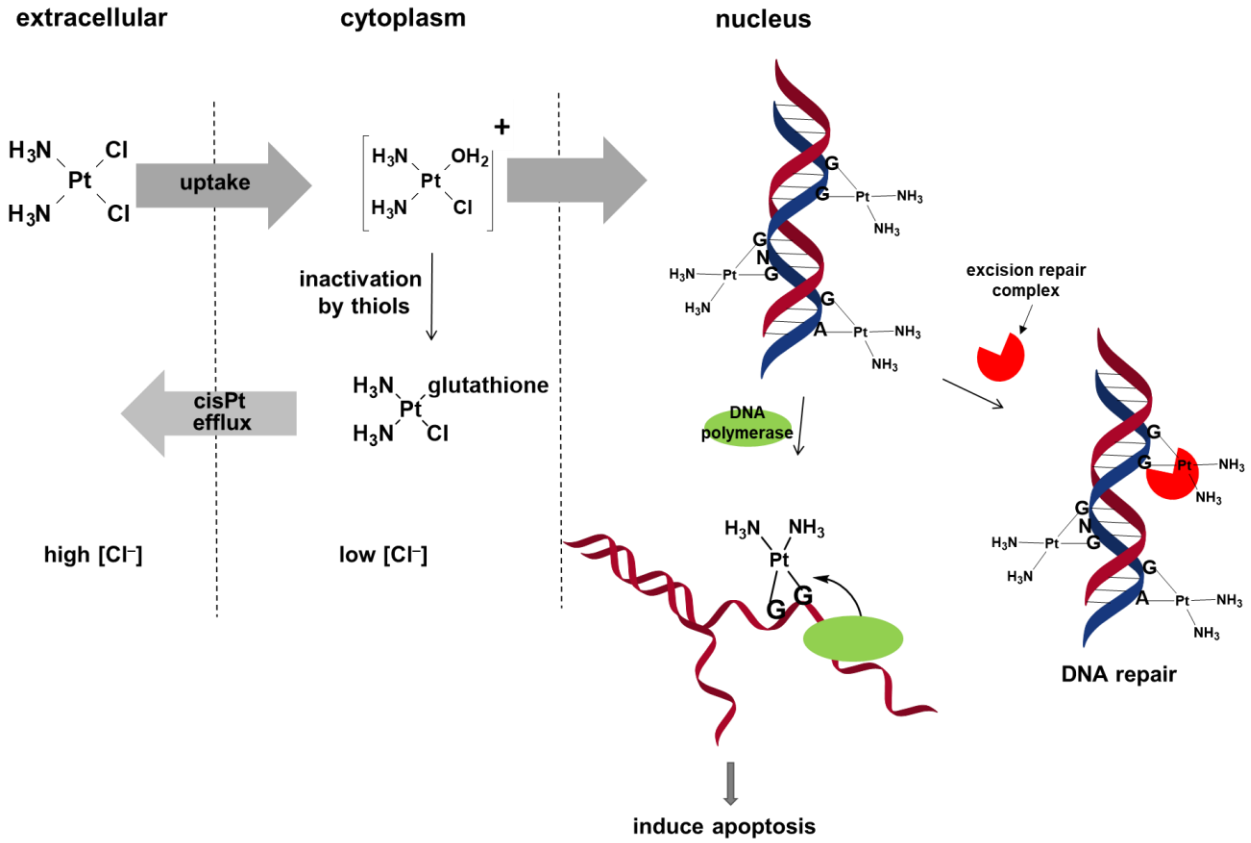

Figure 1.4. Mode of action of cisPt. The mechanism of cisPt antitumor activity includes uptake, aquation, formation of adducts with DNA, inhibition of cellular processes, apoptosis, and possible resistance due to factors such as drug efflux, reactions with other cellular components, and DNA repair. Inhibition of cellular processes such as replication, occurs when cisPt adduct block DNA polymerase. Repair of damaged DNA occurs when the cell removes the platinum adducts using an excision repair complex.

Reactions of the aquated cisPt species with DNA occur under kinetic control, leading to stable adduct formation at the preferred dGuo sites [30, 32]. The coordination of cisPt with DNA involves a number of steps that contribute to the overall reaction rates (**Fig.1.5**). The replacement of the first chlorido ligand with an aqua ligand is the rate-determining step that leads to formation of monoaquated species, $[PtCl(H_2O)NH_3]^+$ [32]. The monoaquated cisPt coordinates with DNA at the N7 position of dGuo residues to form a monofunctional adduct, $[PtCl(N7\text{-}dGuo)NH_3]^+$ [32]. The monofunctional adduct is then hydrolyzed through replacement of the second chlorido to form $[Pt(H_2O)(N7\text{-}dGuo)NH_3]^{2+}$. This aquated monofunctional adduct then coordinates with a nitrogen

(preferably at N7) of the second dGuo residue, leading to formation of a bifunctional adduct, $[Pt(N7\text{-}dGuo)_2NH_3]^{2+}$ (**Fig. 1.5**) [32].

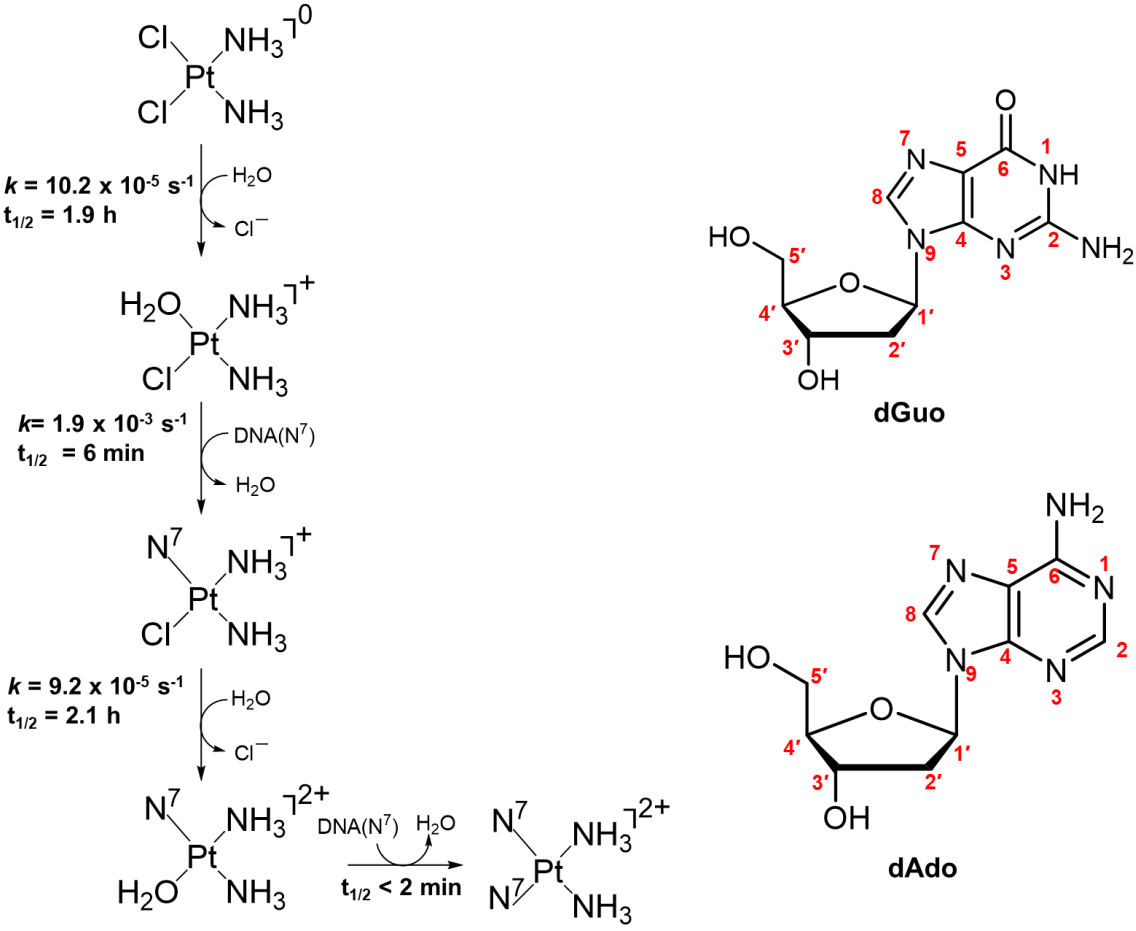

Figure 1.5. **Reaction kinetics of cisPt and DNA**. CisPt loses the first chlorido ligand to form a monoaquated species. The monoaquated species coordinates with DNA at the N7 position of a dGuo residue. The second chlorido of cisPt is then replaced by another aqua ligand. This step is followed by coordination of the complex to the adjacent dGuo residue at the N7 position. The rate constants for each step are indicated [32]. The structures and numbering of dGuo and dAdo are shown on the right.

All of the steps of cisPt coordination to DNA contribute to the kinetics of DNA platination and are therefore important in the cellular activity of cisPt (and other platinum-based compounds as well) [33-36]. For example, *cis*-diammine-1,1-cyclobutane dicarboxylate platinum(II) (carboplatin) is less potent than cisPt, which is partly attributed to its 100-fold slower adduct formation with DNA (more discussion of cisPt analogues will be given in subsequent sections) [34].

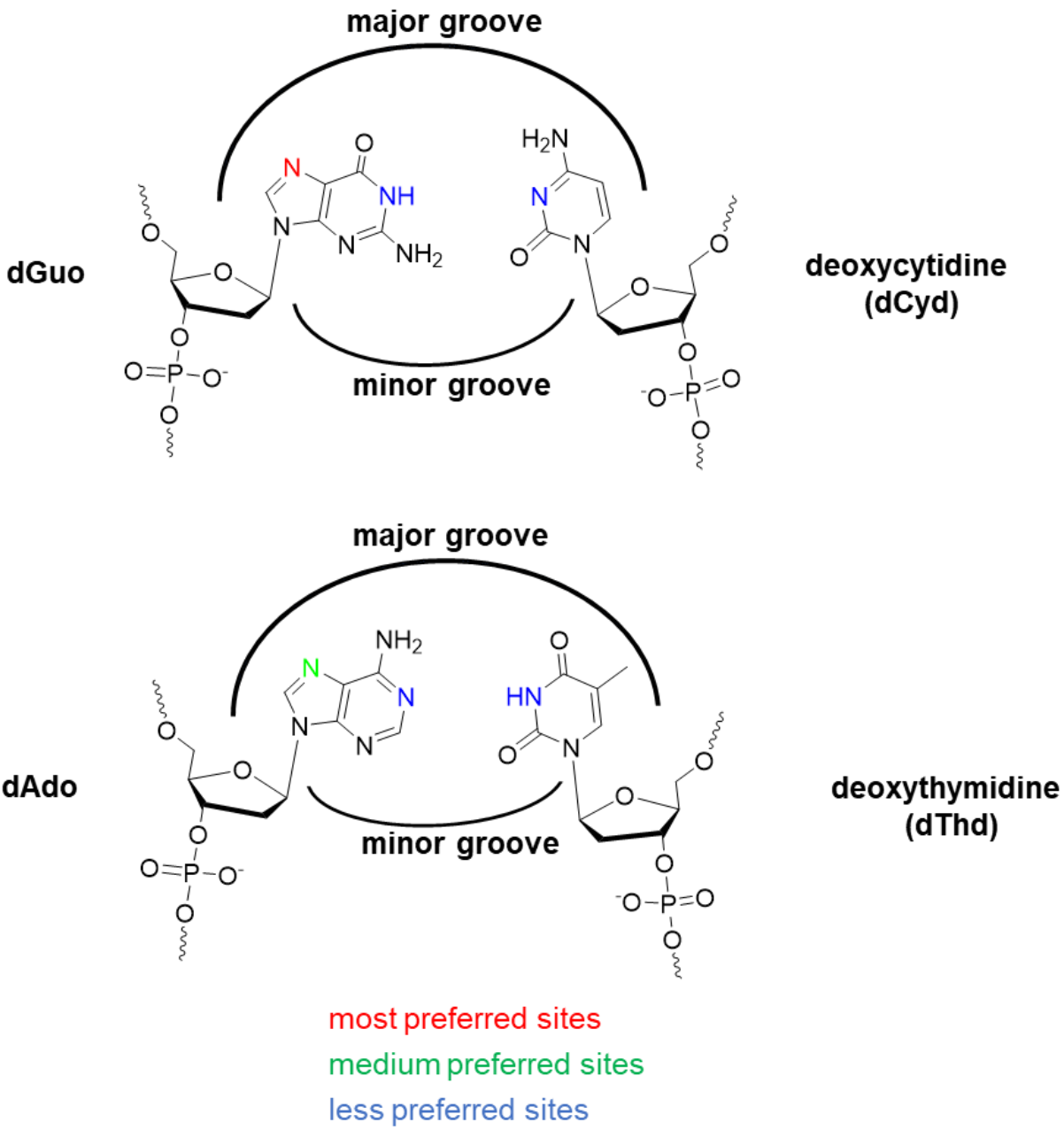

Figure 1.6. **Potential DNA coordination sites for cisPt**. The site preference is dictated by nucleophilicity and accessibility, with the major groove being more accessible to the platinum compounds. Atoms involved in hydrogen bonding between the nucleotide bases are less likely to participate in platinum coordination.

There are several potential binding sites in the DNA for cisPt to coordinate with varying degrees of preference (**Fig. 1.6**). The nitrogen atoms of nucleosides, especially dGuo and

deoxyadenosine (dAdo), are soft bases that provide nucleophilic sites to which the platinum center can coordinate. Coordination occurs preferentially at the N7 position of dGuo due to its high nucleophilicity compared to the nitrogens of other nucleosides or positions of dGuo [10, 37-38]. Furthermore, the N7 position of dGuo is found in the major groove of the DNA, which makes it more accessible for adduct formation by cisPt compared to other sites such as N3 of the same nucleoside [18, 39].

As mentioned above, cisPt can lose two chlorido ligands leading to formation of cross-links. CisPt forms the DNA bifunctional adducts by coordinating to two adjacent dGuo residues at their N7 positions [32, 37, 40]. Of the DNA adducts that are formed, 90–95% are intrastrand cross-links (**Fig. 1.7**). Further analysis shows that 60–65% are 1,2-(dGuo-p-dGuo), 25% are 1,2-(dAdo-p-dGuo), and 5% are 1,3-(dGuo-p-Nuo-p-dGuo) intrastrand cross-links in which the coordination occurs at neighboring nucleotides (1,2) on the same strand or with an intervening nucleotide (1,Nuo,3) (p indicates the phosphate ester bond). The rest of the adducts are a small percentage comprising interstrand cross-links (across two strands of DNA) and monofunctional adducts (**Fig. 1.7**) [37, 41].

Compared to cisPt, transplatin has a different DNA adduct profile owing to its *trans* configuration and therefore large angle (180°) between available coordination sites. While a majority of the adducts formed by cisPt (95%) are bifunctional adducts that are formed by cisPt coordinating with two adjacent nucleosides [37], transplatin forms predominantly monofunctional adducts [38, 42-43]. The *cis* configuration is more compatible with coordination to adjacent sites [37-38, 42]. The angle imparted by the platinum metal center leads to DNA bending [11, 38]. Since transplatin forms predominantly monofunctional adducts, the impact on DNA structure is different [38, 42-43].

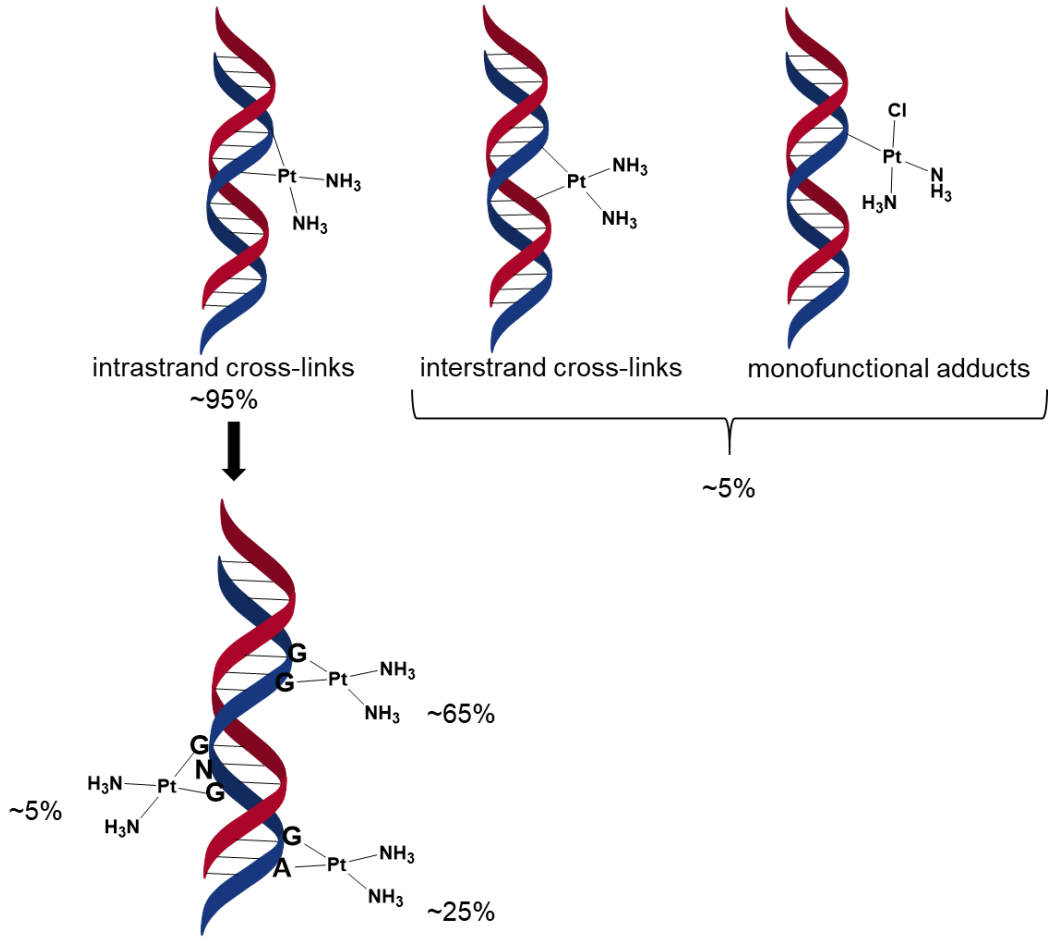

Figure 1.7. **Various types of DNA adducts that are formed by cisPt**. CisPt coordinates with purines at the N7 position and forms intrastrand and interstrand cross-links, and monofunctional adducts with varying abundance [41].

The overall process of cisPt adduct formation such as aquation and DNA platination [34, 36] is influenced by a number of factors associated with the non-leaving group ligand (typically an ammine), including coordination type and hydrogen-bonding properties [35-36]. These factors play roles in target preferences and the types of adducts that are formed. The adducts that are formed when cisPt reacts with dGuo are kinetically inert [27, 35, 44]. The adducts form when the aqua ligand of cisPt is substituted by a nucleobase atom (typically a nitrogen) via a trigonal-bipyramidal transition state [45]. Hydrogen bonding is implicated in the kinetic control of platination [36, 46] and can stabilize the transition state of the cisPt-dGuo reaction [27]. It was demonstrated using computational analysis that during the transition state, cisPt forms a strong hydrogen bond

between its ammine ligand and the oxo at the 6 position of dGuo (**Fig. 1.8**) [27]. As such, this hydrogen-bonding interaction together with charge-charge interactions results in preferential coordination of cisPt to dGuo residues of DNA [27]. In contrast, formation of the cisPt-dAdo adduct is less favored because the dAdo has an amine at the 6 position, which cannot hydrogen bond with the cisPt ammine ligand [27].

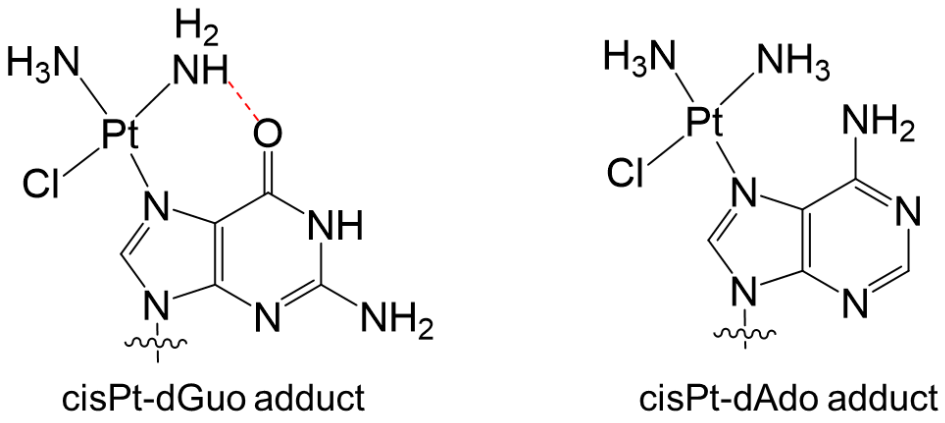

Figure 1.8. **Structure of cisPt-nucleoside adducts**. CisPt binds to the N7 position of dGuo and forms a hydrogen bond between its ammine ligand and the 6-oxo of dGuo. A hydrogen bond would not form in the cisPt-dAdo adduct.

The binding of cisPt in the DNA major groove results in distortion of the helical structure [38]. The distortion of the helix induces the recruitment of proteins that recognize the damage of the DNA structure. These proteins, which include the high-mobility-group (HMG) proteins, recognize and bind to the bent DNA structures and further increase the bend angle [47-48]. The binding of the HMG proteins leads to a cascade of downstream effects that are correlated with cancer cell death and hence mediate the antitumor activity of cisPt [48]. The adducts that are formed also disrupt normal DNA-protein recognition leading to inhibition of important cellular processes, such as replication and transcription [1].

1.3 Introduction to alternative biological targets of cisPt

1.3.1 RNA as a target of platinum-based compounds

Previous studies have shown that RNA is also a biomolecular target of cisPt [49-54]. While the interaction of DNA and cisPt has been largely studied, investigation of the platination of RNA by cisPt and its role in cellular toxicity has been minimal. In recent years there has been increased interest in RNA-cisPt interactions [49-54]. RNA is an important biomolecule that plays crucial roles in cellular functions ranging from translation to regulation of gene expression. Therefore, RNA modifications or damage by small molecules could adversely affect the functions of RNA. By extension, disruption of the RNA integrity and its functions could lead to a cascade of events that ultimately lead to cell death [29, 55-56].

There are various reasons why cellular RNA is a plausible target for cisPt. Unlike DNA, RNA abundance and localization in a cell are not limited to the nucleus, and rRNA, mRNA, and other forms of regulatory RNA can be found in the cytoplasm. Since cisPt is activated to generate its reactive monoaquated species in the cytoplasm, it could interact with cytoplasmic components, including the readily available cytoplasmic RNAs [29, 50, 53-56]. One of the important features that enables coordination of cisPt to DNA nucleotides is their nucleophilicity. RNA also has nucleophilic sites such as the N7 position of guanosine (Guo) residues where cisPt could bind, and therefore modify the RNA and trigger apoptosis [29, 51, 53, 56].

Investigation of the interaction of cisPt with various forms of RNA has been carried out using various techniques. CisPt has been shown to bind to Guo residues of RNAs of varying sizes, structures, and cellular locations, including the ribosome, mRNA, and tRNA [50, 53, 57-58]. Melnikov and coworkers reported a 2.6 Å-resolution X-ray crystal structure of cisPt bound to 70S ribosomes. The structure revealed nine ribosomal target sites in which cisPt coordinated RNA, including six in the 50S subunit (**Fig. 1.9)**, two in the 30S subunit, and one on ribosomal L9 protein [51]. One of the sites (A790 of 16S RNA) is in the mRNA channel; cisPt platinates a nucleotide

that is in direct contact with the mRNA [51]. In inductively coupled plasma mass spectrometry (ICP-MS) quantification of the abundance of cisPt bound to DNA vs. RNA after cellular treatment, it was observed that there is more than four-fold higher accumulation of cisPt on RNA than DNA [59]. The abundance of cisPt adducts on RNA also varies from one form of RNA to another. For example, cells treated with cisPt have up to six-fold higher platinum accumulation on rRNA compared to mRNA [59]. A comparison of the reactivity of small RNA and DNA hairpins with platinum-based compounds indicated that RNA is the kinetically preferred target [49]. Platination of tRNA has also been observed with cisPt coordination occurring at the Guo-Cyd (cytidine) rich regions of the RNA [58]. The platination of long noncoding RNA (lncRNA) has also gained interest due to the importance of lncRNAs in regulation of cellular functions. Previous studies have shown that binding of cisPt to lncRNA plays a role in modulating cancer resistance [60].

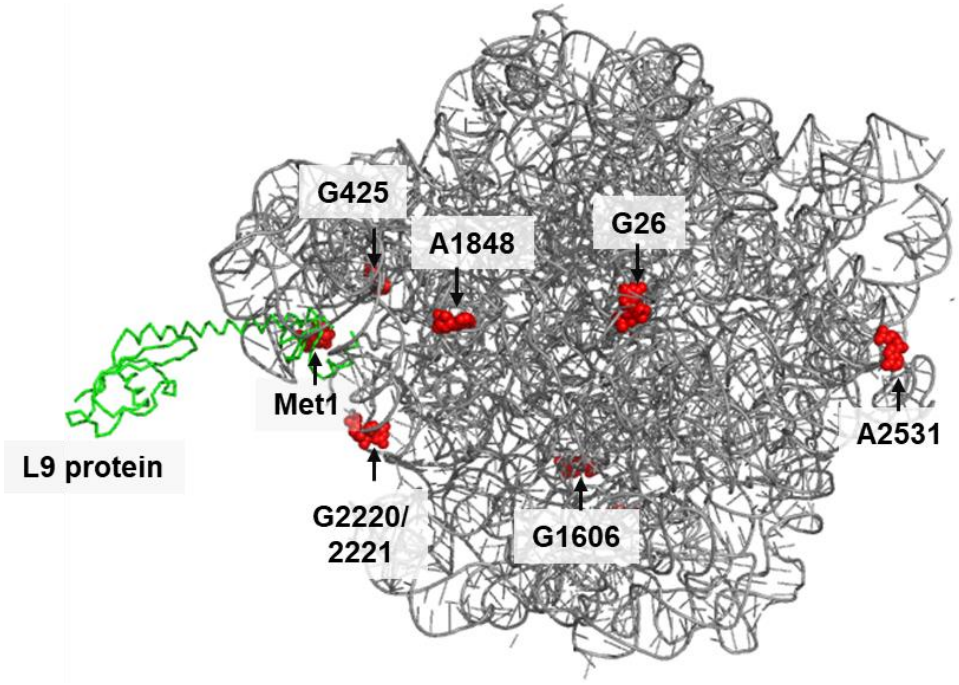

Figure 1.9. **Crystal structure of cisPt bound to 50S RNA (PDB ID: 5J4B) [51]**. Residues modified by cisPt in the 50S subunit of the ribosome are shown by red spheres. The 50S subunit has six cisPt adducts and one adduct on the L9 ribosomal protein (where cisPt binds with a methionine residue). The sequence numbers of the platinated residues are indicated.

Since clinical use of cisPt has become challenging due to cellular resistance through processes such as DNA repair, targeting RNA may provide another avenue for triggering apoptosis while averting resistance. Similar to the target preferences in DNA, aquated cisPt coordinates to accessible Guo residues of RNA [49-54]. Analogues of cisPt that exhibit altered mechanisms of action, such as targeting RNA over DNA, modifying alternative nucleosides rather than dGuo/Guo or altering RNA levels through induced decay pathways, may play a role in circumventing cellular resistance [29, 55-56].

1.3.2 Proteins as targets of platinum-based compounds

There is evidence that cisPt interacts and forms adducts with proteins, especially at locations with sulfur-, nitrogen-, and oxygen-containing amino acids such as cysteine, methionine, and histidine [61]. The coordination of cisPt to cellular proteins plays a role in cisPt uptake, side effects, and resistance [30, 61-62]. As noted earlier in Section 1.2.3, proteins such as copper transporters are crucial for the uptake of cisPt, and their role in facilitating transport causes the cell to be more sensitive towards cisPt treatment [22-24]. Besides facilitating transport, some cellular proteins are biomolecular targets of cisPt and other platinum-based compounds [30, 61-62]. Considering hard-soft acid-base (HSAB) principle, platinum is a soft acid and has a high affinity for soft bases such as sulfur and nitrogen, and therefore readily coordinates to sulfur- and nitrogen-containing biomolecules [15]. Various proteins are rich in sulfur-containing residues such as methionine and cysteine. Therefore, cisPt can coordinate to proteins through such residues. For example, it has been reported that cisPt binds to human superoxide dismutase (hSOD) protein through a cysteine residue (Cys111) (**Fig.1.10**) [61, 63].

Various biochemical and analytical tools have been used to characterize possible platination sites of proteins by cisPt and other platinum-based compounds, and to understand the downstream effects of such platination events [62]. The reactivity of cisPt with proteins such as cytochrome c, superoxide dismutase, lysozyme, myoglobin and ubiquitin have been investigated [62]. These studies were carried out using NMR, mass spectrometry, inductively coupled plasma

optical emission spectroscopy (ICP-OES), and X-ray crystallography [61, 64-67]. These studies have shown that cisPt coordinates with the proteins through their cysteine, histidine, and proline residues [61-63, 68].

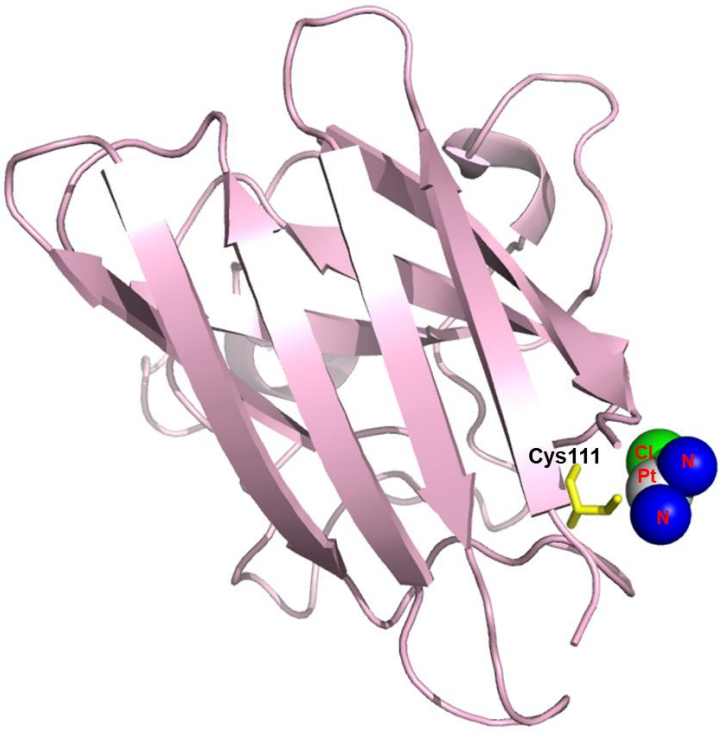

Figure 1.10. **Crystal structure cisPt bound to a protein**. Crystal structure of human superoxide dismutase (hSOD) subunit with cisPt coordinated to its cysteine residue (PDB code 3RE0) [63]. The cisPt coordinates with hSOD through the sulfur atom of Cys111. Cysteine is represented in yellow sticks, whereas Pt and ligands are represented with colored spheres.

1.4 Cellular resistance and toxicity of cisPt; development of cisPt analogues

1.4.1 Toxicity and low selectivity of platinum-based cancer agents

Despite cisPt being used to treat a variety of cancer types, its clinical use may be limited by adverse side effects [69-71]. One of the major side effects of cisPt is nephrotoxicity, which results from cisPt being toxic to cells in several parts of the kidney [69]. CisPt nephrotoxicity includes serious acute kidney injury (AKI), which affects 20–30% of patients [72]. Nephrotoxicity affects cells in the distal convoluted tubules and collecting ducts. CisPt accumulates in the kidney

and causes injury to normal renal epithelial cells, leading to unwanted cell death [72]. Since the effectiveness of cisPt is dose dependent, it is desirable to maximize its dosage for maximal efficacy. However, the effect of nephrotoxicity is also dependent on the dosage and the frequency at which the compound is administered to the patient [72]. Therefore, due to this risk of toxicity, the dosage has to be limited in order to avoid causing renal cell injury [70].

CisPt causes cell death either through apoptosis or necrosis. Apoptosis is programmed cell death, which is induced by cytotoxic drugs such as cisPt [73, 70]. Necrosis is cell death that is caused by damage or injury to the cells [74]. It has been observed that low concentrations (10–100 μM) of cisPt induce apoptosis [70], whereas higher concentrations of cisPt (200–800 μM) lead to necrosis [70, 72, 75]. Nephrotoxins, including cisPt at high concentrations, cause injuries to renal tabular cells, which is characterized by swelling and rupturing [76]. This injury ultimately leads to cell death and activation of an inflammatory response [70, 72, 75-76]. To reduce the nephrotoxic effects of cisPt, the drug is sometimes administered clinically followed by thiol-containing compounds shortly after to react and inactivate excess cisPt in the cells [70, 77]. Such sulfur-containing compounds include methimazole, which reduces nephrotoxicity without reducing the efficacy of cisPt [70, 78].

CisPt can cause other forms of toxicity that are associated a high cellular concentration of the drug. Ototoxicity, which is a form of toxicity that leads to hearing loss, is a side effect of many drugs [10, 79]. High dosages of cisPt induce formation of reactive oxygen species (ROS) in the cochlea cells [10, 79]. The ROS further cause inflammation of the cochlea cells, which ultimately leads to ototoxicity. CisPt has also been implicated in hepatoxicity, which is an effect on the liver [80]. Through a process enhanced by cytochrome P450 2E1, cisPt induces increased levels of ROS and oxidative stress, leading to hepatoxicity [80]. Other forms of cisPt toxicities and side effects that have been noted include nausea, vomiting, hair loss, diarrhea, and cardiotoxicity, among others [10].

1.4.2 Cellular resistance to cisPt

The use of cisPt as a clinical anticancer drug is also limited by cellular resistance [69-71]. Resistance occurs when cancer cells do not undergo apoptosis with the clinically relevant drug dose [71]. There are several factors that lead to cellular resistance, including reduced drug accumulation, inactivation of the drug, and increased DNA repair by the cell [71].

Cancer cells with reduced drug accumulation of cisPt by 20–72% have significant resistance to the compound [81]. There are two main causes of reduced cisPt concentrations in the cell: (1) increased drug efflux from the cell, and (2) inhibition or reduced drug uptake [71]. One or both mechanisms may contribute to resistance [71]. Reduced drug uptake may occur due to a defect in the cell's permeability during passive diffusion or due to aberrant proteins that regulate facilitated transport of cisPt [71]. Development of cisPt resistance due to increased drug efflux is mostly caused by exporter proteins. Multidrug resistance-associated proteins (MRP), found on cellular membranes, have been shown to be upregulated in cancer cells, and have been associated with cellular efflux of various drugs [82]. A member of this protein family called MRP2 is highly abundant in resistant tumor cells, with its upregulation being linked to cisPt resistance [83]. Other proteins that have been linked to cisPt efflux include two copper-transporting Ptype ATPases, ATP7A and ATP7B, which are upregulated in cisPt resistant cancer cells [84-85]. Transfection of ATP7B into tumor cells induces a nine-fold cisPt resistance due to increased drug efflux [85].

CisPt is inactivated when it reacts with certain cytoplasmic nucleophilic metabolites [71], which are usually sulfur-containing. The metabolites that primarily inactivate cisPt include glutathione (GSH) and the cysteine-rich metallothionein [71]. Aquated cisPt is highly reactive towards these metabolites, which then renders it unreactive with DNA. GSH is highly elevated in cancer cells that have chronic exposure to cisPt [71], and therefore can induce resistance by decreasing cisPt levels available for interaction with DNA. Increased levels of GSH in cisPt-resistant cancer cells also upregulates the repair of DNA damaged by cisPt [81]. Metallothionein,

which has sulfur-rich sites for cisPt coordination, has also been demonstrated to have a five-fold higher abundance in cisPt-resistant human tumor cells [86].

Formation and sustaining cisPt-DNA adducts is important for inducing apoptosis. However, the cell can also circumvent cisPt-induced apoptosis by triggering repair of the damaged DNA [71]. Increased rates of removal of the adducts have been shown to attenuate cisPt-induced cytotoxicity [71]. The cell can remove the platinum adducts and repair the damaged DNA through a process known as nucleotide excision repair (NER) [87]. The NER pathway is activated when DNA residues are modified by helix-distorting adducts (**Fig. 1.11**) [87]. First, the adducts are recognized by a sensor complex that includes the XPE protein, followed by recruitment of the excision repair complex [87]. The complex then excises a patch of nucleotides from the region overlapping with the adduct in the damaged DNA (**Fig. 1.11**) [87]. This excision removes approximately 24 nucleotides on the 5′ end of the adduct and three nucleotides on the 3′ side. The remaining complementary single strand is then used as a template for new DNA synthesis (**Fig. 1.11**). After polymerization occurs, the new oligonucleotide is ligated to the rest of the DNA to complete the repair [87]. Studies have shown that aberrant NER proteins or repair pathways lead to sensitivity of a cell to cisPt treatment and that by re-establishing NER, the sensitivity to cisPt returns to original levels [88-89]. Furthermore upregulation of proteins involved in the NER complex lead to an increase in the repair of DNA and cellular resistance to cisPt [89]. Besides NER, a resistant cell can employ other mechanisms to tolerate platinum damage. These include enhancing the DNA replication machinery to replicate past the platinum adducts and allowing the cells to survive high levels of cisPt-mediated DNA modifications [71, 88].

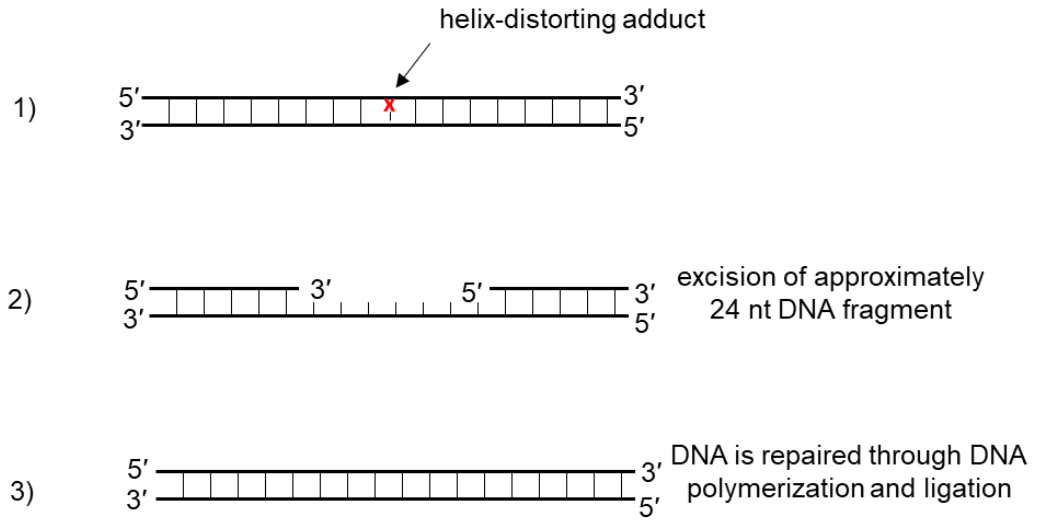

Figure 1.11. **Nucleotide repair mechanism to remove cisPt adducts**. The NER pathway is activated when the DNA helical structure is distorted by adducts (represented by x). Excision of nucleotides removes approximately 24 nucleotides from the 5′ and 3′ ends of the adduct. DNA polymerization then occurs using the complementary single strand as a template. This step is followed by ligation to complete the DNA repair.

1.4.3 Development of cisPt analogues for anticancer therapeutics

Chemoresistance of cancer cells to cisPt and toxic effects to normal cells have led to the development of new platinum-based compounds [90]. Numerous cisPt analogues have been developed to combat the limitations of the parent compound. These analogues exhibit structure-activity relationships that enable them to retain biological activity in cells. More specifically, the active Pt(II) or Pt(IV) complexes are typically coordinated to their ligands in a *cis* geometry and have the general formula *cis*-[PtX_2Z_2] or *cis*-[$PtX_2Y_2Z_2$], in which X is the leaving group ligand, Z is a non-leaving group with at least one N-H moiety, and Y is the axial ligand [91]. Despite these consensus structures, exceptions do exist that violate this structure-activity relationship, and those compounds have been developed using a different approach than for cisPt. Even though thousands of cisPt analogues have been synthesized, only a small number have gone into clinical trials [91]. Carboplatin, oxaliplatin, and nedaplatin are a few examples that have been approved for clinical use worldwide [91].

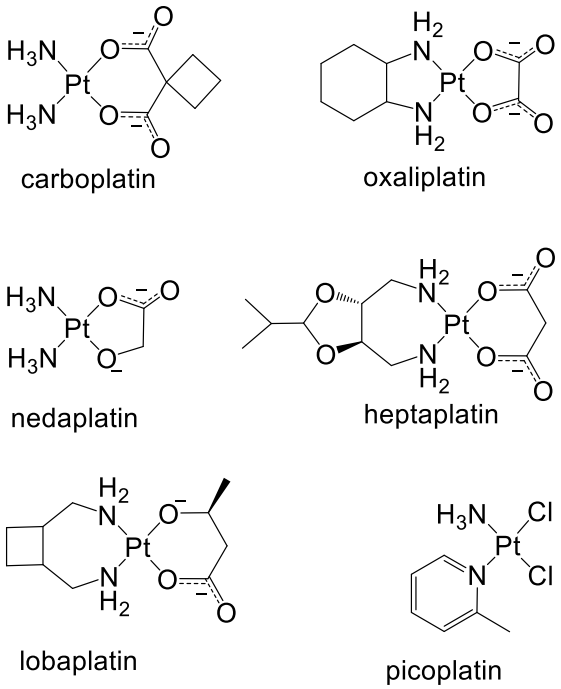

Figure 1.12. **Antitumor platinum-based compounds.** Aside from cisPt, these platinum(II)-based compounds have been clinically used for antitumor targeting either worldwide or in a few regions of the world.

Carboplatin (*cis*-diammine-1,1-cyclobutanedicarboxylate platinum(II)) (**Fig. 1.12**) is a second-generation platinum-based drug with reduced toxic side effects compared to cisPt [33-36]. However, in cancer cells, carboplatin is not as potent as cisPt at similar concentrations [33-36]. The structure of carboplatin consists of a chelating cyclobutanedicarboxylate ligand instead of the two chlorido ligands (in the case of cisPt). The cyclobutanedicarboxylate ligand plays a number of roles such as modulating the rate of aquation and adduct formation, and increasing the solubility of carboplatin, which is important for cell penetration [91]. The chelate ring in the cyclobutanedicarboxylate stabilizes the ligand and slows the reaction rate for ligand exchange with H_2O by two orders of magnitude compared to cisPt [91-92]. The rate of adduct formation with DNA is also 100-fold slower for carboplatin than for cisPt, due to the slower aquation rate [34]. The chemical characteristics of carboplatin have given the compound certain advantages over cisPt such that it can circumvent the toxicity usually caused by high dosage [91]. However, due

to a lower abundance of adducts, carboplatin has a reduced efficacy compared to cisPt, meaning that a much higher dose is required in order to achieve the same effect [16]. Clinically, it has been noted that up to four times as much carboplatin is needed to acquire the same effect as cisPt [16].

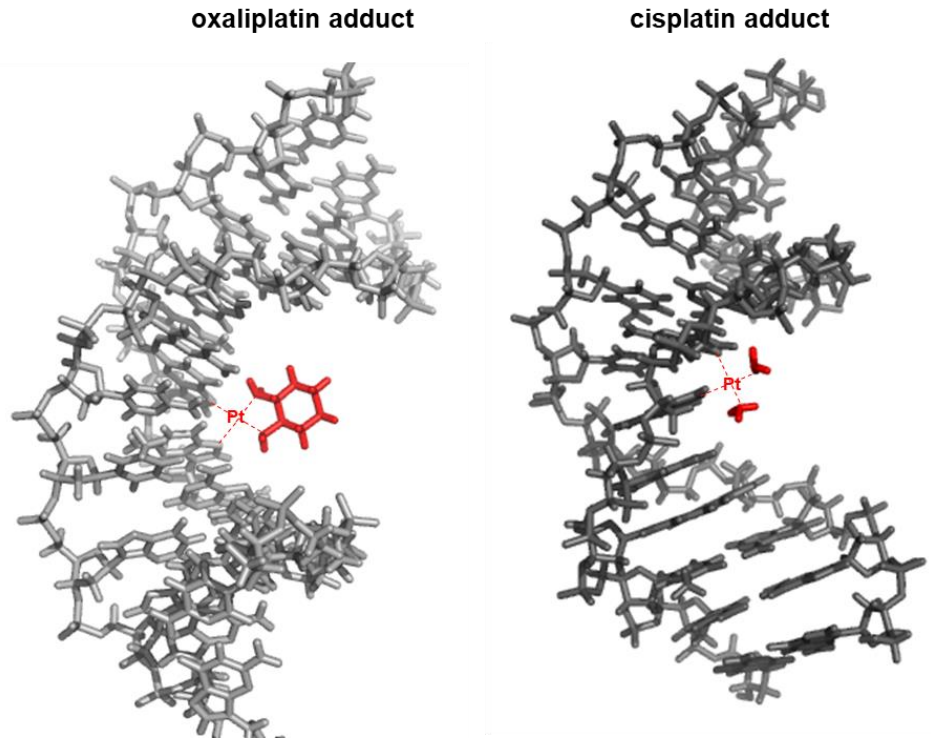

Figure 1.13. **Platinum drugs bound to dGuo residues in the major groove of DNA**. Oxaliplatin has a large DACH ligand that protrudes into the major grove and interferes with DNA replication and transcription machinery (PDB code 1PG9). Compared to oxaliplatin, cisPt forms a smaller adduct that does not efficiently block replication and transcription machinery (PDB code 2NPW).

Oxaliplatin was approved worldwide due to its persistent activity in cisPt-resistant cancers and absence of nephrotoxicity [93]. The non-leaving group ligand of oxaliplatin is a chelated 1,2-diamminocylohexane (DACH) ligand (**Fig. 1.12**). This ligand gives the complex a unique structure-activity relationship that is crucial in averting cellular resistance that challenges utilization of cisPt [91]. As mentioned before, one form of cellular resistance occurs when a cell tolerates the adducts and enables the replication machinery to bypass and read through the platinum adducts [94-95]. Oxaliplatin has been observed to circumvent such resistance, likely because its DACH ligand

protrudes into the major groove of DNA and is more effective at preventing the replication machinery from bypassing the adducts [96, 94] (**Fig. 1.13**). Although oxaliplatin does not exhibit nephrotoxicity, it causes other side effects including neurological toxicity [95]. Oxaliplatin is also not fully effective by itself and normally requires combination therapy with other anticancer agents such as 5-fluorouracil and cisPt [95].

There are several second-generation platinum-based drugs that have received approval in various regions of the world (**Table 1.1**) [93]. Nedaplatin, diammine[hydroxyacetato(2-)-*O,O*] platinum(II), was approved in Japan in 1995 for treatment of lung, oesophageal, and head and neck cancers [93]. It has an added advantage of being more soluble than cisPt as well as having lower nephrotoxicity [97]. Heptaplatin is an approved platinum-based drug used in Korea for treatment of gastric cancer [93]. It also has higher solubility in water and a lower toxicity profile. Lobaplatin, which is used to target chronic myeloid leukemia, has received regional approval in China [93]. Lobaplatin is also in clinical trials in other parts of the world, including the US, South Africa, EU, and Australia, for treatment of breast, ovarian, chronic myeloid leukemia, and lung cancer [93]. The advantage of lobaplatin over cisPt is that its mode of action involves altering the expression of genes that modulate apoptosis, oncogenesis, and cell proliferation [98]. Picoplatin, which entered clinical trials in 1997, has an interesting structural feature that enables aversion of resistance [91]. It has a 2-methylpyridine ring that can tilt by about 102.7°, which results in positioning of the methyl group over the square plane [19, 91] This structural positioning causes steric hindrance to thiol-containing deactivating agents such as glutathione. The tilt can therefore block these metabolites from effectively reacting with the complex. The blocking of the thiol-containing agents is important for circumventing inactivation, so that the platinum complex can form adducts with DNA [19, 91].

Table 1.1. Clinically approved cancer platinum-based drugs [93]

drug	year of approval	country approved	types of cancer treated
carboplatin	1989	worldwide	ovarian, brain, head, neck, cervical, testicular, breast
nedaplatin	1995	Japan	oesophageal, head, neck, lung
oxaliplatin	1996	worldwide	colon
heptaplatin	1999	Korea	advanced gastric
lobaplatin	2010	China	small cell lung, breast, chronic myeloid leukemia

1.4.4 Platinum(IV)-based compounds as antitumor agents

In addition to Pt(II)-based complexes, there are also Pt(IV)-based compounds that exhibit anticancer activity [99]. The Pt(IV) complexes are generally inert and only act as prodrugs that can exert their therapeutic activity after reduction to the reactive Pt(II) complex form [19, 99]. These complexes have the ability to be administered orally in their inactive form, and are converted into the reactive form once in the cell, with potentially high potent activity and low toxicity [99].

As shown in **Fig. 1.14**, Pt(IV) complexes have an octahedral geometry with two *cis* non-leaving ligands (usually ammine ligands), two *cis* leaving groups, and two axial ligands [10, 19]. The Pt(IV) complex can be converted to Pt(II), which by extension leads to the loss of the axial ligands [19]. There are a number of Pt(IV) complexes that have gone into clinical trials for antitumor therapy. Iproplatin has a structure with ligands (including two axial OH groups) that play a role in its high solubility, broad range of activity, and lower toxicity in animal studies (**Fig. 1.15**) [100]. However, iproplatin was dropped in clinical trials after it did not show clear advantages over carboplatin [100]. Tetraplatin (**Fig. 1.15**) is another Pt(IV)-based compound that exhibits advantages over cisPt in animal studies in that it is less nephrotoxic and circumvents cellular resistance. However, it was also abandoned in clinical trials due to severe neurotoxicity in humans [100]. Satraplatin (**Fig. 1.15**) has seen more success in phase 3 clinical trials for hormone-

refractory prostate cancer due to its reduced nephrotoxicity and neurotoxicity [19]. Satraplatin was designed to be an inactive prodrug that can be administered orally, giving it an advantage over the intravenously administered cisPt [19]. Its stability as a prodrug enables it to be distributed in blood plasma in the inactive form before being converted into the active form once inside the cells. It was observed that with oral administration of satraplatin, its cellular potency was comparable to intravenously administered cisPt and carboplatin [100].

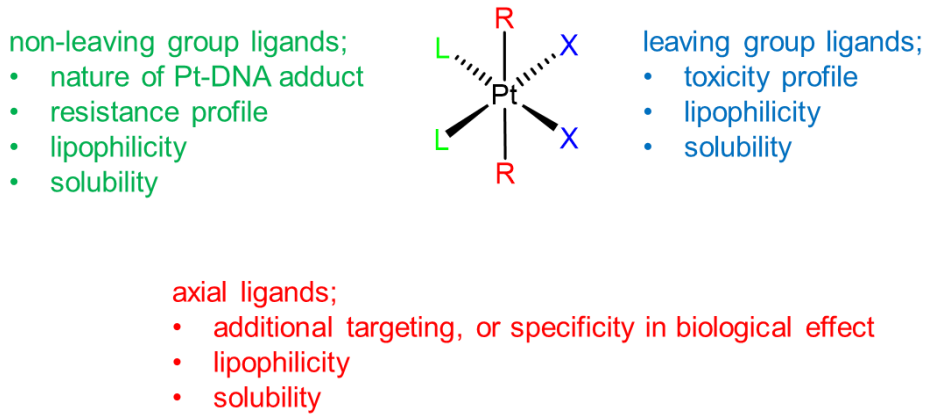

Figure 1.14. **Ligands of Pt(IV)-based complexes and their roles.** Pt(IV)-based antitumor agents have three types of ligands, including leaving group, non-leaving group, and axial ligands. These ligands play different roles in the activity of the compounds towards tumor cells as indicated.

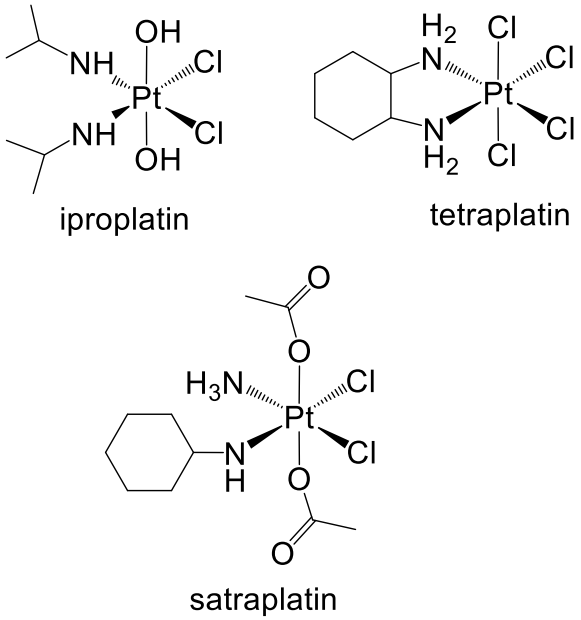

Figure 1.15. **Structures of Pt(IV)-based anticancer agents**. Iproplatin, tetraplatin, and satraplatin are some of the Pt(IV)-based compounds that are or have been used in clinical trials.

In summary, the currently approved antitumor platinum-based drugs have shown significant success in cancer therapies and some analogues have advantages over cisPt in terms of reduced toxic side effects and the ability to circumvent resistance. However, there are still challenges with cancer therapies involving platinum compounds, ranging from DNA repair and off-target inactivation to various forms of toxicity. The reduced toxicity of the second-generation platinum-based drugs is overshadowed by their reduced effectiveness in cells. It is therefore important to develop new cisPt analogues that have alternative biomolecular targets, altered reactivity preferences, and a balance between high efficacy and reduced toxicity.

1.5 Thesis objectives

CisPt exerts its anticancer activity by preferentially coordinating to dGuo residues within DNA [38]. The dGuo adducts that are formed alter the DNA structure and contribute to inhibition of functions such as replication and transcription that ultimately lead to cancer cell death [1, 11]. Nevertheless, cisPt has a number of drawbacks such as cellular resistance that reduce its efficacy [71]. Analogues of cisPt that exhibit altered reactivity with other cellular targets such as RNA or form non-canonical adducts with alternative DNA residues could be useful in circumventing resistance by causing irreparable damage and triggering apoptosis [29, 55].

Aim 1: Synthesize and characterize amino acid-linked platinum(II) compounds

In this thesis work, platinum-based compounds with diversified structures, ligand sizes, and charge distributions were synthesized by coordinating amino acids with platinum. The thesis hypothesis is that modification of cisPt with amino acid ligands of varying sizes and charges will alter the reaction kinetics and nucleoside binding preferences. The amino acids linked to platinum(II) provide an array of compounds (AAPt) with diverse ligands and chemical characteristics. The platinum(II) compounds generated with their corresponding amino acid ligands are AlaPt (alanine), OrnPt (ornithine), and ArgPt (arginine). The amino acid-linked compounds that were successfully synthesized and used for further studies are shown in **Fig.**

1.16. The compounds were characterized by using NMR spectroscopy (^{1}H, ^{13}C, ^{195}Pt), mass spectrometry, and X-ray crystallography.

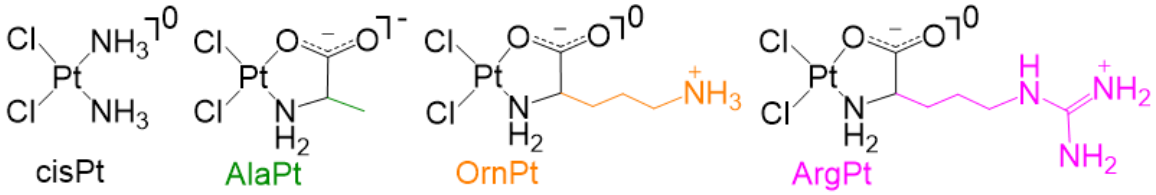

Figure 1.16. The structures of cisPt and amino acid-linked platinum(II) compounds, AlaPt, OrnPt, and ArgPt, are shown.

Aim 2: Characterize non-canonical adducts formed by amino acid-linked platinum(II) compounds with DNA and RNA residues

When cisPt coordinates with DNA, it predominantly platinates the N7 position of dGuo [101-102]. Platinum-based compounds may form intrastrand or interstrand adducts, depending on whether they coordinate to the same strand or two strands, respectively [18, 41]. Adducts can also be defined as monofunctional, bifunctional, or doubly platinated, depending on the platinum:nucleoside ratio (*i.e.*, 1:1, 1:2, or 2:1, respectively). The adduct types also vary, depending on the site of platination on the nucleobase (*e.g.*, N1, N3, or N7). We sought to determine the binding site preferences and to characterize the types of adducts formed by amino acid-linked platinum(II) compounds in DNA and RNA residues. The structures and corresponding chemical properties of various amino acid-linked platinum(II) compounds may alter the preferred sites of reactivity versus those targeted by cisPt. In this work, mass spectrometry was used to determine the composition and type (*e.g.*, mono- or bifunctional) of adducts formed by the platinum-based compounds, and ^{1}H-NMR spectroscopy was used for characterization of the platination sites on the nucleoside. In collaboration with Dr. M. T. Rodgers' laboratory, we also sought to evaluate the effect of platination on the relative glycosidic bond strengths of these non-canonical adducts using tandem mass spectrometry.

Aim 3: Determine reaction kinetics of amino acid-linked platinum(II) compounds with DNA/RNA nucleosides and oligonucleotides

The nucleophilicity and accessibly of the N7 position in dGuo residues of DNA is thought to be favorable for cisPt adduct formation [102]. Less is known about reactivity of other positions such as N7, N3, or N1 of dAdo. The reaction kinetics of three amino acid-linked platinum compounds (AlaPt, OrnPt, and ArgPt) were examined. The rate constants obtained were used to determine how the chemical structures and physical properties of the functional groups of the amino acid ligands relate to reactivity the platinum-based complexes with DNA/RNA nucleosides and oligonucleotides. The DNA/RNA nucleosides or oligonucleotides were reacted with a 50-fold excess of AAPt compound for pseudo-first-order reaction conditions. An HPLC equipped with a C-18 column was utilized to quantify levels of reacted nucleoside/oligonucleotide and the data were analyzed to give the pseudo-first-order kinetics of the platinum compounds. The peak area of unreacted nucleoside/oligonucleotide was monitored over time and the diminishing ratio to the product peaks was determined. The data were fit using an exponential equation assuming pseudo-first-order kinetics. The reaction rate constants obtained from reactions in the nucleoside and oligonucleotide levels were compared in order to understand the reactivity preferences and selectivities of the compounds.

Aim 4: Determine potency of amino acid-linked platinum(II) compounds and quantify their accumulation in cancer and normal cells

At the cellular level, it is important to develop analogues that are more selective than cisPt and can strike a balance between selective potency in cancer cells and reduced toxicity in normal cells. An understanding of the cellular activity of amino acid-linked platinum(II) compounds is important for determining which structural features of the compounds are critical for achieving selective potency and accumulation in cancer cells. The potency of AAPt in human cancer and normal cell lines was determined using the MTT (3-(4,5-dimethylthiaxol-2-yl)-2,5-diphenyltetrazolium bromide) assay. In this assay, IC_{50} values were obtained following treatment

of cell lines with varying concentrations of AAPt compounds (and cisPt for comparison). To determine the cellular abundance of platinum-based compounds, the cell lines were treated with AAPt compounds and cisPt followed by chemical digestion. The abundance of platinum in each sample was then quantified by using ICP-MS. This research will drive the development of new compounds that are not only effective in cancer cells, but can discriminate against normal cells.

CHAPTER 2

AMINO ACID-LINKED PLATINUM(II) COMPOUNDS: SYNTHESIS, CHARACTERIZATION, AND METHODS TO INVESTIGATE THEIR KINETICS, ADDUCTS, AND CELLULAR ACTIVITIES[‡]

[‡]Adapted from Kimutai B, He CC, Roberts A, Jones ML, Bao X, Jiang J, Yang Z, Rodgers MT, Chow CS (2019) J Biol Inorg Chem 24:985-997.

2.1 Abstract

The work in this thesis focuses on synthesis, characterization, adduct formation, kinetics, and biological activity of cisplatin (cisPt) analogues. CisPt analogues can be generated with simple ligand modifications. Small modifications may alter the reactivity preferences of the analogues towards residues that are not preferentially targeted by cisPt. In this work, amino acids are used as ligands and coordinated to a platinum metal center to generate amino acid-linked platinum(II) (AAPt) compounds. The amino acids provide a range of ligands with varied sizes and charge distributions. The AAPt compounds generated may in turn have diversified reactivity profiles compared to cisPt. AAPt compounds that are derivatives of alanine, ornithine, and arginine were synthesized. These compounds are referred to as AlaPt, OrnPt, and ArgPt, respectively. The compounds were characterized using different methods, including ^{1}H-, ^{13}C-, and ^{195}Pt-NMR spectroscopy, mass spectrometry, and X-ray crystallography. A variety of techniques described in this chapter were also used to determine the kinetics of adduct formation, adduct structures, and biological activities of the synthesized compounds. Non-canonical adducts formed by AAPt compounds with nucleosides/oligonucleotides were characterized using mass spectrometry and NMR spectroscopy. The reaction kinetics were determined using HPLC analysis. The influence of AAPt compounds on glycosidic bond stability were investigated using tandem mass spectrometry and survival yield analysis (in collaboration with Dr. M. T. Rodgers' lab). The potency of the compounds in human cell lines was determined using MTT (3-(4,5-

dimethylthiaxol-2-yl)-2,5-diphenyltetrazolium bromide) assays, and their cellular accumulation was quantified using inductively coupled plasma mass spectrometry (ICP-MS).

2.2 Introduction

2.2.1 Application of amino acids as ligands of cisplatin analogues

Despite the application of cisPt in treatment of a variety of cancer types, its clinical use is limited by cellular resistance and adverse side effects emanating from toxicity to normal cells [69-71]. Furthermore, DNA repair and reduced accumulation of cisPt allow cancer cells to continue propagating despite drug treatment [71]. There has been research and development of numerous cisPt analogues aimed at circumventing the limitations of cisPt. However, with thousands of cisPt analogues having been synthesized, only a small number have made it to clinical trials. The few analogues that have been approved for clinical use worldwide include carboplatin, oxaliplatin, and nedaplatin [91]. Therefore, there is still need to develop platinum-based compounds that not only have a balance between potency in cancer cells and toxicity in normal cells, but also have alternative biological targets from those targeted by cisPt.

Amino acids are a great source of ligands with diversified sizes and charge distributions. Based on the chemical and physical properties of their side chains, naturally occurring amino acids can be categorized into groups such as basic, acidic, hydrophobic, and polar. Amino acids with basic side chains include lysine and arginine, whereas the acidic group includes aspartate and glutamate. The nonpolar group includes alanine, leucine, isoleucine, valine, and phenylalanine. Amino acids with polar side chains include serine and cysteine. These amino acids can be linked with a platinum metal center to generate amino acid-linked platinum(II) (AAPt) compounds [103-106]. The diversity of the side chain functional groups together with the contribution of backbone atom metal coordination means that the AAPt compounds can potentially have a wider range of reactivity and targets, which could give them advantages over cisPt. The amino acids are also inexpensive and readily available starting materials, which not only reduces the cost of synthesis but also the number of steps in the synthetic protocols.

There have been a number of previous reports on the synthesis and characterization of AAPt compounds, either with naturally occurring or modified amino acid derivatives [103-104, 107-112]. In these studies, platinum-based derivatives of histidine, serine, methionine, arginine, lysine, and ornithine were synthesized and characterized [103-104, 107-112]. The techniques used for characterization of these platinum-based compounds include ^{195}Pt-NMR spectroscopy, X-ray crystallography, and mass spectrometry. Previous reports focused mainly on the synthesis and characterization of the compounds, but not on the biological applications [107-108, 110, 113]. The platinum(II) metal center was observed to coordinate with the soft bases (nitrogen and sulfur atoms) as well as hard bases (oxygen atoms) of the amino acids [103-104, 107, 110-111]. The general structures of the Pt(II) complexes consist of one chelating amino acid and two chlorine atoms coordinating with the metal center [103-104, 107, 110-111]. Chelation of the amino acid through the backbone nitrogen and oxygen atoms with the Pt(II) center leads to a five-membered ring (N,O binding mode) (**Fig. 2.1**) [103-104, 107, 110-111]. The platinum metal center may also coordinate with the side chain, especially if there is a soft base such as a sulfur atom to form (N,S) type of binding (**Fig. 2.1**) [109]. The presence of an amine in the side chain (*e.g.,* lysine and ornithine) may lead to formation of (N,N) type structures, in which the platinum center coordinates to the nitrogen atoms in the backbone and side chain (**Fig. 2.1**). Even though the (N,N) type structures have not been observed in crystal structures of ornithine and lysine derivatives, they cannot be ruled out. Crystallization conditions may favor only the (N,O) type structures [107].

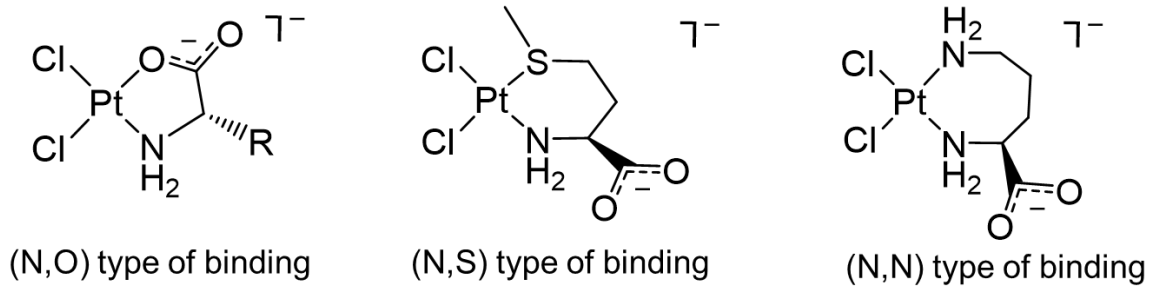

Figure 2.1. Possible structures of AAPt compounds. The platinum(II) metal center can chelate with the amino acid through the backbone or side-chain atoms.

There have been a few applications of AAPt compounds in biological studies. Cellular activity and toxicity of lysine, ornithine, histidine, and methionine derivatives in cancer cell lines were found to be generally lower than that of cisPt [104, 109, 103, 111-112]. Biological applications of the compounds have been minimal and only focused on a few different cell lines and DNA as the biological target [104, 109, 112]. Further studies on the interactions of AAPt compounds with alternative biological targets, as well as comprehensive cellular studies with cisPt-resistant cell lines, are necessary. Previous studies in our lab showed that several AAPt compounds (ornithine and arginine derivatives) interact and form adducts with RNA [106]. There is still a need to understand how the chemical structures and physical properties of the functional groups of the AAPt complexes relate to their reactivity and target preference. Understanding the role of the ligands in target preferences will be important for the rational development of novel compounds that have improved cellular activities and effectiveness.

In this chapter, the synthesis and characterization of several AAPt compounds is described. The derivatives of alanine, ornithine, and arginine (AlaPt, OrnPt, and ArgPt) were successfully synthesized and characterized. These compounds were used in subsequent work to study their reactivities with nucleic acids and also to screen their cellular potency in cancer cells. The synthesized compounds were characterized using ^{1}H-,^{13}C-, and ^{195}Pt-NMR spectroscopy, mass spectrometry, and X-ray crystallography. It was hypothesized that the structures of the synthesized AAPt compounds would have the (N,O) type of binding structures, in which the

platinum(II) center coordinates with the backbone nitrogen and oxygen atoms of the amino acid (**Fig. 2.2**).

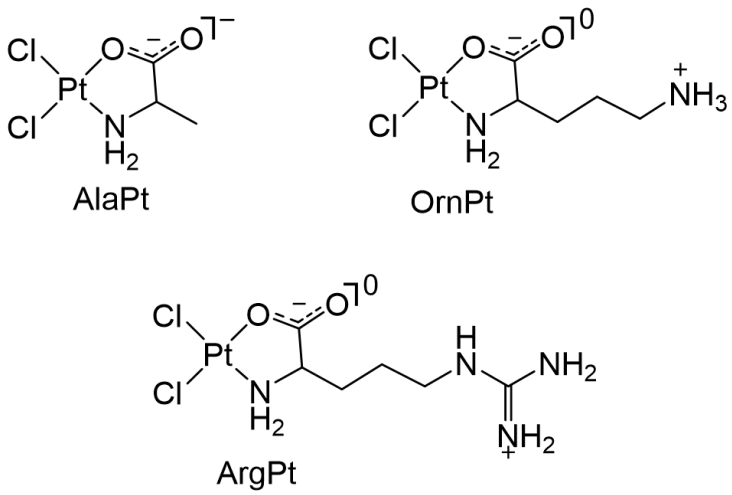

Figure 2.2. The structures of amino acid-linked platinum(II) compounds. The AAPt compounds consist of a platinum(II) metal center coordinated to a chelating amino acid and two chlorido ligands.

2.2.2 Formation and characterization of non-canonical AAPt-nucleic acids adducts

The AAPt compounds form adducts by coordinating with dAdo/Ado residues of DNA and RNA [105-106]. In this thesis work, the adducts formed by AlaPt, OrnPt, and ArgPt with nucleosides and oligonucleotides were characterized to determine the adduct types and sites of platination. AAPt (or cisPt) compounds were first activated to form monoaquated species, which were then reacted with target nucleosides/oligonucleotides. The reactions could result in formation of different types of products that vary in composition, platination sites (N1, N3, or N7), and geometry. The reactions and products formed were monitored using HPLC. The fractions corresponding to adducts were isolated and characterized by using mass spectrometry and NMR spectroscopy.

2.2.3 Kinetics of AAPt with DNA/RNA nucleosides and oligonucleotides

Modifications to cisPt may alter its reactivity and direct the compound towards alternative biological targets. Different behaviors of the platinum-based compounds can be achieved by modifying the ligands to favor different interactions such as hydrogen bonding, charge-charge interactions, and steric hindrance, among others. For example, an analogue of cisPt with a heteroaromatic ligand, 4,4′-dipyrazolylmethane, shows a reactivity preference for the dAdo/dThd-rich regions of DNA rather than the dGuo-rich regions [114]. In this thesis work, the reaction kinetics of three AAPt compounds (AlaPt, OrnPt, and ArgPt) were examined to determine how the chemical structures and physical properties of the functional groups of the amino acids relate to reactivity and nucleoside preferences. The hypothesis is that modification of cisPt with amino acid ligands of varying sizes and charges will alter the reaction kinetics and nucleic acid target preferences. Influence of the oligonucleotide local environment was also investigated since the nucleotides surrounding the target nucleotide may modulate the binding kinetics of cisPt and AAPt and lead to different platination rates and profiles. Timecourse reactions of the AAPt compounds with nucleosides/oligonucleosides were monitored by using HPLC equipped with a C18 column. Pseudo-first-order kinetics were used to compare the preferences of three AAPt compounds (and cisPt) with purine nucleosides and also to understand the impact of local nucleic acid environment on their reactivity with oligonucleotides.

2.2.4 Impact of AAPt compounds on glycosidic bond stability of adducts

Platination of nucleic acids may have unique influences on the chemical properties of the nucleosides such as bond strengths. For example, modifications such as alkylation or protonation of DNA residues have previously been observed to weaken the glycosidic bond and accelerate the process of depurination [115-118]. Thus, hydrolytic instability of purine glycosidic bonds may impact nucleoside integrity, particularly under varying pH and ionic strength conditions and modification states [116, 119-121]. Stability of the glycosidic bond may also be influenced differentially by platination at varying sites on the nucleobase. In this thesis work, the impact of

AlaPt and OrnPt adducts on relative glycosidic bond strengths of adducts is investigated by employing energy-resolved collision-induced dissociation (ER-CID) tandem mass spectrometry and survival yield analysis [116, 122-125].

2.2.5 Potency and accumulation of AAPt compounds in human cancer and normal cells

Application of cisPt in cancer therapy has had major drawbacks due to resistance and adverse side effects, including nephrotoxicity [69-71]. Clinical analogues of cisPt such as carboplatin have low potency, meaning that a higher dose is required to achieve the same effectiveness as cisplatin [16]. Development of new platinum-based compounds will focus on not only maintaining the efficacy of cisPt, but also having reduced side effects and selectivity for cancer cells. Based on Lipinski rules [126], the AAPt compounds could provide another class of metal-based compounds with oral drug-like features. The anticancer potency of AAPt compounds can be evaluated by determining the IC_{50} values in several human cancer cell lines using the 3-(4,5-dimethylthiazol-2-yl)-2,5-diphenyltetrazolium bromide (MTT) assay [127]. This assay utilizes viable cells to convert MTT into a purple-colored formazan. The NAD(P)H-dependent cellular oxidoreductase enzymes in viable cells convert MTT into insoluble purple formazan. The formazan is dissolved by solvents such as DMSO and the optical density (OD) measurements of the resulting solutions are taken using a uv-visible spectrophotometer. The OD measurements are used to determine the percentage of viable cells present following exposure to a given concentration of the cytotoxic compound.

Accumulation of platinum-based compounds inside cells drives the pharmacological impact of the anticancer compound. Low accumulation of cisplatin in cells leads to reduced DNA damage and could potentially stimulate resistance rather than apoptosis [71]. The cellular accumulation of AAPt compounds in comparison to cisplatin in both cancer and normal prostate cells was investigated in this work. Cells were treated with either AAPt compounds or cisPt followed by quantitative measurements of cellular platinum concentrations with inductively coupled plasma mass spectrometry (ICP-MS).

2.3 Materials

2.3.1 Chemicals

Potassium tetrachloroplatinate(II), L-alanine, trimethylsilyl propionate (TSP), 3-(4,5-dimethylthiazol-2-yl)-2,5-diphenyltetrazolium bromide (MTT), 3-hydroxypicolinic acid (3-HPA), and HCl were purchased from Sigma-Aldrich (St. Louis, MO). L-Ornithine, L-arginine, and *cis*-diamminedichloridoplatinum(II) were from Alfa Aesar (Haverhill, MA). Deuterium oxide (D_2O), chloroform-D, and acetonitrile-D_3 were from Cambridge Isotope Laboratories (Tewksbury, MA). Silver nitrate, acetonitrile, ammonium acetate, ethanol, methanol, dimethylsulfoxide, and nitric acid (trace metal grade) were obtained from Fisher Chemical (Hampton, NH). Poly(Ado) RNA was from Pharmacia LKB Biotechnology (Uppsala, Sweden). Sodium phosphate, monobasic and dibasic, were obtained from EMD Millipore (Kankakee, IL). All amino acid-linked platinum(II) compounds were synthesized in the lab (described in **Section 2.4**).

All nucleosides (deoxyguanosine (dGuo), guanosine (Guo), deoxyadenosine (dAdo), and adenosine (Ado)) were purchased from Sigma-Aldrich (St. Louis, MO). Oligonucleotide strands, 5′-d(TTATT)-3′ and 5′-UUAUU-3′, were purchased from Integrated DNA Technologies (Coralville, IA).

2.3.2 Human cell lines and cell culture supplies

The cancer cell lines HeLa (cervical), H1299 (non-small cell lung), MDA-MB-231 (breast), and MDA-MB-453 (breast) [128-132] were obtained from Dr. Young-Hoon Ahn's lab, Wayne State University. DU145 (prostate cancer) [133] was received from Dr. K. V. Honn's lab, Wayne State University. RWPE-1 (normal prostate cell line) [134] was acquired from Dr. Zhihui Qin's lab, Wayne State University. Dulbecco's modified eagle medium (DMEM), keratinocyte serum free medium (K-SFM), human recombinant epidermal growth factor 1-53 (EGF 1-53), bovine pituitary extract (BPE), phosphate buffered saline (PBS), and trypsin-EDTA (0.25%) were purchased from Gibco-ThermoFisher Scientific (Waltham, MA). Transparent flat-bottom 96-well plates were

acquired from USA Scientific (Ocala, FL). Cell culture dishes (60 x 15 mm and 100 x 20 mm) were purchased from Sigma Aldrich (St. Louis, MO).

2.3.3 Instrumentation

Proton and ^{13}C-NMR spectra of the AAPt compounds were recorded on an Agilent MR-400 MHz spectrometer in the Wayne State University Lumigen Instrument Center (LIC). The ^{195}Pt-NMR spectrum of the AlaPt compound was recorded on a Varian VNMRS-500 MHz spectrometer in the LIC. Absorption of nucleosides and oligonucleosides were measured on Beckman Coulter DU730 UV/Vis spectrophotometer (Brea, CA). The ^{1}H and ^{13}C NMR spectra of the AAPt-nucleoside adducts, and two-dimensional heteronuclear single quantum coherence (HSQC) spectroscopy of OrnPt-nucleoside adducts were recorded on a Bruker Avance 700 MHz spectrometer equipped with a TXI cryoprobe in the LIC. The MS analyses were performed by Dr. C. C. He on a 7T Fourier transform ion cyclotron mass spectrometer (FT-ICR MS, solariX, Bruker Daltonics, Billerica, MA) in Dr. M. T. Rodgers' laboratory. X-ray crystallography was performed by Dr. P. Martin on an X-ray single-crystal diffractometer (Bruker X8 APEX) in the LIC. MALDI-MS characterization was performed on a Bruker UltrafleXtreme MALDI-TOF/TOF mass spectrometer (Billerica, MA) in the LIC. HPLC analysis was carried out on a Waters 600 LC with a 717plus autosampler (Milford, MA) fitted with a Sigma-Aldrich Supelco Discovery C18 column (5 μm particle diameter; 4.6 mm × 250 mm, St. Louis, MO) and UV detector set at 254 nm. Platinum-195 quantification was performed on an Agilent 7700X ICP-MS equipped with an ASX-500 series autosampler and Agilent MassHunter software (Santa Clara, CA) (LIC). Orbitrap-MS spectra were obtained on a ThermoScientific LTQ Orbitrap XL (Waltham, MA) (LIC). LC-MS characterization was performed on a Shimadzu 8040 triple quadrupole (Columbia, MD) equipped with ESI (LIC) and a Waters C18 Acquity HSS T3 100 mm column (Milford, MA). Energy-resolved collision-induced dissociation (ER-CID) and survival yield experiments were performed by Dr. C. C. He on a Bruker Daltonics amaZon ETD quadrupole ion trap mass spectrometer (Billerica, MA) in Dr. M. T. Rodgers' laboratory. ER-CID data processing was done by C. C. He using Bruker

Daltonics DataAnalysis 4.0 (Billerica, MA). Survival yield data analysis was performed by Dr. C. C. He using Systat Software SigmaPlot 10.0 (San Jose, CA) and custom software developed in Dr. M. T. Rodgers' laboratory. Optical density measurements for cytotoxicity experiments were performed using a BioTek synergy H1 hybrid reader (Winooski, VT) in Dr. Y. H. Ahn's laboratory.

2.4 Methods

2.4.1 Synthesis and characterization of AlaPt

Synthesis of AlaPt was carried out following a previously described procedure, but with some modifications to improve yield and minimize undesired side reactions [104]. First, 0.17 mmoles (70 mg) of K_2PtCl_4 and five equivalents of L-alanine (75 mg) were dissolved in 2 mL of double-distilled water (ddH_2O) and heated at 50 °C overnight on a Fisher thermoshaker at 950 rpm. The crude product was filtered and vacuum dried for approximately 12 h. Next, 3.0 mL of ice cold ddH_2O was added to the resulting solid, and the solution was mixed by vortexing for one minute, followed by centrifugation at 14,000 rpm for 10 min. The supernatant was removed and discarded. To the pellet was added 3.0 mL of cold 95% ethanol, followed by vortexing and centrifugation at 14,000 rpm for 8 min and removal of the supernatant; this procedure was repeated three times. The solid precipitate was then dried under vacuum overnight. To the dried sample was added 250 µL of 100 mM NaOH, followed by vortexing and filtering under centrifugation (Millipore 10 kDa centrifugal filter) at 14,000 rpm for 10 min to remove high molecular weight aggregates. The filtrate was collected and vacuum dried to obtain a light-yellow product. The final product, obtained in 47% yield (28 mg), was characterized by ^{1}H-NMR spectroscopy, ^{13}C-NMR, ^{195}Pt-NMR, and high-resolution mass spectrometry. Melting point, 249-251 °C; δ/ppm (^{1}H-NMR, D_2O, 400 MHz), 3.50 (1 H, q, J=7.1 Hz, =C<u>H</u>CH_3), 1.28 (3 H, d, J=7.0 Hz, -C<u>H</u>$_3$); δ/ppm (^{13}C-NMR, D_2O, 400 MHz) 193 ((-<u>C</u>OO)CH=), 57 (=<u>C</u>HCH_3), 20 (=CH<u>C</u>H$_3$); δ/ppm (^{195}Pt-NMR, D_2O, 500 MHz, -1639); m/z (electrospray ionization mass spectrometry (ESI-MS)) 352.943 Da/e $[M]^-$; calculated exact mass 352.942 Da $[M]^-$; chemical formula $PtC_3H_6Cl_2NO_2$ ($[M]^-$, at neutral pH).

The synthesized AlaPt was characterized by using ^{1}H-, ^{13}C-, and ^{195}Pt-NMR spectroscopy. The ^{1}H-NMR spectrum of AlaPt was analyzed in comparison to the ^{1}H-NMR spectrum of L-alanine (**Fig. 2.7**). The H_{α} proton peak of alanine has a chemical shift of 3.61 ppm, whereas the corresponding H_{α} peak for AlaPt is shifted upfield by 0.11 ppm (δ 3.50 ppm). The H_{β} proton peak of L-alanine has a chemical shift of 1.31 ppm, whereas the corresponding H_{β} peak for AlaPt is shifted slightly upfield by 0.03 ppm (δ 1.28 ppm). The changes in chemical shifts are consistent with coordination of the amino acid to the platinum center.

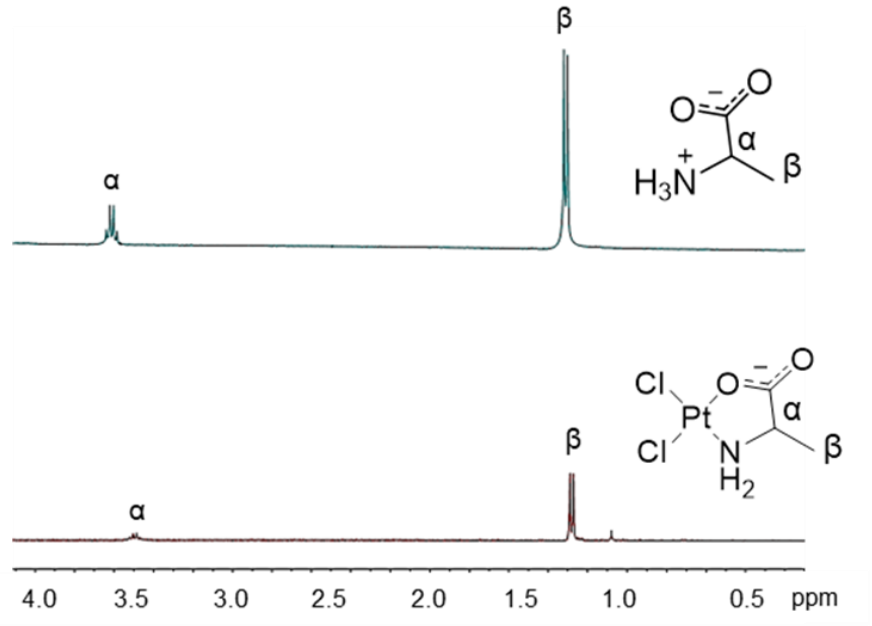

Figure 2.7. **The ^{1}H-NMR spectra of L-alanine (top) and AlaPt (bottom).** For L-alanine; δ/ppm (^{1}H-NMR, D_2O, 400 MHz), 3.61 (1 H, q, J=7.7 Hz, =C<u>H</u>CH$_3$), 1.31 (3 H, d, J=7.6 Hz, -C<u>H</u>$_3$). For AlaPt; δ/ppm (^{1}H-NMR, D_2O, 400 MHz), 3.50 (1 H, q, J=7.1 Hz, =C<u>H</u>CH$_3$), 1.28 (3 H, d, J=7.0 Hz, -C<u>H</u>$_3$).

In the ^{13}C-NMR spectrum, the carboxylate carbon peak for alanine has a chemical shift of 176 ppm, whereas the corresponding peak for AlaPt is at 193 ppm (**Fig. 2.8**). The C_{α} and C_{β} are shifted less (from 50 to 57 ppm and 16 to 20 ppm, respectively) because they are further away from the platinum center. The ^{13}C-NMR spectrum of AlaPt also has extra peaks that are possibly from the aquated AlaPt species. AlaPt is relatively soluble and as much as 100 mg can be dissolved in 1 mL of D_2O. Due to its high solubility, the aquation (replacement of chlorido with

aqua) can occur rapidly. It was observed that when an equivalent ratio of $AgNO_3$ is added to an AlaPt solution, a white precipitate (AgCl) is rapidly formed, possibly due to the fast aquation. To further monitor the presence of aquated species in solution by NMR spectroscopy, AlaPt was mixed with an equivalent ratio of $AgNO_3$ for varying time points of 1, 2, 6, and 24 h. After each time point, the sample was centrifuged to precipitate the AgCl. The supernatant was then characterized with ^{13}C-NMR spectroscopy. It was observed that with increasing time, the peak pattern changed to reflect the diminishing non-aquated AlaPt and the formation of mono- and bis-aquated species (**Fig. 2.9**).

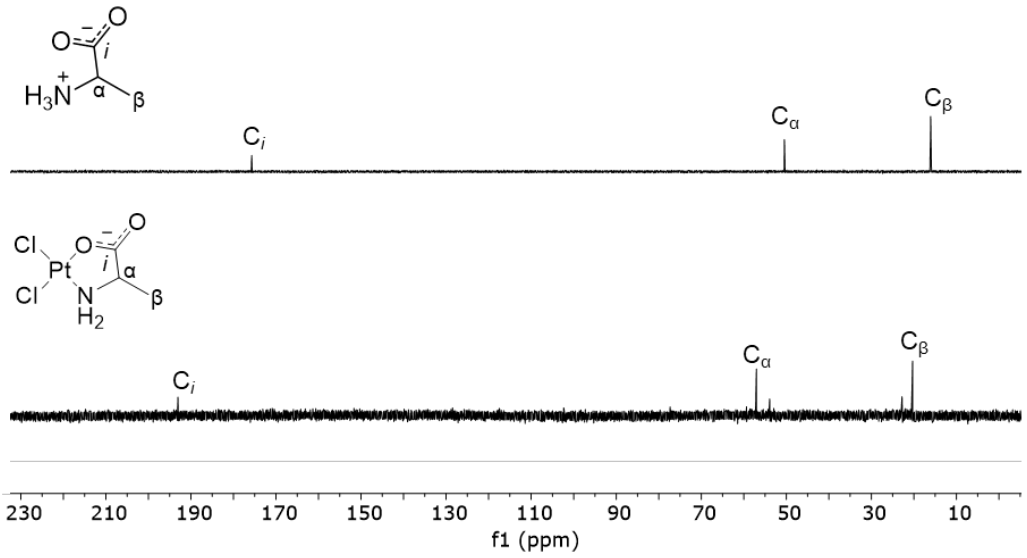

Figure 2.8. **The ^{13}C-NMR spectra of L-alanine (top) and AlaPt (bottom).** For L-alanine; δ/ppm (^{13}C-NMR, D_2O, 400 MHz) 176 ((-COO)CH=), 50 (=CHCH$_3$), 16 (=CHCH$_3$); For AlaPt; δ/ppm (^{13}C-NMR, D_2O, 400 MHz) 193 ((-COO)CH=), 57 (=CHCH$_3$), 20 (=CHCH$_3$). The minor peaks are due to possible aquation of AlaPt which occurs in a H_2O or D_2O environment as described in the introduction (**Section 1.2.3**).

In the ^{195}Pt-NMR spectrum, the chemical shift of the platinum(II) center of AlaPt is compared to that of potassium tetrachloroplatinate(II), which is the starting material for AlaPt synthesis (**Fig. 2.10**). The ^{195}Pt-NMR spectrum shows a ^{195}Pt peak at -1607 ppm for potassium tetrachloroplatinate(II) that shifts to -1639 ppm for the AlaPt product.

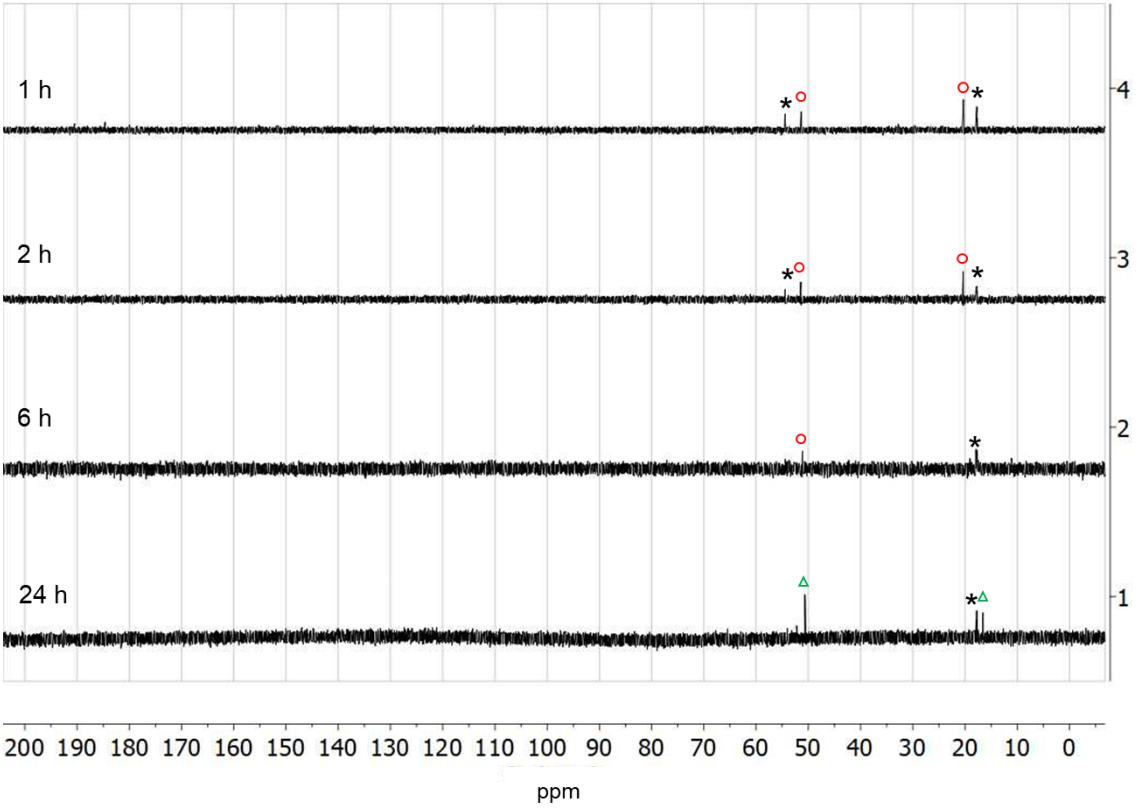

Figure 2.9. The ^{13}C-NMR time course of AlaPt aquation. The spectrum of aquated AlaPt changes over time with different species diminishing or forming at varying proportions. The non-aquated species (black asterisks) are diminished with time. The monoaquated species (red circles) also diminish over time while the bis-aquated species (green triangles) become dominant at longer time periods.

AlaPt was also characterized by using ESI mass spectrometry. The mass analysis gives an observed *m/z* of 352.9 Da/e. This result agrees with the calculated exact mass of 352.9 Da for a singly charged (negative) AlaPt product with a chemical formula $PtC_3H_6Cl_2NO_2$ (**Fig. 2.11**). The mass data are consistent with one amino acid and two chlorido ligands coordinated to a platinum center, with AlaPt having (N,O) type of binding (platinum coordination to the N and O atoms of alanine).

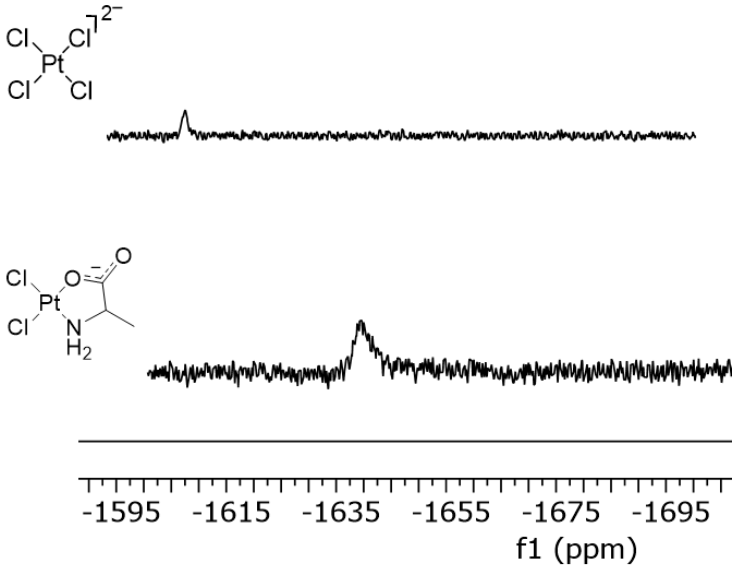

Figure 2.10. **The ^{195}Pt-NMR spectrum of potassium tetrachloroplatinate(II) and AlaPt.** For potassium tetrachloroplatinate(II) (top), δ/ppm (^{195}Pt-NMR, D_2O, 400 MHz) is -1607 ($\underline{Pt}Cl_4$); for AlaPt (bottom), δ/ppm (^{195}Pt-NMR, D_2O, 400 MHz) is -1639 ($\underline{Pt}Cl_2(NH_2)O$). The ^{195}Pt chemical shift for AlaPt is in the same region where peaks for other comparable platinum-based compounds are found [110, 135]. Assistance to obtain these spectra was provided by Dr. Dennis Anderson in the Wayne State University Lumigen Instrument Center.

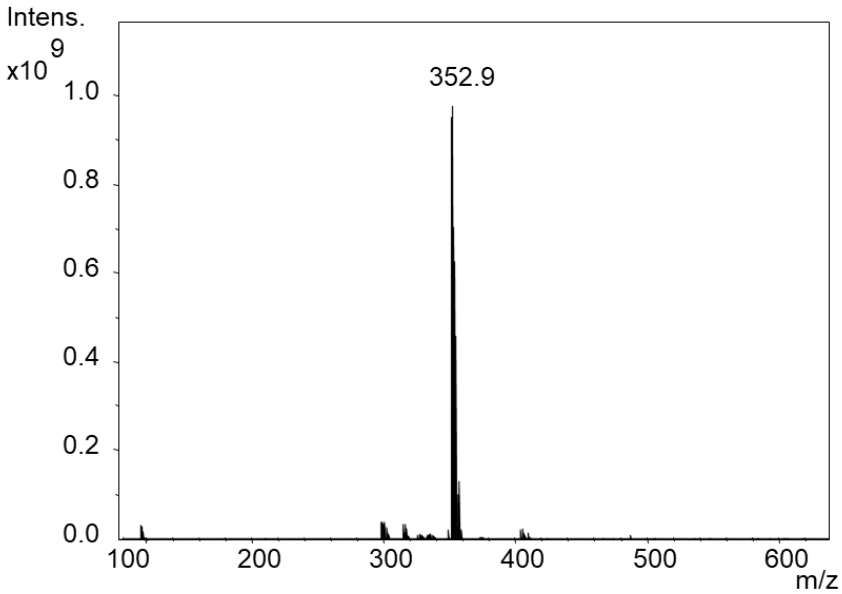

Figure 2.11. **ESI mass spectrum of AlaPt**. *m/z* (ESI-MS) 352.9 Da/e $[AlaPt]^-$; calculated exact mass 352.9 Da $[AlaPt]^-$; chemical formula $PtC_3H_6Cl_2NO_2$ ($[AlaPt]^-$, at neutral pH). The spectrum was obtained by Dr. C. C. He in Dr. M. T. Rodgers' lab.

2.4.2 Synthesis and characterization of OrnPt

Synthesis of OrnPt was carried out as described previously [104]. First, 0.17 mmoles of K_2PtCl_4 and two equivalents of L-ornithine (44 mg) were dissolved in 2 mL of ddH_2O. The mixture was heated at 50 °C overnight on a thermoshaker and afterwards dried under vacuum. The crude product was washed with ice-cold ddH_2O and vacuum dried again. The product, obtained in 40% yield (27 mg), was characterized by ^{1}H-NMR spectroscopy, ^{13}C-NMR spectroscopy and high-resolution mass spectrometry. A sample of OrnPt product was also crystallized to be used for solving its crystal structure through X-ray crystallography. The crystals were first grown through the slow evaporation method. A 10 mM concentration of OrnPt dissolved in ddH_2O was placed in a capped glass tube fitted with a needle-sized hole at the top. The tube was kept in the dark for 3 weeks at room temperature with minimal disturbance. Shiny yellow rod-like crystals were obtained. The biggest crystal was selected, and the structure was solved using a Bruker D8 diffractometer. δ/ppm (^{1}H-NMR, D_2O, 400 MHz), 3.54 (1 H, t, J=6.3 Hz, -C<u>H</u>(NH_2)CH_2-), 2.89 (2 H, t, J=7.9 Hz, -C<u>H</u>$_2$$NH_3$), 1.84–1.69 (4H, m, -CH(NH_2)C<u>H</u>$_2$C<u>H</u>$_2$-); m/z (ESI-MS) 395.986 Da/e $[M–H]^-$; calculated exact mass 395.984 Da $[M–H]^-$; chemical formula $PtC_5H_{11}Cl_2N_2O_2$ ($[M–H]^-$, at neutral pH). The crystal structure shows that the Pt center is coordinated with nitrogen and oxygen of the amino acid.

The OrnPt was characterized by using ^{1}H- and ^{13}C-NMR spectroscopy, mass spectrometry, and X-ray crystallography**.** The ^{1}H-NMR spectrum of OrnPt was compared to that of L-ornithine (**Fig. 2.12**). The chemical shift of the L-ornithine H_α proton peak is 3.60 ppm. The close proximity of the metal center shifts the corresponding H_α proton for OrnPt upfield to 3.50 ppm. The platinum-induced chemical shift is subtle for the H_β and H_γ protons, likely because they are further away from the metal center.

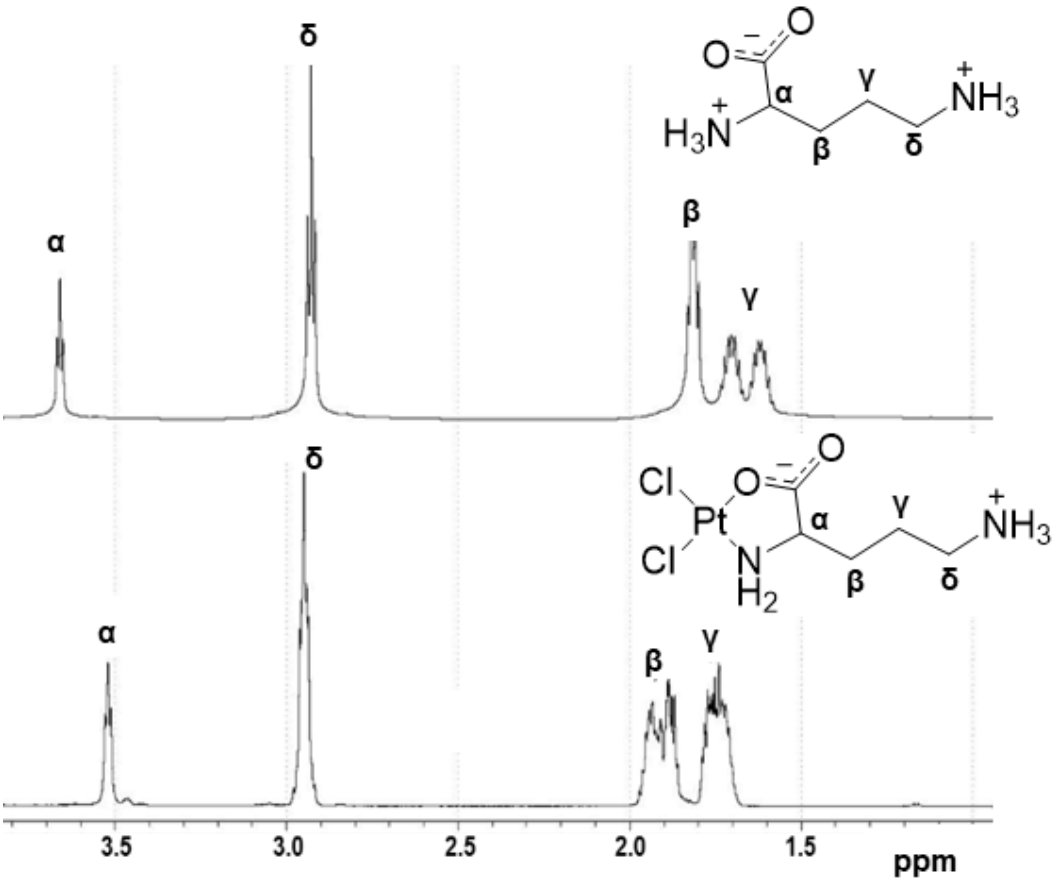

Figure 2.12. **The ^{1}H-NMR spectra of L-ornithine (upper) and OrnPt (lower).** For L-ornithine, δ/ppm (^{1}H-NMR, D_2O, 400 MHz) is 3.63 (1 H, t, J=6.3 Hz, -C<u>H</u>(NH_3)CH_2-), 2.90 (2 H, t, J=8.0 Hz, -C<u>H_2</u>NH_3), 1.82 – 1.52 (4H, m, -CH(NH_3)C<u>H_2</u>C<u>H_2</u>-). For OrnPt; δ/ppm (^{1}H-NMR, D_2O, 400 MHz), 3.54 (1 H, t, J=6.3 Hz, -C<u>H</u>(NH_2)CH_2-), 2.89 (2 H, t, J=7.9 Hz, -C<u>H_2</u>NH_3), and 1.84 – 1.69 (4H, m, -CH(NH_2)C<u>H_2</u>C<u>H_2</u>-). The chemical shifts are consistent with a previously described characterization of OrnPt [104].

In the ^{13}C-NMR spectrum, the peaks from L-ornithine were compared to those for OrnPt. The C_α, C_β, C_γ, and C_δ peaks for L-ornithine are more upfield in comparison to OrnPt (54 to 58 ppm, 37 to 38 ppm, 27 to 29 ppm, and 22 to 23 ppm, respectively) (**Fig. 2.13**). The carboxylate carbon peak for L-ornithine has a chemical shift of 174 ppm. The corresponding peak for OrnPt was not fully resolved likely due to the low solubility of OrnPt in D_2O. OrnPt has moderate solubility in D_2O and gets saturated at approximately 5 mg/mL.

Other solvents that were used to dissolve OrnPt for possible ^{13}C-NMR spectroscopic analysis at higher concentrations include deuterated-acetonitrile, $CDCl_3$, and DMSO. However,

while the solubility of OrnPt is also very low in deuterated-acetonitrile and $CDCl_3$, the DMSO solvent likely reacts with the compound due to the presence of the sulfur, which has been observed to occur when DMSO is mixed with cisPt [136]. The reactivity of OrnPt with DMSO was confirmed by ^{1}H-NMR spectroscopy in which a change in the NMR spectrum is observed (**Fig. 2.14**). For future ^{13}C-NMR analysis, perhaps the carboxylate carbon could be resolved by running the analysis for a longer time period (approx. 24 h in D_2O) or with other solvents such as deuterated-methanol, which can dissolve the compound at higher concentrations.

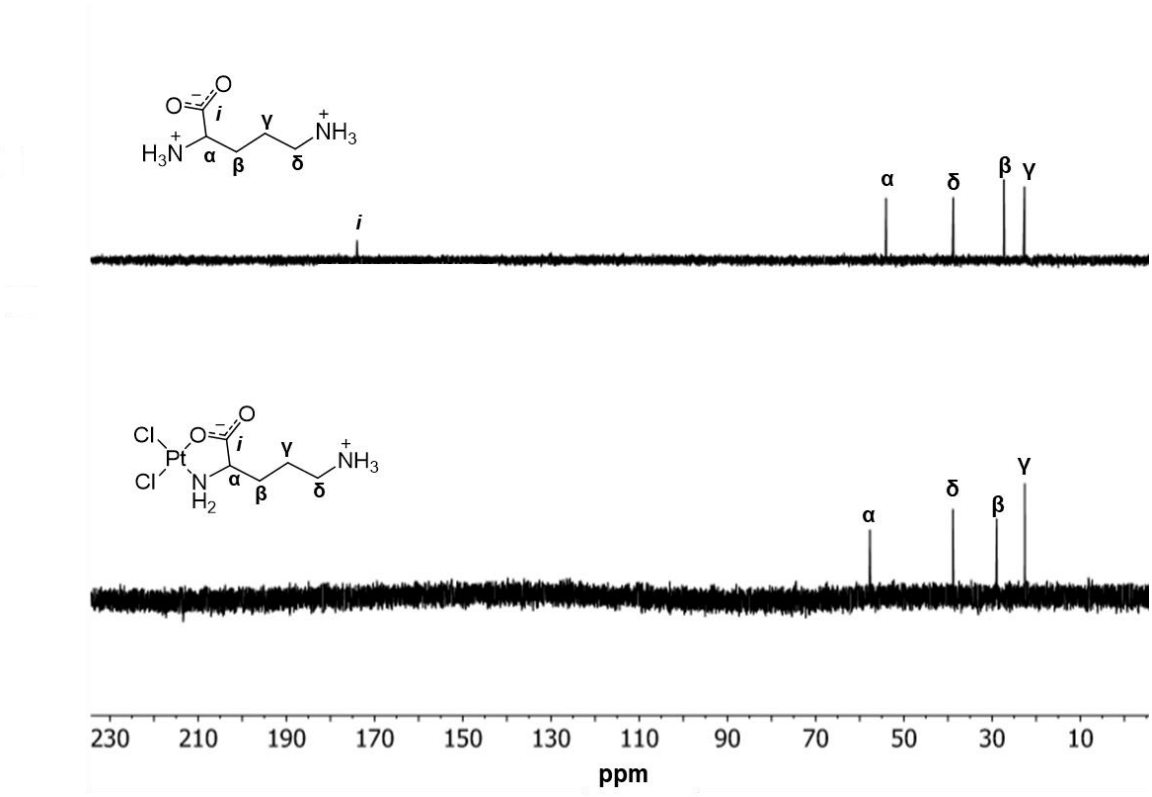

Figure 2.13. The ^{13}C-NMR spectra of L-ornithine and OrnPt. The ^{13}C chemical shifts change between L-ornithine and OrnPt due to coordination of the amino acid with the platinum(II) center. The C_α, C_β ,C_γ, and C_δ are shifted from 54 to 58 ppm, 37 to 38 ppm, 27 to 29 ppm, and 22 to 23 ppm, respectively. The carboxylate carbon peak for OrnPt is not observed due to the relatively low solubility of the compound in D_2O compared to L-ornithine.

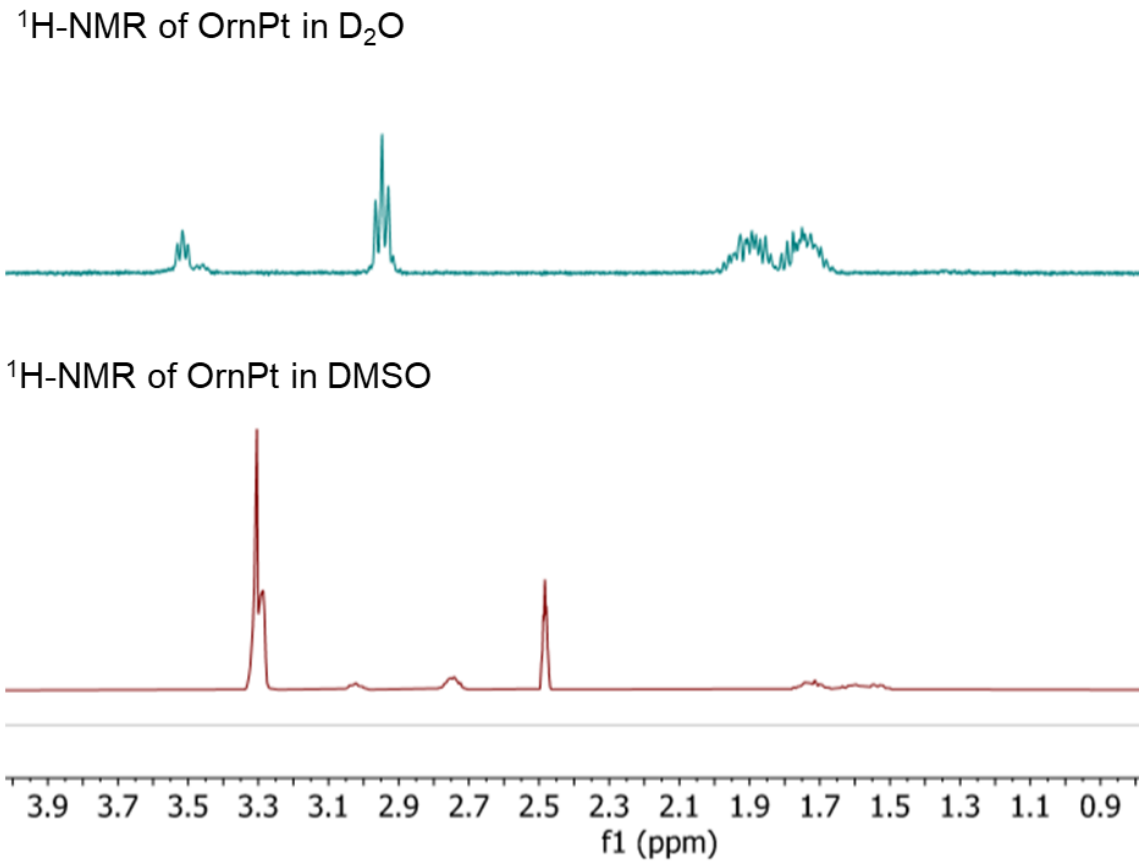

Figure 2.14. **The ^{1}H-NMR spectra of OrnPt in D_2O and DMSO**. DMSO reacts with OrnPt, resulting in an altered ^{1}H-NMR spectrum (bottom) compared to that of OrnPt dissolved in D_2O (top).

Analysis of OrnPt using ESI mass spectrometry gave an observed *m/z* of 395.986 Da/e (**Fig. 2.15**), which is consistent with the calculated exact mass of 395.984 Da for the OrnPt product with the chemical formula $PtC_5H_{11}Cl_2N_2O_2$. A dimer, $[2(OrnPt)-H]^-$, is also observed at 794.975 Da/e. The mass data for OrnPt support a structure with one ornithine and two chlorido ligands coordinated to the platinum center.

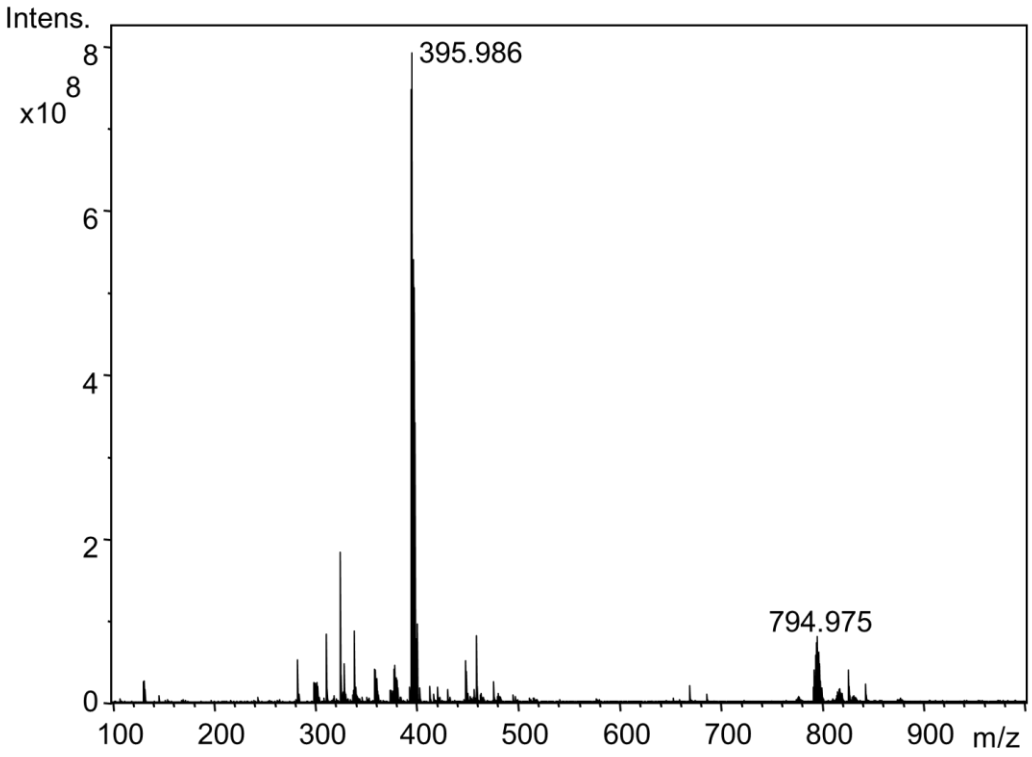

Figure 2.15. ESI mass spectrum of OrnPt. m/z (ESI-MS) 395.986 Da/e $[M-H]^-$; calculated exact mass 395.984 Da $[M-H]^-$; chemical formula $PtC_5H_{11}Cl_2N_2O_2$ ($[OrnPt-H]^-$; at neutral pH); a dimer $[2(OrnPt)-H]^-$ is observed at 794.975 Da/e. This spectrum was obtained by Dr. C. C. He in Dr M.T. Rodgers' lab.

While the above data are consistent with the coordination of one amino acid to a metal center, the spectra do not reveal whether the structure is (N,O) or (N,N) type. In the (N,N) type structure, the propylamine side chain of ornithine could coordinate to the metal center through its nitrogen atom. The structure of OrnPt was therefore analyzed by using X-ray crystallography (**Fig. 2.16**), which shows that the platinum(II) maintains a square-planar geometry and is part of a five-membered ring with (N,O) coordination, consistent with a previous report [104]. The crystallization conditions for OrnPt may favor the (N,O) type, but the presence of (N,N) type structures in solution cannot be ruled out [107].

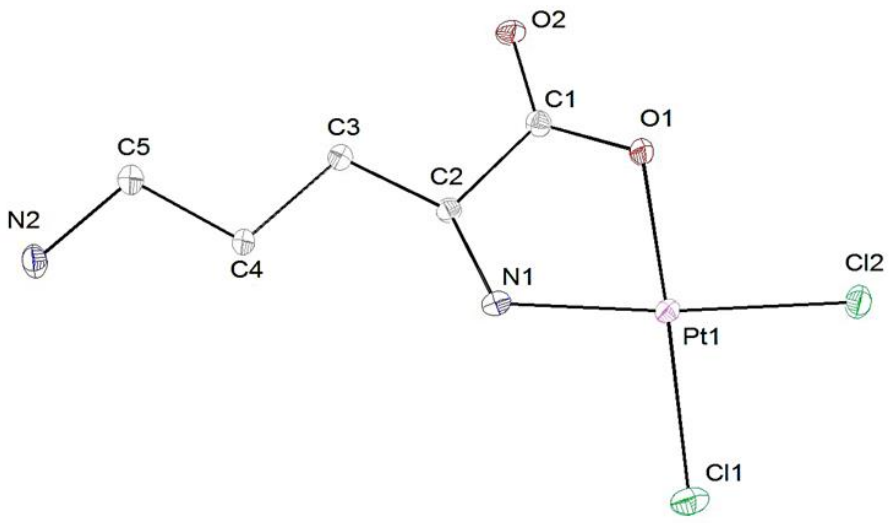

Figure 2.16. Crystal structure of OrnPt. The structure is consistent with a previously described (N_b,O_b) binding structure [104], in which the platinum maintains its square-planar geometry in a five-membered chelation ring. The structure was obtained by Dr. Phil Martin in the Wayne State University Lumigen Instrument Center.

2.4.3 Synthesis and characterization of ArgPt

Synthesis of ArgPt was carried out using L-arginine and K_2PtCl_4 as the starting materials and following the OrnPt synthesis protocol above with several modifications to optimize purity. First, 0.17 mmol of K_2PtCl_4 and one equivalent of L-arginine (29 mg) were mixed in 2 mL ddH_2O. An equivalent amount of KCl (13 mg) was also added to the mixture to inhibit disproportionation of K_2PtCl_4 [112]. The mixture was heated at 50 °C overnight on a thermoshaker at 950 rpm, followed by vacuum drying. The crude product was washed with 1 mL ice-cold ddH_2O three times and vacuum dried again to obtain a light greenish product. The product was obtained in a 23% yield (17 mg) and characterized by ^{1}H-NMR spectroscopy, ^{13}C-NMR, and mass spectrometry. δ/ppm (^{1}H-NMR, D_2O, 400 MHz), 3.49 (1 H, t, J=6.7 Hz, -C<u>H</u>(NH_2)CH_2-), 3.14 (2 H, t, J=6.8 Hz, -C<u>H</u>$_2$NH-), 1.90 – 1.48 (4H, m, -CH(NH)C<u>H</u>$_2$C<u>H</u>$_2$-). m/z (ESI-MS) 439.007 Da/e $[M+H]^+$; calculated exact mass 439.014 Da $[M+H]^+$; chemical formula $PtC_6H_{13}Cl_2N_4O_2$ ($[M-H]^-$, at neutral pH).

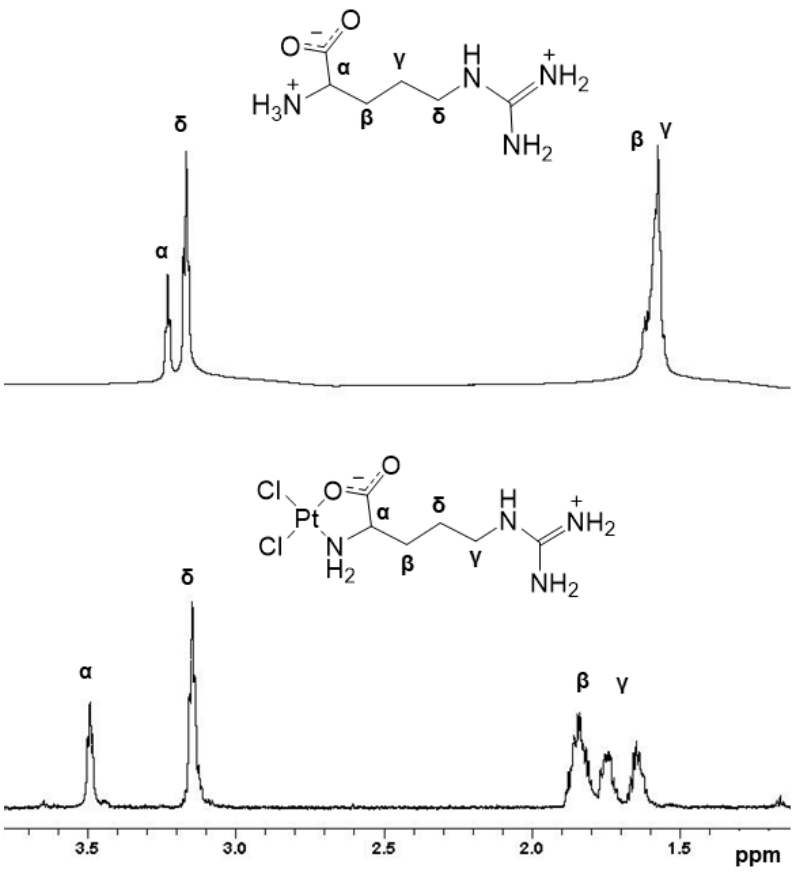

Figure 2.17. **The ^{1}H-NMR spectra of L-arginine and ArgPt.** For L-arginine (upper); δ/ppm (^{1}H-NMR, D_2O, 400 MHz), 3.10 (1 H, t, J=5.5 Hz, -C<u>H</u>(NH_3)CH_2-), 3.04 (2 H, t, J=6.3 Hz, -C<u>H_2</u>NH-), 1.53 – 1.40 (4 H, m, -CH(NH)C<u>H_2</u>C<u>H_2</u>-). For ArgPt (lower); δ/ppm (^{1}H-NMR, D_2O, 400 MHz), 3.49 (1 H, t, J=6.7 Hz, -C<u>H</u>(NH_2)CH_2-), 3.14 (2 H, t, J=6.8 Hz, -C<u>H_2</u>NH-), 1.90 – 1.48 (4 H, m, -CH(NH)C<u>H_2</u>C<u>H_2</u>-).

The ArgPt was characterized by using ^{1}H- and ^{13}C-NMR spectroscopy, and mass spectrometry. The ^{1}H-NMR spectrum of ArgPt was analyzed in comparison to that of L-arginine (**Fig. 2.17**). The chemical shift of the L-arginine H_α proton peak is at 3.10 ppm, whereas the corresponding H_α proton for ArgPt is shifted downfield to 3.49 ppm due to the close proximity of the metal center. Since the H_β and H_γ protons are further away from the metal center, their platinum-induced chemical shift is relatively smaller. In the ^{13}C-NMR spectrum, the peaks from L-arginine were compared to those for ArgPt. The C_α, C_β, C_γ, and C_δ peaks for L-arginine are shifted in comparison to ArgPt (55.5 to 57.8 ppm, 40.8 to 40.5 ppm, 31.5 to 29.3 ppm, and 24.3 to 23.7 ppm, respectively) (**Fig. 2.18**). The C_ε and C_i (carboxylate carbon) peaks of L-arginine have

chemical shifts of 156.8 and 183.2 ppm, respectively. Similar to OrnPt, the corresponding peaks for ArgPt were not fully resolved likely due to the low solubility of ArgPt in D_2O (ArgPt is saturated at approximately 5 mg/mL).

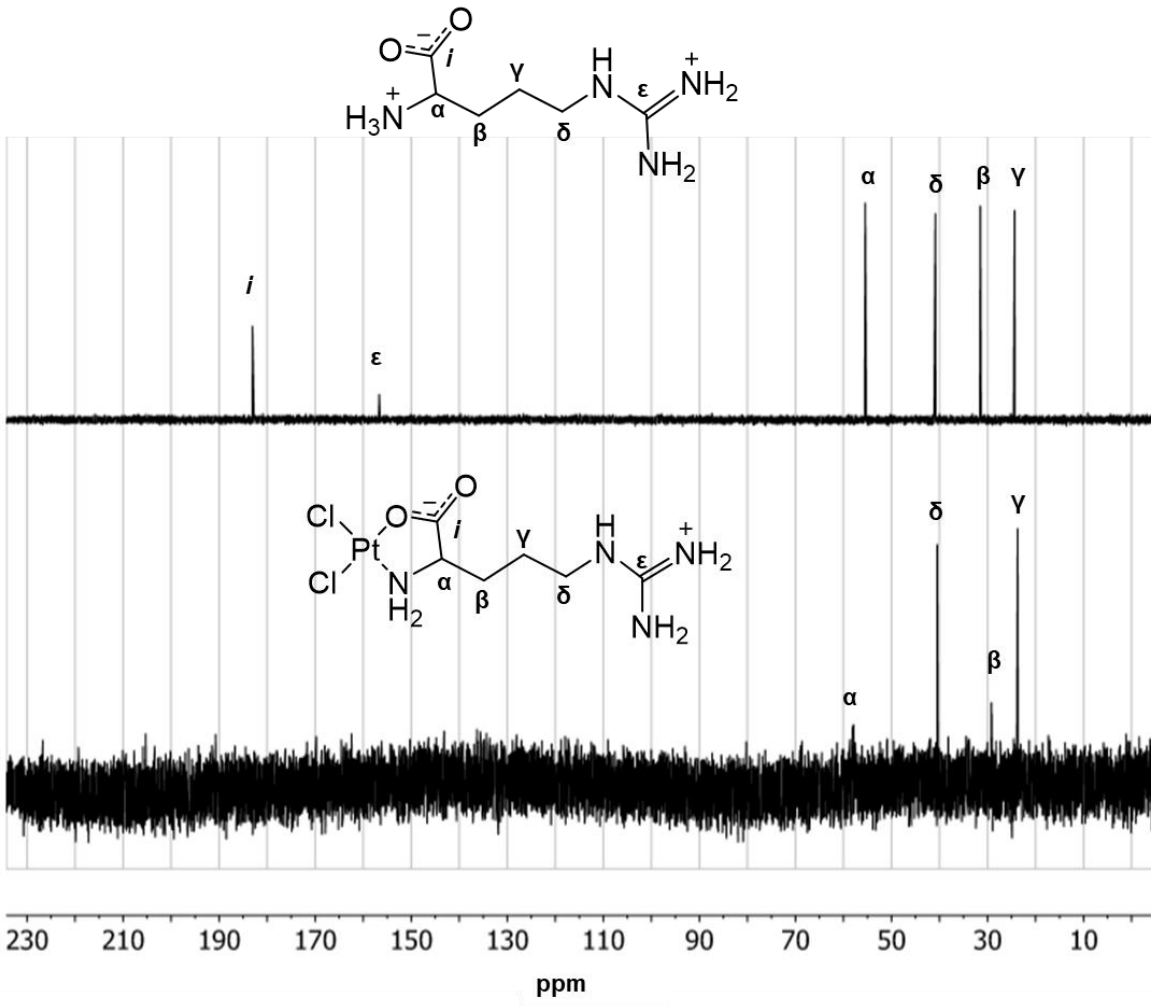

Figure 2.18. The ^{13}C-NMR spectra of L-arginine and ArgPt. The chemical shifts for carbons change between L-arginine and ArgPt due to coordination of the amino acid with the platinum center. The C_α, C_β, C_γ, and C_δ of L-arginine and ArgPt change from 55.5 to 57.8 ppm, 40.8 to 40.5 ppm, 31.5 to 29.3 ppm, and 24.3 to 23.7 ppm, respectively. The C_ε and C_i (carboxylate carbon) peaks for ArgPt are not observed likely due to low solubility of the compound in D_2O compared to L-arginine.

Analysis of ArgPt using ESI mass spectrometry gave an observed *m/z* of 439.007 Da/e (**Fig. 2.19**), which is consistent with the calculated exact mass of 439.015 Da for ArgPt with a chemical formula $PtC_6H_{14}Cl_2N_4O_2$. The mass data suggest that the complex consists on one

arginine and two chlorido ligands coordinated to the platinum(II) center. A dimer, $[2(ArgPt)+Cl]^+$, is observed at 914.993 Da/e. A species, $[(ArgPt)+Cl]^+$, with 474.982 Da/e is also observed.

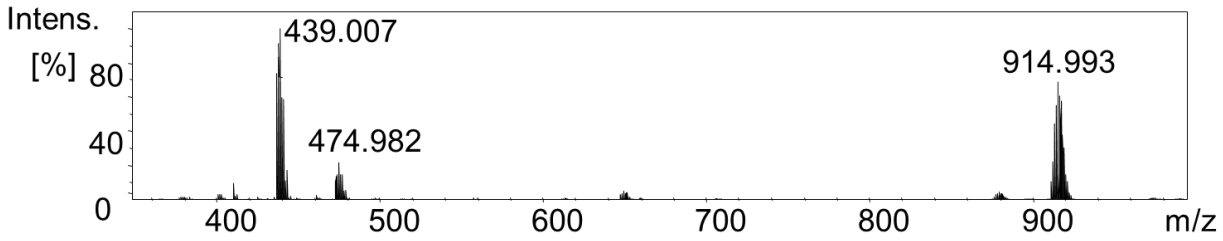

Figure 2.19. Mass analysis of ArgPt using FT-ICR MS. m/z (ESI-MS) 439.007 Da/e $[M+H]^+$; calculated exact mass 439.014 Da $[M+H]^+$; chemical formula $PtC_6H_{14}Cl_2N_4O_2$ ($[M+H]^+$, at neutral pH); Other species include a dimer, $[2(ArgPt)+HCl]^+$, observed at 914.993 Da/e and $[(ArgPt)+Cl]^+$ observed at 474.982 Da/e. This spectrum was obtained by Dr. C. C. He at Dr. M.T. Rodgers' lab.

2.4.4 Preparation of aquated AAPt compounds

For *in vitro* studies, cisPt or AAPt analogues converted into monoaquated species prior to reactions with nucleosides or oligonucleotides. Aquation of AlaPt, OrnPt, and ArgPt to generate the corresponding monoaquated AAPt species, involves replacement of one chlorido with an aqua ligand (**Scheme 2.1**). The AAPt compound (1.8 µmoles) and $AgNO_3$ (1.3 µmoles, ratio of 1:0.7) were dissolved in 300 µL double deionized water (ddH_2O) and agitated (using a vortex shaker) in the dark at room temperature for 15 h. The resulting white precipitate (AgCl) was removed through two centrifugation steps at 14,000 rpm for 10 min each. The supernatant contained the corresponding monoaquated AlaPt, OrnPt, or ArgPt. CisPt was converted to monoaquated cisPt using the same procedure.

Scheme 2.1. Aquation of platinum compounds

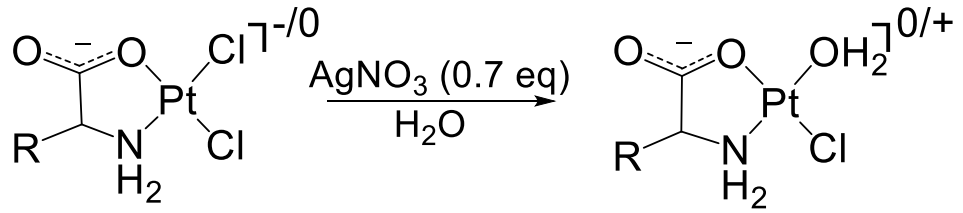

AlaPt: R=CH_3
OrnPt: R=$(CH_2)_3NH_3^+$
ArgPt: R=$(CH_2)_3NHCNH_2NH_2^+$

monoaquated AlaPt
monoaquated OrnPt
monoaquated ArgPt

2.4.5 Preparation of nucleosides and oligonucleotides

To prepare stock solutions, individual nucleosides were dissolved in ddH_2O and filtered through centrifugation. Supernatants were collected and concentrations of the nucleosides were determined by measuring absorption on a DU730 UV/Vis spectrophotometer (Beckman Coulter) at the maximum wavelength and using molar extinction coefficient of the respective nucleoside. The extinction coefficients and wavelengths used were 14,900 M^{-1} cm^{-1} at 260 nm for Ado, 13,600 M^{-1} cm^{-1} at 253 nm for Guo, 15,700 M^{-1} cm^{-1} at 260 nm for dAdo, and 13,000 M^{-1} cm^{-1} at 254 nm for dGuo [137].

HPLC analysis and matrix assisted laser desorption ionization mass spectrometry (MALDI-MS) characterization of 5′-d(TTATT)-3′ (**Figs. 2.20 and 2.21**) and 5′-UUAUU-3′ (**Figs. 2.22 and 2.23**) show that the oligonucleotides were pure and had the expected calculated masses. Concentrations of each strand were determined by measuring absorbance at 260 nm. At this wavelength, the extinction coefficients are 47,000 M^{-1} cm^{-1} for 5′-d(TTATT)-3′ and 52,600 M^{-1} cm^{-1} for 5′-UUAUU-3′.

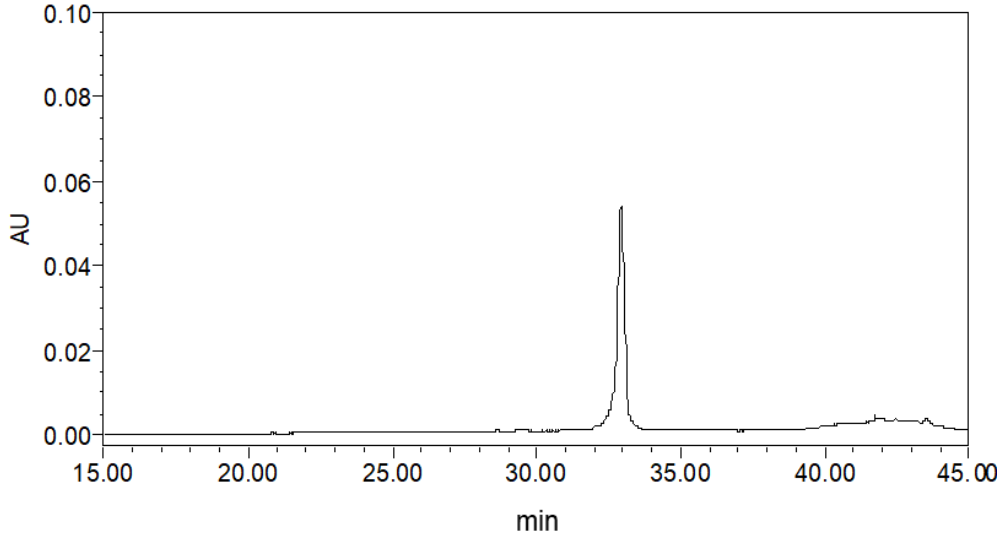

Figure 2.20. HPLC analysis of 5′-d(TTATT)-3′. A single peak for 5′-d(TTATT)-3′ is observed with only minor impurities (C18 column).

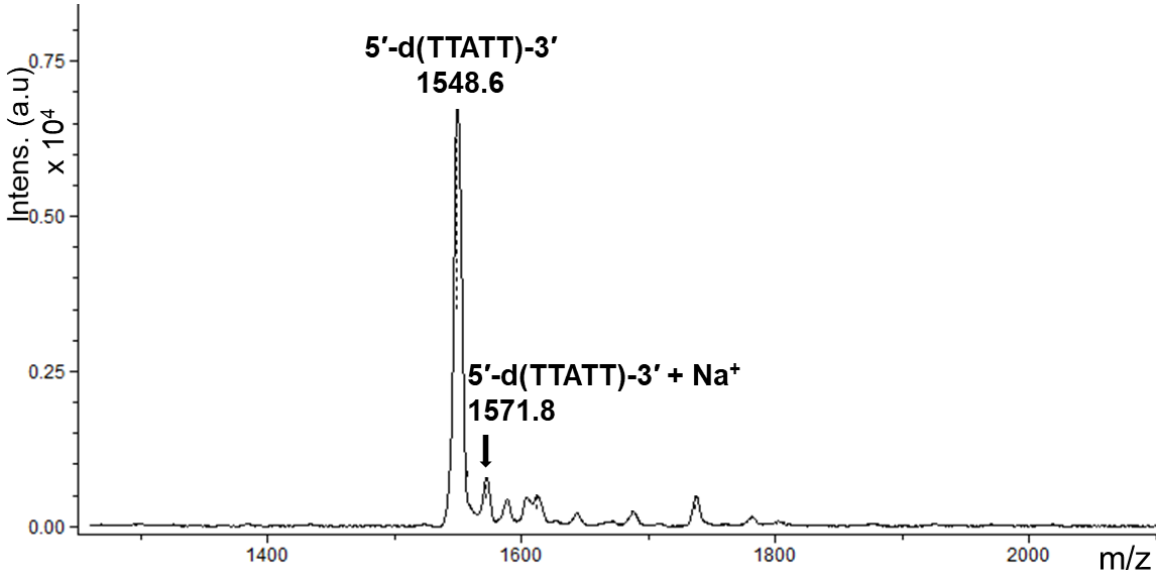

Figure 2.21. MALDI-MS mass spectrum of 5′-d(TTATT)-3′. MALDI analysis (positive mode) of 5′-d(TTATT)-3′ gave an observed m/z of 1548.6 Da/e (calculated exact mass of $[d(TTATT)+H]^+$ is 1548.3 Da). A peak corresponding to the oligonucleotide associated with a sodium ion is observed at m/z 1571.8 Da/e. Other minor peaks associated with multiple sodium ions are observed as well.

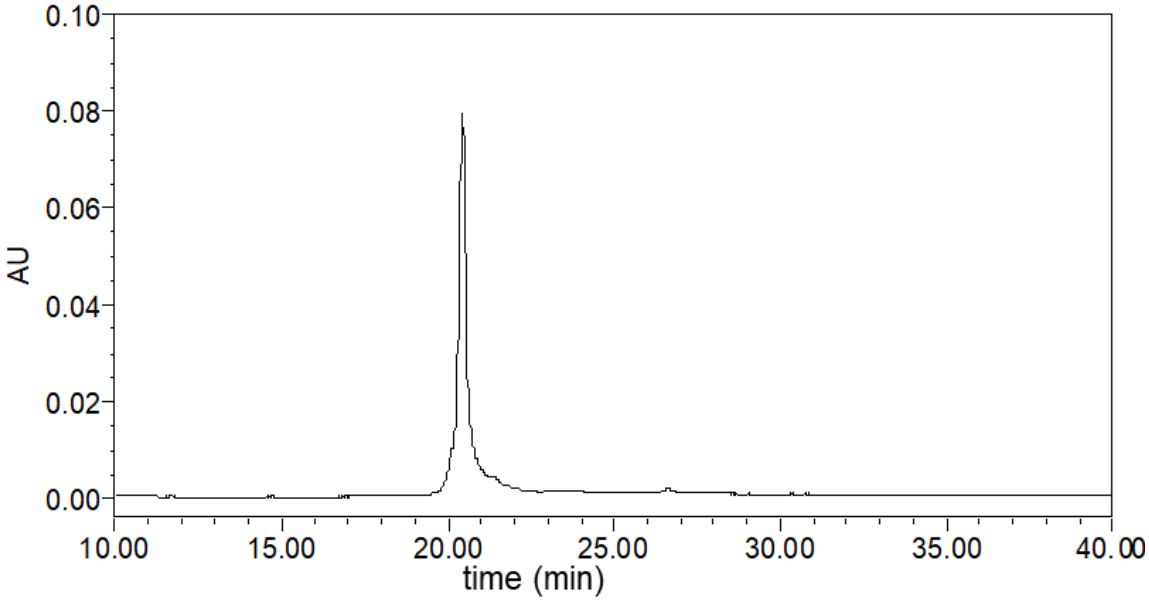

Figure 2.22. HPLC analysis of 5′-UUAUU-3′. A single peak for 5′-UUAUU-3′ is observed with only minor impurities (C18 column).

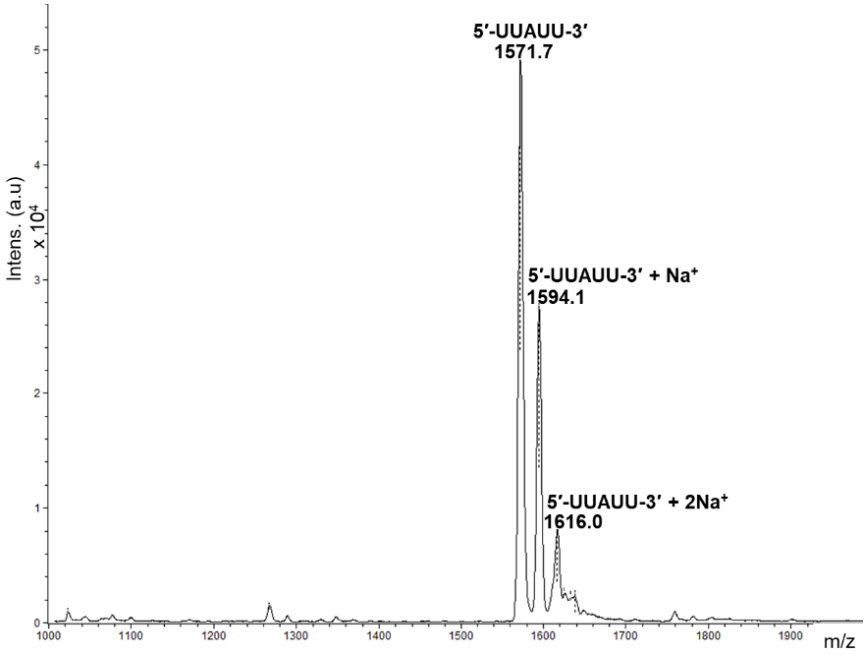

Figure 2.23. MALDI-MS mass spectrum of the 5′-UUAUU-3′. MALDI analysis (positive mode) of 5′- UUAUU-3′ gave an observed m/z of 1571.7 Da/e (calculated exact mass of $[UUAUU+H]^+$ is 1572.1 Da). A peak corresponding to the oligonucleotide associated with one sodium ion is observed at m/z 1594.1 Da/e while an oligonucleotide associated with two sodium ions is observed at m/z 1616.0 Da/e.

2.4.6 Pseudo-first-order reaction kinetics

The monoaquated AAPt compounds (or monoaquated cisPt) were used in 50-fold excess to produce pseudo-first-order reaction conditions. A 0.1 mM solution of the relevant nucleoside (Ado, Guo, dAdo, dGuo) or oligonucleotide was incubated with 5 mM of the aquated platinum complex in 25 mM Na_2HPO_4/NaH_2PO_4 buffer (pH 7) at 37 °C. For nucleoside reactions, six aliquots were collected from the sample at different time points (0, 0.5, 1, 2, 3, 4, and 6 h). For oligonucleotide reactions, six aliquots were collected from the sample at different time points (0, 5, 15, 30, 60, 90, and 120 min). Each aliquot was quenched with NaCl (0.12 M final concentration) and then frozen at -80 °C until HPLC analysis. The HPLC was fitted with the Supelco Discovery C18 column (see instrumentation **Section 2.4.5**). For nucleoside elution, buffers A (40 mM NH_4OAc, pH 6.5) and B (40% acetonitrile, 60% ddH_2O) were employed using isocratic conditions with 5% B for 5 min followed by a linear gradient in which B was increased to 35% over 25 min. For oligonucleotide elution, the same buffers were employed using isocratic conditions with 10% B for 5 min followed by a linear gradient in which B was increased to 20% over 10 min, and further increased to 50% over the next 15 min. The peak area of unreacted nucleoside/oligonucleotide was monitored over the six time points and their diminishing ratio to the product peaks was determined [138]. The unreacted nucleoside/oligonucleotide was monitored because its peak was dominant in area and could also be distinguished from other multiple product peaks based on the retention time of the control. The HPLC calibration curves show a linear relationship between the nucleoside concentration and normalized peak area (**Fig. 2.24**). Therefore, the peak area of the nucleoside at each time point can be integrated quantitatively.

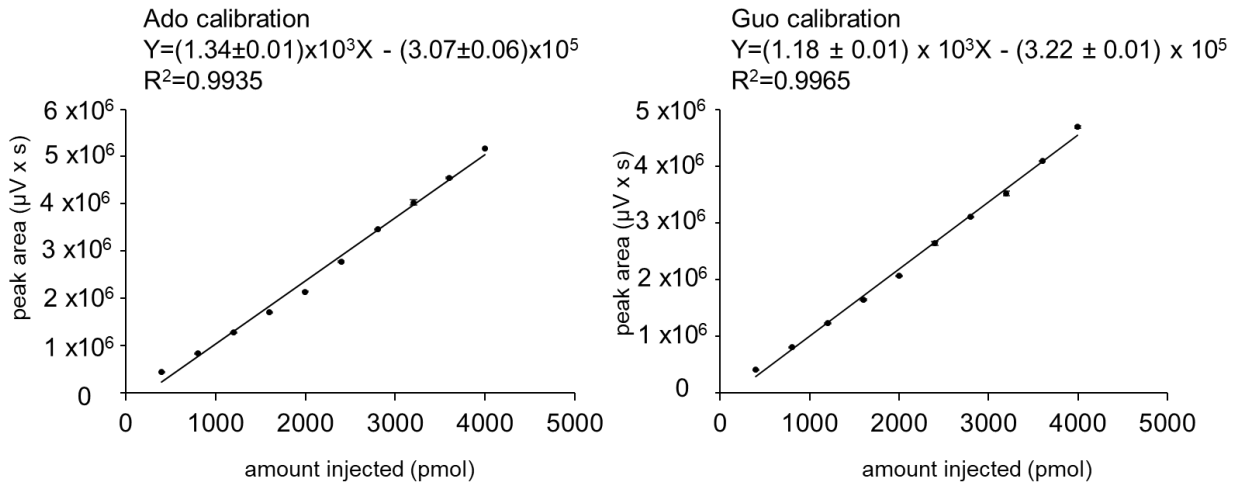

Figure 2.24. HPLC calibration curves for Ado and Guo. There is a linear relationship between the amount of a nucleoside injected and the area under curve.

2.4.7 Fitting data into a kinetic equation

The data were fit using an exponential equation assuming pseudo-first-order kinetics (**Eqs. 2.1-2.5**). The pseudo-first order kinetics equation is derived as follows, in which $AAPt_{aq}$ is the monoaquated compound and Nuo is the nucleoside or oligonucleotide [139]:

$$\text{Nuo} + AAPt_{aq} \xrightarrow{k_{app}} \text{AAPt-Nuo adduct} + H_2O \quad \textbf{(Eq. 2.1)}$$

Depending on the platinum-based compound, various charged species such as monoaquated or bisaquated species can be present in the solution and take part in the reaction [140]. The rate of reaction (V) is given by,

$$V = k_{app}\,[AAPt_{aq}]\,[\text{Nuo}] \quad \textbf{(Eq. 2.2)}$$

in which, k_{app} is the apparent bimolecular rate constant. Under pseudo-first-order conditions, $[AAPt_{aq}] >> [\text{Nuo}]$ (50-fold excess of $AAPt_{aq}$ over Nuo) and remains approximately constant. Under these conditions, the rate constant, k, equals $k_{app}[AAPt_{aq}]$ and the rate (V) is given by,

$$-d[\text{Nuo}]/dt = k\,[\text{Nuo}] \quad \textbf{(Eq. 2.3)}$$

By integration and rearrangement,

$$\ln[Nuo]_t = -kt + \ln[Nuo]_0 \quad \textbf{(Eq. 2.4)}$$

By rewriting the above equation in exponential form,

$$[Nuo]_t = e^{-kt} + [Nuo]_0 \quad \textbf{(Eq. 2.5)}$$

in which $[Nuo]_t$ is the concentration of unreacted nucleoside or oligonucleotide at time t, and $[Nuo]_0$ is the initial concentration of unreacted nucleoside or oligonucleotide. When $[Nuo]_t$ is plotted against t, the decay factor is *k.* The equation was input into KaleidaGraph software and used to fit the data. Experiments were performed in triplicate. The standard error was calculated by dividing the standard of the mean deviation by the square root of the number of replicates.

2.4.8 Mass analysis of HPLC isolated AAPt-nucleoside adducts

The HPLC fractions containing the AAPt-nucleoside adducts were collected and vacuum dried. The samples were redissolved in 50:50 MeOH:ddH_2O (v/v) and ions were generated with an ESI source. The MS analyses were performed using a 7T Fourier transform ion cyclotron mass spectrometer (FT-ICR MS, solariX, Bruker Daltonics). Major ions were identified for each fraction. The dominant AAPt-nucleoside adduct in each fraction was isolated and subjected to CID-tandem mass spectrometry analysis. Fragments were observed and assigned based on their measured m/z values.

2.4.9 NMR spectroscopy of AAPt-nucleoside adducts

The ^{1}H and ^{13}C NMR (700 MHz) spectra of the AAPt-nucleoside adducts were recorded on a Bruker Avance 700 MHz spectrometer equipped with a TXI cryoprobe. The H2 and H8 signals in Ado were assigned by identifying the C2 and C8 chemical shifts in ^{13}C NMR [141] followed by two-dimensional heteronuclear single quantum coherence (HSQC) spectroscopy to correlate C2-H2 and C8-H8. To each sample, 10 μM trimethylsilyl propionate (TSP) was added as an internal standard. The ^{1}H chemical shifts were referenced to the residual HDO (semi-heavy water) signal, which was calibrated against TSP. D_2O (with no buffer) was also chosen as the solvent for the ^{1}H and ^{13}C NMR (700 MHz) spectra of the adducts.

2.4.10 Mass analysis of HPLC isolated AAPt-oligonucleotide adducts

The HPLC fractions containing the AAPt-oligonucleotide adducts were collected and vacuum dried. For MALDI analyses, the dried samples were first redissolved in 10 µL ddH_2O. A 1.5 µL of each sample was mixed with 1.5 µL of saturated 3-HPA and spotted on a MALDI plate. The analyses were carried out on the Bruker UltrafleXtreme MALDI-TOF/TOF. For Orbitrap-ms analyses, the dried HPLC fractions containing the AAPt-nucleoside adducts were redissolved in 100 µL ddH_2O with 0.03% triethylamine. Ions were generated with an ESI source and spectra obtained on the ThermoScientific LTQ Orbitrap XL.

2.4.11 Reactions of AAPt with poly(Ado) RNA, ethanol precipitation, and LC-MS characterization of adducts

For platination reactions with poly(Ado) RNA, monoaquated AAPt was used in 4-fold excess to the RNA molecule. The sample was incubated in 25 mM Na_2HPO_4/NaH_2PO_4 buffer (pH 7) at 37 °C overnight. Afterwards, the RNA was desalted using ethanol precipitation. To carry out ethanol precipitation, the platinum nucleic acid solution (of volume V) was mixed with 2.5 V of 100% ethanol and 0.1 V of 3 M NH_4OAc. The sample mixture was placed on dry ice for 45 min and then centrifuged at 14,000 rpm for 30 min at 4 °C. The supernatant was removed and 100 µL of 70% ethanol was added to the remaining pellet. The sample was centrifuged again at 14,000 rpm for 30 min at 4 °C. The supernatant was removed followed by vacuum drying of the remaining pellet. The dried pellet was redissolved in 50 µL ddH_2O and digested with P1 nuclease (1 unit) for 5 h at 37 °C. This step was followed by calf intestine phosphatase (CIP, 2 units) treatment for another 5 h at 37 °C. The sample was then filtered with centrifugation (Millipore 10 kDa centrifugal filter) at 10,000 rpm for 30 min. The collected sample was vacuum-dried and redissolved in 50:50 MeOH:ddH_2O (v/v).

LC-MS (Shimadzu 8040 triple quadrupole) was used to separate and identify the platinum adducts and corresponding unplatinated material. The LC-MS was equipped with ESI and fitted with a C18 Acquity HSS T3 100mm column. For elution, buffer A (10 mM NH_4OAc, pH 6.5) and

buffer B (9% acetonitrile with 10 mM NH_4OAc in ddH_2O) were employed under isocratic conditions with 0% B for 5 min followed by a linear gradient in which B was increased from 0 to 33% over 20 min.

2.4.12 Energy-resolved collision-induced dissociation (ER-CID) experiments and survival yield analyses

ER-CID experiments of the HPLC fractions containing the AlaPt-Ado, OrnPt-Ado, and ArgPt-Ado adducts were performed on a quadrupole ion trap mass spectrometer (QIT MS, amaZon ETD, Bruker Daltonics). The method has been described in detail in previous work [116, 124-125]. Briefly, HPLC fractions were vacuum dried and then redissolved in a MeOH:ddH_2O (50:50 v/v) mixture. Each HPLC fraction (10 μM) was introduced to the ESI source to generate ions, which were then guided into the ion trap. In the trap, ions were accumulated and mass selected for tandem ER-CID experiments. Helium (1 mtorr) served as both the buffer and collision gas to provide efficient trapping and cooling of the ions as well as to achieve fragmentation of the precursor AAPt-nucleoside complex. The q_z value was set to 0.25 for the ER-CID experiments, which leads to low mass cutoff of 27% of the precursor ion m/z. The rf excitation amplitude was increased from 0 V to the rf excitation amplitude required to produce complete dissociation of the precursor ion at a stepsize of 0.01 V. Experiments were performed in triplicate to assess reproducibility. All data were processed using Data Analysis 4.0 (Bruker Daltonics).

The glycosidic bond cleavage (GBC) survival yield was calculated from the intensities of the precursor and fragment ions, and the ratio of the precursor ion intensity to the total ion intensity was determined using **Eq. 2.6** [142],

$$\text{Survival Yield (GBC)} = (\sum_{x}^{n-x} I_{f_i} + I_p)/(\sum_i I_{f_i} + I_p) \quad (2.6)$$

in which I_{f_i} and I_p are the ion intensities of the fragment and precursor ions, respectively; *x* represents fragments in which the glycosidic bond remains intact. Data analyses were performed using SigmaPlot 10.0 (Systat Software, Inc., San Jose, CA) and custom software developed in

the Rodgers laboratory and reported previously [116, 122-125]. The GBC survival yield was plotted as a function of the rf excitation amplitude. The rf excitation amplitude required to produce 50% glycosidic bond cleavage ($GBC_{50\%}$) was extracted by fitting of the survival yield curve using the four-parameter logistic dynamic equation (**Eq. 2.7)** [116, 124-125].

$$\text{Survival Yield } (GBC_{50\%}) = \min + (\max - \min)/[1 + (rf_{EA}/GBC_{50\%}]^{GBCslope} \quad (2.7)$$

In this equation, max and min are defined as the maximum (1) and minimum (0) values of the survival yield, rf_{EA} is the rf excitation amplitude applied to induce fragmentation, and GBCslope is the slope of the declining region of the survival yield curve.

2.4.13 MTT cytotoxicity assays in human cell lines

The number of cells was first determined using a hemocytometer. The cells (and media) were seeded in a transparent flat-bottom, 96-well plate with each well having 10,000 cells. The seeded plate was placed in an incubator (37 °C, 5% CO_2) for 24 h to allow the cells to attach to the wells. Afterwards, the media was removed and fresh media with varying concentrations of the AAPt compound (or cisPt) added to the wells. In each plate, two types of controls were included. The first, referred to as the growth control, contained cells and media but no platinum compounds. The second, referred to as the blank control, had media only. The plates were incubated for 72 h after which 10 µL of MTT stock (5 mg/mL) was added to each of the wells. The plates were incubated for another 4 h during which time insoluble formazan is produced by viable cells. DMSO (100 µL) was added to the wells and incubated for 10 min to dissolve the formazan. The optical density (OD) of each well was measured at 520 nm using a microplate reader, BioTek synergy H1 hybrid reader in Dr. Y. H. Ahn's lab. The percentage of viable cells for each concentration of platinum compound was determined using **Eq. 2.8**.

$$\%\text{ of viable cells} = \frac{\text{OD for platinum compound concentration} - \text{OD for blank control}}{\text{OD for growth control} - \text{OD for blank control}} \quad (2.8)$$

The IC_{50} plots were generated using GraphPad PRISM®, which fits the concentration of platinum compound (X) and normalized response (percentage of viable cells, Y) into a model equation, **Eq. 2.9.**

$$Y=100/(1+(X^{hillSlope})/(IC_{50}{}^{hillSlope})), \text{ in which hillslope is -1.} \quad (2.9)$$

The protocol for cell culture and maintenance of human cell lines is described in **Appendix A**.

2.4.14 Quantification of cellular accumulation of platinum compounds

The human prostate cancer cell line, DU145, and normal prostate cell line, RWPE-1, were grown in 100 x 20 mm tissue culture dishes until confluency. The cells were then detached from bottom of dishes by treating with trypsin. The suspension was homogenized and the cell number was determined using a hemocytometer. From the stock suspension, 460,000 cells were seeded on 60 x 15 mm culture dishes each and grown in an incubator (37 °C, 5% CO_2) for 18 h. The media was removed and the dishes were washed with 3 mL PBS. In each dish, 3 mL of keratinocyte media with 50 µM of platinum compound was added. The dishes were incubated for another 2 h to allow uptake of the compounds by the attached cells. The media was removed and dishes washed again with 3 mL of PBS. The cells on the dishes were resuspended using 500 µL of trypsin and collected into centrifuge tubes. The cell number in each tube was counted using a hemocytometer. The cells were chemically digested using 300 µL of concentrated HNO_3. The samples were left to further digest at room temperature for 16 h after which they were diluted by adding 2.7 mL of 2% HNO_3 and 0.5% HCl (in ddH_2O) solution prior to ICP-MS quantification.

For ICP-MS calibration, a platinum standard series with 0.5, 1, 5, 10, 25, 50, 100, 200 ppb concentrations was prepared in 2% HNO_3 and 0.5% HCl (in ddH_2O). Aside from the standards and the digested cell samples, solvent blanks and blanks without platinum compounds were also included in the analysis. Quantification was carried out using an Agilent Technologies 7700 series ICP-MS instrument (plasma gas flow 15 L/min, nebulizer pump speed 0.3 rps, spectrum acquisition mode, 100 sweeps per sample, 3 replicates per sample, general purpose plasma

mode). A 10 ppb concentration of ^{209}Bi solution was used as the instrument internal standard. The ^{195}Pt isotope was used for detection since has minimal polyatomic interference [143]. Data were collected under high energy He tune mode in which the internal standard signal was stable and the R value for the calibration curve was closest to 1. For quality control, a 10 ppm standard was run after the samples.

CHAPTER 3

CHARACTERIZATION OF NON-CANONICAL ADDUCTS FORMED BY AMINO ACID-LINKED PLATINUM(II) COMPOUNDS‡

‡Nucleoside level studies are adapted from Kimutai B, He CC, Roberts A, Jones ML, Bao X, Jiang J, Yang Z, Rodgers MT, Chow CS (2019) J Biol Inorg Chem 24:985-997.

3.1 Abstract

Cisplatin (cisPt) is an antitumor drug that preferentially coordinates and forms adducts with deoxyguanosine (dGuo) residues within DNA. These adducts inhibit important cellular functions and ultimately cause cancer cell death. Despite its success as an anticancer drug, cisPt has a number of drawbacks that reduce its efficacy, including repair of adducts and drug resistance. To overcome these problems, other approaches such as development of compounds that form non-canonical adducts by coordinating to other purine nucleobases, including those found in RNA can be pursued. The synthesized amino acid-linked platinum(II) (AAPt) compounds of alanine, ornithine, and arginine (AlaPt, OrnPt, and ArgPt, respectively) have unique reactivities that result in formation of non-canonical adducts with adenosine or deoxyadenosine (Ado or dAdo) residues. In this chapter, the non-canonical adducts formed by the AAPt compounds with nucleosides/oligonucleotides were characterized. Nucleoside-level adducts were separated by HPLC on C18, then characterized by NMR spectroscopy and mass spectrometry (in collaboration with Dr. M. T. Rodgers' lab). The chosen AAPt compounds form predominantly monofunctional adducts by reacting at the N1/N3, or N7 positions of purine nucleobases. The AAPt adducts with oligonucleotides were also isolated by HPLC and characterized by matrix-assisted laser desorption ionization mass spectrometry (MALDI-MS) and liquid chromatography mass spectrometry (LC-MS). The AAPt compounds were observed to form a variety of adduct types with oligonucleotides, including monofunctional, doubly platinated, and bifunctional adducts.

3.2 Introduction

The antitumor drug cisPt platinates neighboring deoxyguanosine (dGuo) residues of DNA by coordinating at their N7 positions and forming bifunctional adducts [18, 37-38]. These adducts alter the DNA helical structure and inhibit important biological processes such as replication and transcription [11]. The adducts trigger a number of cellular responses, including cell cycle arrest, DNA repair, and apoptosis [1]. Despite its success, the application of cisPt as an anticancer drug is limited by cellular resistance and adverse side effects such as nephrotoxicity [69-71]. Resistance, which is caused by factors such as DNA repair and reduced accumulation of drug, enables cancer cells to survive cisPt treatment [71]. Resistance and adverse toxicity can be circumvented by developing other platinum-based compounds that have altered reaction profiles. Platinum analogues may coordinate with DNA sites that are not platinated by cisPt or target other biomolecules such as RNA. These analogues may therefore exhibit unique mechanisms of action that avert resistance, especially when the adducts cause irreparable damage [55-56, 29]. Therefore, the types of adducts formed by platinum-based compounds are important in their cytotoxic mechanism, as exhibited by cisPt-DNA bifunctional adducts that bend the DNA helix and trigger a cascade of events leading to apoptosis [37]. The adducts formed by cisPt or its analogues can be analyzed by using various chemical and analytical methods.

As introduced previously in **Chapter 1**, there are several potential sites in the DNA where cisPt can platinate with varying degrees of preference (**Fig. 3.1**). At these nucleoside residues, cisPt coordinates with nitrogen atoms. The preferred site for cisPt coordination is the N7 position of dGuo [37-38, 10]. This site is situated in the major groove of the DNA, which is highly accessible compared to sites in the minor groove such as N3 [18, 39]. CisPt may form intrastrand or interstrand adducts, depending on whether coordination occurs on the same strand or separate strands, respectively [18, 41]. Adducts can also be defined as monofunctional, bifunctional, or doubly platinated, depending on the platinum:nucleoside ratio (*i.e.*, 1:1, 1:2, or 2:1, respectively).

It has been reported that 90–95% of cisPt-DNA adducts are intrastrand cross-links. whereas the rest are a combination of interstrand cross-links and monofunctional adducts [37, 41].

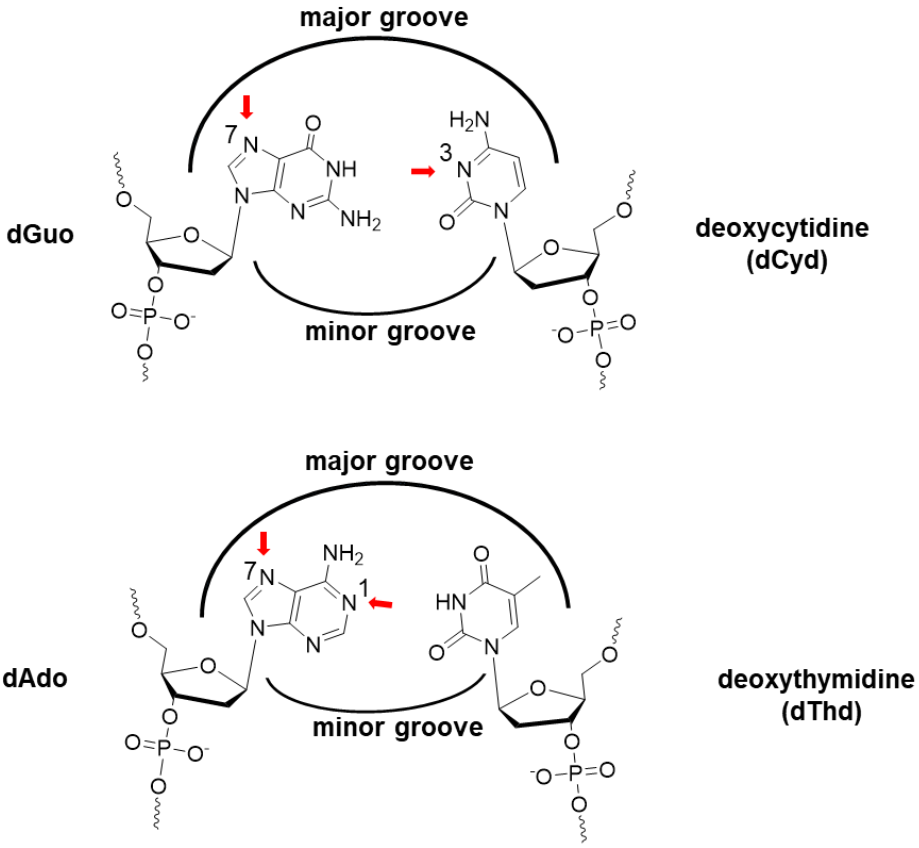

Figure 3.1. Possible coordination sites for cisPt in DNA. The preferred coordination site is dictated by accessibility and nucleophilicity. Arrows point at potential atoms that coordinate with cisPt. The N7 atom of dGuo is preferred since it is in the major groove and more nucleophilic than other DNA sites.

Formation of cisPt adducts with DNA/RNA is influenced by a number of factors (*e.g.*, coordination type and hydrogen-bonding properties) associated with the non-leaving group ligand [35-36]. These factors influence the target preferences and the types of platinum adducts formed with DNA or RNA. For example, hydrogen-bonding interactions are implicated in the preferential coordination of cisPt to dGuo [27]. This preference is because during the transition state, cisPt forms a strong hydrogen bond between its ammine ligand and the oxo at the 6 position of dGuo [27]. In contrast, formation of the cisPt-Ado adduct is less favored because Ado has an amine at

the 6 position, which cannot hydrogen bond with cisPt [27]. The type of ligands associated with cisPt (or other platinum-based compounds) may also affect several factors associated with the adduct structures due to unique interactions with the nucleobase functional groups. These factors include nucleoside platination sites (such as N1, N3, or N7) and geometric or constitutional isomers [105].

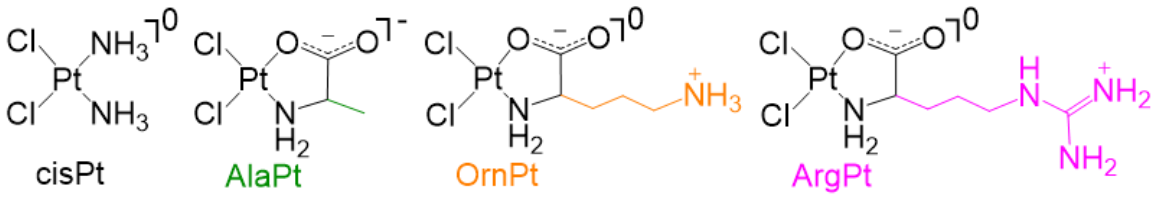

Figure 3.2. **The structures of cisPt and amino acid-linked platinum(II) (AAPt) compounds.** The structures of AAPt compounds consist of a chelated amino acid and two chlorido ligands coordinated to the platinum center.

Previous studies in our lab showed that AAPt compounds such as OrnPt and ArgPt form adducts at Ado residues in RNA [106]. In this chapter, the non-canonical adducts formed by AlaPt, OrnPt, and ArgPt (**Fig. 3.2**) with nucleosides and oligonucleotides were characterized to determine their adduct types and sites of platination. AAPt (or cisPt) compounds were first activated to form the monoaquated species, and then reacted with target nucleosides/oligonucleotides (**Scheme 3.1**). The reactions could in formation of different types of products that potentially vary in composition, platination site (N1, N3, or N7), and geometry. These reactions and products formed were monitored using HPLC. The HPLC fractions corresponding to adducts were isolated and characterized using mass spectrometry and NMR spectroscopy. These characterizations are crucial for understanding how functional groups of the amino acid ligands of AAPt compounds and their chemical features relate to their reactivities and biological target preferences.

Scheme 3.1. Aquation of platinum compounds and subsequent platination of purine residues. Possible coordination sites are highlighted in blue (N7) and red (N1 and N3).

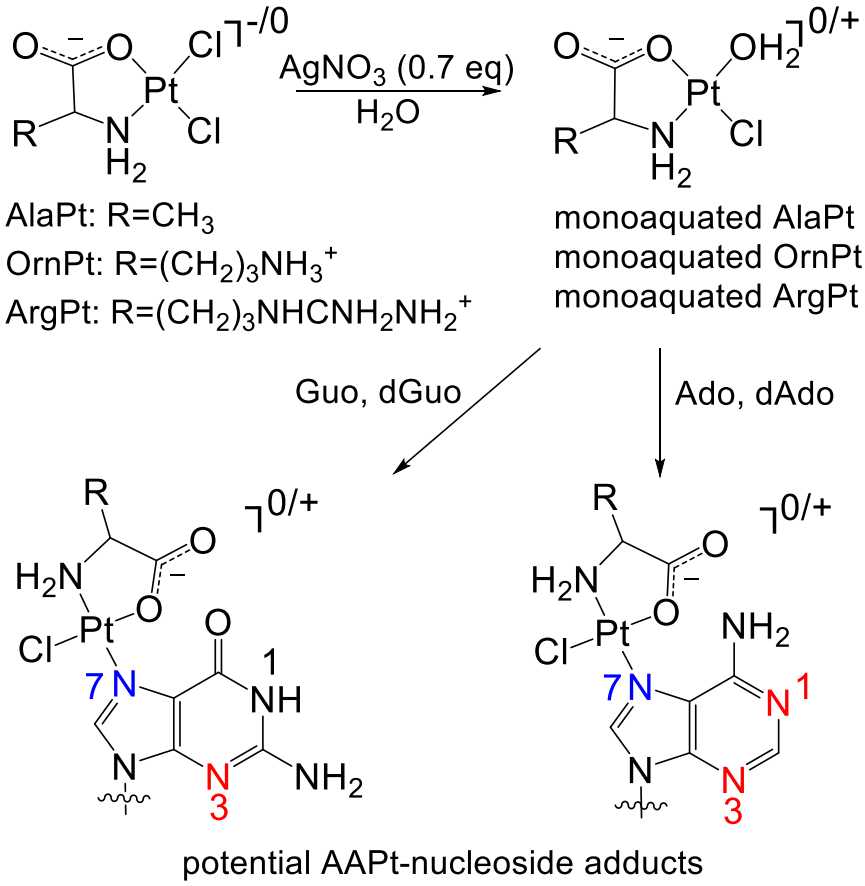

3.3 Results and discussion

3.3.1 Characterization of AAPt-nucleoside adducts

When cisPt coordinates with DNA, it predominantly platinates the N7 position of dGuo [101-102]. In this thesis work, we sought to characterize the non-canonical adducts formed by AAPt compounds and determine their binding site preferences. The structures and corresponding chemical properties of various AAPt compounds may alter the preferred sites of reactivity versus those targeted by cisPt. Mass spectrometry was used to determine the composition and type (*e.g.*, monofunctional, bifunctional, or doubly platinated) of adducts formed by the platinum-based

compounds, and ^{1}H-NMR spectroscopy was used for characterization of the platination sites (*e.g.*, N1, N3, or N7) on the nucleoside.

The reactions of nucleosides with the monoaquated AAPt compounds result in the formation of one or more adducts with longer (AlaPt and ArgPt adducts) or shorter (OrnPt adducts) retention times on a C18 column relative to the unreacted nucleosides (**Fig. 3.3A**). Only one AAPt-Guo adduct was expected based on the known preference for coordination of the aquated cisPt at the dGuo N7 position [101, 144]. Previously in our lab, Dr. Xun Bao characterized the products formed by platination of the Guo nucleoside [145]. HPLC and mass spectrometric analysis showed that platination (by cisPt or OrnPt) led to formation of one major product. NMR spectroscopy was used to determine that platination occurs at the N7 position of Guo [145].

The reactions of Ado with the monoaquated AAPt compounds result in the formation of one or more adducts with longer (AlaPt and ArgPt adducts) or shorter (OrnPt adducts) retention times on a C18 column relative to the unreacted nucleosides (**Fig. 3.3B**). Monoaquated AlaPt reacts with Ado to form two main products (distinct HPLC peaks), referred to as AlaPt-Ado$_{N1/N3}$ and AlaPt-Ado$_{N7}$ (**Fig. 3.3B**). These adducts have longer retention times compared to Ado due to decreased polarity associated with the alanine ligand. Monoaquated OrnPt reacts with Ado to form two major products, OrnPt-Ado$_{N1/N3}$ and OrnPt-Ado$_{N7}$, which have shorter retention times than Ado on C18. Monoaquated ArgPt also reacts with Ado to form three major products, ArgPt-Ado$_{N1/N3}$, ArgPt-Ado$_{N7}$, and ArgPt-Ado$_{mix}$, which have longer retention times than Ado. Although L-ornithine and L-arginine amino acids both have polar side chains (amine and guanidinium, respectively), the adducts formed by their respective AAPt derivatives have different behaviors on the C18 column. The adducts of OrnPt have shorter retention times compared to the adducts of ArgPt. This observation suggests that OrnPt and ArgPt may have different types of structures (N,O vs. N,N) as discussed in **Section 2.4.2**. Furthermore, the two compounds may form adducts that adopt different structural conformations that position their functional groups for favorable interactions or to avoid steric clash. Mass analysis of the fractions obtained from HPLC C18

separation of the AlaPt-Ado, OrnPt-Ado, and ArgPt-Ado adducts was carried out in collaboration with the Rodgers' laboratory using FT-ICR MS equipped with an ESI source.

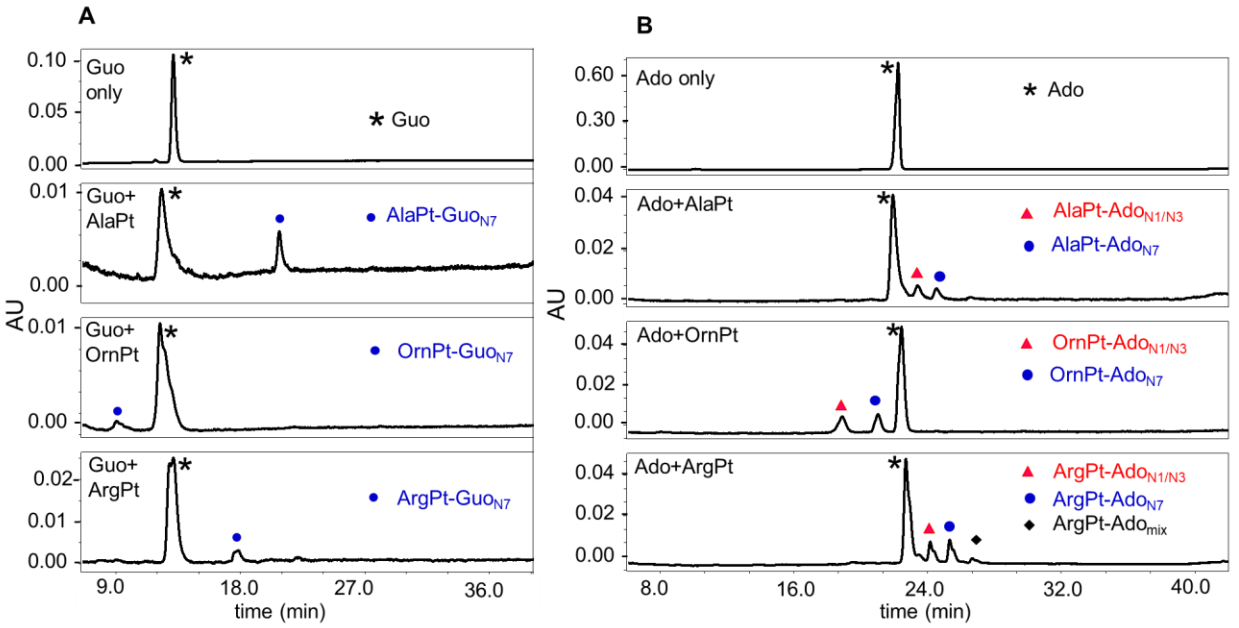

Figure 3.3. HPLC analysis (C18) of platination products. The AAPt-Guo (**A**) or AAPt-Ado (**B**) adduct profiles following reactions with monoaquated AlaPt, OrnPt, or ArgPt are shown. The peaks are labeled as follows; black asterisks for the free nucleosides, blue circles for N7 platination adducts, and red triangles for N1/N3 platination adducts. The controls (unreacted Guo or Ado) are shown as the top traces in (**A**) and (**B**).

Mass analysis of the compounds in the two fractions obtained from HPLC C18 separation of the AlaPt adducts (**Fig. 3.3B**), referred to as AlaPt-Ado$_{N1/N3}$ and AlaPt-Ado$_{N7}$, reveals that they have the same mass, charge, and isotopic distribution, corresponding to a monofunctional adduct, $[Pt(Ado)(Ala)(Cl)+H]^+$ (**Fig. 3.4**). Because they have the same mass, the two adducts are constitutional isomers that may vary at the site of platination (N1, N3, or N7). For the geometric isomers, we expect that the structures shown in **Scheme 3.1** are preferred because of the *trans* effect [146], but these structures still need to be confirmed experimentally. In addition, it would be of interest to understand how the binding types of platinum-based compounds (*i.e.,* (N,N) vs. (N,O)) impact the adduct identities. Other species formed by the loss and addition of neutral molecules are observed (**Fig. 3.5**). These species include $[Pt(Ado)(Ala)(NH_3)]^+$,

$[Pt(Ado)(Ala)(CH_3CO_2H)]^+$, and $[Pt(Ado)(Ala)(CH_3CN)(NH_3)]^+$, which form as a result of the monofunctional adduct losing HCl and generating a complex with NH_3, CH_3CO_2H, or CH_3CN from the HPLC buffer, respectively. Due to the soft ionization conditions offered by ESI, it is not surprising to observe adduction of NH_3 [147].

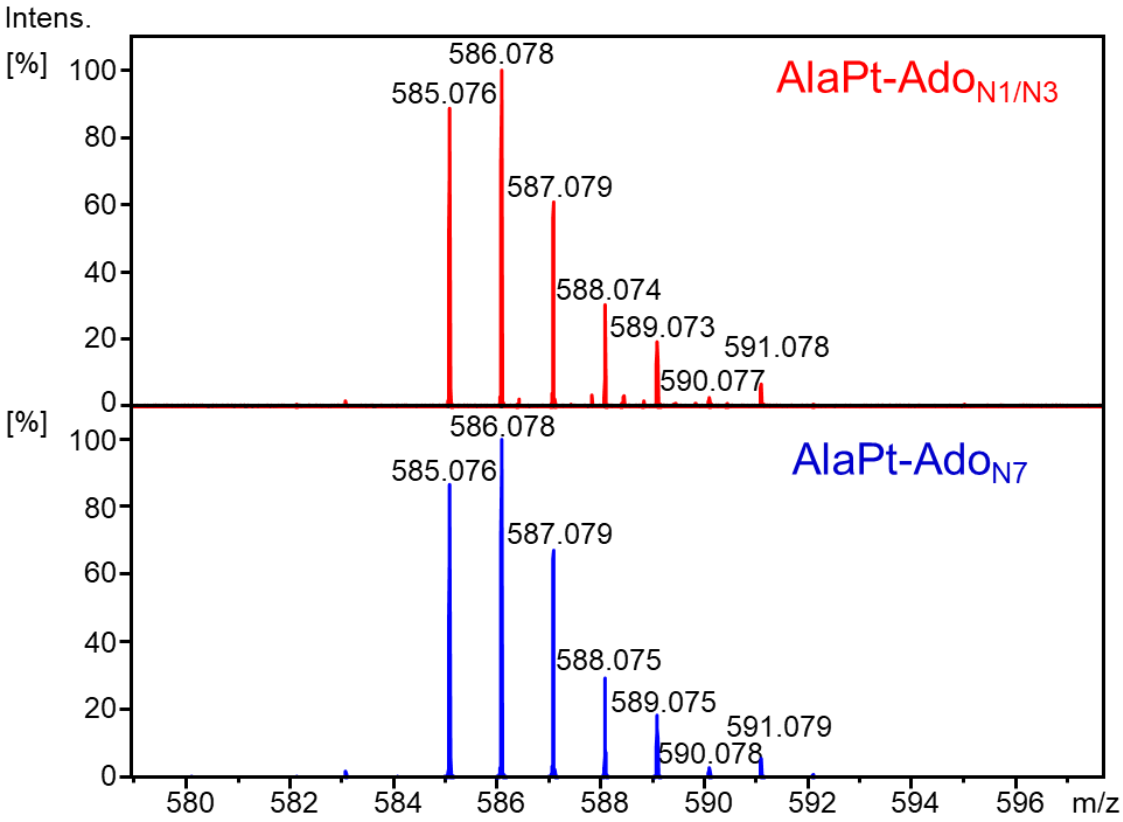

Figure 3.4. Mass spectra of the AlaPt-Ado$_{N1/N3}$ and AlaPt-Ado$_{N7}$ fractions. For both fractions, the monofunctional adduct species $[Pt(Ado)(Ala)(Cl)+H]^+$ is observed with the predicted isotopic distribution. The spectra were obtained by Dr. C. C. He in Dr. M. T. Rodgers' lab.

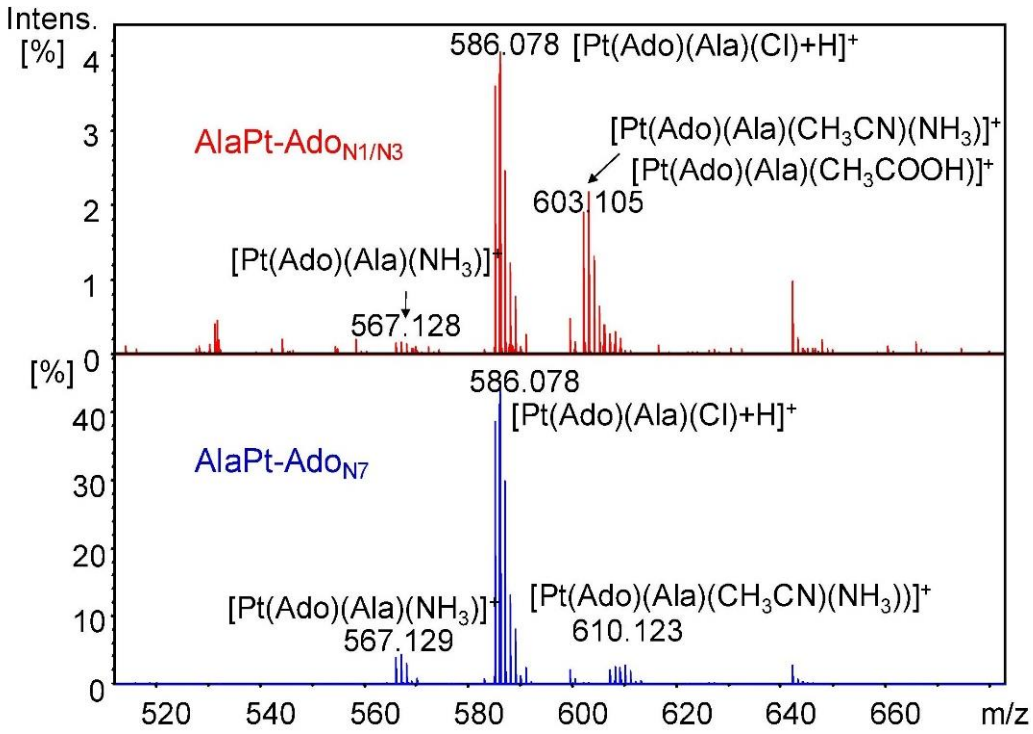

Figure 3.5. Wide range mass spectra of the AlaPt-Ado fractions. Both of the mass spectra for AlaPt-Ado$_{N1/N3}$ (red) and AlaPt-Ado$_{N7}$ (blue) contain the monofunctional adduct species, [Pt(Ado)(Ala)(Cl)+H]$^+$. Other adducts are formed by the loss or addition of neutral molecules to the monofunctional adduct. The spectra were obtained by Dr. C. C. He in Dr. M. T. Rodgers' lab.

Similar to that found for the reactions of AlaPt with Ado, compounds in the OrnPt-Ado HPLC fractions (**Fig. 3.3**), referred to as OrnPt-Ado$_{N1/N3}$ and OrnPt-Ado$_{N7}$, have the same mass, charge, and isotopic distribution corresponding to a monofunctional adduct [Pt(Ado)(Orn)(Cl)]$^+$ (**Fig. 3.6**), *i.e*., the two adducts are constitutional isomers with variation at the site of coordination (*e.g*., N1, N3, or N7) or varying geometries as discussed for AlaPt. Species assigned as [Pt(Ado)(Orn)(NH$_3$)–H]$^+$ and [Pt(Ado)(Orn)(CH$_3$CN)(NH$_3$)–H]$^+$ are also observed, suggesting that ligand substitution of one of the chlorido ligands is facile in solution (**Fig. 3.7**).

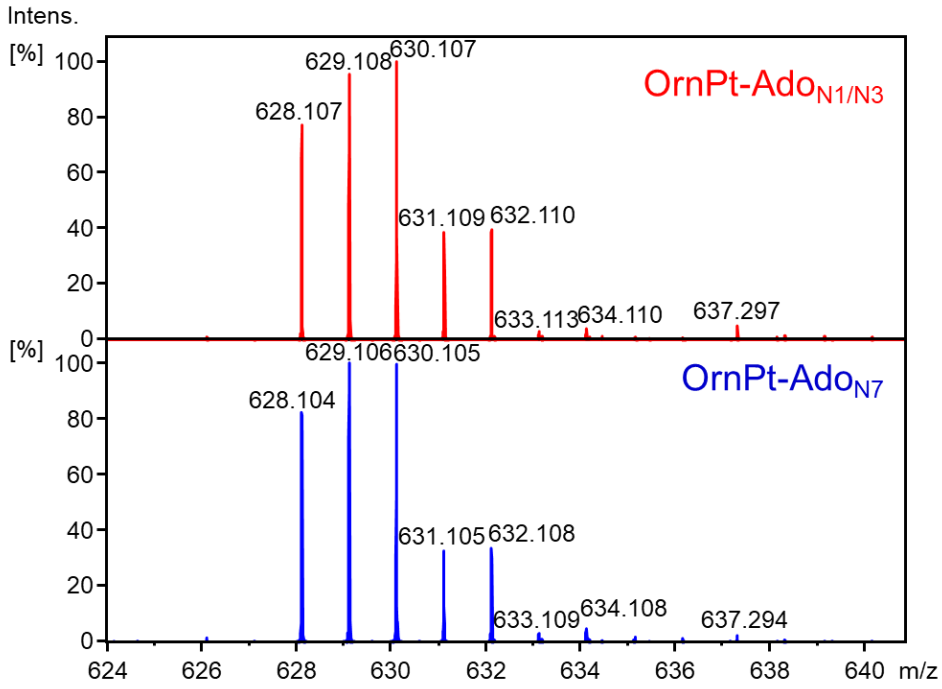

Figure 3.6. Mass spectra of the OrnPt-Ado$_{N1/N3}$ and OrnPt-Ado$_{N7}$ fractions. For both fractions, the monofunctional adduct species $[Pt(Ado)(Orn)(Cl)]^+$ is observed with the predicted isotopic distribution. The spectra were obtained by Dr. C. C. He in Dr. M. T. Rodgers' lab.

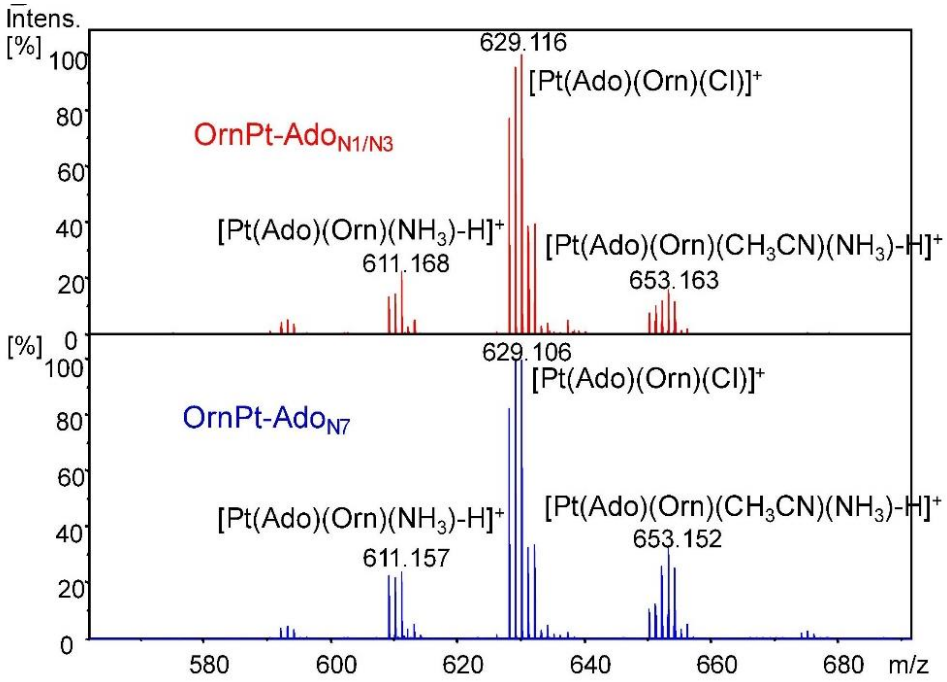

Figure 3.7. Wide range mass spectra of the OrnPt-Ado fractions. Both of the mass spectra for OrnPt-Ado$_{N1/N3}$ (red) and OrnPt-Ado$_{N7}$ (blue) contain the monofunctional adduct species, $[Pt(Ado)(Orn)(Cl)]^+$. Other adducts are formed by the loss or addition of neutral molecules to the monofunctional adduct. The spectra were obtained by Dr. C. C. He in Dr. M. T. Rodgers' lab.

The ArgPt reaction with Ado results in three product HPLC fractions (**Fig. 3.3**). The first two product fractions, referred to as ArgPt-Ado$_{N1/N3}$ and ArgPt-Ado$_{N7}$, have the same mass, charge, and isotopic distribution corresponding to a monofunctional adduct $[Pt(Ado)(Arg)(Cl)]^+$ (**Fig. 3.8**), *i.e.*, the two adducts are constitutional isomers with variation at the site of coordination (*e.g.*, N1, N3, or N7) or varying geometries as discussed for the AlaPt-Ado and OrnPt-Ado adducts. Species assigned as $[Pt(Ado)(Arg)(H_2O)–H]^+$ are also observed, suggesting that ligand substitution of one of the chlorido ligands with H_2O is facile in solution (**Fig. 3.9**). The third fraction, referred to as ArgPt-Ado$_{mix}$, is a mixture of bifunctional ($[Pt(Ado)_2(Arg)]^{2+}$) and doubly platinated ($[Ado(Pt(Arg)Cl)_2]^{2+}$) adducts (**Fig. 3.10**).

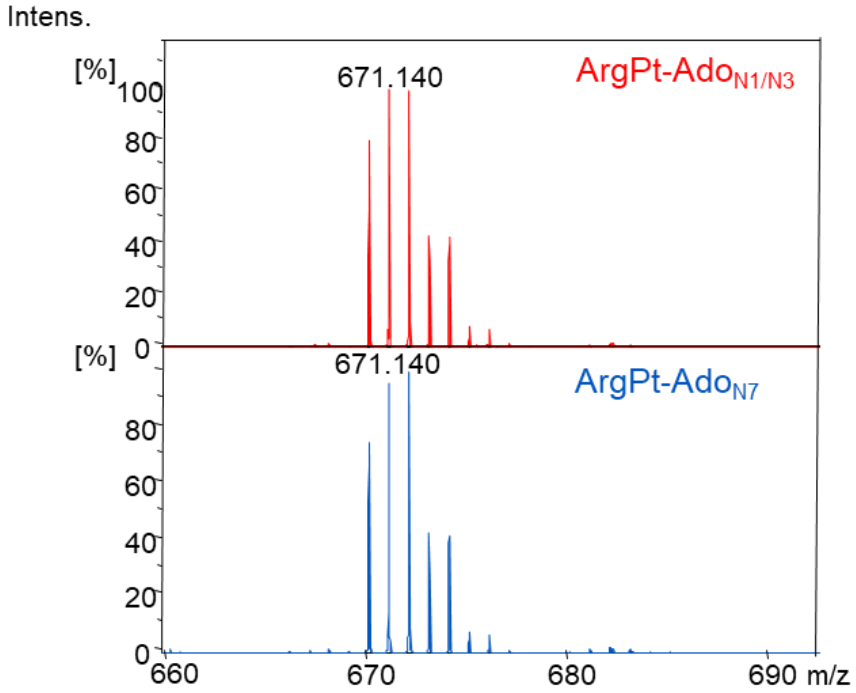

Figure 3.8. Mass spectra of the ArgPt-Ado$_{N1/N3}$ and ArgPt-Ado$_{N7}$ fractions. For both fractions, the monofunctional adduct species $[Pt(Ado)(Arg)(Cl)+H]^+$ is observed with the predicted isotopic distribution. The spectra were obtained by Dr. C. C. He in Dr. M. T. Rodgers' lab.

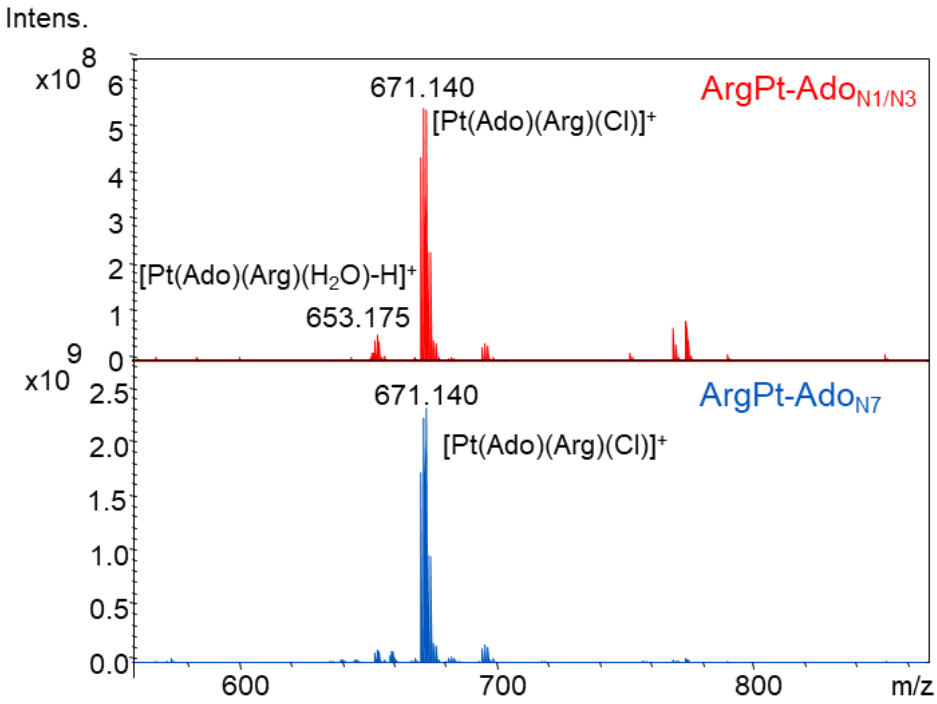

Figure 3.9. Wide range mass spectra of the ArgPt-Ado fractions. Both of the mass spectra for ArgPt-Ado$_{N1/N3}$ (red) and ArgPt-Ado$_{N7}$ (blue) contain the monofunctional adduct species, $[Pt(Ado)(Arg)(Cl)+H]^+$. An adduct, $[Pt(Ado)(Arg)(H_2O)-H]^+$, is also formed through ligand substitution of one of the chlorido ligands with H_2O. The spectra were obtained by Dr. C. C. He in Dr. M. T. Rodgers' lab.

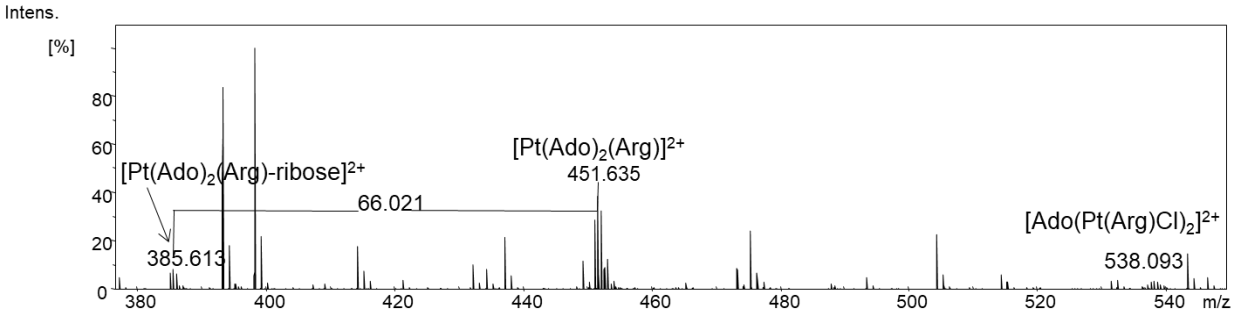

Figure 3.10. Mass spectrum of ArgPt-Ado$_{mix}$ fraction. ArgPt-Ado$_{mix}$ consists of a mixture of bifunctional ($[Pt(Ado)_2(Arg)]^{2+}$) and doubly platinated ($[Ado(Pt(Arg)Cl)_2]^{2+}$) adducts. A fragment of the bifunctional adduct ($[Pt(Ado)_2(Arg)\text{-ribose}]^{2+}$) is also observed, and formed due to the loss of one ribose sugar. All of the adducts are multiply charged and observed in the 2+ states. The spectrum was obtained by Dr. C. C. He in Dr. M. T. Rodgers' lab.

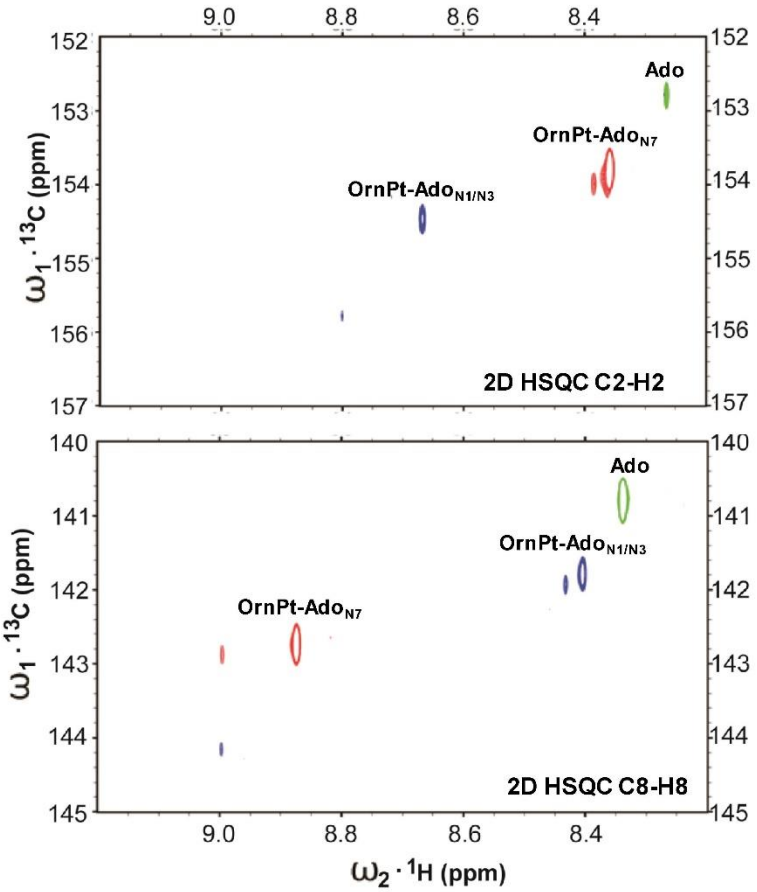

Figure 3.11. The 2D heteronuclear single quantum correlation (HSQC) of OrnPt-Ado$_{N7}$ (top) and OrnPt-Ado$_{N1/N3}$ (bottom). In reference to the signal for Ado C2-H2 (top) [141], the major signal for OrnPt-Ado$_{N1/N3}$ exhibits platination at the N1 (or N3) position. On the other hand, in reference to the Ado C8-H8 (bottom) [141], the major peak for OrnPt-Ado$_{N7}$ exhibits platination at the N7 position. The minor signals observed are for doubly platinated or bifunctional adducts that elute with the major peaks during HPLC separation of the adducts (experiment performed by Dr. Jun Jiang and Dr. Xun Bao).

NMR analysis was used to assign the platination sites of the adducts [138]. Two-dimensional (2D) heteronuclear single quantum correlation (HSQC) spectroscopy was employed to assign the peaks for the H8 and H2 protons of OrnPt-Ado$_{N1/N3}$ and OrnPt-Ado$_{N7}$ (**Fig. 3.11**). ^{1}H-NMR spectroscopy was then employed to determine the specific platination sites of the AlaPt-Ado, OrnPt-Ado, and ArgPt-Ado adducts by comparison of the chemical shifts of the H2 and H8 protons of Ado (**Figs. 3.12, 3.13,** and **3.14**). Compared to the chemical shifts of the H2 and H8 protons of Ado, the corresponding peaks for the species assigned as AlaPt-Ado$_{N1/N3}$ are shifted downfield by 0.4 and 0.1 ppm, respectively (**Table 3.1**). The greater change in chemical shift of

H2 compared to H8 suggests platination at the N1 position in AlaPt-Ado$_{N1/N3}$ because of its proximity to H2 [144, 148]. However, platination at N3 of Ado cannot be ruled out because that adduct would also cause a downfield shift of H2. ^{1}H-NMR analysis of AlaPt-Ado$_{N7}$ shows the peaks assigned as H2 and H8 shifting downfield by 0.1 and 0.5 ppm, respectively (**Table 3.1**), suggesting that platination occurs at the N7 position for this adduct.

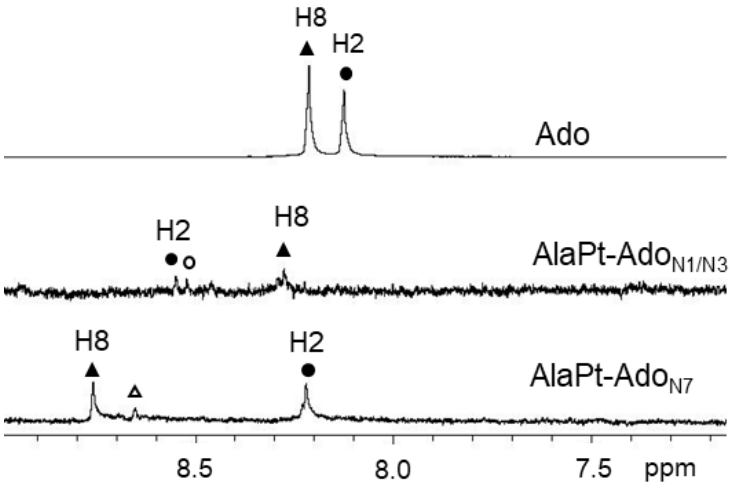

Figure 3.12. Aromatic region of ^{1}H-NMR spectra of AlaPt-Ado HPLC fractions. Ado (top), AlaPt-Ado$_{N1/N3}$ (middle) and AlaPt-Ado$_{N7}$ (bottom); proton signals assigned as H8 and H2 are noted with triangles and circles, respectively. The open circles and triangles are assigned as protons likely from bisaquated AlaPt-Ado species. The extent of proton signal shift is dependent on proximity of the platination site. The data were collected with assistance from Evan Jones in the Lumigen Instrument Center.

Table 3.1. Downfield shifts of protons (in ppm) of AlaPt-Ado adducts relative to Ado protons

	H2	H8
AlaPt-Ado$_{N1/N3}$[a]	0.4	0.1
AlaPt-Ado$_{N7}$[b]	0.1	0.5

[a]monofunctional [Pt(Ado)(Ala)(Cl)] with N1/N3 platination

[b]monofunctional [Pt(Ado)(Ala)(Cl)] with N7 platination

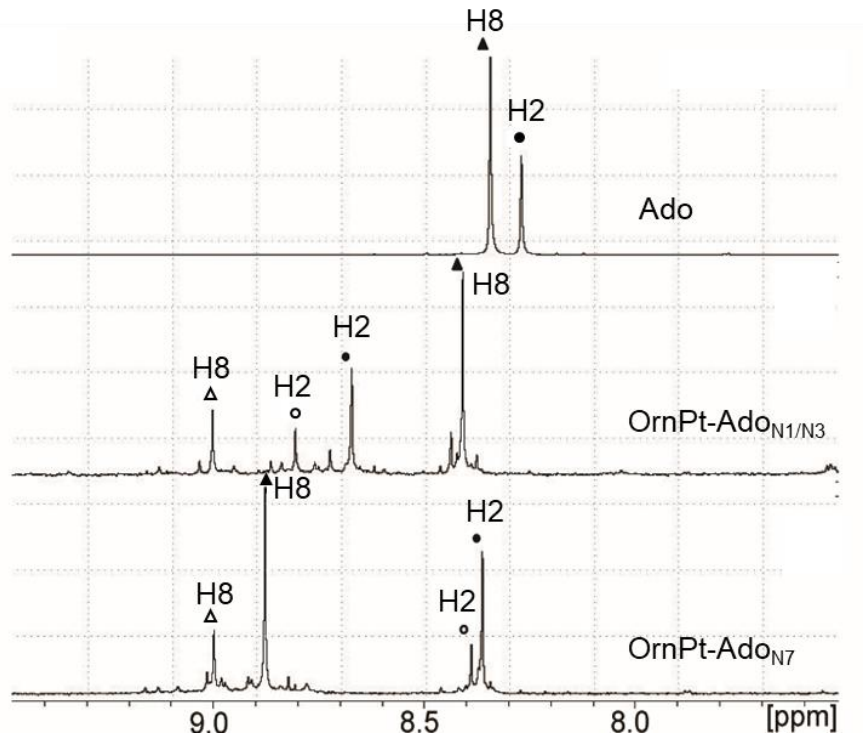

Figure 3.13. Aromatic region of ^{1}H-NMR spectra of OrnPt-Ado HPLC fractions. Ado (top), OrnPt-Ado$_{N1/N3}$ (middle) and OrnPt-Ado$_{N7}$ (bottom); proton signals for H8 and H2 are noted with triangles and circles, respectively. The open circles and triangles are assigned as protons from doubly platinated and bifuctional species that have also been confirmed by mass spectrometry. The extent of proton signal shift is dependent on proximity to the platination site (experiment performed by Dr. Jun Jiang and Dr. Xun Bao).

Table 3.2. Downfield shifts of protons (in ppm) of OrnPt-Ado adducts relative to Ado protons

	H2	H8
OrnPt-Ado$_{N1/N3}$[a]	0.5	0.1
OrnPt-Ado$_{N7}$[b]	0.1	0.5

[a]monofunctional [Pt(Ado)(Orn)(Cl)] with N1/N3 platination

[b]monofunctional [Pt(Ado)(Orn)(Cl)] with N7 platination

The analysis of platination sites on the monoaquated OrnPt adducts is similar to that of the AlaPt adducts (**Fig. 3.13**). In the ^{1}H-NMR spectrum of OrnPt-Ado$_{N1/N3}$, the major peak corresponding to H8 (closed triangle) shows a small chemical shift change (0.1 ppm), whereas the other major peak corresponding to H2 (closed circle) exhibits a 0.5 ppm downfield shift (**Table**

3.2), which suggests that the metal center is most likely coordinated to the N1 (or N3) position of Ado [149]. For OrnPt-Ado$_{N7}$, both peaks for H8 (triangles, open and closed for major products) are shifted downfield by approximately 0.5 ppm, while the corresponding changes in the H2 chemical shifts are only 0.1 ppm (**Fig. 3.13** and **Table 3.2**). The stronger downfield shift observed for the two H8 signals suggests that platination occurs on the neighboring N7 for both products. Therefore, the larger chemical shift change of the H2 peak is consistent with N1/N3 platination of the HPLC fraction assigned as OrnPt-Ado$_{N1/N3}$, whereas OrnPt-Ado$_{N7}$ is assigned as having N7 platination due to the larger chemical shift change of the H8 peak.

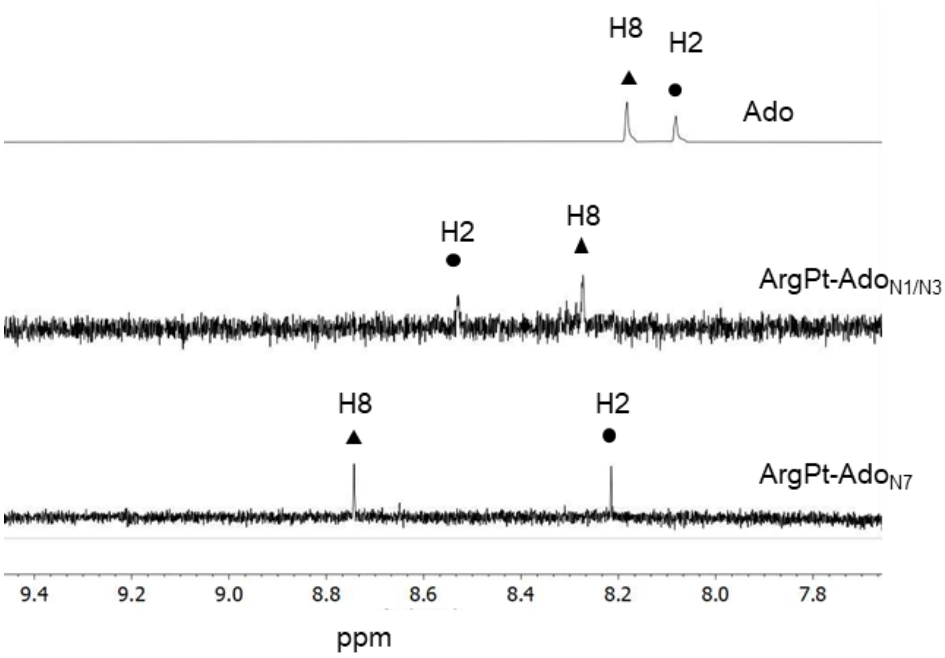

Figure 3.14. Aromatic region of ^{1}H-NMR spectra of ArgPt-Ado HPLC fractions. Ado (top), ArgPt-Ado$_{N1/N3}$ (middle) and ArgPt-Ado$_{N7}$ (bottom); proton signals assigned as H8 and H2 are noted with triangles and circles, respectively. The extent of proton signal shift is dependent on proximity to the platination site.

Table 3.3. Downfield shifts of protons (in ppm) of ArgPt-Ado adducts relative to Ado protons

	H2	H8
ArgPt-Ado$_{N1/N3}$[a]	0.5	0.1
ArgPt-Ado$_{N7}$[b]	0.2	0.6

[a]monofunctional [Pt(Ado)(Arg)(Cl)] with N1/N3 platination

[b]monofunctional [Pt(Ado)(Arg)(Cl)] with N7 platination

The platination sites on the first two adducts of monoaquated ArgPt are also similar to that of the AlaPt and OrnPt adducts (**Fig. 3.14**). Compared to the chemical shifts of H2 and H8 protons of Ado, the corresponding peaks for the species assigned as ArgPt-$Ado_{N1/N3}$ are shifted downfield by 0.5 and 0.1 ppm, respectively (**Table 3.3**). The greater change in chemical shift of H2 compared to H8 suggests that platination occurs at the N1 or N3 position in ArgPt-$Ado_{N1/N3}$ because of its proximity to H2. The ^{1}H-NMR spectrum of ArgPt-Ado_{N7} shows that the peaks assigned as H2 and H8 are shifted downfield by 0.2 and 0.6 ppm, respectively (**Table 3.3**). This change in chemical shift suggests that for the ArgPt-Ado_{N7} product, platination occurs at the N7 position.

3.3.2 Characterization of AAPt-RNA adducts

The local environment of an oligonucleotide may affect the coordination of a platinum-based compound. Elucidation of nucleoside-level adducts provides information about coordination sites, adduct types, and influence of ligands in binding kinetics. However, the nucleotides surrounding the target nucleotide within the context of RNA or DNA oligonucleotides may also modulate the coordination and lead to different platination profiles. The interaction of AAPt compounds with non-canonical targets of cisPt was investigated using the oligonucleotide sequence 5′-UUAUU-3′. This sequence was selected because cisPt and AAPt compounds have low reactivity with Thd (dT) and Urd (U) residues [106, 138]. Therefore, the presence of only one preferred residue (Ado (A)) directs the platination to a single site.

MALDI-MS and ESI-MS were used to determine the composition and type (*e.g.*, mono-, bifunctional, or doubly platinated) of non-canonical adducts formed by AAPt compounds with the 5′-UUAUU-3′ oligonucleotide. The purity of 5′-UUAUU-3′ was first determined by HPLC (C18) as shown in **Chapter 2** (**Fig. 2.22**), where the oligonucleotide was observed with only minor impurity peaks. The oligonucleotide was also further characterized by using MALDI mass spectrometry

(**Chapter 2, Fig. 2.23**). A peak was observed at m/z of 1571.7 Da/e, consistent with a calculated mass of 1571.2 Da for 5′-UUAUU-3′.

Reactions of monoaquated AAPt compounds with 5′-UUAUU-3′ result in formation of adducts with longer retention times on a C18 column relative to the unreacted oligonucleotide. Several reactions were carried out followed by HPLC isolation of the fractions to obtain enough of the products for mass analysis. The fractions obtained were characterized using MALDI-MS or ESI-MS. For the AlaPt reaction, a product peak (AlaPt-UUAUU-1) with a longer retention time than the unreacted 5′-UUAUU-3′ oligonucleotide was formed (**Fig. 3.15**). The HPLC isolated fraction was analyzed by MALDI-MS. However, platinum associated peaks were not observed in the spectrum, likely because of low sample concentration. The sample was reanalyzed an Orbitrap-MS equipped with an ESI source. A triply charged species with the predicted platinum isotopic distribution was observed at 594.073 Da/e (**Fig. 3.16**). This species is assigned as a monofunctional adduct in which one of the uridines is fragmented (base loss) during ionization (calculated exact mass is 1782.150 Da or 594.050 Da/e for the triply charged state)**.** The calculated exact mass of triply charged adduct with all the bases is 1892.161 Da. Since platinum compounds have low reactivity with Urd residues, it is most likely that this adduct involves RNA platination at the Ado residue (**Fig. 3.17**).

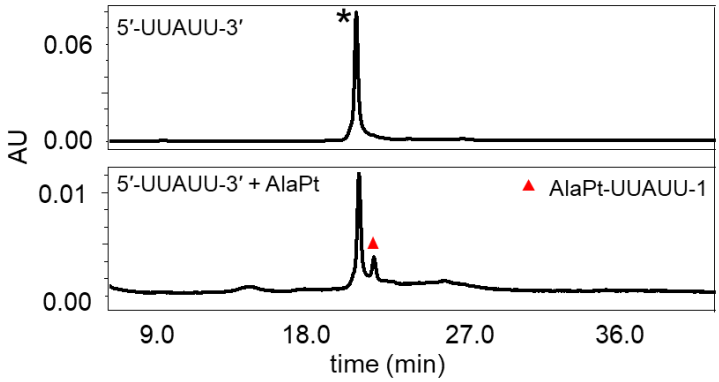

Figure 3.15. HPLC analysis (C18) of AlaPt-UUAUU platination products. The AlaPt-UUAUU adduct profile following reaction with monoaquated OrnPt is shown. A product, AlaPt-UUAUU-1, elutes with a retention time of 21.5 min. The unreacted 5′-UUAUU-3′ has a retention time of 20.5 min.

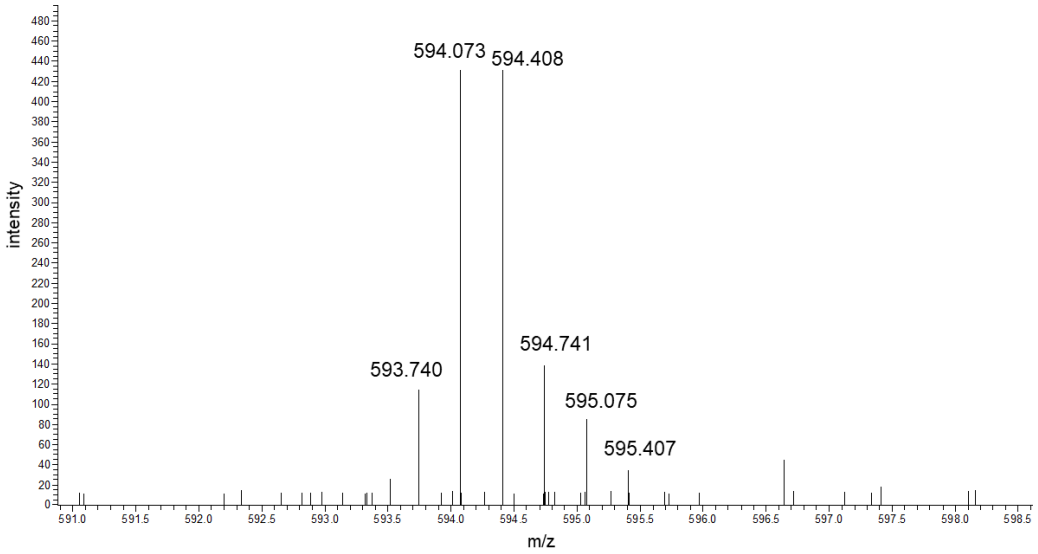

Figure 3.16. ESI mass spectrum of isolated AlaPt-UUAUU-1 product. A triply charged species, $[(M\text{-uracil})+Pt(Ala)Cl+3H]^{3+}$, with the predicted platinum isotopic distribution observed at 594.073 Da/e is assigned as a monofunctional adduct, with a loss of one uracil base. The calculated exact mass of the fragmented adduct is 1782.150 Da (594.050 Da/e for triply charged state), while the unfragmented adduct is 1892.161 Da.

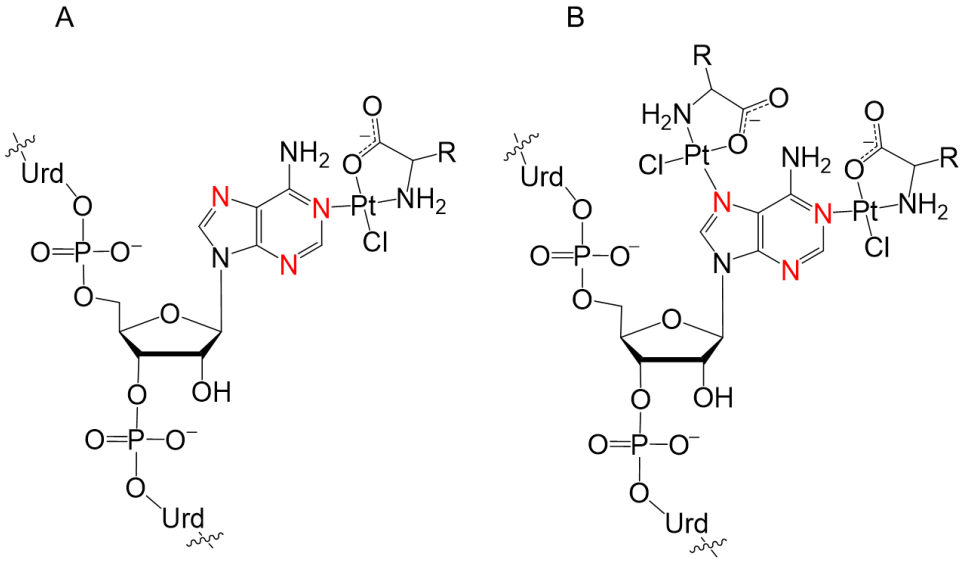

Figure 3.17. Adducts formed by AAPt compounds with 5′-UUAUU-3′ RNA. (**A**) A monofunctional adduct in which one AAPt molecule coordinates with the oligonucleotide at the Ado residue is shown. (**B**) A doubly platinated adduct in which two AAPt molecules coordinate with the oligonucleotide at the Ado residue is shown. Nitrogen atoms are color coded with red at possible sites of coordination.

The reaction of OrnPt with 5′-UUAUU-3′ results in formation of three distinct HPLC product peaks (OrnPt-UUAUU-1, OrnPt-UUAUU-2, and OrnPt-UUAUU-3) that have longer retention times (21.1, 23.0, and 24.0 min, respectively) than the unreacted 5′-UUAUU-3′ oligonucleotide (**Fig. 3.18**). HPLC fractions of the adducts were concentrated and mass analysis was carried out using MALDI-MS. The OrnPt-UUAUU-1 fraction has an observed m/z of 1933.8 Da/e, which is assigned as a monofunctional adduct (calculated exact mass is 1933.2 Da) (**Fig. 3.19**). An unplatinated 5′-UUAUU-3′ is also observed in the mass spectrum and could be formed if fragmentation of the adduct during ionization occurs. Unreacted 5′-UUAUU-3′ could also be present in the sample if there is incomplete HPLC peak separation (especially near the baseline) and residual unreacted 5′-UUAUU-3′ is collected together with the OrnPt-UUAUU-1 fraction.

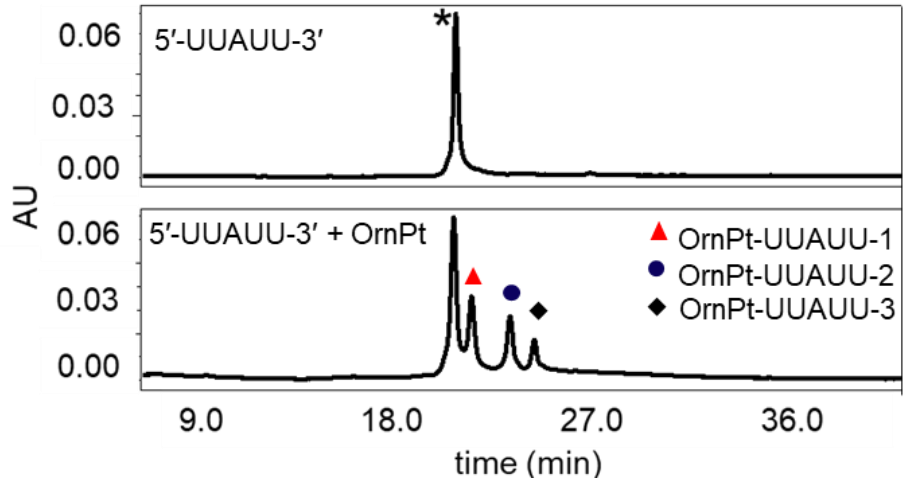

Figure 3.18. HPLC analysis (C18) of OrnPt-UUAUU platination products. The OrnPt-UUAUU adduct profile following reaction of 5′-UUAUU-3′ with monoaquated OrnPt is shown. Three products, OrnPt-UUAUU-1, OrnPt-UUAUU-2, and OrnPt-UUAUU-3, are formed with retention times of 21.1, 23.0, and 24.0 min, respectively. The unreacted 5′-UUAUU-3′ is shown as the top trace.

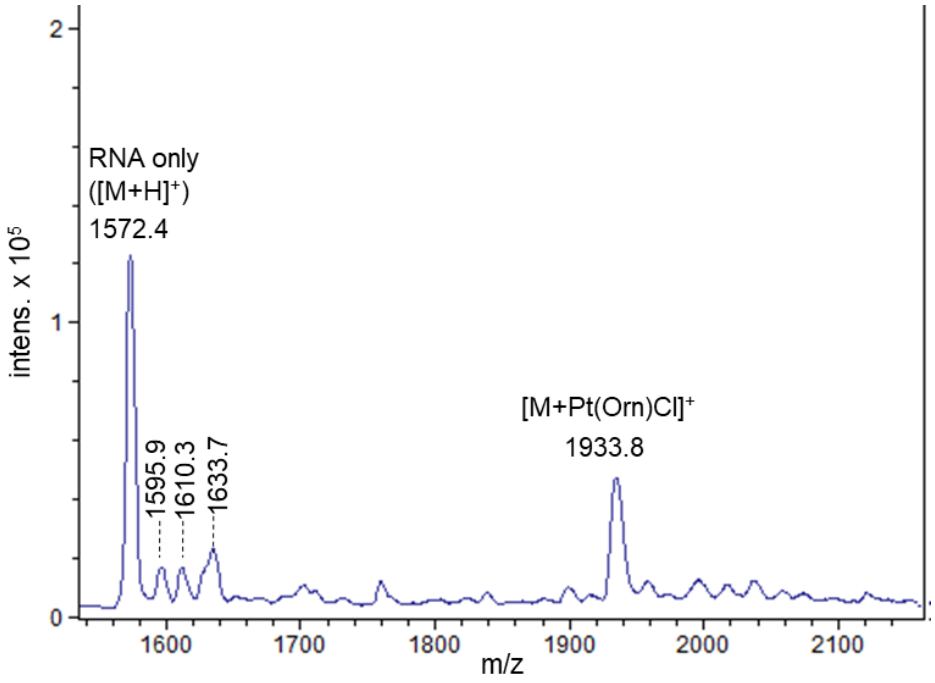

Figure 3.19. MALDI mass spectrum of HPLC isolated OrnPt-UUAUU-1 product. Analysis of HPLC isolated OrnPt-UUAUU-1 indicates an m/z of 1933.8 Da/e, consistent with a monofunctional adduct (calculated exact mass is 1933.2 Da). The unplatinated oligonucleotide (m/z 1572.4 Da/e) is also observed in the spectrum. Adducts of unplatinated oligonucleotide with Na+ (m/z 1595.9 Da/e), Na^++ NH_3 (m/z 1610.3 Da/e), and Na^++ K^+(m/z 1633.7 Da/e) are observed as well.

HPLC fractions for OrnPt-UUAUU-2 and OrnPt-UUAUU-3 peaks were combined during mass analysis due to incomplete separation of the two fractions in some of the HPLC isolations. MALDI-MS data show that the two fractions consist of multiple adducts including a monofunctional adduct observed at m/z 1933.4 Da/e (calculated mass is 1933.2 Da) and a doubly platinated adduct observed at m/z 2295.7 Da/e (calculated exact mass is 2295.2 Da) (**Fig. 3.20**). This result reveals that either the fraction of OrnPt-UUAUU-2 or OrnPt-UUAUU-3 contains a monofunctional adduct while the other contains the doubly platinated adduct. For the doubly platinated adduct structure, it is likely that both OrnPt molecules coordinate to different sites (N1, N3, or N7) of the Ado residue of the oligonucleotide (**Fig. 3.17**). Other minor peaks corresponding to a bisaquated adduct species (m/z 1916.4 Da/e), loss of chlorido ligands (m/z 1898.9 and 2260.1 Da/e), and

association with sodium ions (m/z 1956.6 and 1992.2 Da/e) are observed in the MALDI spectrum as well.

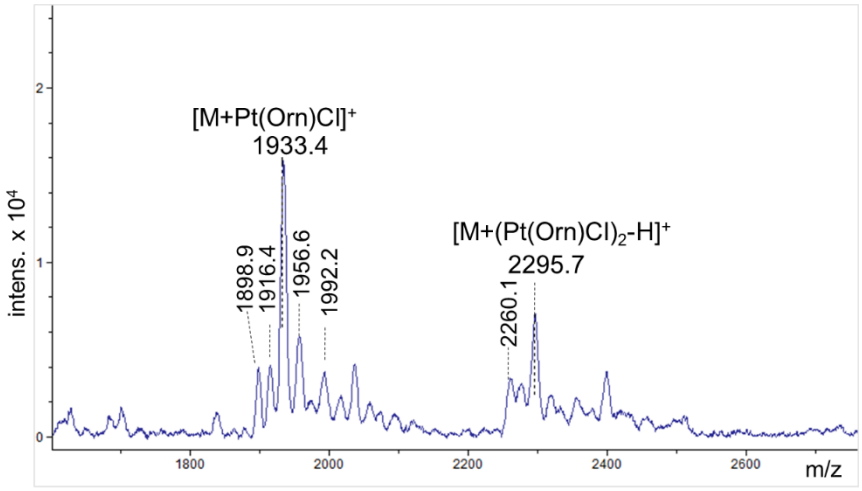

Figure 3.20. MALDI mass spectrum of isolated OrnPt-UUAUU-2 and OrnPt-UUAUU-3 HPLC fractions. Analysis of isolated OrnPt-UUAUU-2, and OrnPt-UUAUU-3 indicate presence of a monofunctional adduct (m/z of 1933.4 Da/e) and doubly platinated adduct (m/z 2295.7 Da). Minor peaks observed (m/z 1898.9, 1916.4, 1956.6, 1992.2, and 2260.1 Da/e) are assigned on bisaquated OrnPt, loss of Cl^-, and association with sodium ions.

The reaction of ArgPt with 5′-UUAUU-3′ was analyzed and three HPLC product peaks (ArgPt-UUAUU-1, ArgPt-UUAUU-2, and ArgPt-UUAUU-3) were observed, which all have longer retention times (22.5, 23.8, and 25.5 min, respectively) than the unreacted 5′-UUAUU-3′ oligonucleotide (**Fig. 3.21**). Fractions were collected and analyzed by MALDI-MS. However, no peaks associated with ArgPt or RNA were observed, likely due to low sample concentration. The MALDI-MS characterization was repeated on a ArgPt-UUAUU reaction mixture that was first desalted through ethanol precipitation. Multiple platinum adducts were observed (**Fig. 3.22**). These include a monofunctional adduct observed at m/z 1979.4 Da/e (calculated mass is 1979.5 Da), a doubly platinated adduct observed at m/z 2405.3 Da/e (calculated exact mass is 2405.5 Da), and an aquated doubly platinated adduct observed at m/z 2366.1 Da/e (calculated exact mass is 2366.5 Da). A species observed at m/z 2511.4 Da/e is likely a complex of doubly

platinated adduct associated with CH_3COOH (from desalting buffers) (calculated exact mass is 2510.7 Da).

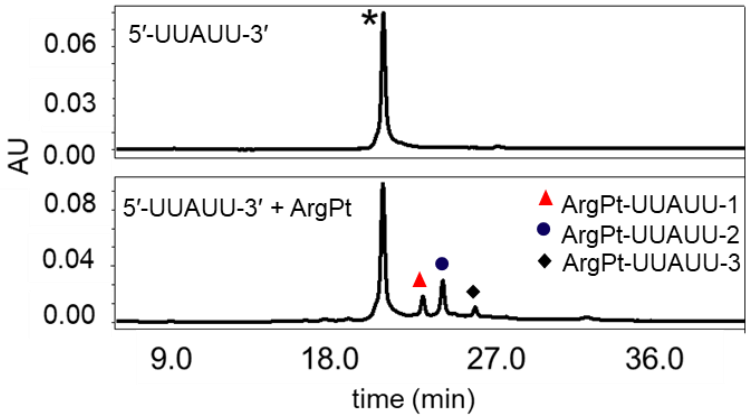

Figure 3.21. HPLC analysis (C18) of ArgPt-UUAUU platination products. The ArgPt-UUAUU adduct profile following reaction of 5′-UUAUU-3′ with monoaquated ArgPt is shown. Three products, ArgPt-UUAUU-1, ArgPt-UUAUU-2, and ArgPt-UUAUU-3, are observed with retention times of 22.5, 23.8, and 25.5 min, respectively. The control (unreacted 5′-UUAUU-3′) is shown as the top trace.

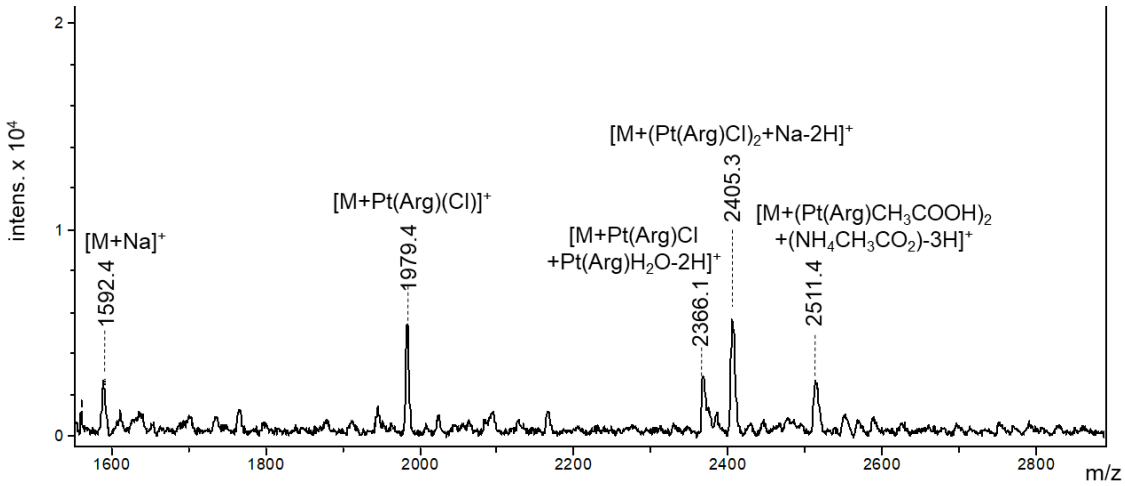

Figure 3.22. MALDI mass spectrum of isolated ArgPt-UUAUU reaction mixtures. Characterization indicates presence of a monofunctional adduct (m/z 1979.4 Da/e), doubly platinated adduct (m/z 2405.3 Da/e), and doubly platinated adduct with bisaquated ArgPt (m/z 2366.1 Da/e). An adduct formed by addition of neutral molecules of CH_3COOH is also observed at 2511.4 Da/e.

In a separate experiment to investigate the formation of ArgPt adducts with RNA, a reaction of poly(Ado) RNA with ArgPt followed by P1 digestion was carried out and analyzed using

LC-MS as described in **Section 2.4.11**. ArgPt reacts with poly(Ado) RNA and forms three product peaks that were resolved on the liquid chromatograph (LC) (**Fig. 3.23**). The three product peaks (ArgPt-poly-1, ArgPt-poly-2, and ArgPt-poly-3) were subjected to mass analysis (**Fig. 3.24**). The first product peak (ArgPt-poly-1) has an observed m/z 482 Da/e, which is assigned as a bifunctional adduct. This adduct is doubly charged (2+) and consistent with ArgPt coordinated with two adjacent residues (Ado-p-Ado) (calculated mass is 964 Da). The second product peak (ArgPt-poly-2) has an observed m/z 672 Da/e, which is assigned as a singly charged (+) monofunctional adduct. This adduct consists of one ArgPt coordinated to a single Ado residue (calculated mass is 671 Da). The third product peak (ArgPt-poly-3) has an observed m/z 647 Da/e. This is another doubly charged (2+) bifunctional adduct, which is consistent with three Ado residues (Ado-p-Ado-p-Ado) coordinated with one ArgPt molecule (calculated exact mass is 1294 Da). The third Ado residue that is part of this adduct may be present because of incomplete digestion by P1 nuclease.

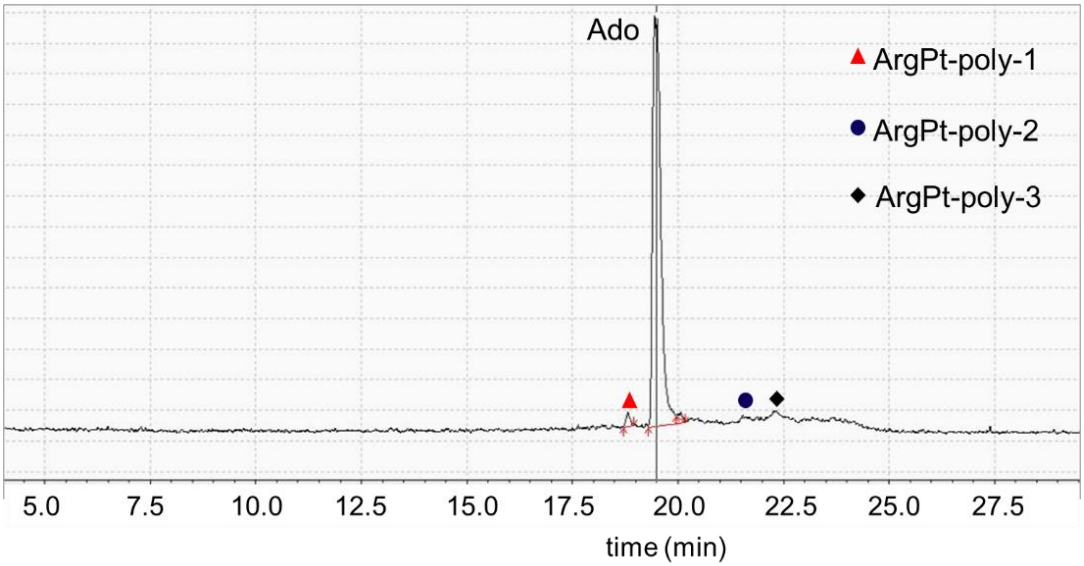

Figure 3.23. LC spectrum of ArgPt-poly(Ado) reaction products. Three peaks referred to as ArgPt-poly-1, ArgPt-poly-2, and ArgPt-poly-3 are formed following a reaction of ArgPt with poly(Ado) RNA.

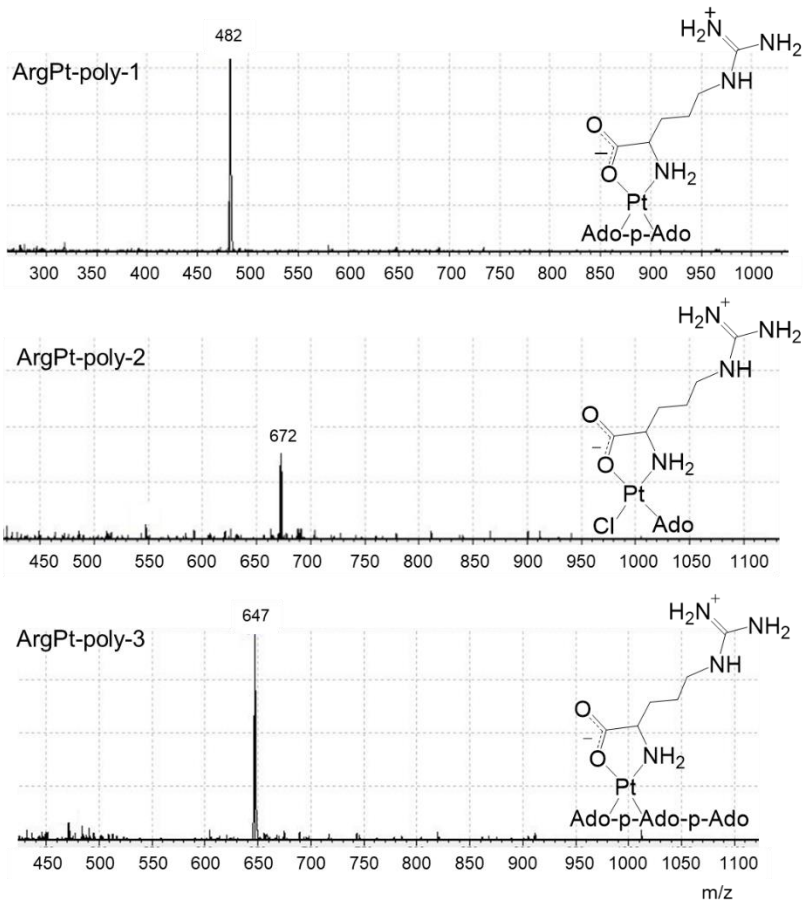

Figure 3.24. LC-MS spectra of ArgPt-poly(Ado) reaction products. Mass spectra (positive mode) of the LC product peaks of ArgPt-poly-1, ArgPt-poly-2, and ArgPt-poly-3 are shown. ArgPt-poly-1 contains a species assigned as a doubly charged bifunctional adduct (m/z 482 Da/e). ArgPt-poly-2 contains a species assigned as the singly charged monofunctional adduct (m/z 672 Da/e), and ArgPt-poly-3 is assigned as a doubly charged bifuntional adduct with an additional Ado residue (m/z 647 Da/e). Representative structures of the adducts are given (p indicates the phosphate ester bond).

3.3.2 Structural isomers of AAPt adducts

In addition to the NMR data, the kinetic *trans* effect and previously reported theoretical calculations were used to propose the structures of the adducts [150]. The adducts likely have several structural orientations that allow maximum stability. We propose that AlaPt-Ado, OrnPt-Ado, and ArgPt-Ado adducts have the *trans* orientation in which the α-NH_2 is *trans* to the Ado platination site (N1, N3, or N7) (**Fig. 3.25**). In the *trans* geometry, the AAPt compounds coordinate to the nucleoside such that the α-amino group and the platinated nitrogen on the nucleoside are

trans to each other. These structures can be used to explain the nucleoside preferences of the platinum-based compounds. The selectivity of cisPt for dGuo has been attributed predominantly to a strong hydrogen bond between the cisPt ammine ligand and the 6-oxo group of dGuo [27]. In contrast, the selectivity of AlaPt, OrnPt, and ArgPt for Ado/dAdo can be explained by a hydrogen-bonding interaction unique to the AAPt compounds. The *trans* adduct structures (*e.g.*, *trans*-Ado-N1 or *trans*-Ado-N7 in **Fig. 3.26**) would position the 6-amine of Ado/dAdo to form a hydrogen bond with the carboxylate ligand of the AAPt compound. Such interactions would stabilize the Ado/dAdo adduct, but are not available for Guo/dGuo, and possibly lead to higher reactivities of Ado/dAdo with the three AAPt compounds studied here. Formation of N3 platination products are less likely due to lack of a stabilizing hydrogen bond with the position 6 functional group of the purine (**Fig. 3.26**).

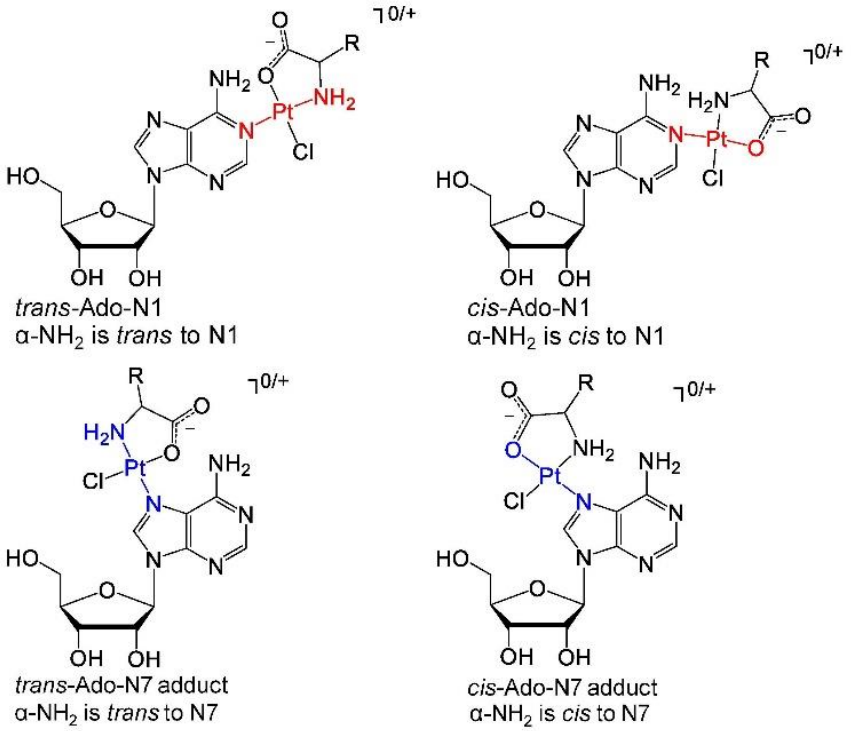

Figure 3.25. Representative geometric and constitutional isomers of AAPt-Ado adducts. Platination occurs at the N1 or N7 positions (N3 platination is also possible). The platinating moiety may have different orientations to position the ligands for favorable interactions with the nucleoside such as hydrogen bonding or to avoid steric clash.

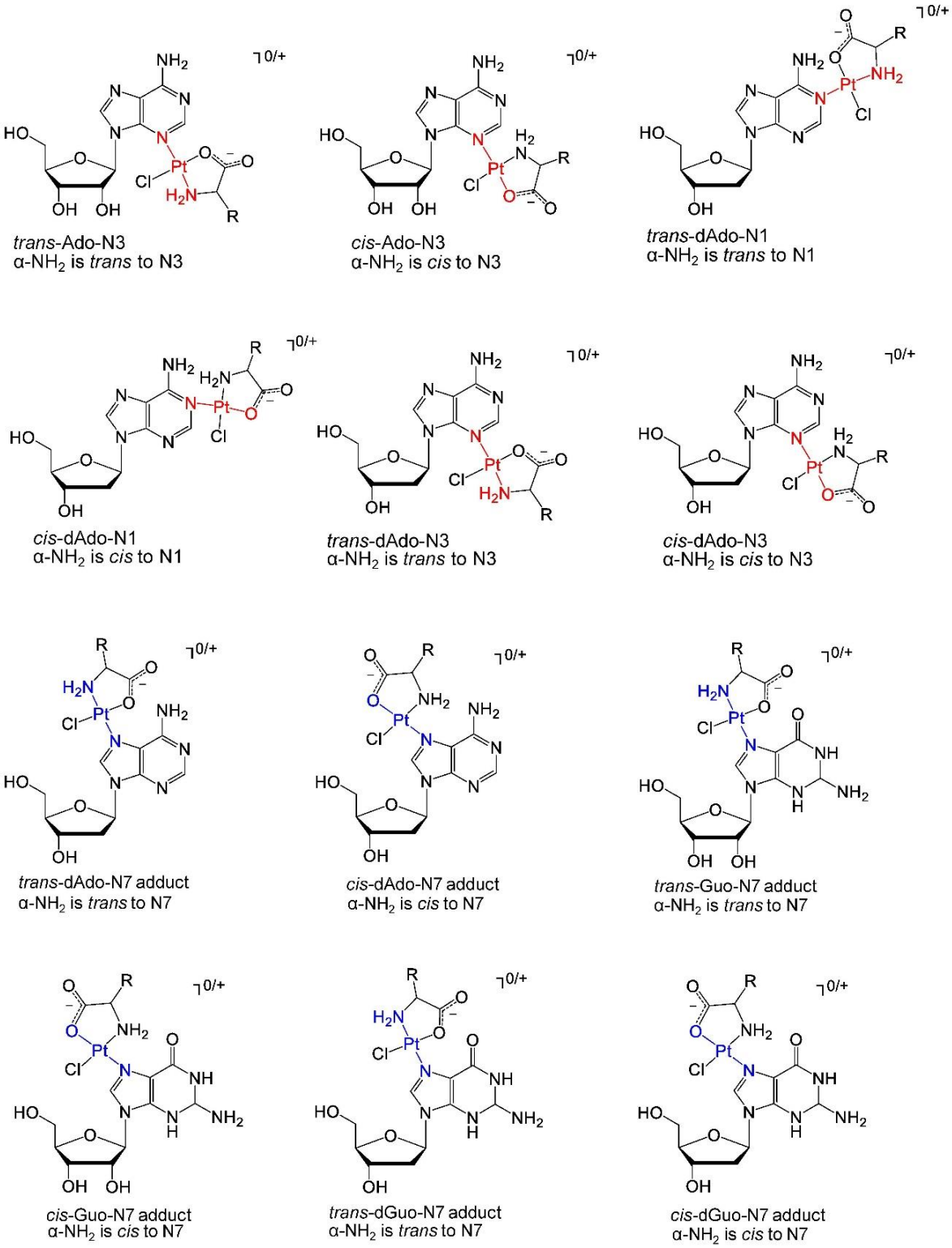

Figure 3.26. Possible adduct structures formed by AAPt with purines. AAPt compounds could coordinate at different sites of purine nucleosides forming various isomers and orientations of the platinum moieties.

3.4 Conclusions

Platination by cisPt occurs predominantly at the N7 position of dGuo residues and results in formation of bifunctional and monofunctional adducts. In contrast, the AAPt compounds (AlaPt, OrnPt, and ArgPt) were observed to form non-canonical adducts by coordinating to multiple sites on Ado/dAdo residues, specifically the N1/N3 and N7 positions of the nucleobases. Various techniques were employed to identify and characterize these adducts. HPLC was used to identify the products formed following the reaction of AAPt compounds with nucleosides or oligonucleotides. The products have different retention times on a C18 column compared to free nucleoside/oligonucleosides and could be isolated for further analysis. ESI-MS characterization was used to identify the composition (*i.e*., Ado vs. Guo) and types of adducts formed. Each of the AAPt compounds reacts with Ado residues and predominantly forms isomeric monofunctional adducts with the same m/z and platinum isotopic distribution pattern. Additionally, bifunctional and doubly platinated adducts are observed. MALDI-MS and ESI-MS were used to identify the types of adducts formed when AAPt compounds platinate short oligonucleotides with single Ado residues. Monofunctional and doubly platinated adducts are formed by AAPt compounds with these oligonucleotides. NMR spectroscopy was employed in differentiating the isomeric adducts formed by AAPt with Ado nucleosides. These isomers vary at their platination sites and could be identified based on the chemical shifts of neighboring protons.

The three compounds coordinate at N1/N3 and N7 positions of Ado residues and the resultant adducts adopt several structural orientations. Although methods such as mass spectrometry and 1D-NMR spectroscopy were used for identifying the types of adducts formed, they give limited information on the structural orientations of the adducts. These orientations can be modulated by factors such as steric hindrance and hydrogen-bonding properties. Differentiating between N1 and N3 platination was also challenging because these sites have similar proximity to H2 proton. However, future studies could employ X-ray crystallography to differentiate between N1 and N3 platination by AAPt compounds.

CHAPTER 4

REACTION KINETICS OF AMINO ACID-LINKED PLATINUM(II) COMPOUNDS WITH DNA/RNA NUCLEOSIDES‡ AND OLIGONUCLEOTIDES

‡Nucleoside level kinetic studies are adapted from Kimutai B, He CC, Roberts A, Jones ML, Bao X, Jiang J, Yang Z, Rodgers MT, Chow CS (2019) J Biol Inorg Chem 24:985-997.

Abstract

The diversity of the side chain functional groups together with the contribution of backbone atoms of amino acid-linked platinum(II) (AAPt) compounds can modulate their reactivities and targets. In this thesis work, the reaction kinetics of alanine-, ornithine-, and arginine-linked platinum(II) compounds (AlaPt, OrnPt, and ArgPt, respectively) were determined. Their reactivity preferences for DNA/RNA nucleosides and oligonucleotides were examined using pseudo-first-order kinetics and HPLC analysis. The rate constants reflect the role of chemical structures and physical properties of the amino acid functional groups in target residue preferences. The oligonucleotide local environment also has an effect on the reactivity of the AAPt compounds.

4.2 Introduction

Platination kinetics have been shown to correlate with cellular activity of cisPt and second-generation analogues [33-36]. For example, *cis*-diammine-1,1-cyclobutane dicarboxylate platinum(II) (carboplatin) is less potent and toxic than cisPt, which is partly attributed to its 100-fold slower adduct formation with DNA [34]. As noted in **Section 1.2.3**, the coordination of platinum-based compounds with DNA involves a number of steps that contribute to the overall reaction rates. Before cisPt reacts with DNA in a cellular setting, it is first aquated to generate *cis*-$[PtCl(NH_3)_2(H_2O)]^+$, whereby a chlorido is replaced with H_2O [32, 151]. Reactions of the aquated cisPt species with DNA then occur under kinetic control, leading to stable adduct formation at the preferred dGuo sites [32, 40]. Therefore, kinetic studies can be used to compare the reactivities of aquated cisPt and AAPt compounds (**Fig. 4.1)**. For *in vitro* studies, cisPt or AAPt analogues are reacted with $AgNO_3$ in order to generate the monoaquated species prior to reactions with

nucleosides or nucleic acids (**Scheme 4.1**) [32]. A number of AAPt-nucleoside adducts form by coordination at the N7 of dGuo/Guo or N1, N3, or N7 positions of dAdo/Ado. By comparing the kinetic rate constants (*k* values) for disappearance of the nucleoside/oligonucleotide over time, the target preferences of aquated cisPt and AAPt (*i.e.,* AlaPt, OrnPt, or ArgPt, **Fig. 4.1**) can be determined [152-153, 58].

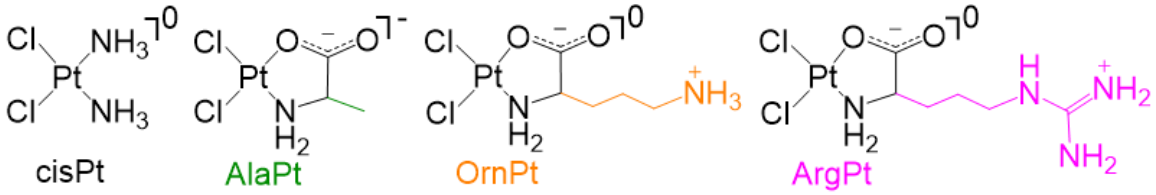

Figure 4.1. **The structures of cisPt (cisPt) and amino acid-linked platinum(II) compounds, AlaPt, OrnPt, and ArgPt.**

Scheme 4.1. Aquation of platinum compounds and subsequent platination of nucleosides/oligonucleotides. Possible coordination sites are highlighted in blue (N7) and red (N1 and N3).

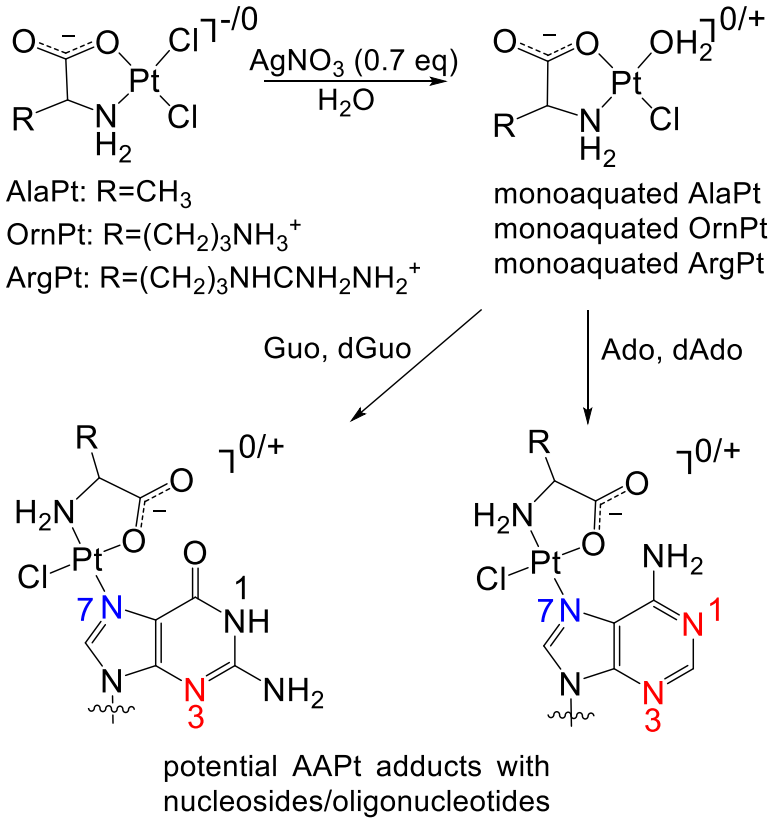

The overall process of cisPt adduct formation such as aquation and DNA platination [34, 36] is influenced by a number of factors associated with the non-leaving group ligand (typically an amine), including coordination type and hydrogen-bonding properties [35-36]. These factors play roles in target preferences and the types of adducts that are formed. CisPt reacts with dGuo of single- and double-stranded DNA leading to formation of kinetically inert adducts [35, 27, 44]. The adduct forms when the aqua ligand is substituted by a nucleobase atom via a trigonal-bipyramidal transition state [45] (**Scheme. 4.2).** Hydrogen bonding is implicated in the kinetic control of platination [36, 46] and can stabilize the transition state of the aquated cisPt-dGuo reaction [27]. More specifically, computational analysis showed that in the transition state, cisPt forms a strong hydrogen bond between its ammine ligand and the oxo at the 6 position of dGuo [27]. As such, this hydrogen-bonding interaction together with charge-charge interactions results in preferential coordination of cisPt to dGuo [27]. In contrast, formation of the cisPt-Ado adduct is less favored because Ado has an amine at the 6 position, which cannot hydrogen bond with cisPt [27].

Scheme 4.2. Associative substitution mechanism of cisPt coordination with dGuo. Hydrogen bonding between ammine and oxo groups stabilizes the trigonal bipyramidal transition state.

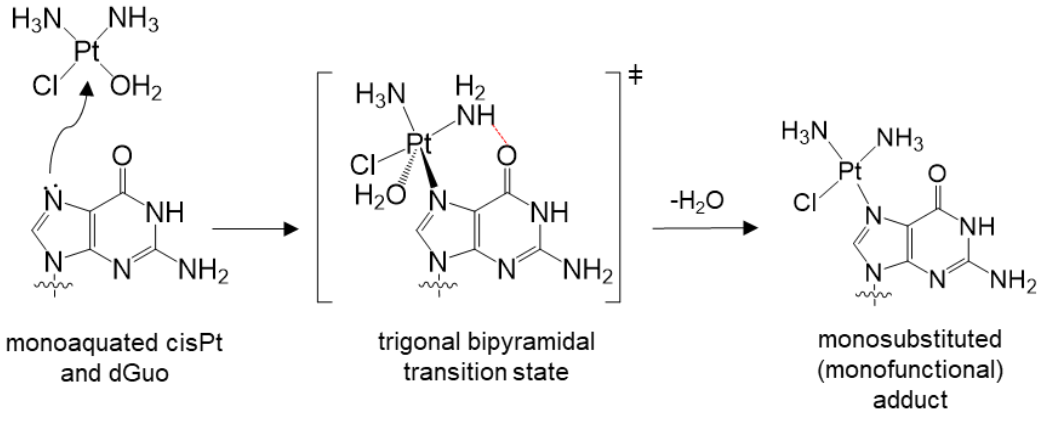

In this thesis work, the reaction kinetics of three AAPt compounds were examined to determine how the chemical structures and physical properties of the functional groups of the

amino acid relate to reactivity and nucleoside preference. Pseudo-first-order kinetics were used to compare the reactivity of the three AAPt compounds with purine nucleosides. The hypothesis is that modification of cisPt with amino acid ligands of varying sizes and charges would alter the reaction kinetics and nucleic acid target preferences. Influence of the oligonucleotide local environment was also investigated since the nucleotides surrounding the target nucleotide may modulate the binding kinetics of cisPt and AAPt and lead to different platination rates and profiles. The impact of this local environment was determined by comparing the reactivities and preferences of AAPt compounds with oligonucleotides and nucleosides. The oligonucleotide sequences chosen were 5′-UUAUU-3′ for RNA and 5′-d(TTATT)-3′ for DNA. These sequences were selected because cisPt and AAPt compounds have low reactivity with Thd (dT) or Urd (U) residues [106, 138]. Therefore, the presence of only one preferred residue (Ado (A) or dAdo (dA)) directs the platination to a single site. By excluding competing reactivity with the flanking residues, the influence of the oligonucleotide local environment on platination at the preferred residue can be analyzed. Understanding reactivity and selectivity of platinum-based compounds at both the nucleoside and oligonucleotide level is needed to drive the development of new compounds that target alternative biological residues or molecules such as RNA [55, 29, 154]. This approach could potentially be important in achieving improved cellular activities and effectiveness.

4.3 Results and discussion

4.3.1 Kinetics of platination reactions with DNA/RNA purine nucleosides

The reactions of (deoxy)nucleosides with the monoaquated AAPt compounds result in the formation of one or more adducts with longer (AlaPt and ArgPt adducts) or shorter (OrnPt adducts) retention times on a C18 column relative to the unreacted (deoxy)nucleosides (**Fig. 3.3, Section 3.3.1**). The adduct characterization was described in previous chapter (**Section 3.3.1**). In summary, monoaquated AlaPt, OrnPt, and ArgPt each reacts with Guo to form one major product (distinct HPLC peak), referred to as AlaPt-Guo_{N7}, OrnPt-Guo_{N7}, and ArgPt-Guo_{N7}, respectively. In

contrast, platination of Ado leads to formation of multiple adducts. Monoaquated AlaPt reacts with Ado to form two main products, AlaPt-Ado$_{N1/N3}$ and AlaPt-Ado$_{N7}$. Monoaquated OrnPt also reacts with Ado to form two major products, OrnPt-Ado$_{N1/N3}$ and OrnPt-Ado$_{N7}$. Monoaquated ArgPt reacts with Ado to form three major products, ArgPt-Ado$_{N1/N3}$, ArgPt-Ado$_{N7}$, and ArgPt-Ado$_{mix}$, which have longer retention times than Ado. The subscripts refer to coordination sites at the adducts. The rate of formation of products varies depending on the identity of the AAPt compound and the target nucleoside. By monitoring the rates of formation of products, the rate constants (*k* values) and reactivity preference of each platinum compound can be determined.

Kinetic rate constants (*k* values) were used to reveal the preferred target nucleoside of each AAPt compound relative to cisPt. Under pseudo-first-order reaction conditions for the monoaquated AAPt (or cisPt) and purine nucleosides, the peak areas of the unreacted nucleosides were monitored by HPLC and observed to decrease with time (**Fig. 4.2**). The rate of decrease of the peak area corresponding to the unreacted nucleoside (Ado, Guo, dAdo, or dGuo) varies, depending on the identity of the platinum compound (monoaquated AlaPt, OrnPt, or ArgPt). As described in **Section 2.4.7,** the peak area of the nucleoside at each time point can be integrated quantitatively, plotted, and fitted to an exponential decay equation (**Eq. 4.1**) to extract the pseudo-first-order rate constant (*k*).

$$[\text{Nuo}]_t = e^{-kt} + [\text{Nuo}]_0 \quad \textbf{(Eq. 4.1)}$$

From **Eq. 4.1**, $[\text{Nuo}]_t$ is the concentration of unreacted nucleoside or oligonucleotide at time t, and $[\text{Nuo}]_0$ is the initial concentration of unreacted nucleoside or oligonucleotide. When $[\text{Nuo}]_t$ is plotted against t, the decay factor is *k.* The *k* values for each AAPt analogue with DNA/RNA nucleosides were obtained (summarized in **Table 4.1** and shown graphically in **Fig. 4.3**).

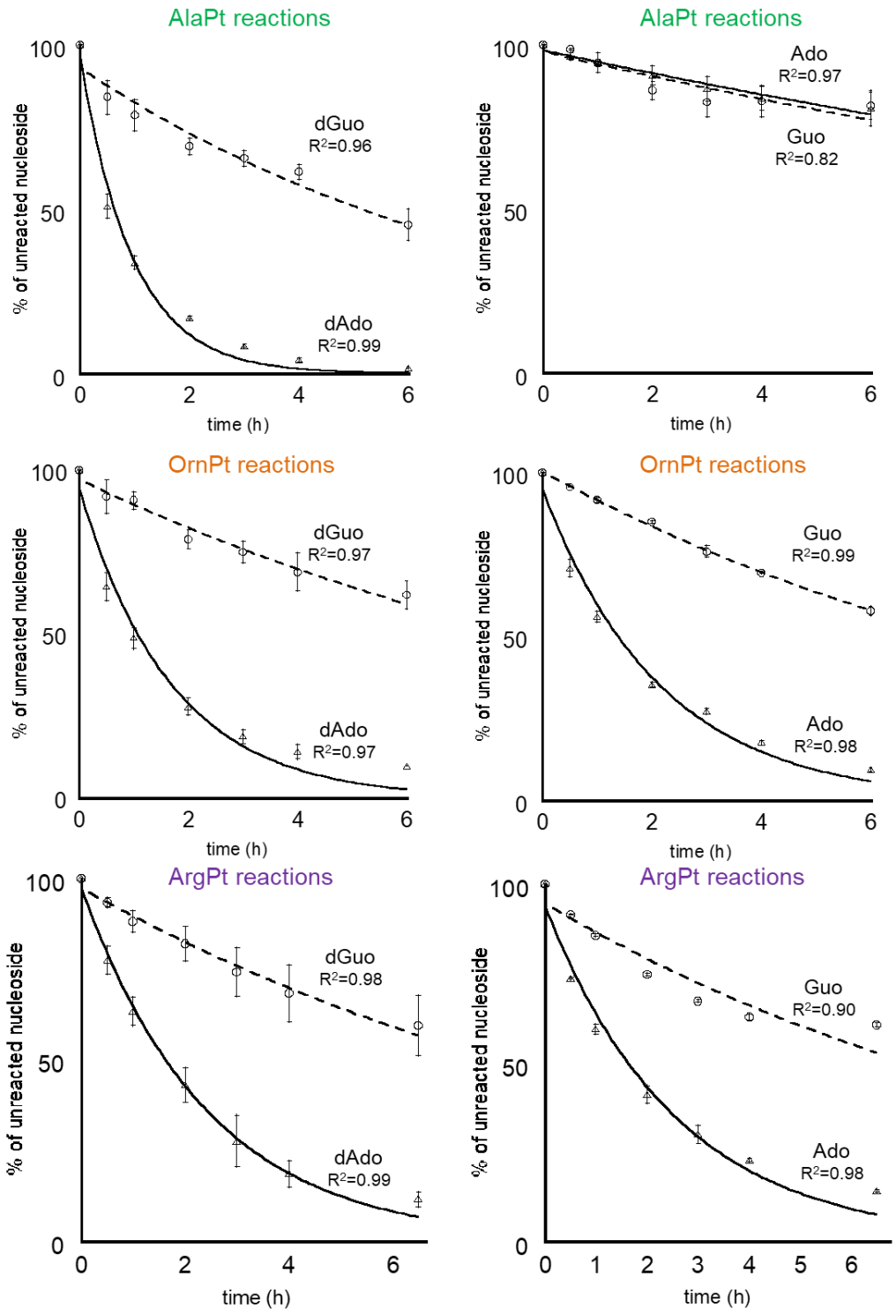

Figure 4.2. Reaction rates of monoaquated AlaPt, OrnPt, and ArgPt with purine nucleosides. Representative kinetic traces of reactions of monoaquated AlaPt, OrnPt, or ArgPt with the purine nucleosides showing the fraction of the unreacted nucleoside diminishing over time. Measurements were done in triplicate.

Table 4.1. Pseudo-first-order rate constants, *k* (μs^{-1})[a]

	dGuo	Guo	dAdo	Ado
cisPt[b]	49±1	25±2	6±1	6±2
AlaPt[b]	19±7	9±4	176±9	9±4
OrnPt[b]	20±1	24±1	125±1	100±1
ArgPt[b]	23±2	25±1	115±15	108±1

[a] triplicate runs in 25 mM Na_2HPO_4/NaH_2PO_4 buffer (pH 7) at 37 °C;
[b] monoaquated compounds

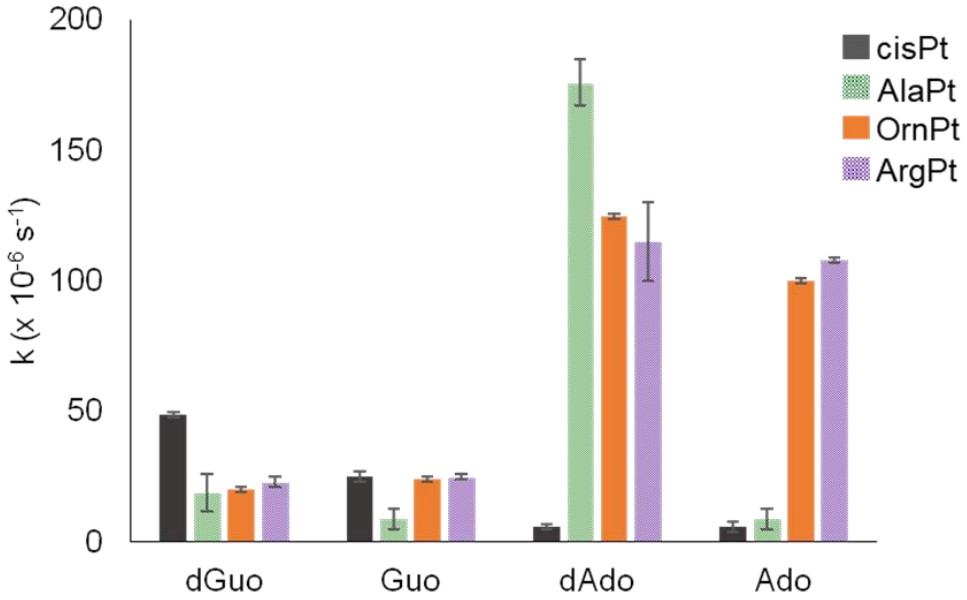

Figure 4.3. Comparisons of rate constants (*k*) for reaction of monoaquated cisPt (grey) and AAPt compounds (monoaquated AlaPt, green; monoaquated OrnPt, orange; monoaquated ArgPt, violet) with DNA/RNA purine nucleosides (dGuo, Guo, dAdo, and Ado) are shown.

CisPt is known to preferentially target dGuo over other residues of DNA [38, 33, 101, 41]. This selectivity was confirmed here with the nucleoside-level kinetic studies, in which the highest reaction rate constant (*k*) of aquated cisPt is with dGuo (49×10^{-6} s^{-1}) (**Table 4.1**). The reactivity of monoaquated cisPt with Guo, dAdo, and Ado is lower than dGuo by two- to eight-fold. The AAPt compounds display a wide range of reactivities as shown in **Fig. 4.3**. The highest reactivity of monoaquated AlaPt is with dAdo (176×10^{-6} s^{-1}), which is nine to twenty-fold higher than that of reactions with Guo and dGuo, and demonstrates that monoaquated AlaPt prefers dAdo. The

reactivity of monoaquated AlaPt is strongly influenced by both the identity of the purine base as well the functional group at the 2′ position (*e.g.,* H or OH), with a preference for dAdo over Ado. The highest reaction rates for OrnPt are with dAdo and Ado (125×10^{-6} s^{-1} and 100×10^{-6} s^{-1}, respectively). These rates of reactions for monoaquated OrnPt with Ado/dAdo are four- to six-fold higher than reactions with Guo/dGuo (**Table 4.1** and **Fig. 4.3**), demonstrating its preference for the adenine moiety. The highest reactivity of monoaquated ArgPt is with dAdo and Ado (115×10^{-6} s^{-1} and 108×10^{-6} s^{-1}), which is four- to five-fold higher than its reactivity with Guo/dGuo, and demonstrates that monoaquated ArgPt also has a preference for the adenine moiety (**Table 4.1** and **Fig. 4.3**).

4.3.2 Kinetics of platination reactions with DNA/RNA oligonucleotides

CisPt reacts with DNA and RNA constructs by preferentially targeting the Guo/dGuo residues. The reactivity of cisPt is modulated by the local conditions such as salt concentrations and pH [155-156, 49]. Previous literature reports and work from our lab focused on the reaction kinetics of cisPt with various DNA and RNA constructs. Representative *k* values are shown in **Table 4.2**. These values vary depending on the type of DNA/RNA construct and the conditions (*i.e*., salt concentration, buffer type, etc.) of the experiments. Kinetic experiments with cisPt often employ sequences with dGuo/Guo residues due to its preference for such residues. In this thesis work, the reaction of cisPt (and AAPt compounds) with DNA/RNA constructs that do not have dGuo/Guo residues, but instead have dAdo/Ado as the target sites were investigated.

The monoaquated cisPt or AAPt compounds react with DNA and RNA oligonucleotides (5′-d(TTATT)-3′ and 5′-UUAUU-3′, respectively), resulting in formation of multiple product peaks with longer retention times on a C18 column relative to the unreacted oligonucleotides (**Fig. 4.4**). Multiple peaks result from formation of different types of adducts (*e.g.,* monofunctional and doubly platinated). Monoaquated cisPt reacts with the RNA oligonucleotide to form one major product, which has longer retention times than the free RNA on C18 (**Fig. 4.4A**) Monoaquated AlaPt reacts

with the RNA oligonucleotide to form two major products, that have longer retention times than the free RNA on C18 (**Fig. 4.4B**). These AlaPt-UUAUU products likely have decreased polarity due to the associated alanine ligand, leading to longer retention times compared to those of unreacted oligonucleotide. Monoaquated OrnPt reacts with 5′-UUAUU-3′ to form three products, which also have longer retention times on a C18 column relative to the unreacted oligonucleotides (**Fig. 4.4C**). Similarly, monoaquated ArgPt reacts with the RNA oligo to form three products that also have longer retention times on a C18 column relative to the free oligonucleotides (**Fig. 4.4D**). Factors that could increase the retention time of platinated oligonucleotides relative to the free oligonucleotides include neutralization of the oligonucleotide local charge by platinum compounds, structural changes, and increased size of the oligonucleotide after platination.

Table 4.2. Rate constants of cisPt reactions with various DNA/RNA constructs

	sequence	***k* values ($x10^{-4}$ s^{-1}) [ref]**	**conditions**
RNA	5′-CGCGUUGUUCGCG-3′	4.4 ± 0.4 [49]	35 mM Na^+, pH 6.0, 37 °C
DNA	5′- $(T)_{10}$-GG-$(T)_{10}$-3′	7.4 ± 0.8 [156]	10 mM K^+, 5 mM Na^+, pH 6.2, 37 °C
RNA	5′- $(U)_{10}$-GG-$(U)_{10}$-3′	3.3 ± 0.7 [156]	10 mM K^+, 5 mM Na^+, pH 6.2, 37 °C
DNA	5′- $(T)_{10}$-GG-$(T)_{10}$-3′	24 ± 5 [156]	10 mM K^+, 20 mM Na^+, pH 6.2, 37 °C
RNA	5′- $(U)_{10}$-GG-$(U)_{10}$-3′	33 ± 10 [156]	10 mM K^+, 20 mM Na^+, pH 6.2, 37 °C
RNA	5′-GGCCGΨAACΨAΨAACGGUC-3′	13.3 ± 0.9 [155]	10 mM K^+, 20 mM Na^+, pH 6.2, 37 °C
RNA	5′-GCAGGAUUAGAUACCCUGC-3′	16.2 ± 1.1 [155]	10 mM K^+, 20 mM Na^+, pH 6.2, 37 °C

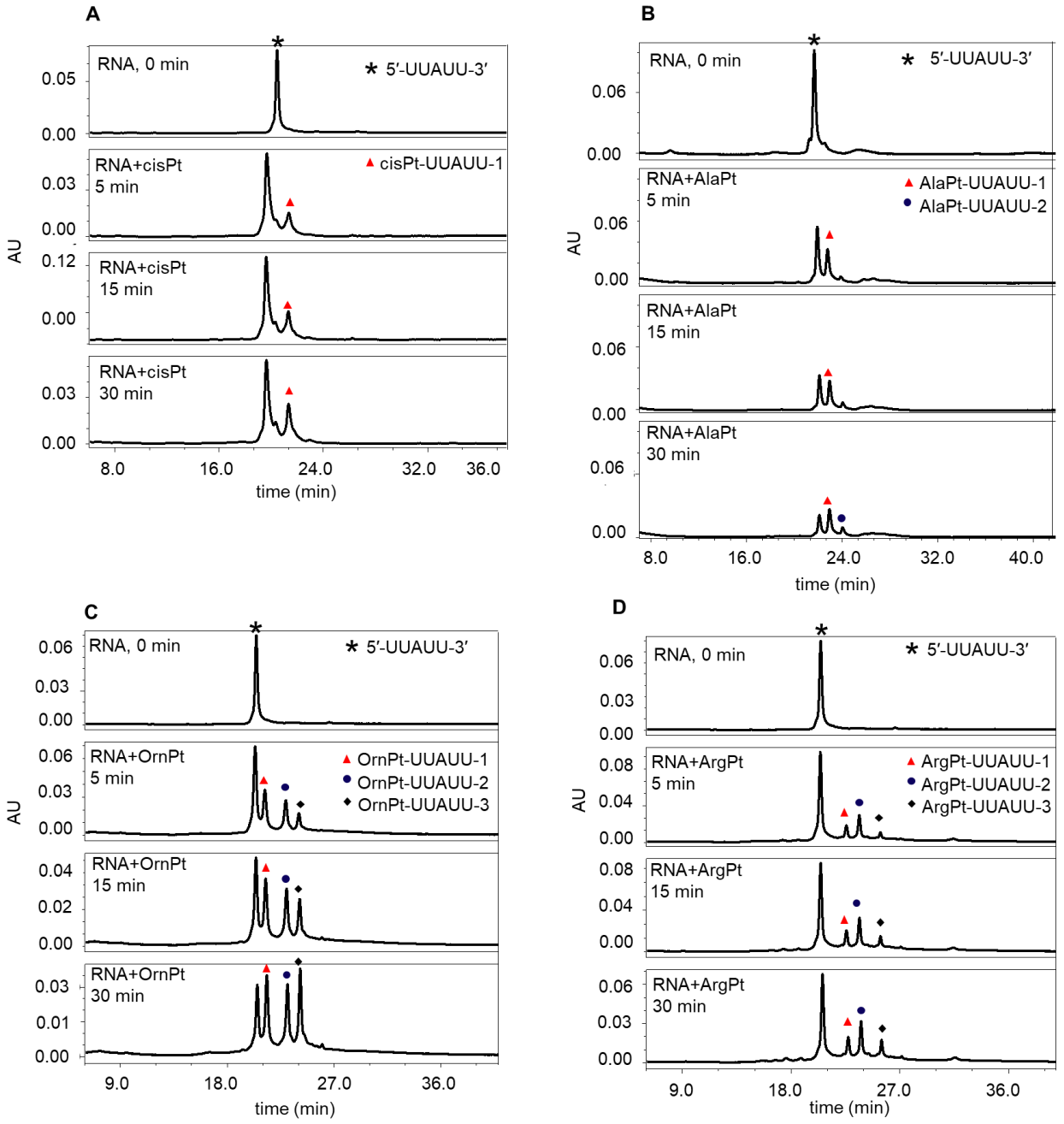

Figure 4.4. HPLC analysis (C18) of platinated RNA products. The adduct profiles following reactions of 5′-UUAUU-3′ with monoaquated cisPt (**A**), AlaPt (**B**), OrnPt (**C**), and ArgPt (**D**) are given. Multilple product peaks (indicated in the figure) are formed during the reactions. The reaction times are indicated and the controls (unreacted oligonucleotides with buffer, black asterisks) are shown as the top traces.

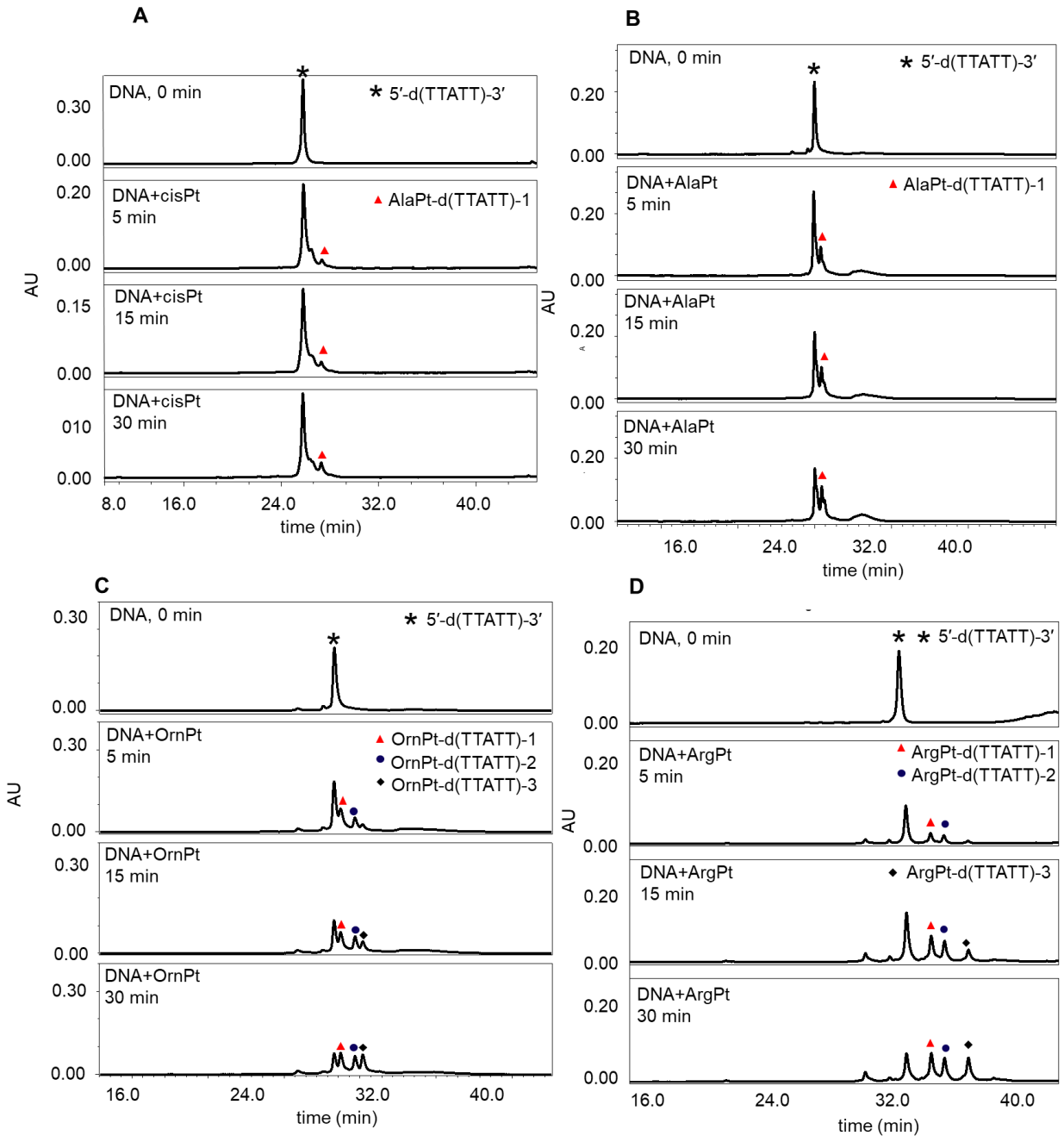

Figure 4.5. HPLC analysis (C18) of platinated DNA products. The adduct profiles following reactions of 5′-d(TTATT)-3′ with monoaquated cisPt (**A**), AlaPt (**B**), OrnPt (**C**), and ArgPt (**D**) are given. Multilple product peaks (indicated in the figure) are formed during the reactions. The reaction times are indicated and the controls (unreacted oligonucleotides with buffer, black asterisks) are shown as the top traces. Some minor peaks with short retention time were also formed in OrnPt and ArgPt reactions.

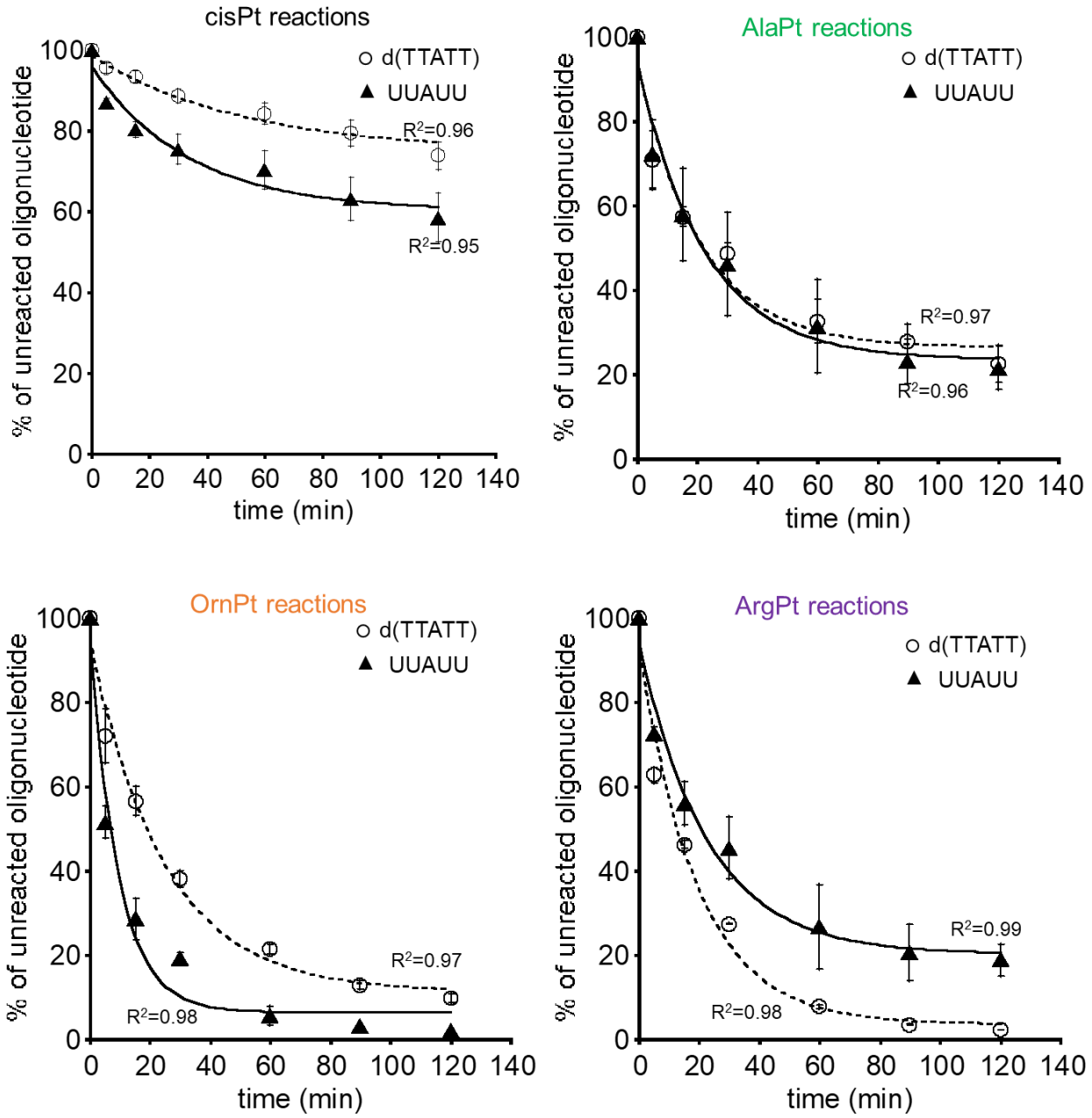

Figure 4.6. Reaction rates of AlaPt, OrnPt, and ArgPt with RNA and DNA oligonucleotides. Kinetic traces of reactions of monoaquated cisPt, AlaPt, OrnPt, or ArgPt with RNA and DNA oligonucleotides showing the fraction of unreacted oligonucleotide diminishing over time. 5′-UUAUU-3′ is represented by a solid line and 5′-d(TTATT)-3′ is represented by a dashed line.

Similarly, AAPt compounds (and cisPt) react and form products with DNA oligos (**Fig. 4.5**). The number of products and their retention time in relation to free oligonucleotides are similar to reactions with RNA oligonucleotides. AlaPt reacts with 5′-d(TTATT)-3′ to form one main product, which has a longer retention time than the free DNA oligo (**Fig. 4.5B**). Monoaquated OrnPt reacts

with 5′-d(TTATT)-3′ to form three major products, which have longer retention times than the free DNA oligo on the C18 column (**Fig. 4.5C**). Monoaquated ArgPt also reacts with 5′-d(TTATT)-3′ to form three major products that have longer retention times than the unreacted DNA oligo (**Fig. 4.5D**).

The *k* values were used to compare the reactivities of cisPt and each AAPt compound with the oligonucleotides. Similar to the nucleoside level analysis, the peak areas of the oligonucleotides at each time point can be integrated quantitatively, plotted, and fitted to an exponential decay equation (**Eq. 4.1**) to extract the pseudo-first-order rate constants (*k* values). The HPLC peak areas of the unreacted oligonucleotides (5′-UUAUU-3′ or 5′-d(TTATT)-3′) were monitored and observed to decrease at different rates depending on the identity of the platinum compound (monoaquated cisPt, AlaPt, OrnPt, or ArgPt) (**Fig. 4.6**). The *k* values for each AAPt analogue with the oligonucleotides are summarized in **Table 4.3** and shown graphically in **Fig. 4.7**.

Table 4.3. Pseudo-first-order rate constants, *k* ($x10^{-4}$ s^{-1})[a]

	5′-d(TTATT)-3′	5′-UUAUU-3′
cisPt[b]	3.2 ± 0.1	5.0 ± 0.1
AlaPt[b]	7.9 ± 0.1	7.5 ± 1.2
OrnPt[b]	8.0 ± 0.5	17.7 ± 2.1
ArgPt[b]	8.7 ± 0.2	7.4 ± 0.8

[a] triplicate runs in 25 mM Na_2HPO_4/NaH_2PO_4 buffer (pH 7) at 37 °C;
[b] monoaquated compounds

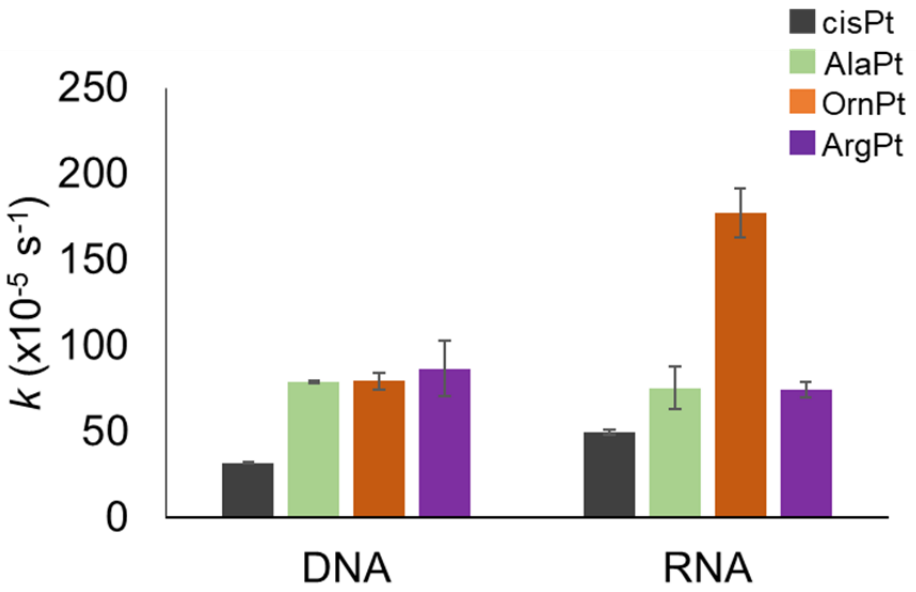

Figure 4.7. Comparison of reactivity of platinum-based compounds with oligonucleotides. The rate constants (*k*) for reaction of monoaquated cisPt, AlaPt, OrnPt, and ArgPt with DNA oligonucleotides and RNA oligonucleotides are shown.

A comparison of the *k* values for cisPt with the chosen RNA (5.0×10^{-4} s^{-1}) and DNA (3.2×10^{-4} s^{-1}) oligonucleotides indicates that cisPt is moderately selective in its reactivity with the two nucleic acids (less than two-fold difference) under low salt conditions (25 mM Na_2HPO_4/NaH_2PO_4). The *k* values for reaction kinetics of cisPt with the chosen sequences are in the same range as other reported literature values and previous work in our lab, with variation that is consistent with the preferred targets of cisPt and salt conditions (**Tables 4.2 and 4.3)** [155-156, 49]. Based on the *k* values, cisPt reactivity with 5′-UUAUU-3′ or 5′-d(TTATT)-3′ is relatively lower compared to its reactivity with constructs that have Guo/dGuo residues. This is not surprising due to the preference of cisPt for Guo residues [33, 38, 101, 41]. Compared to the three AAPt compounds, cisPt has the lowest *k* values when reacting with 5′-UUAUU-3′ and 5′-d(TTATT)-3′ because of the lack of its preferred Guo/dGuo target in the sequences (**Table 4.3**).

The range of *k* values for the reactions of AAPt compounds with oligos are as shown in **Fig. 4.7**. The AAPt compounds are generally more reactive than cisPt with the chosen DNA/RNA constructs, with *k* values that are two- to six-fold higher than those of cisPt. This difference was

also observed when the compounds react with nucleosides (**Section 4.3.1**). Monoaquated AlaPt has similar reactivity with both DNA and RNA oligonucleotides (7.9×10^{-4} s^{-1} and 7.5×10^{-4} s^{-1}, respectively) (**Table 4.3** and **Fig. 4.7)**. Monoaquated OrnPt exhibits a two-fold preference for RNA over DNA with *k* values of 17.7×10^{-4} s^{-1} and 8.0×10^{-4} s^{-1}, respectively (**Table 4.3** and **Fig. 4.7**) demonstrating its preference for the ribose moiety. The functional group at the 2′ position (*e.g.,* H or OH) of the nucleic acid appears to influence the OrnPt reactivity. The *k* values of monoaquated ArgPt with DNA and RNA oligonucleotides are similar (8.7×10^{-4} s^{-1} and 7.4×10^{-4} s^{-1}, respectively).

There is generally higher reactivity between AAPt compounds with RNA/DNA oligonucleotides than with free nucleosides, as exhibited by the increased *k* values in the oligonucleotide level reactions (**Tables 4.1** and **4.3**). The oligonucleotide local environment enhances reactivity of the AAPt compounds, likely due to factors such as negatively charged phosphate groups that attract the positively charged side chains of OrnPt and ArgPt. The backbone phosphate group of the oligonucleotides could also provide hydrogen-bond acceptors that stabilize interactions with the AAPt compounds. AlaPt exhibits discrimination between Ado and dAdo at the nucleoside level (**Table 4.1**) likely because its reactivity is more strongly influenced by the functional group at the 2′ position (*e.g.,* H or OH). This influence is minimized at the oligonucleotide level where the phosphate backbone may have a larger influence on reactivity. Similar reactivity is observed for AlaPt with 5′-UUAUU-3′ and 5′-d(TTATT)-3′ oligonucleotides. In contrast, OrnPt does not discriminate between Ado and dAdo nucleosides, but has a two-fold higher reactivity with 5′-UUAUU-3′ than with 5′-d(TTATT)-3′. This result implies that the presence of a backbone phosphate group, along with other factors (*e.g*., the functional group at the 2′ position), plays a role in either diminishing or amplifying the selectivity of AAPt compounds, depending on their side chain identity.

4.4 Conclusions

CisPt preferentially coordinates with dGuo residues, which is correlated with its anticancer activity [33, 38, 101]. Finding platinum-based compounds that preferentially platinate alternative targets has been an attractive goal, but has yielded little success to date. In this thesis work, platinum-based compounds AlaPt, OrnPt, and ArgPt have been shown to exhibit kinetic preferences for Ado/dAdo residues. These monoaquated AAPt compounds exhibit altered reactivity and different nucleoside preferences compared to monoaquated cisPt. OrnPt exhibits a greater than five-fold increase in reactivity with Ado/dAdo nucleosides over Guo/dGuo, and AlaPt has over nine-fold higher selectivity for dAdo over all other purines. The AAPt compounds exhibit unique differences in their reactivity by having altered preferences with non-canonical targets of cisPt. These differences suggest that the mode of amino acid coordination (*e.g.*, N vs. O) plays a role in modulating the rate of reactivity. While cisPt only has only (N,N) type of binding, the amino acid complexes can have (N,O) or (N,N) coordination.

The AAPt compounds have generally an increased reactivity with oligonucleotides compared to nucleosides. The local environment flanking the target residues in a DNA or RNA oligonucleotide, such as phosphate groups with associated cations, likely enhances the binding kinetics of cisPt and AAPt. The negatively charged phosphate groups can interact favorably with positively charged AAPt compounds or provide hydrogen bond acceptors that stabilize the interactions of AAPt compounds with their targets. OrnPt has a two-fold higher preference for RNA oligonucleotides over DNA, demonstrating that certain features of platinum-based compounds could modulate selective targeting of one nucleic acid over another. This preference could also be important in the development of compounds that target either DNA or RNA with high selectivity.

HPLC fitted with a C18 column has been used previously to monitor kinetic reactions of platinum-based compounds with their targets and to extract rate constants [138, 157]. In this thesis chapter, HPLC fitted with a C18 column was also used for kinetic studies of AAPt with their

nucleic acid targets. The rate constants were extracted after plotting the ratio of diminishing reactants as a function of time. Although the formation of individual AAPt-nucleoside or AAPt-oligonucleotide products could also be monitored, the identification of their rate of formation was challenging since one adduct could be converted to another type of adduct during the course of reaction (*e.g.* a monofunctional adduct converting into a bifunctional adduct). In the future, this method could be modified to include an internal standard so as to ascertain and correct for variability between injections. There are other alternative methods such as NMR spectroscopy and mass spectrometry that could also be used to monitor kinetic reactions and extract rate constants [32, 34, 149, 158]. These methods could be used to confirm the reaction kinetics and selectivity of AAPt compounds with their targets.

The AAPt compounds studied here have altered selectivity compared to cisPt and are therefore candidates for an alternative pathway of cytotoxicity that could involve non-canonical targets such as dAdo residues of DNA as well as Ado residues of RNA. Since platination of biomolecules such as proteins are often overlooked [30, 61-62], AAPt compounds may also have reactivity that extends beyond the current scope of targets.

CHAPTER 5

IMPACT OF AMINO ACID-LINKED PLATINUM(II) COMPOUNDS ON GLYCOSIDIC BOND STABILITY OF ADDUCTS[‡]

[‡]Adapted from Kimutai B, He CC, Roberts A, Jones ML, Bao X, Jiang J, Yang Z, Rodgers MT, Chow CS (2019) J Biol Inorg Chem 24:985-997

5.1 Abstract

Destabilization of glycosidic bonds accelerate depurination and formation of abasic sites in nucleic acids, which could ultimately contribute to cell cytotoxicity. Unstable glycosidic bonds can be caused by a change in chemical composition of the nucleoside due to modifications. Platination of deoxyguanosine (dGuo) residues by cisplatin (cisPt) has been reported to have no destabilizing effect on the adduct glycosidic bonds. However, changes in stabilization may occur in non-canonical target residues that are modified by other platinum-based analogues. Amino acid-linked platinum(II) (AAPt) compounds of alanine, ornithine, and arginine (AlaPt, OrnPt, and ArgPt, respectively) have unique reactivities that result in altered preferences for adenosine (Ado) or deoxyadenosine (dAdo) residues. The compounds predominantly form monofunctional adducts by reacting at the N1, N3, or N7 positions of purine nucleobases. Features of the AAPt compounds that impact glycosidic bond stability of Ado residues were explored in this chapter. The glycosidic bond cleavage of the adducts was investigated using energy-resolved collision-induced dissociation (ER-CID) tandem mass spectrometry and survival yield analysis (in collaboration with Dr. M.T. Rodgers' lab). Our results indicate that glycosidic bond cleavage is activated differentially for AlaPt-Ado and OrnPt-Ado isomers. Formation of unique adducts at non-canonical residues and subsequent destabilization of the glycosidic bonds are important features that could circumvent cisPt-based drug resistance.

5.2 Introduction

Modification of nucleic acid residues may have unique influences on the chemical properties of nucleosides such as bond strengths. Alkylation or protonation of DNA residues have previously been reported to weaken the glycosidic bonds and accelerate the process of depurination [115-118]. Hydrolytic instability of purine glycosidic bonds may impact nucleoside integrity, particularly under varying pH and ionic strength conditions and modification states [116, 119-121]. Stability of the glycosidic bonds is important for maintaining the integrity of nucleic acids and crucial for cell viability [159-160]. Previous experiments with *N*-glycosydases showed that hydrolytic cleavage of particular Ado glycosidic bonds in rRNA is toxic, as it causes inactivation of the ribosome [159].

In a previous theoretical study, evaluation of the effects of cisPt modification indicated that platination at N7 does not impact stability of the dGuo glycosidic bond [26]. However, platination of nucleic acids by other cisPt analogues may have an impact on glycosidic bond strengths. To the best of our knowledge, the influence of platination on the glycosidic bonds of dAdo or Ado adducts has not been investigated, likely because cisPt and other platinum-based compounds coordinate preferentially with dGuo (or Guo) residues. AAPt compounds, including AlaPt, OrnPt, and ArgPt, have reactivity preferences for Ado and dAdo residues (discussed in **Chapters 3** and **4**). A previous report from our lab also showed that OrnPt has the ability to modify Ado residues in folded RNA [106]. We therefore sought to evaluate the relative glycosidic bond strengths of these non-canonical structures.

Structural and chemical features of platinum-based compounds could determine the extent of glycosidic bond stability once coordination with a nucleotide occurs. For AAPt compounds, the type of side chain and the backbone atoms may affect stability of the adduct. Glycosidic bond strength may also be affected differentially depending on the position of the nucleobase at which the AAPt compounds platinate. The reactions of monoaquated AAPt compounds with Ado result in formation of multiple monofunctional adduct isomers. These

constitutional isomers vary at the sites at which platination occurs, including N1, N3, or N7 positions (**Fig. 5.1**). Understanding the features that promote glycosidic bond destabilization in nucleic acids is important for development of analogues that trigger unique cytotoxic responses not exhibited by cisPt [55, 29, 154]. Possible destabilization that activates cleavage of the glycosidic bonds in AAPt-Ado adducts could also be exploited as a therapeutic pathway against cisPt resistant cancer cells. This is also potentially useful in understanding features of platinum-based drug candidates that have improved cellular activities and effectiveness in cancer cells.

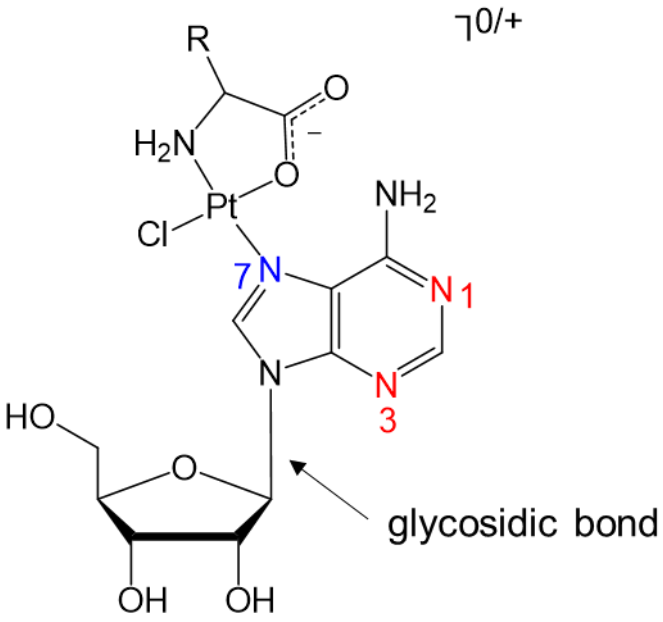

Figure 5.1 Structure of monofunctional AAPt-Ado adduct. The AAPt compounds (AlaPt, OrnPt, or ArgPt) can coordinate at the N1, N3, or N7 position of nucleobase forming constitutional isomers. The glycosidic bond of the adduct is shown.

In this collaborative project, I first carried out the synthesis of AAPt compounds followed by reactions with Ado nucleosides as described in **Chapter 2**. Using HPLC fitted with a C18 column, I isolated products from each individual reaction so as to obtain enough samples for NMR

spectroscopy characterization and subsequent tandem mass spectrometry analysis. Energy-resolved collision-induced dissociation (ER-CID) tandem mass spectrometry and survival yield analysis was carried out by Dr. C. C. He in Dr. M. T. Rodgers' lab.

ER-CID tandem mass spectrometry and survival yield analysis have been used previously to investigate glycosidic bond stabilities [116, 122-125]. In this thesis work, the techniques were also applied to investigate the impact of AAPt coordination on relative glycosidic bond strengths. In ER-CID tandem mass spectrometry, isolated HPLC fractions containing the nucleoside-platinum adducts are first ionized in the ESI source. The nucleoside-platinum precursor ions are mass selected and guided into the ion trap where cleavage of adduct ions is activated using ER-CID. This step is followed by mass analysis and detection of the resultant fragments (**Fig. 5.2**). Survival yield analysis is a method that monitors the fragmentation patterns of ions as a function of excitation voltage [142]. The setup of ER-CID experiments and survival yield analysis was described in **Section 2.4.12**.

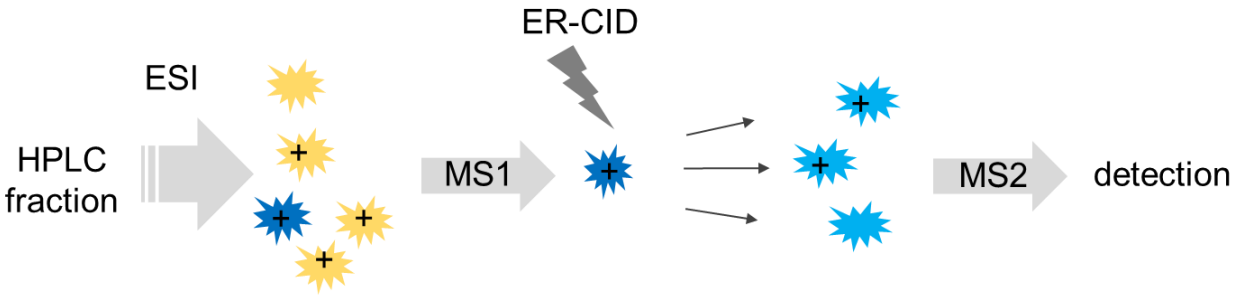

Figure 5.2. Schematic representation of the ER-CID experiment. HPLC isolated adduct fractions are ionized in the ESI source. Precursor ions are mass selected in MS1 and guided into the ion trap where they are fragmented by ER-CID. Fragments are then mass analyzed in MS2 followed by detection.

5.3 Results and discussion

5.3.1 Non-canonical AAPt-Ado adduct isomers and their differential fragmentation patterns

The reactions of Ado with the monoaquated AAPt compounds result in the formation of more than one product as discussed in **Chapter 3**. These products were separated by HPLC using a C18 column (**Chapter 3, Fig. 3.3B)**. Characterization of the HPLC isolated products using mass spectrometry and NMR spectroscopy were discussed in **Section 3.3.1.**

The fragmentation pattern of these adducts and the stability of their glycosidic bonds can be affected differentially depending on the type of amino acid ligand linked to the platinum center of the AAPt compound. Furthermore, isomers can also exhibit differences in stability dictated by the site of platination (N1, N3, or N7). Cleavage of AAPt-Ado$_{N1/N3}$ and AAPt-Ado$_{N7}$ isomers was activated through CID and composition of the fragments was determined by using tandem mass spectrometry in which several fragmentation products (both charged and neutral) could be formed, depending on the bond stability (**Fig. 5.3**).

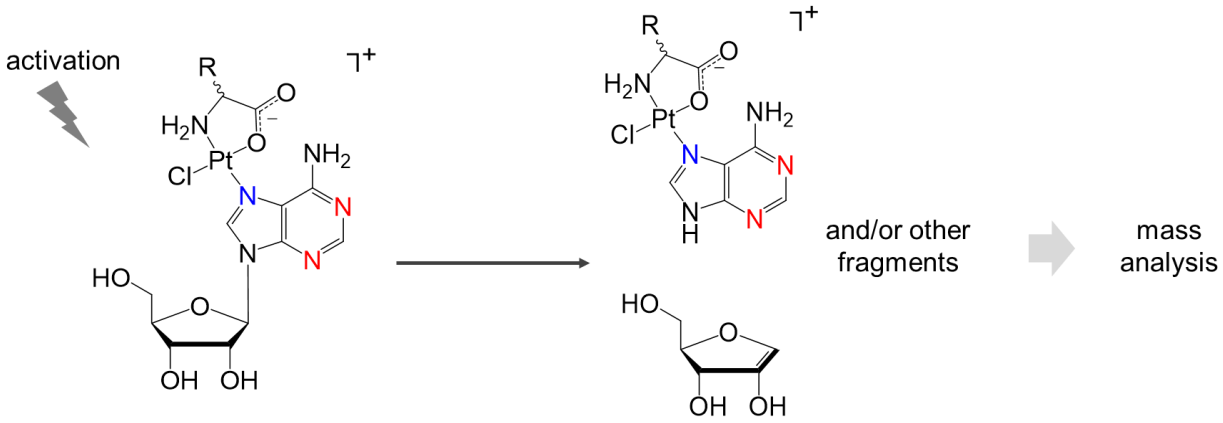

Figure 5.3. Activation of AAPt-Ado adduct towards cleavage. Activation by CID of the precursor ion results in cleavage of different bonds including the glycosidic bond. Charged and neutral fragments are formed, depending on which functional groups are lost.

Despite having different platination sites, the N1/N3 and N7 adducts of AlaPt-Ado produce comparable fragmentation patterns with a major fragment (m/z: 454.036 Da) formed by loss of the ribose sugar (132.042 Da) (**Fig. 5.4**). The loss occurs via glycosidic bond cleavage following

proton transfer of H2' to the nucleobase [120]. Minor neutral losses of HCl, H_2O, and [Pt(Ala)(Cl)–H] from AlaPt-Ado$_{N1/N3}$ (m/z: 550.101, 532.091 and 268.104 Da, respectively) are also observed.

In contrast to the AlaPt-Ado adducts, fragmentation patterns of the OrnPt-Ado adducts vary between the isomers, despite being subjected to similar fragmentation conditions (**Fig. 5.5**). Two groups of fragments are observed in each CID mass spectrum. The first group contains fragments formed by loss of neutral molecules of NH_3, HCl, and (NH_3 + HCl) from OrnPt-Ado (m/z: 612.080, 593.130, and 576.103 Da, respectively); the second group corresponds to fragments involving glycosidic bond cleavage ions resulting in loss of the ribose sugar and the same neutral losses (m/z: 497.063, 480.036, 461.085, and 444.058 Da, respectively). For OrnPt-Ado$_{N1/N3}$, both groups have approximately the same intensity, whereas for OrnPt-Ado$_{N7}$, the second group of fragments dominate. This result indicates a difference in the overall stability of the glycosidic bonds of these two OrnPt-Ado isomers.

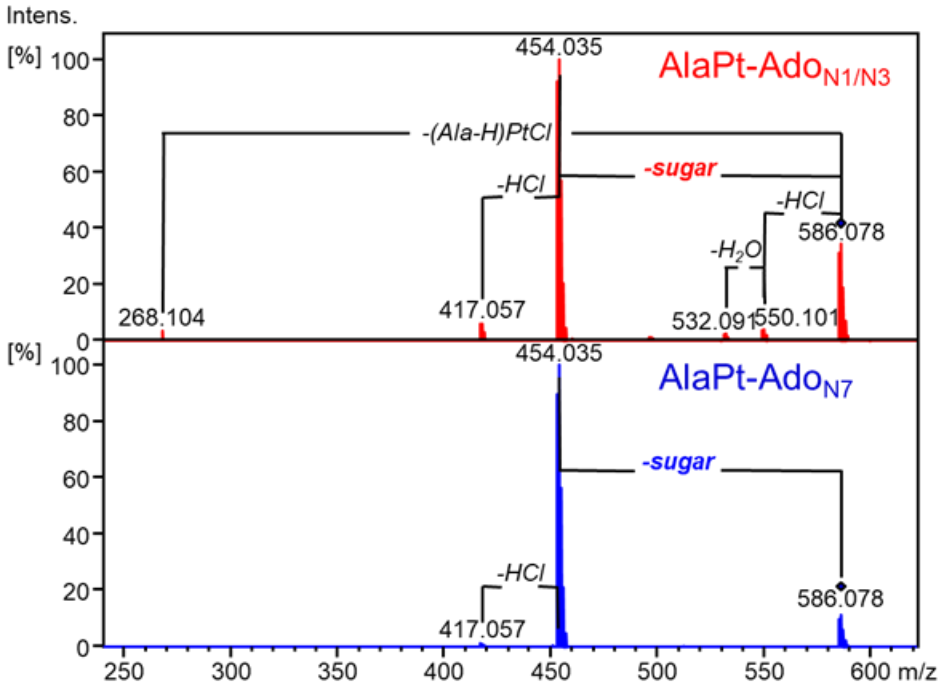

Figure 5.4. **CID fragmentation patterns of AlaPt-Ado adducts.** AlaPt-Ado$_{N1}$ (or AlaPt-Ado$_{N3}$) and AlaPt-Ado$_{N7}$ fragmentation patterns are shown. The spectra were obtained by Dr. C. C. He in Dr. M. T. Rodgers' lab.

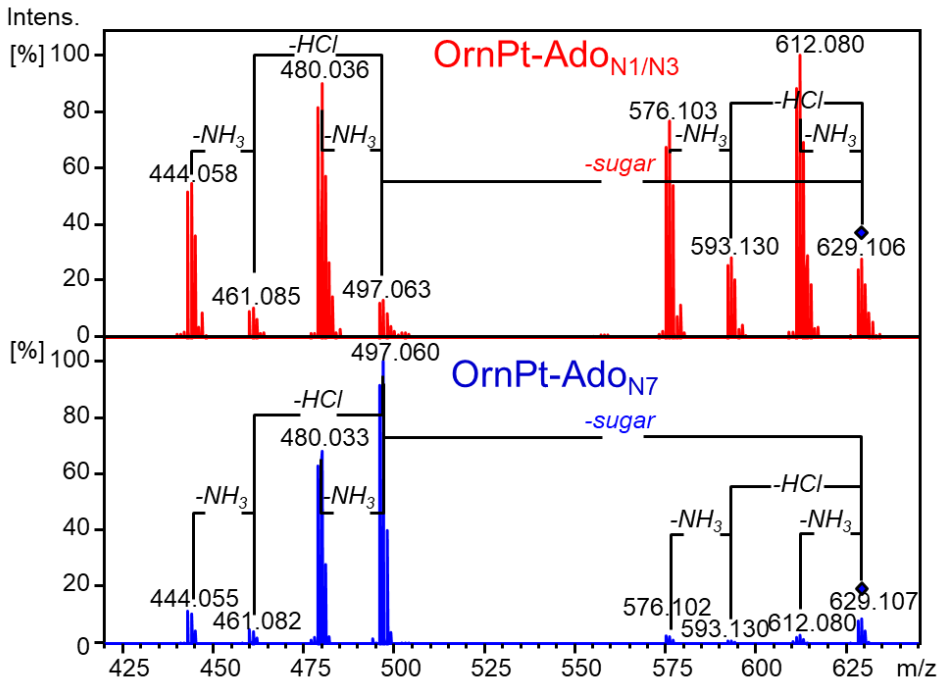

Figure 5.5. **CID fragmentation patterns of OrnPt-Ado adducts.** OrnPt-Ado$_{N1}$ (or OrnPt-Ado$_{N3}$) and OrnPt-Ado$_{N7}$ fragmentation patterns are given. The spectra were obtained by Dr. C. C. He in Dr. M. T. Rodgers' lab.

Similar to the OrnPt-Ado adducts, fragmentation patterns of the ArgPt-Ado adducts also vary between the isomers, despite being subjected to similar fragmentation conditions (**Fig. 5.6**). Two groups of fragments are also observed in each CID mass spectrum. The first group contains fragments formed by loss of neutral molecules of H_2O, HCl, and CH_4N_2O from ArgPt-Ado (m/z: 653.131, 635.165, and 611.110 Da, respectively); the second group corresponds to fragments involving glycosidic bond cleavage ions resulting in loss of the ribose sugar and the same neutral losses (m/z: 539.099, 521.088, 503.123, and 479.067 Da, respectively). For ArgPt-Ado$_{N1/N3}$, both groups have a wide range of intensities, with the loss of CH_4N_2O being the most intense. For ArgPt-Ado$_{N7}$, both groups have a wide range of intensities, but the loss of the sugar is more dominant. This result indicates a difference in the overall stability of the glycosidic bonds of these two ArgPt-Ado isomers.

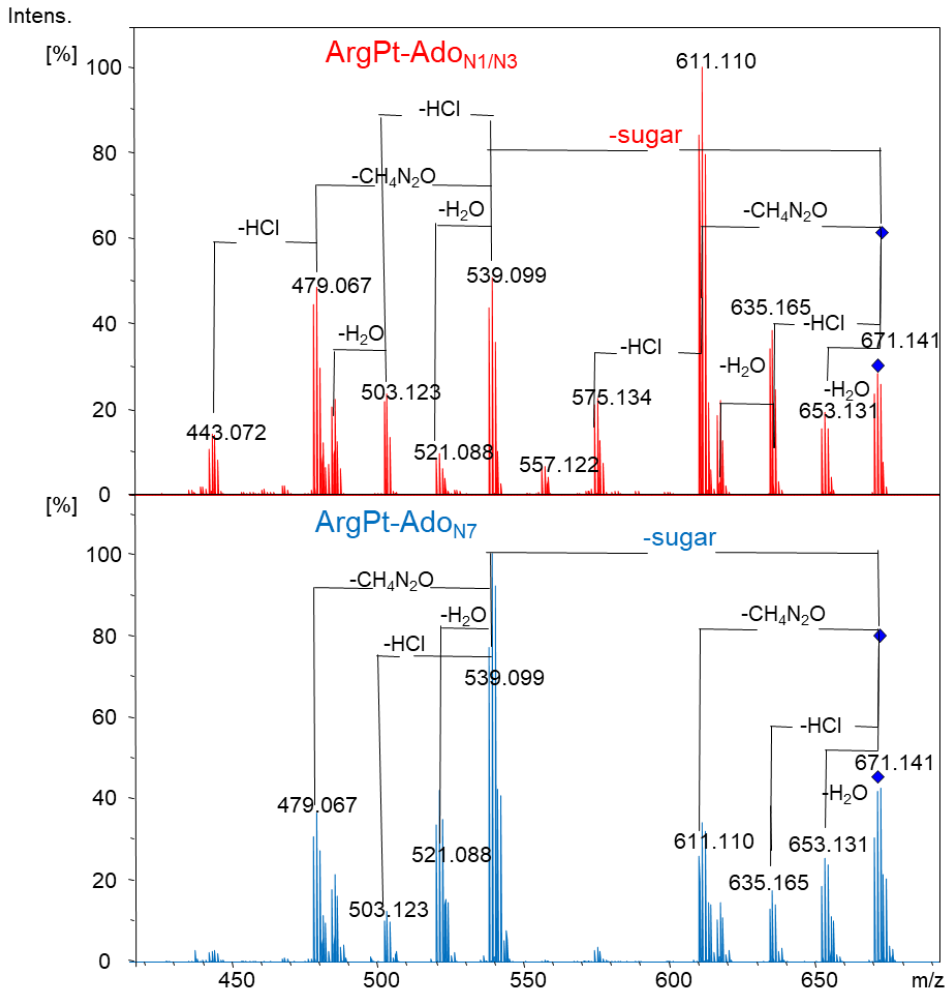

Figure 5.6. **CID fragmentation patterns of ArgPt-Ado adducts.** ArgPt-Ado$_{N1}$ (or ArgPt-Ado$_{N3}$) and ArgPt-Ado$_{N7}$ mass spectra are shown. The spectra were obtained by Dr. C. C. He in Dr. M. T. Rodgers' lab.

5.3.2 Differential activation of AAPt-Ado isomers towards glycosidic bond cleavage

Glycosidic bond survival yield analysis employing ER-CID tandem mass spectrometry has been used previously to study relative stabilities of the glycosidic bonds in the context of cationization and protonation of purine (deoxy)nucleosides [120, 124, 161-162]. In this study, we aimed at investigating the glycosidic bond stabilities of AAPt-nucleoside adduct isomers. First, I carried out reactions of AAPt compounds with Ado and isolated the adducts by HPLC using a C18 column. This was followed by survival yield analysis carried out by Dr. C. C. He. Glycosidic bond survival yield of the two AlaPt-Ado adducts (referred to as N1/N3 and N7, depending on the

platination site) were compared in order to determine their relative glycosidic bond stabilities. Because the adducts are isomers, they have an equal number of atoms and degrees of freedom, and thus internal energy and dissociation lifetime effects on the fragmentation should be very similar such that differences in the survival yield can be directly correlated to glycosidic bond stability. The two OrnPt-Ado adducts were compared in a similar fashion.

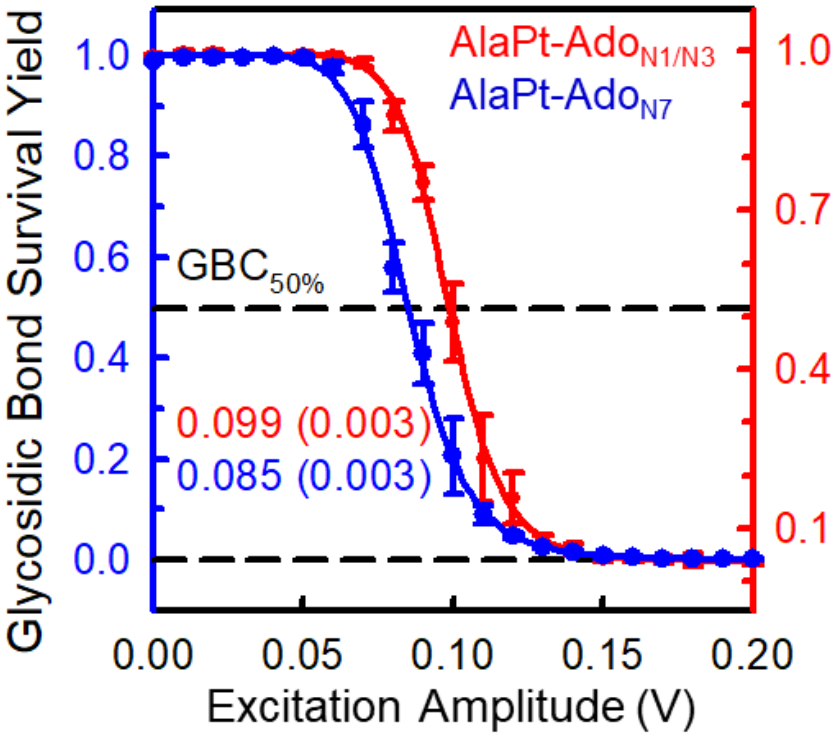

Figure 5.7. Glycosidic bond survival yield curves of AlaPt adduct isomers. Glycosidic bond survival yield curves of AlaPt-Ado$_{N1/N3}$ in red and AlaPt-Ado$_{N7}$ in blue. The spectrum was obtained by Dr. C. C. He in Dr. M. T. Rodgers' lab.

Fits to the survival yield curves of the AlaPt-Ado isomers produce GBC$_{50\%}$ values for AlaPt-Ado$_{N1/N3}$ and AlaPt-Ado$_{N7}$ of 0.099 V and 0.085 V, respectively (**Fig. 5.7**). Platination in both isomers activates dissociation primarily through cleavage of the glycosidic bond with 95% and 100% of the fragmentation of AlaPt-Ado$_{N1/N3}$ and AlaPt-Ado$_{N7}$ occurring via glycosidic bond cleavage, respectively, *i.e.*, neutral losses account for 5% or less of the dissociation behavior for both AlaPt-Ado isomers. Trends in the GBC$_{50\%}$ values indicate that N7 platination is more activating than N1/N3 platination.

The $GBC_{50\%}$ values determined for OrnPt-$Ado_{N1/N3}$ and OrnPt-Ado_{N7} are much larger, 0.364 V and 0.351 V, respectively (**Fig. 5.8**). The trend in these values again indicates that N7 platination activates the glycosidic bond more effectively than N1/N3 coordination of platinum. Furthermore, both OrnPt-Ado adducts exhibit significant competition between glycosidic bond cleavage and neutral loss pathways. Indeed, neutral loss pathways account for 60% and 10% of dissociation for OrnPt-$Ado_{N1/N3}$ and OrnPt-Ado_{N7} adducts, respectively. Because AlaPt and OrnPt-Ado differ in size, direct comparison of $GBC_{50\%}$ values may be problematic, but the large shifts in these values determined for the AlaPt-Ado vs. OrnPt-Ado adducts strongly suggest that binding of AlaPt activates the glycosidic bond more effectively than OrnPt binding. The increased competition with the neutral loss pathways in OrnPt-Ado compared to AlaPt-Ado adducts also supports this conclusion.

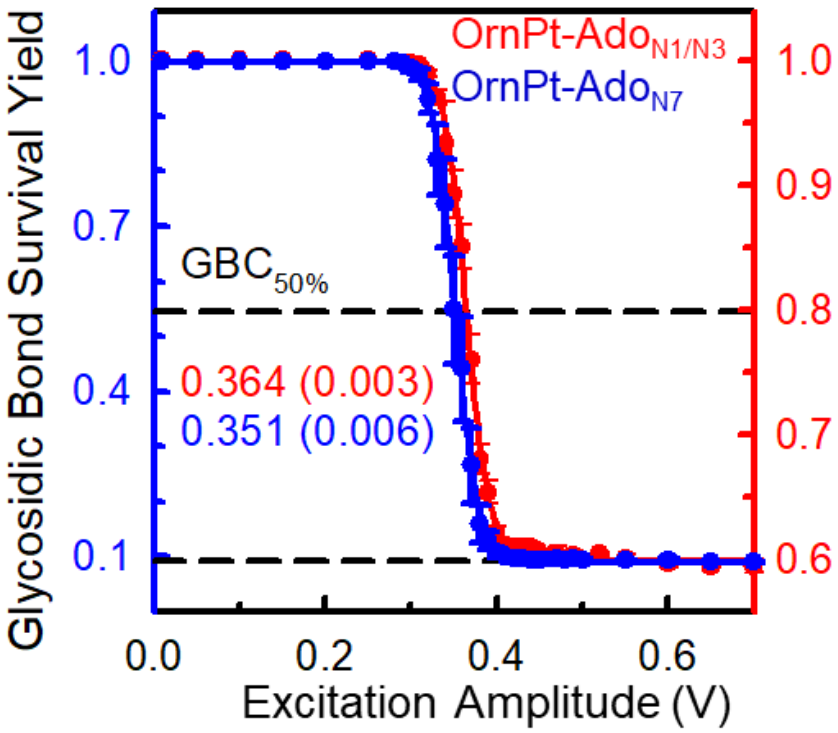

Figure 5.8. Glycosidic bond survival yield curves of OrnPt adduct isomers. Glycosidic bond survival yield curves of OrnPt-$Ado_{N1/N3}$ in red and OrnPt-Ado_{N7} in blue. The spectrum was obtained by Dr. C. C. He in Dr. M. T. Rodgers' lab.

The survival yield analysis of ArgPt-Ado isomers (ArgPt-Ado$_{N1/N3}$ and ArgPt-Ado$_{N7}$) will be performed in the future. Because of the observed difference in CID fragmentation pattern (**Fig. 5.6),** they are predicted to have different behaviors in their glycosidic bond cleavage and neutral loss pathways.

The difference in stability between the adduct isomers suggests that two factors can influence the glycosidic bond stability, the type of amino acid ligand linked to the platinum center, and the site at which the AAPt coordinates with the nucleoside. Platination by monoaquated AlaPt results in adduct isomers that have relatively lower glycosidic bond stabilities than adduct isomers formed by monoaquated OrnPt. The fact that N7 platination by AlaPt and OrnPt results in lower adduct glycosidic bond stability compared to N1 (or N3) platination suggests that the closer the proximity of the platination site to the ribose sugar, the greater the destabilization of the glycosidic bond. Protonation or platination modifications on the nucleoside can accelerate the depurination reaction by reducing the transition state energy [26]. The ligands of AlaPt or OrnPt may cause electron-density withdrawal at the N9 position in a manner that is dependent on proximity of the platinum atom. In the future, further tandem mass spectrometry and spectroscopic studies, including computational analysis, will be performed in an effort to elucidate detailed mechanisms for glycosidic bond cleavage of the N7 and N1/N3 AlaPt , OrnPt, and ArgPt adduct species, as done previously with both standard and modified nucleosides [116, 120, 163] .

5.4 Conclusions

Enzymatic cleavage of Ado glycosidic bonds in RNA and subsequent depurination are lethal to cells [159, 164]. Alternatively, cleavage through activation of glycosidic bonds could lead to fragmentation of nucleic acids [115-118]. In this collaborative work with Rodgers' laboratory, glycosidic bond survival yield analysis was applied to determine the impact of AAPt coordination on the relative glycosidic bond strength of an RNA-based nucleoside, Ado. When either AlaPt or OrnPt coordinate to the N7 position of Ado, they destabilize the glycosidic bond to a greater extent than when coordination occurs at the N1/N3 position. Overall, AlaPt almost exclusively activates

the resulting AlaPt-Ado adduct via cleavage of the glycosidic bond. In contrast, OrnPt is less activating of the glycosidic bonds such that fragmentation of OrnPt-Ado also involves other neutral loss pathways. Such activation of AAPt-Ado adducts is particularly important considering that cisPt is reported to have no destabilizing effect on the glycosidic bonds of target dGuo residues [26]. Within a biological context, AlaPt and OrnPt could potentially exert destabilization of glycosidic bonds in nucleic acid residues and lead to abasic sites. Formation of abasic sites, especially in RNA, could possibly trigger apoptosis, as well as provide an alternative pathway of cytotoxicity that circumvents cisPt resistance. The variation in the influence of AlaPt and OrnPt on Ado also highlights the importance of structure for other classes of platinum-based drugs in determining their preferred target residues and impact on adduct stability.

CHAPTER 6

POTENCY AND ACCUMULATION OF AMINO ACID-LINKED PLATINUM COMPOUNDS IN HUMAN CANCER AND NORMAL CELLS

6.1 Abstract

Although cisplatin (cisPt) is widely used for treatment of a variety of cancer types, its therapeutic application has major drawbacks due to resistance, adverse toxicity, and reduced accumulation. Second generation analogues including carboplatin and oxaliplatin have reduced toxicity and resistance, but have low potency compared to cisPt. It is therefore important to develop more ideal platinum-based compounds that balance between potency, selectivity for cancer cells, and reduced toxicity in normal cells. Amino acid-linked platinum(II) (AAPt) compounds including AlaPt, OrnPt, and ArgPt provide another class of metal-based compounds with oral drug-like features that conform with Lipinski rules. At the molecular level, these compounds have been demonstrated to have altered reactivity preferences and form non-canonical adducts compared to cisPt. The altered reactivity preference could translate to unique activity at the cellular level that triggers different cytotoxic responses in cancer and normal cells. In this thesis chapter, the half maximal inhibitory concentration (IC_{50}) values of AAPt compounds with various cancer and normal cells are reported. The values were determined using the MTT (3-(4,5-dimethylthiaxol-2-yl)-2,5-diphenyltetrazolium bromide) assay. AlaPt, OrnPt, and ArgPt are observed to have a wide range of potencies in the chosen cell lines. Whereas cisPt does not exhibit selective potency with these cell lines, ArgPt exhibits selective potency in prostate cancer cells over normal cells. The uptake and accumulation of platinum-based compounds in cancer cells determines the extent of the cellular response that leads to apoptosis. Accumulation of the AAPt compounds in prostate cancer and other cancer cell lines was determined using inductively coupled plasma mass spectrometry (ICP-MS). Compared to cisPt, ArgPt has significantly higher accumulation in prostate cancer cells. These studies are important for correlating potency and

uptake of platinum-based compounds with other factors such as structural features of the compound and DNA/RNA adducts.

6.2 Introduction

CisPt is a common metal-based anticancer drug used for the treatment of a variety of cancer types [18, 11]. It has a cure rate of up to 80% in some forms of cancer such as testicular cancer [18, 11]. However, cisplatin cancer applications have been hindered by drawbacks such as resistance and adverse side effects such as nephrotoxicity [165-166, 71]. Resistance occurs when cancerous cells do not undergo apoptosis within the clinically relevant drug doses. Factors that lead to resistance include reduced drug accumulation, increased thiol levels that inactivate cisPt, and increased DNA damage repair that removes cisPt adducts [71]. CisPt can also cause major toxic side effects including nephrotoxicity, which occurs when cisPt accumulates in the kidney and causes injury to renal epithelial cells, leading to undesirable death of healthy cells [167]. To mitigate these challenges, analogues of cisPt such as carboplatin and oxaliplatin have been developed with the goal of reducing toxicity and resistance [16]. The chemical characteristics of carboplatin gives it an advantage over cisPt, and toxicity can be circumvented due to its lower reactivity and adduct formation (discussed in **Chapter 1, Section 1.4.3**) [91]. Despite having reduced toxicity and lower cellular resistance, the activity of analogues such as carboplatin has been hampered by lower potency. As high as 90% of administered carboplatin does not react with the target and is excreted, meaning that a much higher dose is required in order to achieve the same effectiveness as cisPt [16]. It is therefore desirable to develop new platinum-based compounds that have the same or better efficacy than cisPt while being selective for cancer cells in order to reduce the toxic side effects. The compounds should also be able to circumvent cellular resistance so as to impart apoptosis of tumor cells even with long-term use.

The potency of platinum-based compounds can be determined using their IC_{50} values. An IC_{50} value refers to the concentration of a compound that causes a reduction in cell viability by 50%. IC_{50} values of compounds can be determined by using quantitative colorimetric techniques

such as the MTT assay (discussed in **Chapter 2, Section 2.4.13**) [168]. This assay is used to quantify the number of viable cells based on the amount of metabolic activity that is detected. In this assay, the mitochondrial NAD(P)H-dependent reductase enzymes in viable cells reduce the MTT into the insoluble, purple compound known as formazan [169]. Formazan crystallizes on the cell surface and is then dissolved by solvents such as dimethyl sulfoxide (DMSO) [168-169]. Absorbance measurements of the resulting solutions are taken using a spectrophotometer. The absorbance readings are correlated with the percentage of viable cells and plotted as a function of compound concentration [170]. The fitted dose-response curves are used to extract the IC_{50} values.

The MTT assay has been modified in which tetrazolium is used to determine the IC_{50} values of compounds in cells. The alternative reagents also include MTS (3-(4,5-dimethylthiazol 2-yl)-5-(3-carboxymethoxyphenyl)-2-(4-sulfophenyl)-2H-tetrazolium), XTT (2,3-bis-(2-methoxy-4-nitro-5-sulfophenyl)-2H-tetrazolium-5-carboxanilide), and WST (2-(2-methoxy-4-nitrophenyl)-3-(4-nitrophenyl)-5-(2,4-disulfophenyl)-2H-tetrazolium) [170]. These assays have been modified to eliminate the need for washing and solvent solubilization steps because they generate water-soluble products [171]. However, the MTT assay is still preferred for investigating cell viability and proliferation [171] because of its higher sensitivity and validated use in miniaturized high-throughput assays [171]. This technique is also preferred over alternatives such as the radioactive isotope-based thymidine incorporation assay, which is more time consuming and expensive [171-172]. Other techniques such as counting total viable cells using a hemocytometer are cumbersome and require a large number of samples to be processed [172].

The IC_{50} values of FDA-approved platinum compounds varies depending on the compound, the type of cells being treated, and the length of time of treatment [173-182]. In **Table 6.1**, examples of IC_{50} values of the FDA-approved platinum-based drugs in common cell lines are given. Generally, the IC_{50} values of cisPt are lower than carboplatin [33-36]. For example, cisPt has an IC_{50} value of 21 μM in a lung H1299 cell line following 72 h of treatment, whereas

carboplatin achieves a similar value after 5 days of treatment (**Table 6.1**) [174, 180]. In lung cell lines A549 and MCF7, oxaliplatin has similar or lower IC_{50} values than cisPt (**Table 6.1**) [178-179, 182]. This may be attributed to the structural characteristics of oxaliplatin, which includes its relatively larger non-leaving ligand that triggers cell death by protruding into the major groove and effectively blocking DNA replication and transcription (discussed in **Chapter 1, Section 1.4.3**) [94, 96].

Table 6.1. IC_{50} (μM) values of cisPt, carboplatin, and oxaliplatin in human cancer cell lines

tissue	**cell line [ref]**	**cisPt (time) [ref]**	**carboplatin (time) [ref]**	**oxaliplatin (time) [ref]**
lung	lung H1299 [129]	21 ± 4 (72 h) [180]	19 ± 3 (5 d) [174]	-
cervical	HeLa [132]	2 ± 1 (72 h) [181]	5 ± 2 (96 h) [175]	12 ± 1 (72 h) [181]
breast	MDA-MB-231 [130]	1.4 ± 0.2 (5 h) [182]	8 ± 1 (5 d) [182]	23 ± 1 (72 h) [176]
lung	A549 [183]	3 ± 1 (5 d) [182]	20 ± 1 (5 h) [182]	0.9 ± 0.1 (72 h) [178]
lung	MCF7 [184]	16 ± 6 (24 h) [179]	4 (48 h) [173]	2 ± 1 (24 h) [179]
prostate	DU145 [133]	3 (72 h) [177]	10 ± 1 (48 h) [174]	2.1 ± 0.2 (72 h) [178]

The AAPt compounds could provide another class of metal-based compounds with oral drug-like features according to Lipinski rules [126]. The Lipinski rules are a set of requirements that predict the overall cell absorption and drug-likeness of a compound. The Lipinski criteria

require that compounds should not violate more than one of the four rules, which include having: 1) less than 500 Da in molecular weight, 2) less than five hydrogen-bond donors, 3) less than ten hydrogen-bond acceptors, and 4) log*P* values of not greater than five [185]. The structural characteristics and molecular weights of AAPt compounds conform with the Lipinski rules (**Fig. 6.1**). There has been limited previous attempts to investigate the activity and potency of AAPt compounds in cancer cell lines. The cytotoxicity of ArgPt, LysPt (lysine-linked platinum(II)), and several LysPt-related derivatives were previously investigated in HeLa and KM-12 cell lines using colony counting method [112, 103]. In these studies, ArgPt and LysPt exhibited promising IC_{50} values of 25 µM in a HeLa cell line following 24 h of treatment and further 7-10 days of cell growth [112]. There is still a need to investigate the potency of AAPt compounds (including AlaPt and OrnPt) in a larger variety of cancer cell lines including cisPt-resistant and cisPt-sensitive cells. The results would provide a deeper understanding of the features of platinum-based compounds that promote their activity, selectivity, and circumvention of resistance.

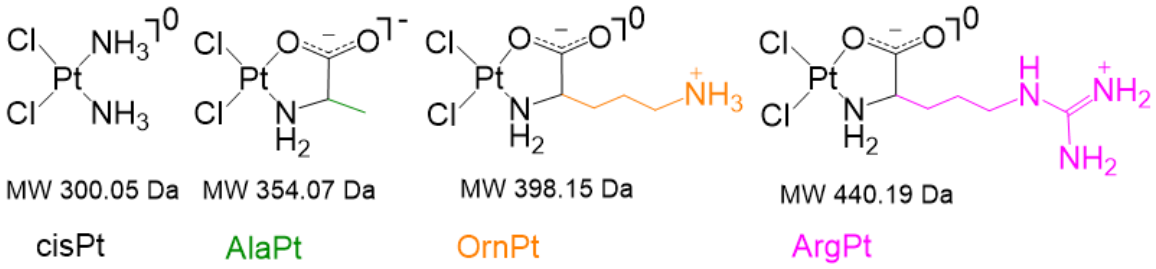

Figure 6.1. The structures of cisPt and AAPt compounds. The structures and molecular weights of cisPt, AlaPt, OrnPt, and ArgPt are given.

The drawbacks of cisPt therapy such as resistance due to DNA repair, non-selectivity, and toxicity limit its effectiveness, but could possibly be mitigated by compounds that form adducts at novel targets that are not preferentially platinated by cisPt. CisPt preferentially binds with DNA dGuo residues, which plays a role in its anticancer activity [18, 27, 40, 38]. Formation of adducts at non-canonical sites could be important in circumventing resistance and triggering alternative cytotoxic pathways in tumor cells. In **Chapter 4**, it was demonstrated that AAPt compounds

(AlaPt, OrnPt, and ArgPt) have altered reactivity compared to cisPt. AAPt compounds have reactivity preferences for dAdo and Ado residues of DNA and RNA [105-106]. These AAPt compounds could become candidates that induce alternative cytotoxic pathways by involving non-canonical targets such as dAdo residues of DNA as well as Ado residues of RNA. The features of compounds that lead to tumor cell death can be investigated at both the molecular and cellular levels.

In this thesis chapter, the anticancer potency of AAPt compounds at the cellular level is reported. The IC_{50} were determined in several human cancer cell lines by using MTT assay. The potency of the compounds was investigated in prostate, breast, and lung cancer cell lines. Prostate and lung cancers are the leading causes of cancer-related deaths among men in the United States, whereas breast and lung cancers are the leading causes of cancer-related deaths among women [186]. CisPt chemotherapy has been applied in the treatment of lung, breast, and prostate cancer [187-189], but has been hindered by adverse toxicity, side effects, and resistance [187-188]. Therefore, there is a need to develop other platinum-based compounds that have better activity and selectivity than cisPt in these forms of cancer.

The accumulation of anticancer compounds inside cells is an important aspect that drives their pharmacological impacts. Low accumulation of cisPt in cells causes DNA damage, which potentially stimulates resistance rather than apoptosis [71]. Reduced cellular accumulation of cisPt is caused by factors such as disruption of drug uptake or increased efflux [71]. Higher cellular accumulation of cisPt (or other platinum-based compounds) is important for formation of a sufficient number of DNA adducts to trigger apoptosis. Therefore, accumulation of the compounds in cells can be correlated with their potency and IC_{50} values, in which higher accumulation corresponds to higher potency (and lower IC_{50} values). Previously, whole cell cisPt uptake in cisPt-sensitive and cisPt-resistant lung tumor cells was determined by using ICP-MS [190]. It was observed that cisPt-resistant cancer cells have four-fold lower uptake of cisPt compared to the cisPt-sensitive cells following exposure to the drug for a similar period of time [190]. The amount

of cisPt bound to biological targets such as DNA and RNA, has been quantified in other studies by using ICP-MS [59]. In the thesis work reported in this chapter, cellular accumulation of AAPt compounds in comparison to cisPt in both cancer and normal cells was determined using ICP-MS. The structural characteristics of AAPt compounds could be important for efficient cellular uptake and accumulation. The positively charged ligand side chains of ArgPt and OrnPt could promote cell penetration due to electrostatic interactions with the anionic plasma membrane [191]. Cancer cells have a net negative charge on the surface on their cell membranes compared to normal cells [192-194]. This can be attributed to high levels of lactate anions secreted by cancer cells that minimize the presence of cations on the cell surface and promote a net negative charge [195]. This behavior is unique to cancer cells, which have an active metabolism that causes glycolysis to form high amounts of lactate anions compared to normal cells [196]. Furthermore, cancer cells have upregulation of negatively charged sulfated proteoglycans on the cell surface that further contribute to the negative charge [197-198]. Favorable interactions with the negative cell surface prior to uptake could favor selective targeting of cancer cells.

6.3 Results and discussion

6.3.1 Potency of AAPt compounds in human cancer and normal cells

The potency of AAPt compounds in prostate (DU145), lung (H1299), breast (MDA-MB-453 and MDA-MB-231), and cervical (Hela) cancer cell lines was investigated by using the MTT assay. The activities of platinum-based compounds in prostate normal (RWPE-1) and prostate cancer (DU145) cell lines were also determined so as to understand their selective potency. The MTT assay, as described in **Section 2.4.13**, was used to investigate the viability of cells following treatment with the AAPt compounds and cisPt. The percentage of viable cells as a function of increasing concentration of platinum-based compounds was plotted and used to extract the IC_{50} values.

The DU145 cell line was treated with the AAPt compounds (and cisPt) for 72 h. The dose-response curves show that the percentage of viable cells decreases with an increase in the

concentration of platinum-based compound (**Fig. 6.2**). The degree in which the number of viable cells decreases depends on the identity of the platinum compound (cisPt, AlaPt, OrnPt, and ArgPt). These results suggest that the different structural forms of the platinum-based compounds have different uptake levels and/or trigger different cytotoxic responses in the cells.

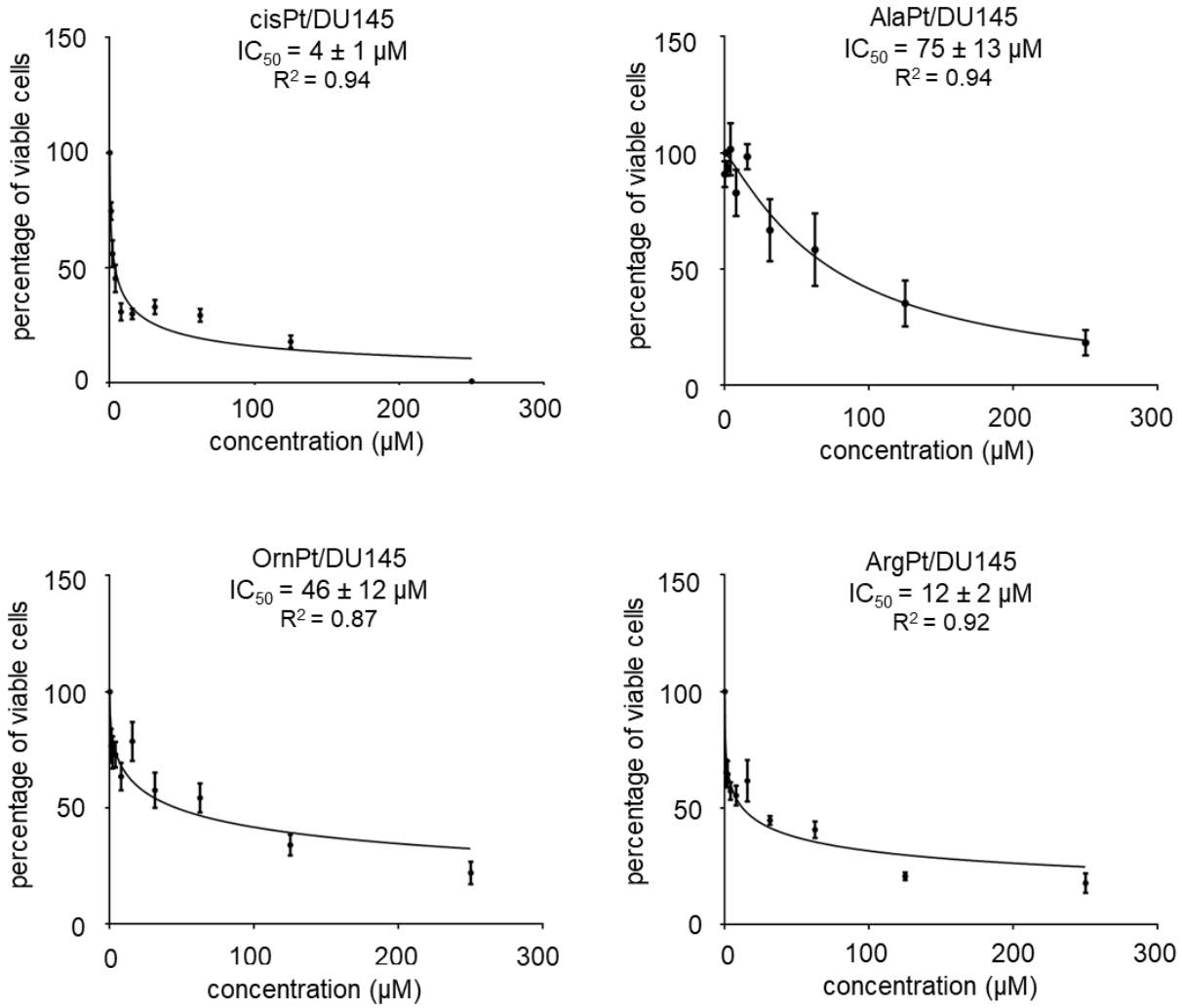

Figure 6.2. Dose-response curves of AAPt compounds (and cisPt) in prostate cancer (DU145) cell line. The MTT assay was used to determine the percentage of viable cells as a function of increasing concentration of platinum-based compound. The type of cancer cell line and platinum-based compound used are indicated in the plots. All cells were treated for 72 h. Cells have varied responses to the different compounds used in the assay. GraphPad PRISM software was used for curve fitting using the model equation $Y=100/(1+(X^{hillSlope})/(IC_{50}{}^{hillSlope}))$, in which hillslope is -1. IC_{50} values were extracted from the plots. Each plot is from at least two biological replicates.

From the dose-response curves, the AAPt concentrations that resulted in 50% reduction of viable cells (IC_{50} values) were extracted. The IC_{50} value of cisPt was compared to those of AAPt compounds (**Table 6.2**). Cispt has an IC_{50} value of 4 µM in prostate cancer cells following the 72 h treatment. This value is consistent with a reported IC_{50} value of 3 µM following treatment of the same cell line with cisPt over 72 h [177]. AlaPt has an IC_{50} value of 75 µM in the DU145 cell line, which is 19-fold higher than cisPt value (**Table 6.2**). This result shows that in this cell line, AlaPt is less potent (or has lower uptake) and its chemical structure does not elicit cytotoxic responses comparable to cisPt. OrnPt has an IC_{50} value of 46 µM in the DU145 cell line which is 11-fold higher than cisPt (**Table 6.2**). This result shows that OrnPt is also less potent in prostate cancer cells compared to cisPt.

Table 6.2. Comparison of potency of AAPt compounds, cisPt, and carboplatin in DU145 cell line

Compounds (ref)	**cell line (ref)**	**IC_{50} value (µM)[‡]**
cisPt	DU145 [133]	4 ± 1
AlaPt	DU145 [133]	75 ± 13
OrnPt	DU145 [133]	46 ± 12
ArgPt	DU145 [133]	12 ± 2
carboplatin [174]	DU145 [133]	10 ± 1

[‡]error is from at least two biological replicates

ArgPt has an IC_{50} value of 12 µM in the DU145 cell line (**Table 6.2**). This value is three-fold higher than that of cisPt, showing only a moderately lower potency. Although the low IC_{50} value of cisPt may translate to high potency, the high activity may also cause toxicity to rapidly dividing cells and other side effects [165-166, 71] and hence, a three-fold lower activity of ArgPt could be more ideal in cancer targeting. Carboplatin is reported to have an IC_{50} value of 10 µM in DU145 [174], which is similar to that of ArgPt in the same cell line (**Table 6.2**). Therefore, ArgPt and the clinically used carboplatin have the same potency in prostate cancer cells, but are

potentially less toxic than cisPt in normal cell lines. The lower potency of carboplatin is advantageous in circumventing the adverse toxicity usually caused by high dosages of platinum compounds [91]. For ArgPt, having an IC_{50} value that is comparable to carboplatin could be important in balancing selective potency in cancer cells and toxicity in normal cells. ArgPt and carboplatin may have structural features that promote both potency and reduced toxicity.

Because of the potency of ArgPt in prostate cancer cells, its activity in a prostate normal (RWPE-1) cell line was also investigated and compared to cisPt. In RWPE-1, cisPt has an IC_{50} value of 4 µM after a 72 h treatment (**Fig. 6.3** and **Table 6.3**). This low micromolar value is similar to its IC_{50} value in the DU145 cancer cell line, meaning that cisPt is highly potent and not selective for cancer over normal prostate cells. This result was expected because cisPt is known to be non-selective and toxic to normal cells [199-200].

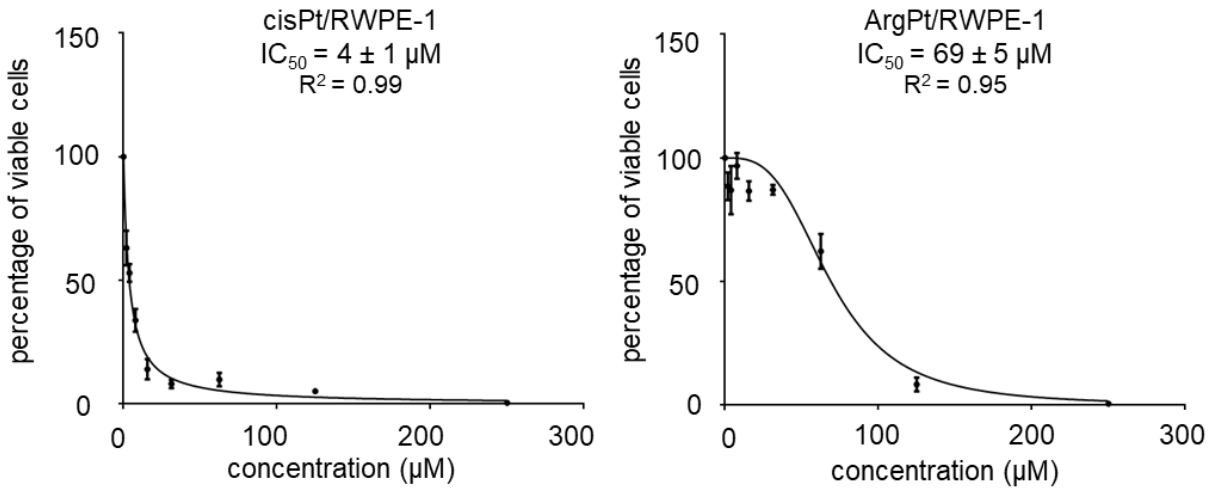

Figure 6.3. Dose-response curves of cisPt and ArgPt in normal prostate (RWPE-1) cell lines. An MTT assay was used to determine the percentage of viable cells as a function of increasing concentration of platinum-based compound. The type of cancer cell line and platinum-based compound used are indicated in the plots. The cell lines were treated for 72 h. Cells have varied responses to the different compounds used in the assay. GraphPad PRISM software was used for curve fitting using the model equation $Y=100/(1+(X^{hillSlope})/(IC_{50}{}^{hillSlope}))$, in which hillslope is -1. IC_{50} values were extracted from the plots. Each plot is from at least two biological replicates.

Table 6.3. Comparison of IC_{50} (μM) values of cisPt and ArgPt in normal and cancer cell lines

tissue	cell line (ref)	disease	cisPt‡	ArgPt‡
prostate	DU145 [133]	carcinoma	4 ± 1	12 ± 2
prostate	RWPE-1 [134]	normal	4 ± 1	69 ± 5
		fold change in IC_{50} values	1	6

‡error is from at least two biological replicates

ArgPt has a low IC_{50} value of 12 μM in prostate cancer cells and a moderately high IC_{50} value of 69 μM in prostate normal cells (**Fig. 6.3** and **Table 6.3**). The six-fold difference in the IC_{50} values of ArgPt in prostate cancer and normal cells shows that ArgPt is moderately selective for the cancer cells. The selective potency of ArgPt in the cancer cell line compared to normal cells could be due to its ligand side chains. Cancer cells have been reported to have a higher net negative charge on their cell surface compared to normal cells [192-194] and also upregulation of negatively charged sulfated proteoglycans on the cell surface [197-198]. The negative surface and sulfated sugars may enable favorable electrostatic interactions with the positive guanidinium side chains [201, 195] leading to attraction of ArgPt towards cancer cells and promoting uptake by the same cells.

Although OrnPt has a positive side chain, its four-fold lower potency could be related to its different amine side chain (compared to guanidinium). The positively charged amine may not possess favorable interactions with cancer cells compared to the guanidinium in ArgPt. This difference is observed in various cell penetrating peptides (CPP), in which the arginine moiety stimulates higher cellular uptake compared to lysine (which has similar amine moiety as ornithine) [202, 201, 203]. An example is where arginine-enriched peptides stimulates more cellular internalization through endocytosis than lysine-enriched peptides [202]. Efficient uptake of both arginine- and lysine-rich peptides is also attributed to their interactions with cell surface proteoglycans, however, absence of proteoglycans does not limit internalization of arginine-rich

peptides meaning that the arginine moiety modulates cell penetration through several pathways that may not be available for the lysine moiety [201]. Furthermore, as mentioned in **Section 2.4.2**, it is possible that OrnPt may exist with an (N, N) type of structure. The (N, O) and (N, N) type of structures could elicit different cytotoxic responses in cells. Therefore, among the three AAPt compounds investigated, ArgPt has higher potency in cancer cells over normal cells, a feature that could be advantageous over cisPt.

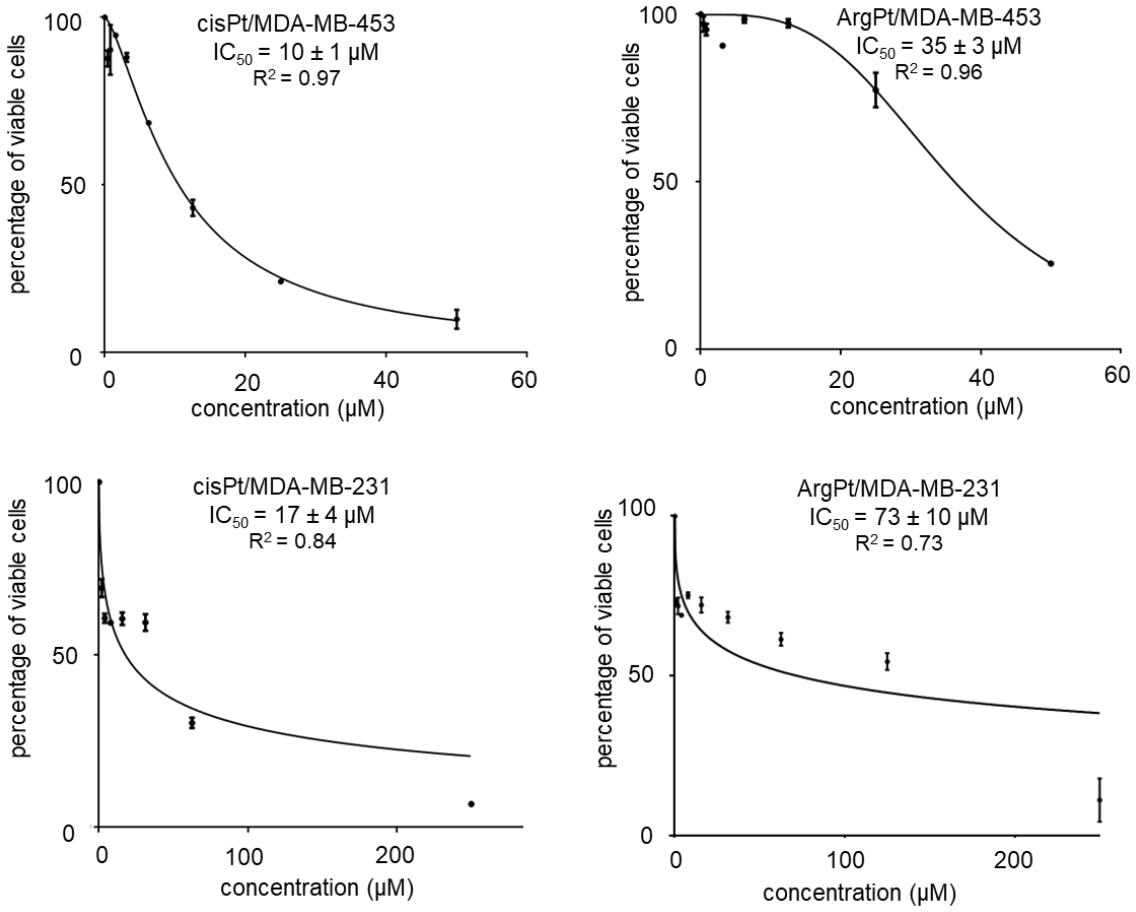

Figure 6.4. Dose-response curves of cisPt and ArgPt in breast cancer cell lines. An MTT assay was used to determine the percentage of viable cells as a function of increasing concentration of platinum-based compound. The type of cancer cell line and platinum-based compound used are indicated in the plots. All cells were treated for 48 h except MDA-MB-453 which was treated for 64 h. GraphPad PRISM software was used for curve fitting using the model equation $Y=100/(1+(X^{hillSlope})/(IC_{50}{}^{hillSlope}))$, in which hillslope is -1. IC_{50} values were extracted from the plots. Each plot is from at least two biological replicates.

As mentioned before, breast and lung cancer are the leading causes of cancer-related deaths among women in the United States [186]. Because of the promising results of ArgPt with prostate cancer cell lines, its potency in breast (**Fig. 6.4** and **Table 6.4**) and lung (**Fig. 6.5** and **Table 6.4**) cancer cell lines was also investigated in comparison to cisPt using the MTT assay. The potency of the compounds in a cervical cancer cell line (HeLa) was also determined (**Figs. 6.4 and 6.5**). The dose-response curves of all cell lines tested show that the percentage of viable cells is diminished with an increase in the concentration of platinum compounds depending on the type of cell line and identity of the platinum compound. ArgPt has an IC_{50} value of 35 μM in the breast cancer cell line MDA-MB-453 and 73 μM in breast cancer cell line MDA-MB-231 (**Table 6.4**). The response to ArgPt treatment is therefore different in the two breast cancer cell lines under investigation, with a two-fold higher potency in MDA-MB-453 cells compared to MDA-MB-231 cells. ArgPt has an IC_{50} value of 73 μM in the H1299 cell line and 78 μM in the HeLa cell line. The IC_{50} values in all four cell lines indicate that ArgPt has only moderate activity in these cell lines. Compared to cisPt, ArgPt has significantly less potency in the same cell lines (**Table 6.4**). To confirm that the cellular potent activity is only from the complexes of amino acids linked with a platinum center and not the free amino acids, future experiments will involve the use of respective amino acids as controls.

Table 6.4. IC_{50} (μM) values ArgPt in comparison with cisPt

tissue	**cell line (ref)**	**treatment time**	**cisPt**[‡]	**ArgPt**[‡]
breast	MDA-MB-231 [130]	48 h	17 ± 4	73 ± 10
breast	MDA-MB-453 [128]	64 h	10 ± 1	35 ± 3
lung	H1299 [129]	48 h	25 ± 2	73 ± 5
cervical	HeLa [132]	48 h	23 ± 2	78 ± 9

[‡]error is from at least two biological replicates

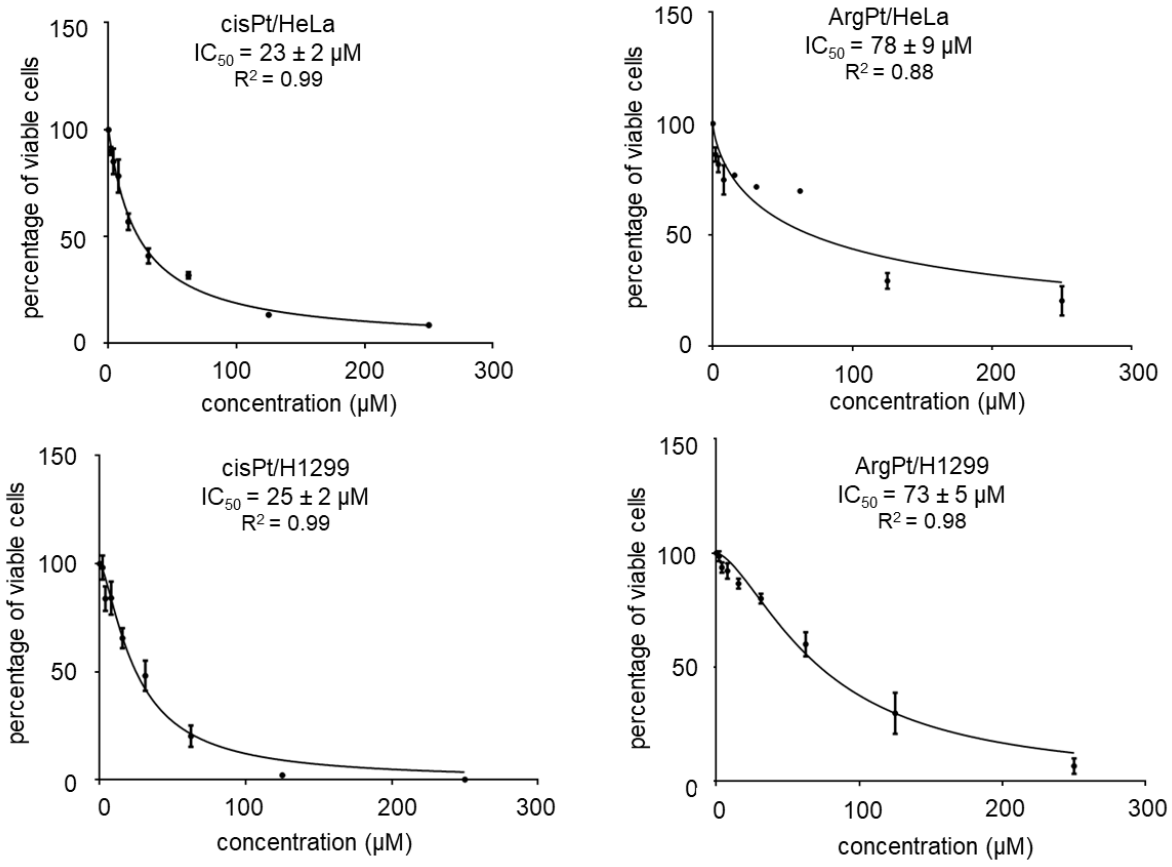

Figure 6.5. Dose-response curves of ArgPt and cisPt in cervical and lung cancer cell lines. MTT assays were used to determine the percentage of viable cells as a function of increasing concentration of platinum-based compound. GraphPad PRISM software was used for curve fitting using the model equation $Y=100/(1+(X^{hillSlope})/(IC_{50}{}^{hillSlope}))$, in which hillslope is -1. IC_{50} values were extracted from the plots. Each plot is from at least two biological replicates.

6.3.2 Quantification of platinum abundance in cells

In this thesis work, the cellular accumulation of AAPt compounds and cisPt in DU145 and RWPE-1 cell lines was determined. Because of the selective potency of ArgPt in prostate cancer cells compared to normal cells, it was of interest in this thesis work to determine the possible difference in uptake and accumulation of the compound in both cell types. Cells were treated with either AAPt or cisPt compounds and their cellular platinum concentration determined quantitatively by using ICP-MS (**Chapter 2, Section 2.4.14**). The ICP-MS has four tune modes from which quantification can be carried out. Quantification was done in the high energy helium

(HEHe) tune mode because the internal standard signal was stable and the R value of calibration was closest to 1. The calibration curves from the four tune modes are shown in the Appendix (**Figs. 1A-4A**). As shown in **Table 6.5**, accumulation of the platinum-based compounds varies depending on the cell line and the identity of compound. To confirm the consistency of the quantification, the samples were diluted 2X and 10X, followed by measurements on the ICP-MS and correction of dilution factors (**Table 6.6**). Readings for respective samples were consistent with each other with a low error percentage ranging from 0.1 to 7.8%.

Table 6.5. Accumulation of platinum compounds in prostate cancer and normal cells

disease	cell line	Pt compound	amount (nmol/10^6 cells)
normal	RWPE-1	cisPt	0.9 ± 0.3
carcinoma	DU145	cisPt	15 ± 8
normal	RWPE-1	OrnPt	0.9 ± 0.2
carcinoma	DU145	OrnPt	28 ± 11
normal	RWPE-1	ArgPt	3.2 ± 0.1
carcinoma	DU145	ArgPt	96 ± 16

Table 6.6. ICP-MS analysis of diluted samples of cells treated with platinum-based compounds

	original	2X dilution	10X dilution	average	percentage error
normal/cisPt	0.9	0.9	0.9	0.9	<0.1
cancer/cisPt	15	16	16	16	1.9
normal/OrnPt	0.9	1.1	1.1	1.0	<0.1
cancer/OrnPt	28	30	28	29	2.4
normal/ArgPt	3.2	4.2	4.1	3.8	7.8
cancer/ArgPt	96	114	111	107	5.2

CisPt has an accumulation of 15.3 nmol per million cancer cells, which is 17-fold higher than its accumulation in normal cells (**Table 6.5** and **Fig. 6.6**). OrnPt has an accumulation of 28 nmol per million cancer cells, which is thirty-fold higher than its accumulation in normal cells. ArgPt has an accumulation of 96 nmol per million cancer cells, which also represents a 30-fold higher accumulation than in normal prostate cells. Therefore, OrnPt and ArgPt exhibit higher fold changes in their accumulation in cancer cells over normal cells compared to cisPt. The considerably higher accumulation in cancer cells than normal cells could be important in triggering selective potency. The 30-fold higher ArgPt accumulation in cancer cells translated to a six-fold selective potency in the same cells compared to normal cells (**Tables 6.2** and **6.3**). The presence of a positively charged guanidinium on the side chain of ArgPt may be important for its penetration and potency in cells. It has been reported that positively charged residues including arginine promote cell penetration due to strong electrostatic interactions with anionic plasma membranes [204] and through their interactions with the negative sulfated proteoglycans [201-202]. Cancer cells have a higher net negative surfaces on their cell membranes [192-194] and upregulated levels of proteoglycans [197-198], which would likely interact favorably with the positive ArgPt side chains. Therefore, it is plausible that ArgPt has favorable interactions with the surfaces of cancer cells and transit through the cell membrane followed by interactions with the negatively charged nucleic acids inside cells. Although OrnPt also has a positive amine on its ligand side chain, it has a four-fold lower potency and three-fold lower accumulation than ArgPt in DU145 cell line. This is likely because the guanidinium moiety of arginine is more efficient in promoting cell internalization compared to the amine moiety of ornithine (or lysine) [201-202]. This also means that other properties of ArgPt in addition to its positively charged guanidinium on the side chain could play a role in mediating potency and accumulation.

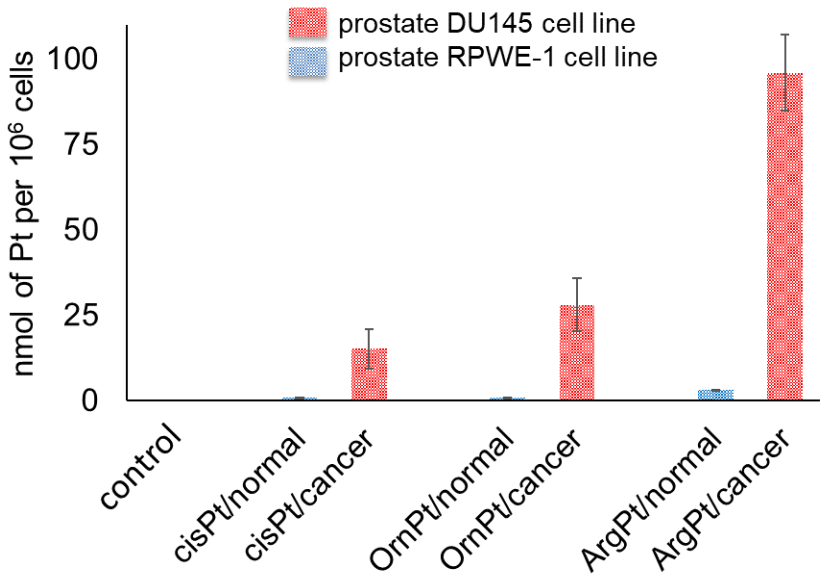

Figure 6.6. Accumulation of platinum-based compounds in prostate normal (blue, DU145 cell line) and cancer (red, RWPE-1) cell lines. Error is calculated fom three repeats.

While cellular uptake of the AAPt compounds (and cisPt) is crucial in adduct formation and triggering cell death, other factors associated with the cells could also play a role in mediating the extent of potency once uptake occurs. The difference in potency of ArgPt in all the cell lines investigated in this thesis work could be explained by their p53 status. It is suggested that antitumor agents including cisPt induce apoptosis through involvement of the tumor suppressor p53 protein [205-206]. Cell lines with downregulated or mutated p53 proteins are less chemosensitive to cisPt [205-206]. The p53 status and cisPt sensitivity in the cell lines investigated in this thesis work are consistent. If ArgPt induces apoptosis through involvement of p53 proteins in a manner similar to cisPt, then cells with this tumor suppressor would be more chemosensitive to ArgPt. Breast cancer cell line MDA-MB-453 has full length p53 [207] while its related MDA-MB-231 has mutated p53 proteins [208]. The response to ArgPt by these two cell lines are consistent with their p53 status in which MDA-MB-453 is two-fold more sensitive to ArgPt than the MDA-MB-231 cell line. H1299 and HeLa cell lines are p53 null [209-210] and this may explain why ArgPt has relatively low potency in these cell lines. The DU145 cell line also

expresses p53 [211], and this could also contribute to the observed high sensitivity to ArgPt as indicated by the low IC_{50} value.

6.4 Conclusions

At the cellular level, ArgPt exhibits increased potency and accumulation compared to cisPt. While cisPt is potent in both cancer and normal prostate cells, ArgPt is selective in potency towards prostate cancer cells compared to normal cells. ArgPt also has higher accumulation in prostate cancer cells, which correlates with its lower IC_{50} value and higher potency. ArgPt is observed to have a 30-fold higher accumulation in prostate cancer cells than normal cells, which translates into a six-fold selective potency in cancer cells. Structural characteristics of AAPt compounds could enable the compounds to have unique cell penetration properties and potency compared to cisPt. The positively charged guanidinium on side chain of ArgPt could promote cell penetration due to electrostatic interaction with anionic plasma membrane. Unique features of cancer cells including the higher net negative charge on the surface of cell membranes or the presence of negatively charged sulfated proteoglycans could also recruit ArgPt towards cancer cells and promote selective uptake of the compounds. Although, OrnPt is also observed to have higher accumulation in prostate cancer cells than normal cells, its potency in prostate cancer cells is relatively low compared to ArgPt. The possible existence of OrnPt adducts with an (N, N) type of structure of metal complex could explain this difference, especially if the (N, N) type of structures do not have favorable interactions with cells compared to (N, O) type of structures.

Future directions will involve using respective free amino acids during MTT assays as controls so as to ascertain if the complex of platinum center together with the amino acid ligand induce the potent activity of AAPt compound as opposed to free amino acid alone. Furthermore, competition studies of cellular uptake of free amino acids and AAPt compounds could be carried out by incubating cells with the compounds prior to ICP-MS quantification of platinum accumulation. These studies may give further information on possible cell receptors or transporters that could be aiding the uptake of AAPt compounds.

Inherent cellular features including the status of tumor suppressors such as p53, could also modulate the extent of potency in a given cancer cell line. Cell lines with low p53 abundance or mutated p53 have lower sensitivity towards not only cisPt but also OrnPt and ArgPt. This tumor suppressor may play a role in mediating the cytotoxic pathway of ArgPt and OrnPt in a manner similar to cisPt, but this has to be tested with further experimentation. The high accumulation of AAPt compounds in cancer cells combined with selective potency and non-canonical targets (reported in previous chapters) could enable the compounds to have a robust and unique cytotoxic pathway that circumvents challenges hindering cisPt application.

CHAPTER 7

CONCLUSIONS AND FUTURE DIRECTIONS

7.1 Overall conclusions

Cisplatin (cisPt) was approved over 40 years ago for anticancer therapy and has since been used for treatment of several forms of cancer [9, 11]. CisPt preferentially form adducts with deoxyguanosine (dGuo) residues, which alters the DNA structure and inhibits biological processes such as replication and transcription [11, 38]. The adducts trigger other cellular responses, including cell cycle arrest, DNA repair, and apoptosis [1]. The clinical use of cisPt has been limited by cellular resistance and adverse side effects such as nephrotoxicity [69-71]. These drawbacks have provided the inspiration to explore other modified cisPt ligands and research their structure-activity relationships. The parent cisPt has two ammine and two chlorido ligands that modulate its various chemical properties ranging from reaction kinetics to preferred biological targets of the compound [16-18].

The ligands of second generation cisPt analogues possess unique biochemical effects that have played a role in improving their therapeutic activities. In carboplatin for example, the chelate ring in cyclobutanedicarboxylate stabilizes the leaving ligand and slows the aquation rate [91-92]. This in turn slows the rate of adduct formation with DNA, which ultimately reduces the reactivity and toxicity of the compound compared to cisPt at high dosage [91, 34]. The non-leaving 1,2-diamminocylohexane ligand in oxaliplatin protrudes into the major groove of DNA where it effectively blocks the replication machinery from bypassing the adduct [94, 96]. This is important in circumventing a form of resistance that occurs in cancer cells where the replication machinery is able to read through cisPt adducts. Although the second-generation antitumor platinum-based drugs have advantages over cisPt in terms of reduced toxic side effects and the ability to circumvent resistance, they are limited by their low efficacy [16]. The compounds also require combination therapy with other anticancer agents in order to be fully effective [95].

There is still a need to develop platinum-based compounds that can balance high potency, reduced resistance, and low toxicity in cells. Since cisPt and second-generation platinum drugs are known to target dGuo residues of DNA, platinum-based compounds that have alternative target residues or biomolecules such as RNA could trigger unique biochemical events compared to cisPt. However, there has been limited success in finding platinum-based compounds that preferentially platinate alternative non-cisPt targets. Previous work in our lab showed that amino acid-linked platinum(II) (AAPt) compounds coordinate with RNA residues [106]. The work in this thesis focused on synthesis of AAPt compounds and characterization of the non-canonical adducts that form with adenosine (Ado) residues. The reaction kinetics, impact on glycosidic bond stability, potency, and accumulation of AAPt compounds in cancer cells were also investigated.

AAPt compounds are generated by attaching amino acids to a platinum metal center [106, 103-105]. In **Chapter 2**, the synthesis and characterization of three AAPt compounds (AlaPt, OrnPt, and ArgPt) were described. The structural characterization of the compounds demonstrated that the respective amino acid is chelated with the Pt(II) center through the backbone nitrogen and oxygen atoms giving a five-membered ring ((N,O) type of structure) [104-105]. Even though the (N,N) type structure in OrnPt was not observed in the X-ray crystal structure, it was not ruled out since crystallization conditions may have favored only the (N,O) type structure [107].

CisPt predominantly targets the N7 position of Guo residues and results in formation of bifunctional and monofunctional types of adducts. Compared to cisPt, the AAPt compounds have a wider range of reactivities and targets because of the diversity of the side chain functional groups together with the contribution of backbone atom metal coordination. AAPt compounds form adducts with non-cisPt targets including Ado/dAdo residues of RNA and DNA. In **Chapter 3**, the non-canonical adducts formed by AAPt compounds (AlaPt, OrnPt, and ArgPt) were characterized. The adducts formed are monofunctional isomeric adducts that vary at the platination sites. The compounds coordinate specifically at the N1/N3 and N7 positions of the Ado

nucleobases. In this thesis, mass spectrometry and 1D-NMR spectroscopy methods were used to identify the types of adducts formed. However, these methods give limited information on the structural orientations of the adducts which are modulated by factors such as steric hindrance and hydrogen-bonding properties. The ^{1}H-NMR spectroscopy is also limited in differentiating between N1 and N3 platination sites because of their similar proximity to H2 proton. Future studies could employ X-ray crystallography or 2D-NMR spectroscopy to differentiate between N1 and N3 platination.

Kinetic studies in **Chapter 4** indicate that monoaquated AlaPt, OrnPt, and ArgPt have altered reactivity and different target preferences compared to cisPt [105]. AlaPt has nine to 20-fold higher selectivity for dAdo over all other purines. OrnPt exhibits a four to six-fold increased reactivity with Ado/dAdo nucleosides over Guo/dGuo, whereas ArgPt has four- to five-fold higher reactivity with dAdo/dAdo than with Guo/dGuo. Since cisPt only has the (N,N) type of structure while the amino acid complexes can have (N,O) type of structures, the altered reactivity preferences suggest that the mode of amino acid coordination together with the ligand side chain play a role in modulating the nucleoside preferences and rates of reactivity. Furthermore, the selectivity of cisPt for dGuo is attributed to formation of a hydrogen bond between the cisPt ammine ligand and the 6-oxo group of Guo during transition state [27]. In contrast, the preferences of AlaPt, OrnPt, and ArgPt could be due to hydrogen-bonding interactions with Ado/dAdo functional groups. The *trans* adduct structures of AAPt-Ado are stabilized because of hydrogen bonding between the 6-amine of Ado and carboxylate ligand of the AAPt compound. The lower reactivities of the selected AAPt compounds with Guo/dGuo are likely lower due to the lack of such an interaction. HPLC fitted with a C18 column was used to monitor the rate of diminishing reactants prior to extracting the rate constants. It was challenging to monitor rate of formation of individual products since there is possible conversion from one type of adduct to another with different retention time. There are other methods available such as NMR spectroscopy and mass spectrometry that have been used previously to investigate the reaction kinetics of platinum-

based compounds [32, 34, 149, 158] and could also be used to confirm the reactivities and preferences of AAPt compounds with their nucleic acid targets.

The reaction kinetics of AAPt compounds (and cisPt) with 5′-UUAUU-3′ and 5′-TTATT-3′ oligonucleotides were also studied in which monofunctional and doubly platinated adducts were observed. The reactivities of the compounds with these oligonucleotides generally increased compared to reactions with nucleosides, as exhibited by the increased *k* values. The local environment flanking the target residues in DNA or RNA oligonucleotide, such as the phospho-diester backbone, likely enhances reactivity with AAPt compounds. The negatively charged phosphate groups could interact with the positive ligands of the AAPt compounds (OrnPt and ArgPt). The functional groups of the backbone could also hydrogen bond with functional groups of AAPt, which would stabilize the coordination of the compounds with their targets. OrnPt was also observed to have a two-fold higher preference for the RNA oligonucleotide than the corresponding DNA, which means that its structural features could be important in development of nucleic acid-selective platinum-based compounds. To further understand the impact of local environment on the reactivities of AAPt compounds, other oligonucleotides aside from 5′-UUAUU-3′ and 5′-TTATT-3′, could also be used in reaction kinetics. Oligonucleotides with varied lengths, different sequences flanking target sites, or changing positions of Ado residues would provide further understanding on how target positions in relation to flanking sequences or oligonucleotide length could affect the reactivities of AAPt compounds.

Platination of nucleosides could influence the stability of nucleic acids as reported in **Chapter 5**. Collision induced dissociation (CID) and glycosidic bond survival yield analysis were applied to determine the impact of platination on the relative glycosidic bond strength of non-canonical AAPt-Ado adducts. When either AlaPt, OrnPt, or ArgPt coordinate to the N7 position of Ado, they destabilize the glycosidic bonds to a greater extent than when they coordinate at the N1 or N3 positions. Depending on the proximity of the platinum atom, the ligands of the selected AAPt compounds could cause electron-density withdrawal at the N9 position leading to

destabilization of the glycosidic bonds. Overall, AlaPt-Ado adducts are observed to predominantly fragment via cleavage of the glycosidic bond. In contrast, fragmentation of OrnPt-Ado involves cleavage of the glycosidic bonds and other neutral loss pathways. Activation of glycosidic bond cleavage is particularly unique to the selected AAPt compounds considering that cisPt is reported to have no destabilizing effect on the glycosidic bonds of target dGuo residues [26]. Destabilization of glycosidic bonds could be biologically relevant considering that AAPt compounds could exert formation of abasic sites in nucleic acids. Irreparable abasic sites, especially in RNA, could trigger apoptosis and provide an alternative cytotoxic pathway that averts cisPt resistance.

To explore features of ligands that improve activity and selectivity of platinum-based compounds, the potency and accumulation of AAPt compounds was investigated in **Chapter 6**. The MTT assay was used to investigate cellular potency, whereas ICP-MS was used to assess accumulation of AAPt compounds in comparison with cisPt. While cisPt is potent in both cancer and normal prostate cells, ArgPt selectively accumulates and is more potent in prostate cancer cells. ArgPt has a 30-fold higher accumulation and a six-fold selective potency in cancer cells compared to normal cells. The unique uptake and potency of ArgPt compared to cisPt could be attributed to its ligands. The positively charged guanidinium ligand side chain in ArgPt likely has favorable electrostatic interactions with plasma membranes, which could recruit the compound and enhance cell penetration. Unique features of cancer cells such as the net negative charge on the surface of cell membranes and presence of higher levels of negative sulfated glycoproteins [193, 195, 194, 201, 197-198] could also recruit ArgPt towards cancer cells and promote selective uptake of the compound. Other factors that modulate the extent of chemosensitivity in cancer cells include their tumor suppressor p53 status. Cell lines with downregulated or mutated p53 are less sensitive towards cisPt treatment [209, 206]. This tumor suppressor may also play a role in chemosensitivity of cancer cells towards AAPt compounds, but this has to be confirmed with further experiments.

Overall, the different attributes of the selected AAPt compounds (AlaPt, OrnPt, and ArgPt) investigated in this thesis work are important in development of cisPt analogues that have improved anticancer activity. These aspects, which include unique platination sites, formation of non-canonical adducts, reaction kinetics, selective potency, and high accumulation in cancer cells, could enable platinum-based compounds to have robust and unique antitumor activities that avert chemoresistance and adverse toxicity. To ascertain if the complex of platinum center together with the amino acid ligand induce the potent activity of AAPt compound as opposed to free amino acid alone, MTT assays could be carried out using respective free amino acids as controls. Studying competitive cellular uptake and accumulation of free amino acids and AAPt compounds may give further information on the mode of uptake or possible transporters that could be aiding the cell penetration of AAPt compounds.

7.2 Future directions

7.2.1 Impact of platinum adducts on hydrolytic cleavage of RNA oligonucleotides

The impact of platination on cleavage of glycosidic bonds of nucleoside adducts was investigated using glycosidic bond survival yield analysis as described in **Chapter 5**. It would be of interest to follow up on these experiments by investigating the rates of depurination of oligonucleotides using HPLC or UV analysis. The presence of alkylated or non-canonical bases in nucleic acids may promote cleavage of the glycosidic bonds [212-213], and modifications could promote hydrolysis of glycosidic bonds leading to damage of DNA through depurination [213]. Modification of DNA/RNA oligonucleotides by AAPt compounds may also promote hydrolysis of glycosidic bonds. The impact of platination on hydrolysis and damage of DNA/RNA oligonucleotides could be investigated by platinating nucleic acids with AAPt compounds (and cisPt) under physiological conditions and monitoring depurination kinetics using HPLC/UV analysis. The resulting depurination products could be characterized by using mass spectrometry.

7.2.2 Quantification of AAPt compounds bound to cellular DNA and RNA

In **Chapter 6**, the whole cell abundance of AAPt compounds in comparison with cisPt was described. It would also be of interest to quantify the number of adducts formed by platinum-based compounds with cellular biological targets so as to understand their distribution, localization, and preferred targets. Platinum metals bound to RNA versus DNA need to be quantified and compared to understand the preferred nucleic acid target of the compounds. These studies would involve treating cells with platinum-based compounds followed by isolation of DNA and RNA. Because of the elemental quantification capability and robust detection limit of ICP-MS, it could be employed to quantify the platinum-based compounds bound to the respective nucleic acids.

7.2.3 Downstream effects of AAPt platination of mRNA

Since platination by AAPt compounds occurs preferentially with Ado/dAdo sites of nucleic acids as described in **Chapters 3 and 4**, their cellular activities could lead to inhibition of unique downstream protein functions that are dependent on Ado/dAdo-rich sites. Cancerous cells have an upregulation of mRNA polyadenylation [214-215], which could provide an important selective target over normal cells. The mRNA has been reported to be platinated by cisPt [55] and could also be one of the biological targets of AAPt compounds. The poly(Ado) tail of mRNA would provide an Ado-rich region for which the selected AAPt compounds (AlaPt, OrnPt, and ArgPt) could platinate preferentially. Since mRNA associates with a number of proteins such as poly(Ado) binding protein (PABP), which are crucial in facilitating nuclear export and translation processes [216], it would be of interest to understand the impact of platination on such RNA-protein interactions and their downstream effects. Such *in vitro* experiments could be analyzed using gel electrophoresis and mass spectrometric analysis.

APPENDIX A

PROTOCOL FOR HUMAN CANCER AND NORMAL CELL CULTURE

This information describes the protocol for maintaining both cancer and normal cell lines used in **Chapter 6.**

General

Cell culturing was carried out in an aseptic laminar flow hood to ensure protection from contaminants. The hood was cleaned with 70% ethanol before and after every use. Before introducing items such as media into the hood, their container surfaces were sterilized with 70% ethanol. Autoclaved tubes/tips and sterile cell plates/dishes were used in all experiments. For cancer cells, Dulbecco's modified eagle medium (DMEM) supplemented with 10% fetal bovine serum (FBS), penicillin (5 units/mL), and streptomycin (0.1 mg/mL) was used. For normal cells, keratinocyte serum free medium (K-SFM) supplemented with human recombinant epidermal growth factor 1-53 (EGF 1-53), bovine pituitary extract (BPE), penicillin (5 units/mL), and streptomycin (0.1 mg/mL) was used. The cell culture incubator was always kept at 37 °C and 5% CO_2. All the cell lines used in this thesis work are monolayer cell cultures that attach to the bottom of plate/dish when they are viable and are only suspended when treated with trypsin or if they are dead.

Recovery of cryopreserved cells

Cells are usually cryopreserved in liquid nitrogen in a cryovial with DMSO/media solution. Their recovery should ensure minimal cell death and removal of DMSO from cell solution before cell growth is reestablished. The cryovial with cells was removed from the liquid nitrogen and quickly placed in 37 °C waterbath. After one minute of agitating, the vial was sterilized with 70% ethanol before opening the cap. The cell solution was transferred into a centrifuge tube with an additional 1 mL of appropriate media and centrifuged at 1000 rpm for 4 min at 25 °C. The supernatant was removed, mixed with another 1 mL of media to resuspend the cells, and centrifuged again. The supernatant was removed again, and the cell pellet resuspended with 1

mL media before transferring all contents into a cell culture dish (60 x 15 mm) with an additional 3 mL of media. The seeded dish was stored in the incubator to allow the cells to attach to the plate and grow.

Some cells usually die due to stress conditions of storage and therefore the cell growth of new culture is recovered by seeding the dishes with a high density of cells. The dishes should be checked periodically under microscope to ensure cell growth, confluency, and availability of media. Fresh media can be added after 3-5 days.

Trypsinizing and passaging monolayer cells

When cells reach over 80% confluency, they were passaged (split) into secondary dishes as described below.

Cancer cells

To split the cell culture, the media was first removed from the dish. The cell dish was washed with 2 mL of PBS. Trypsin-EDTA (0.25%, 0.5 mL) was added into the dish and incubated for 2-5 min at 37 °C to detach the cells from surface of dish. Fresh media (2.5 mL) was added to the dish to inactivate the trypsin. Equal volume of cell suspension were distributed into secondary dishes. More media was added into the secondary plates for a total volume of 8 mL in each 100 x 20 mm secondary dish (or 3 mL if using 60 x 15 mm dishes). The cells were then stored in the incubator until they were used for experiments or until they reached over 80% confluency (where they were split again into tertiary dishes).

Normal cells

The normal cells are treated differently from cancer cells because their media do not contain FBS to deactivate the trypsin. The media was first removed from the confluent cell culture dish and washed with 2 mL of PBS. Trypsin (0.05%, 0.5 mL) was added and incubated for 2-5 min at 37 °C to suspend the cells. To the dish, 0.5 mL of 10% FBS is added, agitated, and transferred into a centrifuge tube. The tube was centrifuged at 1000 rpm for 4 min at 25 °C followed by removal of supernatant. The cell pellet was resuspended with 3 mL of appropriate

media. Equal volume of cell suspension were distributed into secondary dishes. More media was added into the secondary plates for a total volume of 8 mL in each 100 x 20 mm secondary dish (or 3 mL if using 60 x 15 mm dishes). The cells were then stored in the incubator until they were used for experiments or until they reached over 80% confluency (where they were split again into tertiary dishes).

Storage of cells for future experiments

Cancer cells

The cells were resuspended with 0.5 mL trypsin (0.25%). Appropriate media (1.5 mL) was added to the suspension and mixed. The contents were transferred into a centrifuge tube and centrifuged at 1000 rpm for 4 min at 25 °C. The supernatant was removed and 1 mL of appropriate fresh media was added to the tube. Another 1 mL of DMSO was also added into the tube and mixed. The contents were transferred into sterile cryovial, capped and placed in -80 °C overnight. The cryovials were then placed in liquid nitrogen freezer for long term storage.

Normal cells

The cells were resuspended with 0.5 mL trypsin (0.05%). After the cells were dispersed, 0.5 mL of 10% FBS was added into the dish and mixed. The contents were transferred into a centrifuge tube and centrifuged at 1000 rpm for 4 min at 25 °C. The supernatant was removed and 1 mL of appropriate fresh media was added to the tube. Another 1 mL of DMSO was also added into the tube and mixed. The contents were transferred into sterile cryovial, capped and placed in -80 °C overnight. The cryovials were then placed in liquid nitrogen freezer for long term storage.

ICP-MS CALIBRATION AND INTERNAL STANDARDS

The ICP-MS was calibrated in four different tune modes using ^{195}Pt and two internal standards (^{209}Bi and ^{115}In). The calibration graph with R value closest to 1 and stable internal standards was selected for quantification of samples (**Fig. 1A-4A**).

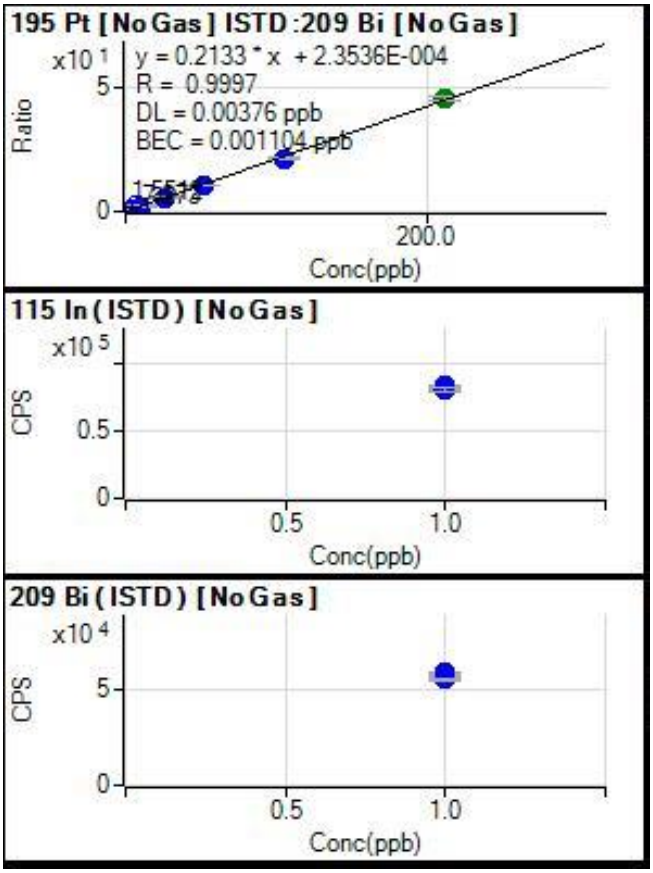

Figure 1A. ICP-MS Calibration graph with no gas tune mode. The calibration graph together with measurements of internal standards (Bi-209 and In-115) in the same mode are given. DL is detection limit and BEC is background equivalent concentrations.

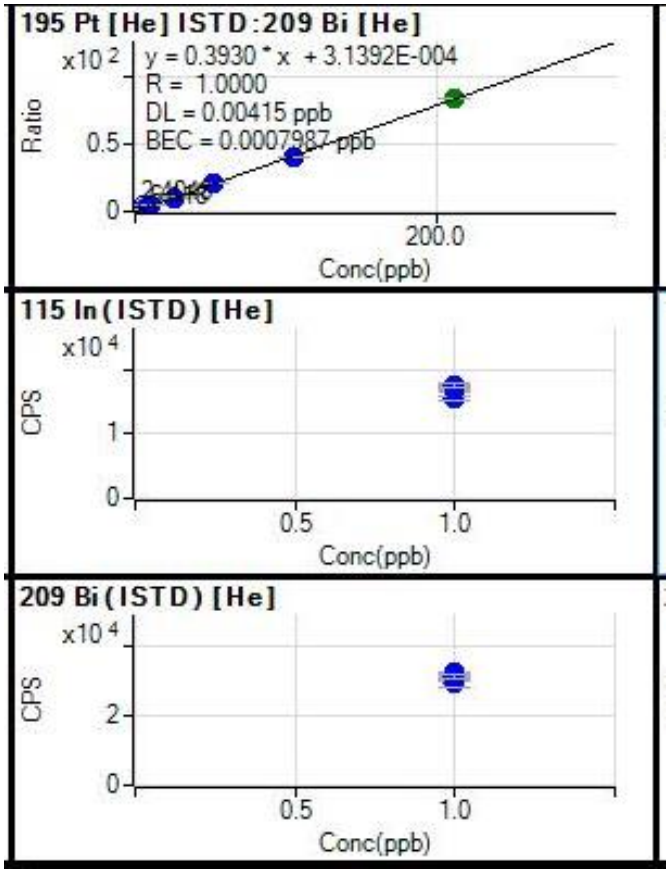

Figure 2A. ICP-MS calibration graph in helium tune mode. The calibration graph together with measurements of internal standards (Bi-209 and In-115) in the same mode are given. DL is detection limit and BEC is background equivalent concentrations.

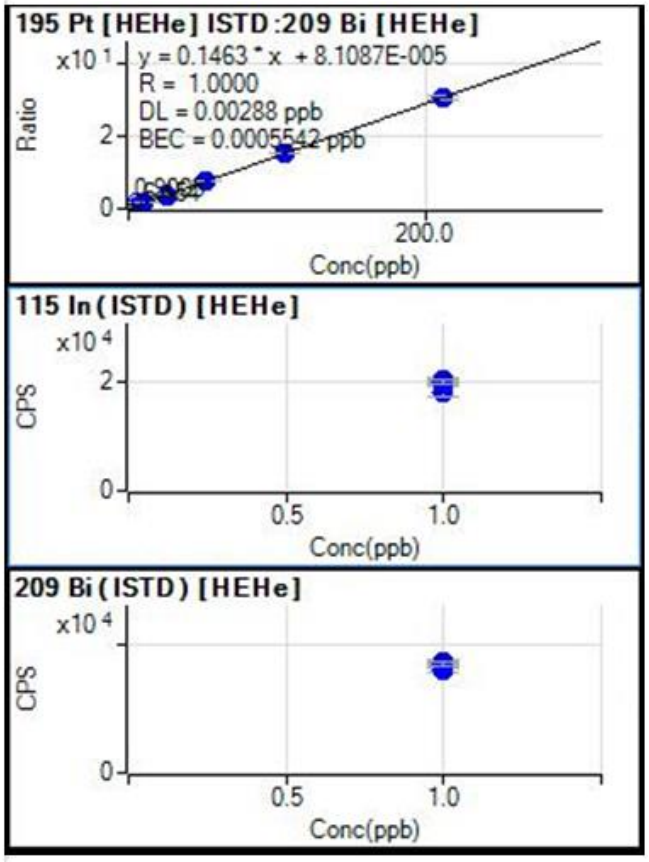

Figure 3A. ICP-MS calibration graph in high energy helium (HEHe) tune mode. The calibration graph together with measurements of internal standards (Bi-209 and In-115) in the same mode are given. DL is detection limit and BEC is background equivalent concentrations.

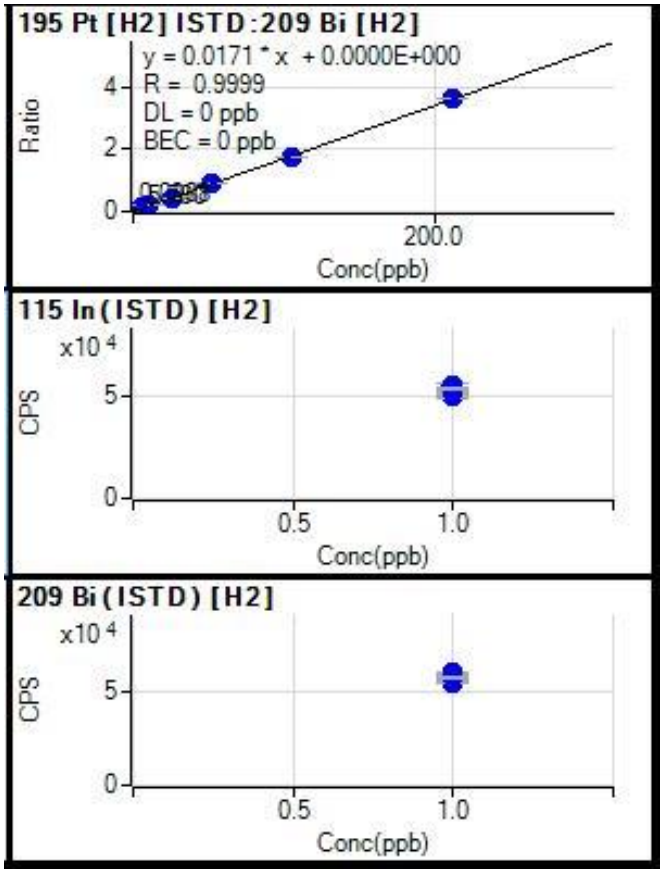

Figure 4A. ICP-MS calibration graph in hydrogen tune mode. The calibration graph together with measurements of internal standards (Bi-209 and In-115) in the same mode are given. DL is detection limit and BEC is background equivalent concentrations.

References

1. Wang D, Lippard SJ (2005) Nat Rev Drug Discov 4:307-320
2. Peyrone M (1844) Annalen der Chemie und Pharmacie 51:1-29
3. Kauffman GB, Pentimalli R, Doldi S, Hall MD (2010) Platin Met Rev 54:250-256
4. Crichton RR, In *Biol Inorg Chem*, Elsevier: Oxford, (2012); pp 415-432.
5. Milburn GHW, Truter MR (1966) J Chem Soc A:1609-1616
6. Rosenberg B, VanCamp L, Krigas T (1965) Nature 205:698-699
7. Rosenberg B, VanCamp L, Trosko JE, Mansour VH (1969) Nature 222:385-386
8. Rosenberg B (1978) Interdiscipl Sci Rev 3:134-147
9. Kelland L (2007) Nat Rev Cancer 7:573-584
10. Ghosh S (2019) Bioorg Chem 88:102925
11. Jung Y, Lippard SJ (2007) Chem Rev 107:1387-1407
12. Raghavan D (2003) Oncology 17:218-228
13. Sarin N, Engel F, Kalayda GV, Mannewitz M, Cinatl J, Jr., Rothweiler F, Michaelis M, Saafan H, Ritter CA, Jaehde U, Frotschl R (2017) PloS one 12:e0181081
14. Lai SL, Hwang J, Perng RP, Whang-Peng J (1995) Oncol Res 7:31-38
15. Ho T-L (1975) Chem Rev 75:1-20
16. Dasari S, Tchounwou PB (2014) Eur J Pharmacol 740:364-378
17. Goodsell DS (2006) Stem cell 24:514-515
18. Jamieson ER, Lippard SJ (1999) Chem Rev 99:2467-2498
19. Alderden RA, Hall MD, Hambley TW (2006) J Chem Educ 83:728
20. Gately DP, Howell SB (1993) Br J Cancer 67:1171-1176
21. Sharp SY, Rogers PM, Kelland LR (1995) Clin Cancer Res 1:981-989
22. Ishida S, Lee J, Thiele DJ, Herskowitz I (2002) Proc Natl Acad Sci USA 99:14298-14302

23. Holzer AK, Samimi G, Katano K, Naerdemann W, Lin X, Safaei R, Howell SB (2004) Mol Pharmacol 66:817-823

24. Lin X, Okuda T, Holzer A, Howell SB (2002) Mol Pharmacol 62:1154-1159

25. Fuertes MA, Castilla J, Alonso C, Perez JM (2003) Curr Med Chem 10:257-266

26. Baik M-H, Friesner RA, Lippard SJ (2002) J Am Chem Soc 124:4495-4503

27. Baik M-H, Friesner RA, Lippard SJ (2003) J Am Chem Soc 125:14082-14092

28. Andrews PA, Howell SB (1990) Cancer Cell 2:35-43

29. Bellacosa A, Moss EG (2003) Curr Biol 13:R482-484

30. Reedijk J (1996) Chem Comm:801-806

31. Perez RP (1998) Eur J Cancer 34:1535-1542

32. Bancroft DP, Lepre CA, Lippard SJ (1990) J Am Chem Soc 112:6860-6871

33. Blommaert FA, van Dijk-Knijnenburg HCM, Dijt FJ, den Engelse L, Baan RA, Berends F, Fichtinger-Schepman AMJ (1995) Biochemistry 34:8474-8480

34. Hah SS, Stivers KM, de Vere White RW, Henderson PT (2006) Chem Res Toxicol 19:622-626

35. Reedijk J (2008) Platin Met Rev 52:2-11

36. Reedijk J (2003) Proc Natl Acad Sci USA 100:3611-3616

37. Kartalou M, Essigmann JM (2001) Mutat Res 478:1-21

38. Sherman SE, Gibson D, Wang AHJ, Lippard SJ (1985) Science 230:412-417

39. Yang X-L, Wang AHJ (1999) Pharmacol Ther 83:181-215

40. Mantri Y, Lippard SJ, Baik M-H (2007) J Am Chem Soc 129:5023-5030

41. Fichtinger-Schepman AMJ, van der Veer JL, den Hartog JHJ, Lohman PHM, Reedijk J (1985) Biochemistry 24:707-713

42. Eastman A, Barry MA (1987) Biochemistry 26:3303-3307

43. Kasparkova J, Marini V, Bursova V, Brabec V (2008) Biophys J 95:4361-4371

44. Johnson NP, Hoeschele JD, Rahn RO (1980) Chem-Biol Interact 30:151-169

45. Deeth RJ, Elding LI (1996) Inorg Chem 35:5019-5026

46. Reedijk J (1992) Inorganica Chim Acta 198-200:873-881

47. Chow CS, Whitehead JP, Lippard SJ (1994) Biochemistry 33:15124-15130

48. Ohndorf UM, Rould MA, He Q, Pabo CO, Lippard SJ (1999) Nature 399:708-712

49. Hägerlöf M, Papsai P, Chow CS, Elmroth SKC (2006) J Biol Inorg Chem 11:974-990

50. Hostetter AA, Chapman EG, DeRose VJ (2009) J Am Chem Soc 131:9250-9257

51. Melnikov SV, Söll D, Steitz TA, Polikanov YS (2016) Nucleic Acids Res 44:4978-4987

52. Plakos K, DeRose VJ (2017) Chem Comm 53:12746-12749

53. Rijal K, Chow CS (2009) Chem Comm:107-109

54. Saunders AM, DeRose VJ (2016) Curr Opin Chem Biol 31:153-159

55. Becker JP, Weiss J, Theile D (2014) Toxicol Lett 225:43-47

56. Bruno PM, Liu Y, Park GY, Murai J, Koch CE, Eisen TJ, Pritchard JR, Pommier Y, Lippard SJ, Hemann MT (2017) Nat Med 23:461-471

57. Chapman EG, Hostetter AA, Osborn MF, Miller AL, DeRose VJ, (2011) Structural and Catalytic Roles of Metal Ions in RNA, The Royal Society of Chemistry: 347-377.

58. Papsai P, Aldag J, Persson T, Elmroth SKC (2006) Dalton Trans:3515-3517

59. Hostetter AA, Osborn MF, DeRose VJ (2012) ACS Chem Biol 7:218-225

60. Abu N, Hon KW, Jeyaraman S, Jamal R (2018) Future Oncol 14:3085-3095

61. Messori L, Merlino A (2016) Coord Chem Rev 315:67-89

62. Casini A, Reedijk J (2012) Chem Sci 3:3135-3144

63. Banci L, Bertini I, Blaževitš O, Calderone V, Cantini F, Mao J, Trapananti A, Vieru M, Amori I, Cozzolino M, Carrì MT (2012) J Am Chem Soc 134:7009-7014

64. Einhäuser TJ, Galanski M, Keppler BK (1996) J Anal Atom Spectrom 11:747-750

65. Li H, Zhao Y, Phillips HIA, Qi Y, Lin T-Y, Sadler PJ, O'Connor PB (2011) Anal Chem 83:5369-5376

66. Ming X, Groehler A, Michaelson-Richie ED, Villalta PW, Campbell C, Tretyakova NY (2017) Chem Res Toxicol 30:980-995

67. Vinje J, Sletten E (2007) Anticancer Agents Med Chem 7:35-54

68. Peng J, Mandal R, Sawyer M, Li XF (2005) Clin Chem 51:2274-2281

69. Gonzales-Vitale JC, Hayes DM, Cvitkovic E, Sternberg SS (1977) Cancer 39:1362-1371

70. Hanigan MH, Devarajan P (2003) Cancer Ther 1:47-61

71. Siddik ZH (2003) Oncogene 22:7265-7279

72. Miller RP, Tadagavadi RK, Ramesh G, Reeves WB (2010) Toxins 2:2490-2518

73. Friesen C, Fulda S, Debatin KM (1999) Leukemia 13:1854-1858

74. Kanduc D, Mittelman A, Serpico R, Sinigaglia E, Sinha AA, Natale C, Santacroce R, Di Corcia MG, Lucchese A, Dini L, Pani P, Santacroce S, Simone S, Bucci R, Farber E (2002) Int J Oncol 21:165-170

75. Lieberthal W, Triaca V, Levine J (1996) Am J Physiol 270:F700-708

76. Thadhani R, Pascual M, Bonventre JV (1996) N Engl J Med 334:1448-1460

77. Tedeschi M, De Cesare A, Oriana S, Perego P, Silva A, Venturino P, Zunino F (1991) Cancer Treat Rev 18:253-259

78. Osman AM, El-Sayed EM, El-Demerdash E, Al-Hyder A, El-Didi M, Attia AS, Hamada FM (2000) Pharmacol Res 41:113-119

79. Sheth S, Mukherjea D, Rybak LP, Ramkumar V (2017) Front Cell Neurosci 11:338

80. Lu Y, Cederbaum AI (2006) Toxicol Sci 89:515-523

81. Kelland LR (1993) Crit Rev Oncol Hematol 15:191-219

82. Borst P, Evers R, Kool M, Wijnholds J (2000) J Natl Cancer Inst 92:1295-1302

83. Kool M, de Haas M, Scheffer GL, Scheper RJ, van Eijk MJ, Juijn JA, Baas F, Borst P (1997) Cancer Res 57:3537-3547

84. Katano K, Kondo A, Safaei R, Holzer A, Samimi G, Mishima M, Kuo YM, Rochdi M, Howell SB (2002) Cancer Res 62:6559-6565

85. Komatsu M, Sumizawa T, Mutoh M, Chen ZS, Terada K, Furukawa T, Yang XL, Gao H, Miura N, Sugiyama T, Akiyama S (2000) Cancer Res 60:1312-1316

86. Kasahara K, Fujiwara Y, Nishio K, Ohmori T, Sugimoto Y, Komiya K, Matsuda T, Saijo N (1991) Cancer Res 51:3237-3242

87. D'Andrea AD, The Molecular Basis of Cancer, W.B. Saunders: 2008 39-55.

88. Chaney SG, Sancar A (1996) J Natl Cancer Inst 88:1346-1360

89. Reed E (1998) Cancer Treat Rev 24:331-344

90. Galluzzi L, Senovilla L, Vitale I, Michels J, Martins I, Kepp O, Castedo M, Kroemer G (2012) Oncogene 31:1869-1883

91. Wong E, Giandomenico CM (1999) Chem Rev 99:2451-2466

92. Knox RJ, Friedlos F, Lydall DA, Roberts JJ (1986) Cancer Res 46:1972-1979

93. Boulikas T, Pantos A, Bellis E, Christofis P, (2007) Cancer Ther. 5:537-583.

94. Alian OM, Azmi AS, Mohammad RM (2012) Clin Transl Med 1:26

95. Misset JL (1998) Br J Cancer 77 Suppl 4:4-7

96. Raymond E, Faivre S, Woynarowski JM, Chaney SG (1998) Semin Oncol 25:4-12

97. Kuwahara A, Yamamori M, Nishiguchi K, Okuno T, Chayahara N, Miki I, Tamura T, Inokuma T, Takemoto Y, Nakamura T, Kataoka K, Sakaeda T (2009) Int J Med Sci 6:305-311

98. McKeage MJ (2001) Expert Opin Investig Drugs 10:119-128

99. Hall MD, Hambley TW (2002) Coord Chem Rev 232:49-67

100. Lebwohl D, Canetta R (1998) Eur J Cancer 34:1522-1534

101. Takahara PM, Frederick CA, Lippard SJ (1996) J Am Chem Soc 118:12309-12321

102. Stachowicz-Kuśnierz A, Korchowiec J (2016) Struct Chem 27:543-555

103. Sandman KE, Fuhrmann P, Lippard SJ (1998) J Biol Inorg Chem 3:74-80

104. Dalla Via L, Gia O, Magno SM, Dolmella A, Marton D, Di Noto V (2006) Inorg Chim Acta 359:4197-4206

105. Kimutai B, He CC, Roberts A, Jones ML, Bao X, Jiang J, Yang Z, Rodgers MT, Chow CS (2019) J Biol Inorg Chem 24:985-997

106. Rijal K, Bao X, Chow CS (2014) Chem Comm 50:3918-3920

107. Altman J, Wilchek M, Warshawsky A (1985) Inorg Chim Acta 107:165-168

108. Bino A, Cohen S, Altman J, Wilchek M (1988) Inorg Chimica Acta 147:99-102

109. Hambley TW, Webster LK (1994) J Inorg Biochem 55:175-181

110. Watabe M, Kai M, Goto K, Ohmuro H, Furukawa S, Chikaraishi N, Takayama T, Koike Y (2003) J Inorg Biochem 97:240-248

111. Ye Q-S, Xie M-J, Liu W-P, Chen X-Z, Yu Y, Chang Q-W, Hou S-Q (2009) Chem Pharm Bull 57:424-427

112. Ziegler CJ, Sandman KE, Liang CH, Lippard SJ (1999) J Biol Inorg Chem 4:402-411

113. Baidina IA, Slyudkin OP, Borisov SV (1985) J Struct Chem 26:955-958

114. Collins JG, Wheate NJ (2004) J Inorg Biochem 98:1578-1584

115. Boysen G, Pachkowski BF, Nakamura J, Swenberg JA (2009) Mutat Res 678:76-94

116. Zhu Y, Hamlow LA, He CC, Strobehn SF, Lee JK, Gao J, Berden G, Oomens J, Rodgers MT (2016) J Phys Chem B 120:8892-8904

117. Prakash AS, Gibson NW (1992) Carcinogenesis 13:425-431

118. Roger M, Hotchkiss RD (1961) Proc Natl Acad Sci USA 47:653-669

119. Gates KS (2009) Chem Res Toxicol 22:1747-1760

120. Wu RR, Rodgers MT (2016) Phys Chem Chem Phys 18:16021-16032

121. He CC, Hamlow LA, Devereaux ZJ, Zhu Y, Nei Y-w, Fan L, McNary CP, Maitre P, Steinmetz V, Schindler B, Compagnon I, Armentrout PB, Rodgers MT (2018) J Phys Chem B 122:9147-9160

122. Zhu Y, Roy HA, Cunningham NA, Strobehn SF, Gao J, Munshi MU, Berden G, Oomens J, Rodgers MT (2017) Phys Chem Chem Phys 19:17637-17652

123. Zhu Y, Yang Z, Rodgers MT (2017) J Am Soc Mass Spectrom 28:2602-2613

124. Zhu Y, Hamlow LA, He CC, Lee JK, Gao J, Berden G, Oomens J, Rodgers MT (2017) J Phys Chem B 121:4048-4060

125. Zhu Y, Roy HA, Cunningham NA, Strobehn SF, Gao J, Munshi MU, Berden G, Oomens J, Rodgers MT (2017) J Am Soc Mass Spectrom 28:2423-2437

126. Leeson P (2012) Nature 481:455

127. Mosmann T (1983) J Immunol Methods 65:55-63

128. Cailleau R, Olive M, Cruciger QV (1978) In vitro 14:911-915

129. Mitsudomi T, Steinberg SM, Nau MM, Carbone D, D'Amico D, Bodner S, Oie HK, Linnoila RI, Mulshine JL, Minna JD, Gazdar AF (1992) Oncogene 7:171-180

130. Cailleau R, Young R, Olivé M, Reeves WJ, Jr. (1974) J Natl Cancer Inst 53:661-674

131. Lucey BP, Nelson-Rees WA, Hutchins GM (2009) Arch Pathol Lab Med 133:1463-1467

132. Scherer WF, Syverton JT, Gey GO (1953) J Exp Med 97:695-710

133. Stone KR, Mickey DD, Wunderli H, Mickey GH, Paulson DF (1978) Int J Cancer 21:274-281

134. Bello D, Webber MM, Kleinman HK, Wartinger DD, Rhim JS (1997) Carcinogenesis 18:1215-1223

135. Still BM, Kumar PGA, Aldrich-Wright JR, Price WS (2007) Chem Soc Rev 36:665-686

136. Fischer SJ, Benson LM, Fauq A, Naylor S, Windebank AJ (2008) Neurotoxicol 29:444-452

137. Lundblad R, Macdonald F (2010) Handbook of Biochemistry and Molecular Biology, 4th Edn CRC Press: Boca Raton

138. Eastman A (1982) Biochemistry 21:6732-6736

139. Corbett JF (1972) J Chem Educ 49:663

140. Lee KW, Martin Jr DS (1976) Inorganica Chim Acta 17:105-110

141. Ulrich EL, Akutsu H, Doreleijers JF, Harano Y, Ioannidis YE, Lin J, Livny M, Mading S, Maziuk D, Miller Z, Nakatani E, Schulte CF, Tolmie DE, Kent Wenger R, Yao H, Markley JL (2008) Nucleic Acids Res 36:D402-D408

142. Kertesz TM, Hall LH, Hill DW, Grant DF (2009) J Am Soc Mass Spectrom 20:1759-1767

143. Zhang T, Cai S, Forrest WC, Mohr E, Yang Q, Forrest ML (2016) Appl Spectrosc 70:1529-1536

144. Marcelis AT, den Hartog JHJ, van der Marel GA, Wille G, Reedijk J (1983) Eur J Biochem 135:343-349

145. Bao X, Ph. D. Dissertation, Wayne State University 2015.

146. Quagliano JV, Schubert LEO (1952) Chem Rev 50:201-260

147. Beck JL, Colgrave ML, Ralph SF, Sheil MM (2001) Mass Spectrom Rev 20:61-87

148. Lemaire D, Fouchet M-H, Kozelka J (1994) J Inorg Biochem 53:261-271

149. Eastman A (1982) Biochemistry 21:6732-6736

150. Coe BJ, Glenwright SJ (2000) Coord Chem Rev 203:5-80

151. Davies MS, Berners-Price SJ, Hambley TW (2000) Inorg Chem 39:5603-5613

152. Arpalahti J, Mikola M, Mauristo S (1993) Inorg Chem 32:3327-3332

153. Kjellström J, Elmroth SKC (2003) Dalton Trans:2867-2871

154. van Zutphen S, Reedijk J (2005) Coord Chem Rev 249:2845-2853

155. Dedduwa-Mudalige NG, Ph.D. Dissertation, Wayne State University 2015.

156. Gamage ST, Ph.D. Dissertation, Wayne State University 2019.

157. Jennerwein MM, Eastman A, Khokhar A (1989) Chem-Biol Interact 70:39-49

158. Höfer D, Galanski M, Keppler BK (2017) Eur J Inorg Chem 2017:2347-2354

159. Endo Y, Tsurugi K (1987) J Biol Chem 262:8128-8130

160. Guillet M, Boiteux S (2002) EMBO J 21:2833-2841

161. Cody RB, Burnier RC, Freiser BS (1982) Anal Chem 54:96-101

162. Coon JJ (2009) Anal Chem 81:3208-3215

163. Devereaux ZJ, Zhu Y, Rodgers MT (2019) Eur J Mass Spectrom 25:16-29

164. May KL, Yan Q, Tumer NE (2013) Toxicon 69:143-151

165. Gonzales-Vitale JC, Hayes DM, Cvitkovic E, Sternberg SS (1977) Cancer 39:1362-1371

166. Hanigan MH, Devarajan P (2003) Cancer therapy 1:47-61

167. Miller RP, Tadagavadi RK, Ramesh G, Reeves WB (2010) Toxins 2:2490-2518

168. Mosmann T (1983) J Immunol Methods 65:55-63

169. Chacon E, Acosta D, Lemasters JJ, Academic Press: San Diego, (1997) In Vitro Methods in Pharmaceutical Research 209-223.

170. Stepanenko AA, Dmitrenko VV (2015) Gene 574:193-203

171. van Tonder A, Joubert AM, Cromarty AD (2015) BMC Res Notes 8:47-47

172. Fanning J, Biddle WC, Goldrosen M, Crickard K, Crickard U, Piver MS, Foon KA (1990) Gynecol Oncol 39:119-122

173. Alami N, Li Z, Engel J, Leyland-Jones B (2007) Cancer Res 67:4780-4780

174. Ambrosini G, Sambol EB, Carvajal D, Vassilev LT, Singer S, Schwartz GK (2006) Oncogene 26:3473-3481

175. Hartinger CG, Nazarov AA, Ashraf SM, Dyson PJ, Keppler BK (2008) Curr Med Chem 15:2574-2591

176. Huang R, Sun Y, Gao Q, Wang Q, Sun B (2015) Anticancer Drug 26:957-963

177. Imrali A, Mao X, Yeste-Velasco M, Shamash J, Lu Y (2016) Am J Cancer Res 6:1772-1784

178. Liu R, Fu Z, Zhao M, Gao X, Li H, Mi Q, Liu P, Yang J, Yao Z, Gao Q (2017) Oncotarget 8:39476-39496

179. Lovejoy KS, Serova M, Bieche I, Emami S, D'Incalci M, Broggini M, Erba E, Gespach C, Cvitkovic E, Faivre S, Raymond E, Lippard SJ (2011) Mol Cancer Ther 10:1709-1719

180. Navanesan S, Wahab NA, Manickam S, Sim KS (2015) BMC Complem Altern Med 15:186

181. Park GY, Wilson JJ, Song Y, Lippard SJ (2012) Proc Natl Acad Sci USA 109:11987-11992

182. Silva H, Barra CV, Rocha FV, Frézard F, Lopes MTP, Fontes APS (2010) J Braz Chem Soc 21:1961-1967

183. Giard DJ, Aaronson SA, Todaro GJ, Arnstein P, Kersey JH, Dosik H, Parks WP (1973) J Natl Cancer Inst 51:1417-1423

184. Soule HD, Vazquez J, Long A, Albert S, Brennan M (1973) J Natl Cancer Inst 51:1409-1416

185. Leeson P (2012) Nature 481:455-456

186. Jemal A, Siegel R, Ward E, Hao Y, Xu J, Murray T, Thun MJ (2008) CA Cancer J Clin 58:71-96

187. Dasari S, Tchounwou PB (2014) European journal of pharmacology 0:364-378

188. Dhar S, Kolishetti N, Lippard SJ, Farokhzad OC (2011) Proc Natl Acad Sci USA 108:1850-1855

189. Tsimberidou AM, Braiteh F, Stewart DJ, Kurzrock R (2009) J Clin Oncol 27:6243-6250

190. Barr MP, Gray SG, Hoffmann AC, Hilger RA, Thomale J, O'Flaherty JD, Fennell DA, Richard D, O'Leary JJ, O'Byrne KJ (2013) PloS one 8:e54193-e54193

191. Schmidt N, Mishra A, Lai GH, Wong GC (2010) FEBS Lett 584:1806-1813

192. Chen B, Le W, Wang Y, Li Z, Wang D, Ren L, Lin L, Cui S, Hu JJ, Hu Y, Yang P, Ewing RC, Shi D, Cui Z (2016) Theranostics 6:1887-1898

193. Abercrombie M, Ambrose EJ (1962) Cancer Res 22:525-548

194. Le W, Chen B, Cui Z, Liu Z, Shi D (2019) Biophysics Report 5:10-18

195. Chen B, Le W, Wang Y, Li Z, Wang D, Ren L, Lin L, Cui S, Hu JJ, Hu Y, Yang P, Ewing RC, Shi D, Cui Z (2016) Theranostics 6:1887-1898

196. Romero-Garcia S, Moreno-Altamirano MMB, Prado-Garcia H, Sánchez-García FJ (2016) Front Immunol 7:52-52

197. Ferguson BW, Datta S (2011) Prostate cancer 2011:893208

198. Nagarajan A, Malvi P, Wajapeyee N (2018) Front Endocrinol 9:483-483

199. Basu S, Ma R, Boyle PJ, Mikulla B, Bradley M, Smith B, Basu M, Banerjee S (2003) Glycoconj J 20:563-577

200. Florea A-M, Büsselberg D (2011) Cancers (Basel) 3:1351-1371

201. Åmand HL, Rydberg HA, Fornander LH, Lincoln P, Nordén B, Esbjörner EK (2012) Biochim Biophys Acta 1818:2669-2678

202. Amand HL, Fant K, Norden B, Esbjorner EK (2008) Biochem Biophys Res Commun 371:621-625

203. Guidotti G, Brambilla L, Rossi D (2017) Trends Pharmacol Sci 38:406-424

204. Schmidt N, Mishra A, Lai GH, Wong GCL (2010) FEBS Letters 584:1806-1813

205. Lai SL, Perng RP, Hwang J (2000) J Biomed Sci 7:64-70

206. Perego P, Giarola M, Righetti SC, Supino R, Caserini C, Delia D, Pierotti MA, Miyashita T, Reed JC, Zunino F (1996) Cancer Res 56:556

207. Vranic S, Gatalica Z, Wang Z-Y (2011) Oncol Lett 2:1131-1137

208. Hui L, Zheng Y, Yan Y, Bargonetti J, Foster DA (2006) Oncogene 25:7305-7310

209. Matlashewski G, Banks L, Pim D, Crawford L (1986) Eur J Biochem 154:665-672

210. Leroy B, Girard L, Hollestelle A, Minna JD, Gazdar AF, Soussi T (2014) Hum Mutat 35:756-765

211. Bajgelman MC, Strauss BE (2006) Prostate 66:1455-1462

212. Devereaux ZJ, Zhu Y, Rodgers MT (2018) Eur J Mass Spectrom

213. Rios AC, Yu HT, Tor Y (2015) J Phys Org Chem 28:173-180

214. Topalian SL, Gonzales MI, Ward Y, Wang X, Wang R-F (2002) Cancer Res 62:5505-5509

215. Topalian SL, Kaneko S, Gonzales MI, Bond GL, Ward Y, Manley JL (2001) Mol Cell Biol 21:5614-5623

216. Schmid M, Olszewski P, Pelechano V, Gupta I, Steinmetz Lars M, Jensen Torben H (2015) Cell Rep 12:128-139

ABSTRACT

NON-CANONICAL TARGETS, REACTION KINETICS, AND CELLULAR POTENCY OF AMINO ACID-LINKED PLATINUM(II) COMPOUNDS

by

BETT KIMUTAI

May 2020

Advisor: Dr. Christine S. Chow

Major: Chemistry (Biochemistry)

Degree: Doctor of Philosophy

Although cisplatin (cisPt) has been used for several years in cancer therapy, its application has faced challenges of adverse toxicity, lack of selectivity, and cellular resistance. Several second-generation cisPt analogues have been synthesized, but only a few have been approved worldwide for anticancer usage. The approved analogues, which include carboplatin, oxaliplatin, and nedaplatin, have advantages in averting adverse toxicity and resistance in their antitumor application. However, compared to the parent cisPt, these analogues have low potency and usually require to be administered with other compounds in order to be effective. There is still a need to develop alternative platinum-based compounds with balanced potency, selectivity for cancer cells, and reduced side effects.

CisPt is known to target deoxyguanosine (dGuo) residues of DNA and coordinate at their N7 positions. New analogues could be developed to selectively coordinate with alternative targets and form non-canonical adducts that could potentially be important in avoiding resistance and lack of selectivity. Efforts to find compounds that coordinate with alternative sites of DNA or RNA have had limited success. Previous work in our lab showed that positively charged amino acid-linked platinum(II) (AAPt) compounds have altered reactivity compared to cisPt when reacting with folded RNA. In this thesis, AAPt compounds of alanine, ornithine, and arginine (AlaPt, OrnPt, and ArgPt, respectively) were synthesized. The structures of these AAPt compounds consist of

one chelating amino acid and two chlorido ligands that coordinate with the platinum center to form a five-membered ring. The objectives of this thesis were to characterize the non-canonical adducts formed by AAPt compounds, investigate their reaction kinetics with nucleic acids, study their impact on glycosidic bond stability, and investigate their cellular potency and accumulation.

AlaPt, OrnPt, or ArgPt react with Ado nucleosides to form multiple products that were isolated from HPLC and further characterized using mass spectrometry and NMR spectroscopy. The compounds coordinate with Ado to predominantly form isomeric monofunctional adducts that vary at their platination sites (N1, N3, or N7). The compounds also react with oligonucleotide sequences 5′-d(TTATT)-3′ and 5′-UUAUU-3′ in which monofunctional and doubly platinated adducts are observed. Kinetic reactions of AAPt compounds with purine nucleosides indicate that AlaPt, OrnPt and ArgPt have reactivity preferences for Ado/dAdo residues over Guo/dGuo residues. These AAPt compounds have between five- to nine-fold higher reactivity with Ado/dAdo nucleosides than with Guo/dGuo. The reactivity of these compounds with DNA/RNA oligonucleotides is enhanced compared to their reactivity with nucleosides. This preference is likely because the negatively charged backbone phosphate groups could interact favorably with the AAPt compounds or provide hydrogen-bond acceptors that stabilize the interactions of AAPt with the oligonucleotides.

Changes in the chemical composition of a molecule affect its stability. Modification of nucleoside residues due to coordination with platinum-based compounds could also impact their adduct bond stabilities. The fragmentation and stability of glycosidic bonds were investigated using collision induced dissociation (CID) and glycosidic bond survival yield analysis. It was observed that platination by AlaPt and OrnPt at the N7 position destabilizes the glycosidic bonds more than platination at the N1 or N3 positions. Comparatively, AlaPt activates fragmentation of the adducts predominantly through glycosidic bond cleavage, while OrnPt activates fragmentation through glycosidic bond cleavage and significant neutral losses.

The cellular potency of AAPt compounds in human cancer and normal cells was investigated using MTT assays. The potent activity of these compounds was observed in several cell lines including prostate cancer cell line (DU145). While cisPt exhibits potency in both prostate cancer and normal cell lines, ArgPt is more selective with a six-fold higher potency in prostate cancer cells over normal cells. The uptake and accumulation of platinum-based compounds could contribute to the selective potency of platinum-based compounds. Therefore, the accumulation of the compounds was investigated in prostate normal and cancer cells using inductively coupled plasma mass spectrometry (ICP-MS). ArgPt exhibits a thirty-fold higher accumulation in cancer cells compared to normal cells, which likely translates to its observed selective potency.

The work in this thesis could be important in providing important structural and chemical information that can be applied in the development of newer platinum-based drugs that have improved anticancer activities. Characteristics that enable formation of non-canonical adducts and altered reactivity preferences could be important in circumventing cellular resistance. Features that promote selective potency and increased uptake by cancer cells are also crucial in reducing toxic side effects.

AUTOBIOGRAPHICAL STATEMENT

BETT KIMUTAI

ADVISOR: Dr. Christine S. Chow

THESIS TITLE: NON-CANONICAL TARGETS, REACTION KINETICS, AND CELLULAR POTENCY OF AMINO ACID-LINKED PLATINUM(II) COMPOUNDS

EDUCATION:

- **PhD; Biological Chemistry, 2019, Wayne State University, Detroit, MI, USA**
- **B.S; Biochemistry, 2012, Fairleigh Dickinson University, Teaneck, NJ, USA**

PUBLICATIONS

1. **Kimutai B**, He CC, Roberts A, Jones ML, Bao X, Jiang J, Yang Z, Rodgers MT, Chow CS, Amino acid-linked platinum(II) compounds: non-canonical nucleoside preferences and influence on glycosidic bond stabilities (2019) J Biol Inorg Chem 24:985-997
2. He CC, **Kimutai B**, Bao X, Hamlow L, Zhu Y, Strobehn SF, Gao J, Berden G, Oomens J, Chow CS, Rodgers MT, Evaluation of hybrid theoretical approaches for structural determination of a glycine-linked cisplatin derivative via infrared multiple photon dissociation (IRMPD) action spectroscopy (2015) J Phys Chem A 119:10980-10987